“Enhanced Wellbore Stabilization and Reservoir Productivity with Aphron Drilling Fluid Technology”

FINAL REPORT

October 1, 2003 – September 30, 2005

by

Fred Growcock

Issued October, 2005

DOE Award Number DE-FC26-03NT42000

MASI Technologies *LLC*

5950 N. Course Dr.

Houston, Texas 77072

DISCLAIMER

ABSTRACT

The thrust of this Project was to obtain laboratory evidence for the field-proven capability of aphron drilling fluids to limit fluid invasion in permeable formations with little permanent formation damage and provide a sound scientific basis for this behavior. The results demonstrate how and to what extent aphron drilling fluids reduce whole mud loss and minimize collateral damage to high-permeability porous media. Now the industry can utilize this technology with greater confidence and, by doing so, recover hydrocarbons more economically.

Aphrons – long-lived air-filled bubbles -- serve as a first line of defense to prevent leak-off during the initial invasion period after a drill bit cuts into rock. What makes this possible is their resistance to loss of air at downhole pressures and their ability to move rapidly to the fluid front via a phenomenon called "Bubbly Flow." In contrast to conventional bubbles, which do not survive long past a few hundred psi, aphrons can survive compression to at least 27.3 MPa (4000 psi); their longevity is influenced by the system pressure, bubble size, rate of pressurization, shear rate, fluid composition and concentration of nitrogen in solution.

Bubbly Flow of aphrons can be described by the Navier-Stokes equation, which states that the velocity of a bubble relative to the liquid phase is proportional to the pressure gradient and bubble diameter and inversely proportional to the fluid viscosity. Thus, aphrons can accumulate at the fluid front and inhibit movement of the liquid, particularly during the initial stages of fluid invasion, when fluid viscosity is lowest and the pressure gradient is the highest.

Aphron drilling fluids contain a cellulosic material that acts as an efficient oxygen scavenger and leaves the aphrons filled with nitrogen, thus eliminating oxygen-induced corrosion. Although this reduces aphron diameter by about 7%, the impact on aphron performance is minor. Depending on salinity, the cellulosic material can also interact with the xanthan gum-based viscosifier and alkalinity control agent MgO to produce a microgel that is able to form a soft seal that helps to reduce the rate of invasion of fluid into pores and microfractures.

Aphrons shrink and expand with pressure in the same manner as conventional bubbles, i.e. as prescribed by the Modified Ideal Gas Law (Volume $\propto$ 1/Pressure). However, at elevated pressures (below the solubility limit of nitrogen in water), conventional bubbles begin to lose air rap-

idly via diffusion into the surrounding aqueous medium. Aphrons lose nitrogen, too, but the low permeability of the aphron shell slows the rate of diffusion considerably.

When shrinking aphrons reach a size of about 25 μm diameter, they undergo a structural change that leads to rapid expulsion and dissolution of the remaining nitrogen into the fluid. The rate of pressurization also affects the longevity of aphrons. Rapid pressurization produces longer-lived aphrons than slow pressurization, and rapid depressurization brings nitrogen out of solution faster than gradual depressurization. Because the drilling fluid contains a very small amount of air – 15 vol %, or 0.02 wt % -- system pressure must be below a couple hundred psi before the nitrogen reaches saturation and comes out of solution; when it does, it tends to become incorporated into aphrons that have survived pressurization.

Examination of the key components of the polymer-based aphron drilling fluid revealed that a smaller amount (3.5 vs 5.0 lb/bbl) of the viscosifier, GO-DEVIL II, and a larger amount (0.5 vs 0.3 lb/bbl) of the aphron stabilizer, PLASTISIZER, improve the longevity of aphrons.

During flow of an aphron drilling fluid through pores and microfractures, aphrons are sheared and comminuted to sizes that correspond to those of the openings in the rock. During this period, they are much more vulnerable to loss of nitrogen. However, if enough of the aphrons survive transport to the fluid front, the fluid in the aphron band becomes saturated with nitrogen; aphrons which arrive thereafter will survive, accumulating and acting as conventional bridging material. Microgel-forming particulates supplement this bridging action. Aphrons and microgel, coupled with radial flow in the invasion zone, reduce the velocity of the fluid sufficiently that the viscosity of the highly shear-thinning base fluid rises rapidly. This viscosity increase further slows the fluid, which raises the viscosity more, etc. and the fluid essentially stops. A Fluid Invasion Model was developed that simulates these phenomena.

Formation damage potential of aphron drilling fluids is of similar magnitude to that of conventional reservoir drilling fluids. The latter produce high return permeabilities by forming a thin, tight external filter cake that limits invasion of insoluble components. Aphron drilling fluids, on the other hand, produce high return permeabilities because they are very compatible with produced fluids. Aphrons themselves are minimally damaging, because they possess little affinity for each other or for the mineral surfaces in the pores of drilled formations; thus, reversing the pressure differential to produce hydrocarbons from a reservoir removes the aphrons with ease.

TABLE OF CONTENTS

LIST OF FIGURES

INTRODUCTION

Aphron drilling fluids have been used successfully in 300+ applications worldwide to drill depleted reservoirs in mature oil and gas fields, high-permeability formations and micro-fractured rock. Aphrons are specially designed air-filled bubbles that are usually incorporated into the drilling fluid with conventional mud mixing equipment, thereby reducing costs and safety concerns associated with air or foam drilling. Because the amount of air in the fluid is very low, the density of the fluid at downhole pressures is essentially that of the base fluid. Nevertheless, the fluid is able to seal loss zones effectively, minimize loss of whole mud and differential sticking and avoid formation damage. Consequently, aphron drilling fluids are marketed as cost-effective alternatives to underbalanced drilling.[1-4]

Aphron drilling fluids possess two chief attributes that serve to minimize fluid invasion and damage to the formation. First, the base fluid is very shear-thinning and exhibits an extraordinarily high LSRV (Low-Shear-Rate Viscosity); this high viscosity is thought to reduce the flow rate of the fluid dramatically upon entering a loss zone. Second, the fluid contains bubbles that are designed to be very tough and flexible. These stabilized bubbles, or "aphrons," are essential to sealing the problem area by forming an internal bridge that acts as a lost circulation material.

Water-based aphron drilling fluids, such as APHRON ICS™ and HYSSTER™ systems, are the subject of this study. Aphrons consist of two essential elements: a spherical core of air and a protective outer shell.[5] In contrast to a conventional air bubble, which is stabilized by a surfactant monolayer, the outer shell of the aphron is thought to consist of a much more robust surfactant tri-layer. This tri-layer consists of an inner surfactant film enveloped by a viscous water layer, outside of which is an outer bilayer of surfactants that provides rigidity and low permeability to the structure while imparting some hydrophilic character to it. Under quiescent conditions, the structure is compatible with the aqueous bulk fluid. It has been speculated that, in an environment where the aphrons undergo shear, the outermost surfactant layer is stripped away to leave a structure with residual hydrophobic character that has little affinity for water-wet mineral surfaces.[4]

Aphrons are claimed to act as a unique bridging material, forming a micro-environment in a pore network or fracture that appears to behave in some ways like a foam, and in other ways like a solid, but flexible bridging material. As is the case with any bridging material, concentration and size of the aphrons are critical to the mud's ability to seal thief zones. Aphrons are created and entrained in the bulk fluid with standard mud mixing equipment, which reduces the safety concerns and costs associated with high-pressure hoses and compressors commonly utilized in air or foam drilling.[6] Although each application is customized to the individual operator's needs, the mud system is generally designed to contain 12-15% by volume air. Aphrons are thought to be sized or polished at the drill bit to achieve a size of 15-100 μm diameter, which is typical of many bridging materials.

Various aspects of the aphrons, particularly their physicochemical properties, need to be evaluated further to understand the way that they function and to enhance their performance. Greater application of aphron technology and the consequent reduction in drilling costs would be facilitated by a systematic and thorough evaluation of the structure and behavior of aphron drilling fluids under downhole conditions.

The objectives of this project were threefold: (a) develop a comprehensive understanding of how aphrons behave at elevated pressures and temperatures; (b) measure the ability of aphron drilling fluids to seal permeable and fractured formations under simulated downhole conditions; and (c) determine the role played by each component of the drilling fluid.

The Project was divided into two phases. Phase I (Year 1) focused on developing evidence for the ways in which aphrons behave differently from ordinary surfactant-stabilized bubbles, particularly how they seal permeable and micro-fractured formations during drilling operations. Various methods were evaluated for characterizing the properties of aphrons, including acoustic Bubble Spectrometry, optical and electronic micro-imaging and interfacial tension. Key properties that were investigated included the effects of pressure on bubble size, the influence of environmental parameters on aphron stability, the affinity of aphrons for each other and for the mineral surfaces in rock pores and micro-fractures, and the nature of aphron seals in permeable and micro-fractured rock. Initial sealing and formation damage tests were carried out, using lab-scale apparati designed to simulate permeable and micro-fractured environments. Phase II (Year 2) focused on optimization of the structure of aphrons and composition of aphron drilling fluids, quantifying the flow properties of the fluids (radial vs linear flow, shear effects and Bubbly Flow phenomena), and understanding formation sealing and damage under simulated downhole conditions, so as to furnish irrefutable evidence for this technology and provide field-usable data.

The schedule of tasks in Phases I and II is provided in Figure 1.

Figure 1. Schedule of Tasks in Aphron Drilling Fluid Project

	2003	2004				2005		
Task	4th Q	1st Q	2nd Q	3rd Q	4th Q	1st Q	2nd Q	3rd Q
1. Aphron Compressibility								
1.1 Aphron Visualization	X	X	X					
1.2 Fluid Density	X	X	X					
1.3 Aphron Air Diffusivity	X	X	X	X				
2. Sealing Mechanism								
2.1 In Situ Visualization			X	X				
2.2 Pressure Transmissibility	X	X	X					
2.3 Aphron Shell Hydrophobicity			X	X				
3. Leak-Off/Formation Damage - Initial Tests								
3.1 Sealing of Permeable Media			X	X				
3.2 Sealing of Fractured Media			X	X				
4. Aphron Drilling Fluid Optimization								
4.1 Microstructure					X	X	X	X
4.2 Performance					X	X	X	X
5. Flow Properties								
5.1 Geometry of Medium					X	X	X	
5.2 Fluid Rheology						X	X	X
5.3 Multi-Phase Flow Effects						X	X	X
6. Leak-Off/Formation Damage Perm Media						X	X	X

Phase I ran from Oct. 1, 2003 through Sept. 30, 2004 and consisted of Task Areas 1-3. Topical Reports were written summarizing all of these tasks and submitted to NETL AAD Document Control, along with the four Quarterly Progress Reports that cover Phase I. Phase II ran from Oct. 1, 2004 through Sept. 30, 2005 and consisted of Task Areas 4-6. Quarterly Progress Reports for the first three Quarters of Phase II were submitted to NETL AAD Document Control. All of the tasks were completed, as scheduled, and are indicated in Figure 1 by an X.

EXECUTIVE SUMMARY

This Project was designed with two ultimate objectives: to gain greater acceptance for aphron drilling fluid technology and to decrease the costs of drilling mature and multiple-pressure formations in oil and gas wells. Aphron drilling fluids are very high low-shear-rate viscosity fluids laden with specially designed microbubbles, or "aphrons." The distinguishing characteristic of this drilling fluid is its ability to enable drilling of low-pressure formations -- including depleted production zones – with minimal mud loss and formation damage, while drilling overbalanced (wellbore pressure > pore pressure). Thus, aphron drilling fluids serve as alternatives to underbalanced drilling fluids without the economic and safety risks associated with use of low-pressure fluids. However, there is little mechanistic evidence that aphron drilling fluids perform as claimed, and it would be very helpful for the U.S. drilling industry and the U.S. consumer to develop some understanding of how these fluids behave under downhole conditions in a well-controlled laboratory environment.

The results obtained in this Project demonstrate how and to what extent aphron drilling fluids reduce whole mud loss and minimize collateral damage to high-permeability porous media. Consequently, the industry now can utilize this technology with greater confidence to drill oil and gas wells and, by doing so, recover the hydrocarbons more economically.

Five individuals with suitable credentials were constituted into a team to carry out the work. This Project team installed laboratory facilities and purchased and constructed the equipment required to carry out the Project plan. Four of the individuals also received training at the M-I SWACO Customer Mud School. Work areas were combined to permit centralized data acquisition and communication with internal and external file servers, and electronic and hard-copy filing systems were set up to be compatible with ISO 9001 guidelines. Finally, near the end of Phase I, the laboratory facilities for MASI Technologies LLC were consolidated at a new location: 8275 El Rio, Suite 130, Houston, TX 77054.

All of the tasks undertaken in Phases I (Year 1) and II (Year 2) of this Project were completed. The results are presented as outlined below:

- Aphron Visualization
  - Ambient Conditions
  - Elevated Pressure and Temperature
- Aphron Longevity
  - Effect of Pressure
  - Effect of Compression/Decompression
  - Effect of Shear
  - Effect of Method of Generating Aphrons
  - Effect of Fluid Composition
- Pressure Transmissibility through Aphron Drilling Fluids
- Sealing of Permeable Media by Aphron Drilling Fluids
  - Core Leak-Off Tests

- Disk Leak-Off Tests
- Syringe Sand Pack Leak-Off Tests
- Capillary Suction Tests
- Effects of Chemical Composition on Drilling Fluid Invasion

➢ Flow Properties of Aphron Drilling Fluids
- Multi-Phase Flow
- Fluid Rheology
- Modeling of Drilling Fluid Invasion in Permeable Media
- Radial Flow of Aphron Drilling Fluids

➢ Wettability and Formation Damage Potential of Aphron Drilling Fluids

To study the behavior of aphrons, Acoustic Bubble Spectrometry (ABS) was evaluated and found to be unacceptable. ABS-derived bubble size distributions (BSD) in APHRON ICS™ drilling fluids do not correlate well with BSD determined via conventional laser light scattering (LLS) and optical imaging. In addition, the calculated total void fraction (fraction of air) is several orders of magnitude too low. By contrast, direct optical imaging of the bubbles was found to be a very suitable method, providing accurate and consistent BSD. Direct optical imaging not only reveals the dimensions of a population of bubbles, but also the dimensions of single bubbles, so that the technique can be used to characterize the effects of environmental variables on bubble size. The development of an ultra-thin high-pressure viewing cell – the VRD, or Variable Reservoir Depth, Viewing Cell -- enabled imaging of opaque fluids, too, thus obviating the need for the ABS. All high-pressure imaging of whole drilling fluids was carried out in the VRD Viewing Cell. A large-chamber Canty Viewing Cell was also employed, but strictly for qualitative imaging of transparent fluids. Magnification of the images was carried out with conventional light microscopes at magnifications up to 400x . Finally, a locally available Environmental Scanning Electron Microscope was found to provide very clear images of the fluid and its interaction with surfaces; although the low sample chamber pressure removed all air and left only residual voids, high concentrations of the polymers and surfactants were evident at the edges of the residual voids.

Aphron stability was found to depend on a number of system variables. First, it was learned that the oxygen dissolved in the fluid and entrained in aphrons is quickly scavenged by a cellulosic polymer in the base fluid, leaving the aphrons filled essentially with nitrogen. Although this reduces their size (diameter) by about 7%, sealing of permeable and fractured formations should be affected very little, and any concerns about enhanced corrosivity or biodegradability should be put to rest.

Aphrons can survive compression to at least 27.3 MPa (4000 psig). By contrast, conventional bubbles do not survive compression beyond a few hundred psi. This finding is of enormous significance, in that it provides the first clear evidence that aphron technology may be useful at pressures higher than previously thought (20.5 MPa, or 3000 psig). Like conventional bubbles, compression of aphrons initially results in volume reduction as predicted by the modified Ideal Gas Law, i.e. Volume $\propto$ 1/Pressure. However, conventional bubbles do not survive a few hundred psi for more than a few seconds, whereas aphrons can survive a few thousand psi for at least a few minutes. The solubility of nitrogen in the drilling fluid closely follows Henry's Law, which stipulates that Solubility $\propto$ Pressure. For a fluid containing 12 vol % nitrogen at ambient temperature, all of the nitrogen can potentially dissolve at pressures exceeding ~ 50 psig. Above this pressure, aphrons lose nitrogen via diffusion and dissolution into the surrounding fluid. The rate of shrinkage of the aphrons depends on pressure, bubble size, initial rate of compression, shear rate, concentration of nitrogen in solution and fluid composition.

The rate of loss of nitrogen is a function of the surface area of the bubble. However, when the aphrons reach a critical minimum size, on the order of 25 to 50 μm diameter, they undergo a structural change that leads to rapid collapse.

When an aphron-containing fluid at elevated pressure is depressurized, surviving aphrons increase in size as per the modified Ideal Gas Law. Nitrogen that was lost from aphrons and is in solution can be released, albeit slowly, if the pressure is reduced to a level low enough that the aqueous medium becomes supersaturated with nitrogen. The released air preferentially enters existing aphrons, but new aphrons can be formed, too.

As resistant as the aphrons may be to high pressures, it may be possible to reduce their permeability even more and to improve their resistance to shear. Optimization of the APHRON ICS™ formulation showed that reducing the concentration of the viscosifier GO-DEVIL II from 5.0 to 3.5 lb/bbl and increasing the concentration of PLASTISIZER from 0.3 to at least 0.4 lb/bbl increases the longevity of aphrons. Greater improvements may be possible with other additives.

The mechanics of the aphron generation process were also explored to optimize aphron longevity. In the laboratory, Silverson, Prince Castle and Hamilton Beach mixers entrained similar amounts of air with similar bubble size distributions (BSD), whereas a kitchen blender entrained much more air with a higher BSD and bubbles that were much less stable. Pumping the APHRON ICS fluid through a pressure drop in a Gaulin Homogenizer or a jet designed to simulate a drill bit comminuted the bubbles but did not enhance their stability or generate additional aphrons. Indeed, in flow tests through an orifice using an inlet pressure of 2000 psig and an outlet pressure of 1500 psig, it was demonstrated that aphrons cannot be formed, even if the APHRON ICS™ mud contains dissolved air equivalent to 15 vol % at ambient pressure.

Pressure transmissibility tests demonstrated that pulses through APHRON ICS™ fluids and other reference drilling fluids are transmitted very quickly (msec/m), so that variations in fluid composition do not yield observable differences in the rate of pressure transmission. On the other hand, significant differences <u>were</u> observed in pressure loss under both flow and static conditions. Under flowing conditions, the base fluid in APHRON ICS™ muds was shown to yield a significantly larger pressure loss (or, for a fixed pressure drop, lower flow rate) in long conduits than any conventional high-viscosity drilling fluid. Interestingly, aphrons had no observable effect. If flow was restricted or stopped, again APHRON ICS™ fluids (at a fixed wellbore pressure) generated significantly lower downstream pressures than did other muds. The same phenomena were evident in permeable sands at low pressure, with one important exception: in unconsolidated sands of permeability up to at least 100 darcy, the aphrons themselves slowed the rate of fluid invasion and increased the pressure drop across the sands.

Invasion of APHRON ICS™ drilling fluids into permeable and fractured formations was simulated using various types of laboratory tests, including high-pressure Core Leak-Off tests, Disk Leak-

Off tests, Syringe Sand Pack Leak-Off tests, Capillary Suction tests and Capillary Flow tests. These tests demonstrated that sealing of permeable rock and capillary tubes is accomplished by several of the constituents of the drilling fluid working together.

First, properly designed aphrons can form an internal bridge. Flow visualization tests indicate that aphrons move more rapidly through permeable media than the base fluid. This phenomenon, called "Bubbly Flow," follows conventional Navier-Stokes theory, which is as applicable to flow in a conduit and in a permeable medium (flow in opposition to a pressure differential) as it is to buoyancy (upward flow of bubbles in opposition to gravity). According to this theory, the velocity of a bubble relative to the liquid phase is proportional to the pressure gradient and bubble diameter and inversely proportional to the fluid viscosity. Thus, aphrons can accumulate at the fluid front and inhibit movement of the liquid particularly during the initial stages of fluid invasion, when fluid viscosity is lowest and the pressure gradient is the highest. Although the amount of air in a typical aphron drilling fluid is very small (15 vol % air at ambient temperature and pressure constitutes only 0.02 wt % air), Bubbly Flow can cause the aphrons to move at a velocity greater than the liquid phase, thus accumulating at the fluid front and inhibiting movement of the liquid.

Second, the cellulosic material that scavenges the oxygen in the system also interacts with the xanthan gum-based viscosifier and alkalinity control agent MgO to produce a microgel that is able to form a soft seal which helps to reduce the rate of invasion of fluid into pores and microfractures. In addition, the surfactants in BLUE STREAK and APHRONIZER A also appear to function in some manner that is not well understood to slow progress of the fluid.

Finally, the viscosifier, because of its highly shear-thinning nature and almost total lack of thixotropy can rapidly build viscosity to a level much higher than that of any conventional drilling fluid. The complex workings of all of these components make it possible to seal loss zones as permeable as 80 darcy.

The rheology of the APHRON ICS™ fluid can be described very well by a Power Law model, as is the case for the rheology of typical reservoir drilling fluids. However, the viscosity at any given shear rate is several times higher for the APHRON ICS™ fluid. Essentially all of the viscosity is generated by the xanthan gum-based viscosifier GO DEVIL II. No effects on viscosity were observed for any of the other components in the APHRON ICS™ fluid, including aphrons. However, at concentrations of air in excess of 15 vol % (at ambient pressure), high-shear-rate viscosity increased with increasing amount of air. No significant effect was observed at low shear rates. Oily additives, such as ACTIGUARD or produced fluids did not affect the viscosity either, though they resulted in lower levels of entrained air.

A multi-phase Fluid Invasion model was developed which shows that under downhole conditions, the rheology of the APHRON ICS™ fluid can control its depth of invasion in high-permeability formations to a couple of meters. The flow equations are solved numerically to give exact solutions that fit lab data very well at both low and high shear rates. Bubbly Flow of aphrons is incorporated in the model, but the direct effects of aphrons, particulates and surfactants are not yet included. Neither is comminution of aphrons; during invasion of the drilling fluid into a pore network, comminution will produce bubbles comparable in size to the pore throats. Bubbly flow will ensure that the concentration of the comminuted bubbles at the fluid front will be high. Some bubbles will not survive the passage, but they will eventually saturate the fluid front with dissolved nitrogen. Comminuted bubbles that come later to the fluid front will survive and will slow whole mud invasion by decreasing the viscosity and bridging the pore throats. This process is favored at low pressures, low fluid viscosity and high pressure gradient.

Linear, static Leak-Off tests at 200 ^{o}F, Fore-Pressure = 2000 psig and Back-Pressure = 1000 psig showed that Solids-Free APHRON ICS^{TM} fluid can seal Aloxite cores ranging in permeability from 2 to 10 darcy; the Leak-Off is commensurate with the permeability of the core. Other work has shown the fluid to be able to seal cores with permeabilities as high as 80 darcy. A "solids-free" standard reservoir drilling fluid (RDF), on the other hand, is not able to seal a 2-darcy core, even with the fluid's LSRV raised to a value comparable to that of the APHRON ICS^{TM} fluid. In other core Leak-Off tests, no detectable change in Leak-Off was observed with change in back pressure from 500 to 1500 psig. With addition of 30 ppb of 40-μm $CaCO_3$, Leak-Off for both fluids decreased significantly. When prepared in 10% NaCl, the two $CaCO_3$-laden fluids provided similar ultra-low Leak-Off; in fresh water, the Leak-Off of the APHRON ICS^{TM} fluid was a little higher. This is attributed to the interaction of $CaCO_3$ with various components of the APHRON ICS^{TM} system, which can coat the $CaCO_3$ and make it less effective as an <u>externa</u>l bridging material.

While the temperature and pressure specifications for these Leak-Off tests are reasonable and practical, the flow geometry (linear), shortness of the cores (5 cm, or 2 in) and fluid loading (static) may not adequately simulate invasion of fluids like APHRON ICS^{TM} that are thought to seal internally. To remove these limitations, a novel Radial Flow Apparatus was constructed that has a pie wedge shape (radial invasion profile), is quite long (69 cm, or 27 in), and fluid is pumped across the face of the inlet (dynamic loading). While the fragile nature of its polycarbonate construction limits operation of the Apparatus to pressures of only a few psig, fluids can be viewed fully as they flow radially through a packed bed of particles. Tests conducted in the Radial Flow Apparatus demonstrated the accuracy of the Fluid Invasion model, e.g. showing that the band of aphrons formed at the fluid front has a constant thickness, and showed that the APHRON ICS fluid will nearly stop its progress, whereas a typical reservoir drilling fluid continues does not stop and gives Leak-Off values an order of magnitude greater than the APHRON ICS fluid.

Six key surface interactions were identified as important during drilling fluid invasion and production of crude oil: Bubble-Bubble, Bubble-Mineral Surface (Pore Wall) and Drilling Fluid-Produced Fluid. Visual observations of Bubble-Bubble and Bubble-Mineral Surface interactions during fluid flow tests in beds of packed beads indicate that aphrons have very little affinity for each other or for the mineral surfaces in rock formations encountered during drilling. Even aphrons that are forcibly brought together, separate with the slightest amount of fluid movement. Thus, aphrons resist aggregation and coalescence; in a reservoir, aphrons are expected to be produced back easily by reversing the pressure differential, thus minimizing formation damage.

APHRON ICS^{TM} drilling fluids themselves appear to be very compatible with oils, such as produced fluids. Seven oils – including four crude oils -- were examined, using various emulsion compatibility and spreading tests. In every case, the oil and aphron drilling fluid mixed readily with each other, generating little or no effect on bulk properties, and in most cases generating water-continuous emulsions with oil/mud volume ratios as high as 50/50. In addition, when spread over each other, the APHRON ICS fluid and the oils gave very low contact angles. Finally, fluid displacement studies in cells packed with glass beads demonstrated that the surfactants in APHRON ICS™ systems facilitate transport of low-toxicity mineral oil through mud-saturated beds.

Several opportunities presented themselves to share the latest aphron drilling fluid technology with potential Project collaborators and clients. Several meetings were held with DOE representatives:

- Project Kick-Off Meeting with NETL DOE Project Team in Morgantown , W. Va. on Jan 23rd , 2004, followed by a visit to Dynaflow, Inc. (supplier of HTHP ABS System) in Jessup, Md. on Jan 26th, 2004.
- Informal technical update and lab tour with Gary Covatch and John Rogers at the M-I Technology Center and Applied Engineering Lab, Houston, TX, where the DOE Project Team is temporarily ensconced, Feb. 18, 2004.
- 3rd Quarter DEA Meeting in Houston Aug. 19, 2004.
- Drilling Fluids Training of personnel at NETL in Morgantown, W. Va., Feb. 14 & 15, 2005.
- Annual Project Review of DOE Project at NETL in Morgantown, W. Va., Feb. 16, 2005.

In addition, meetings and publications proved to be fruitful ways to bring potential clients up to date on the Project:

- Brief trip to Lafayette, LA Feb. 19 & 20, 2004 to meet with attendees at Formation Damage Symposium, including Sandra Cobianco of ENI Tecnologie (Milano, Italy) and Dr. Ergun Kuru of the University of Alberta (Edmonton, Canada) re formation damage and extensional viscosity of aphron drilling fluids. Also met with Jack Cowan of ActiSystems Inc. (partner in MASI Technologies LLC) to return that company's ABS System and discuss collaborative efforts. Finally, a brief meeting was held with Dr. Nick Takach of the University of Tulsa to discuss flow of foams and energized fluids; Dr. Takach invited the team to participate in the TUDRP/ACTS (Tulsa University Drilling Research Program/ Advanced Cuttings Transport Study) annual meeting in May.
- Publication and presentation of paper SPE 87134, "Alternative Aphron-Based Drilling Fluid," at IADC/SPE Drilling Conference in Dallas, TX, March 2-4, 2004.
- Exhibit Booth duty at SPE Coiled Tubing Conference & Exhibition, The Woodlands, TX, March 23- 24, 2004.
- Publication and presentation of paper # AADE-04-DF-HO-18, "Applications of Novel Aphron Drilling Fluids," at AADE 2004 Drilling Fluids Conference, Houston, Texas, April 6-7, 2004.
- Presentation of Project update to M-I SWACO R&D management, Houston, Texas, April 1, 2004.

- Presentation of Project update to ActiSystems at M-I SWACO, Houston, Texas, April 20, 2004.
- Exhibit Booth duty at *Offshore Technology Conference*, Houston, Texas, May 3-6, 2004.
- Featuring of aphron technology in Technology Applications section of May, 2004 issue of ***Journal of Petroleum Technology***.
- Attendance at *Tulsa University Drilling Research Program/Advanced Cuttings Transport Study* Annual Review, Tulsa, OK, May 10, 11, 2004.
- Publication and presentation of paper entitled, "Development of Aphron Drilling Fluids," at *SEFLU y CEMPO*, Margarita Island, Venezuela, May 24-28, 2004.[7]
- Exhibit Booth duty and attendance of a few presentations at *DEA Workshop*, Galveston, Texas, June 22 & 23, 2004.
- Operations Meeting of Shell Exploration & Production Co. (SEPCO) in New Orleans, Aug. 26, 2004.
- Meeting with faculty and students at Texas A&M University (College Station, TX) on Sept. 9 to discuss collaboration on the mechanics of Bubbly Flow.
- Exhibit Booth duty at SPE Annual Technology Conference and Exhibition Sept 27-29, 2004.
- Exhibit Booth duty at SPE/IADC Underbalanced Drilling Meeting, The Woodlands, Texas, Oct. 11 & 12, 2004.
- Overview of DOE Aphron Drilling Fluid project to M-I SWACO Technical Service, M-I Corporate Center, Houston, Texas, Oct. 14, 2004.
- Briefing of M. Kilchrist of ActiSystems, Inc. on aphron drilling fluid test procedures, MASI Technologies *LLC* laboratory, Oct. 18, 2004.
- Workshop for HiTech (Canada) personnel and associates on aphron drilling fluid test procedures, MASI Technologies *LLC* Laboratory, Oct. 20 & 21, 2004.
- Collaborative work with Cory Sikora and Mike George of Celanese Corp on Aphronizer B alternatives, MASI Technologies *LLC* Laboratory, several meetings throughout 2003-2005.
- Decision by MASI and Prof. Ergun Kuru of the University of Alberta, Canada to share APHRON ICS™ sample products, mixing procedures, and results of surface chemistry studies of aphron drilling fluids.
- Publication of article entitled, "Aphron Grant in Year 2" in ***Momentum*** M-I SWACO newsletter 4th Q 2004.
- Presentation of work entitled, "Static Leak-Off Tests of APHRON ICS™ Drilling Fluids," to Eric van Oort at Shell Exploration & Production Co., New Orleans, LA, Feb. 16, 2005.
- Presentation of recent findings of DOE project to M-I SWACO Tech Service, March 14, 2005.

- Tour of MASI Technologies lab and review of DOE Project for Hank Bakker, Devon Canada Corporation, March 31.
- Submission of testimony to Energy & Water Subcommittees of the House and Senate Committees on Appropriations regarding the necessity and value of the Aphron Drilling Fluids Project, March 2005.
- Publication and presentation of AADE-05-NTCE-73, "Drilling Fluid Selection to Minimize Formation Invasion," at 2005 AADE National Technical Conference and Exhibition, Houston, April 5-7, 2005.[8]
- Exhibit Booth duty at Coiled Tubing Conference, Houston, April 12-14, 2005.
- Project update and tour of MASI Technologies Lab to Mark Stansbury, M-I SWACO Yemen Country Manager, April 18, 2005.
- Exhibit Booth duty at 2005 IADC/SPE Managed Pressure Drilling Conference & Exhibition, San Antonio, April 20-21, 2005.
- Tour of MASI Technologies to Selim Molla, Drilling Superintendent, and Finance Minister from Albania, along with representatives of M-I SWACO, May 4, 2005.
- Discussions with Robert Jenkerson, Nanoactive Technologies on nano-sized particulates, May 27, 2005.
- Discussions with Lee Conn and Tom Heinz re training engineers to handle APHRON ICS™ systems in the field, May 27, 2005.
- Tour of MASI Technologies Lab to Mike Gascho (M-I SWACO) in preparation for work in Yemen, May 27, 2005.
- Publication of article, **"**Enhanced Wellbore Stabilization and Reservoir Productivity with Aphron Drilling Fluid Technology," in **GasTIPS**, Summer 2005**.**[9]
- Publication of article, "US DOE-Backed R&D Validates Effectiveness of Aphron Drilling Fluids in Depleted Zones," in IADC **Drilling Contractor**, May/June 2005.[10]
- Presentation of "Avances en Fluidos de Perforacion de Afrones" at Primer Encuentro Tecnologico de Perforacion y Rehabilitacion de Pozos, San Tome, Venezuela, May 23-26, 2005.[11]
- Summary of Project results since Oct. 1, 2003 at M-I SWACO R&D Project Review, June 15, 2005.
- Tour and training of M-I SWACO Tech Service Engineers Nick Hilbig, Steve Smith and Andres Diaz, June 20 and 21, 2005.
- Training and Tech Service Strategy Meeting, M-I SWACO, June 22, 2005.
- Publication and presentation of article entitled "Drilling Fractured Granite in Yemen with Solids-Free Aphron Fluid," with Michel Gregoire (Total) and Nick Hilbig, Mark Stansbury and Saleh Al-Yemeni (M-I SWACO) at IADC World Drilling 2005, Rome, Italy, June 9-10, 2005.[12]
- Meeting with Troy Gamble, M-I SWACO re application of APHRON ICS™ on Nexen Yemen wells, July 7, 2005.

- Lab tour and presentation of aphron drilling fluid technology to Eric Messier, Devon Energy, July 12, 2005.
- Attendance at M-I SWACO Technical Conference, Sugarland, TX, Aug. 29-31, 2005.
- Submission of article and preparation of poster and slide show presentation for SPE 96145, "How Aphron Drilling Fluids Work," to be presented at SPE Annual Technical Conference & Exhibition, Oct. 9-12, Dallas, TX.[13]
- Submission of article and preparation of slide show presentation for EXPL-2-FG-13, "New Insights into Aphron Drilling Fluids," to be presented at V INGEPET, Lima, Peru, Nov. 8-11, 2005.[14]

EXPERIMENTAL APPROACH

The tasks undertaken in this Project were organized in chronological order as follows:

Phase I

1. Aphron Compressibility
   1.1. Aphron Visualization
   1.2. Fluid Density
   1.3. Aphron Air Diffusivity
2. Sealing Mechanism
   2.1. In Situ Visualization
   2.2. Pressure Transmissibility
   2.3. Aphron Shell Hydrophobicity
3. Leak-Off and Formation Damage
   3.1. Leak-Off in Permeable Formations
   3.2. Leak-Off in Fractured Formations

Phase II

4. Aphron Drilling Fluid Optimization
   4.1. Microstructure
   4.2. Performance
5. Flow Properties
   5.1. Fluid Flow Pattern
   5.2. Rheology
   5.3. Multi-Phase Flow Effects
6. Formation Invasion and Damage Potential

For this Final Report, however, the results are organized so as to provide a more logical framework for the subject matter and a more cohesive story:

Aphron Visualization
Ambient Conditions
Elevated Pressure and Temperature
Aphron Longevity
Effect of Pressure
Effect of Compression/Decompression
Effect of Shear
Effect of Method of Generating Aphrons
Effect of Fluid Composition
Pressure Transmissibility through Aphron Drilling Fluids
Sealing of Permeable Media by Aphron Drilling Fluids
Core Leak-Off Tests
Disk Leak-Off Tests
Syringe Sand Pack Leak-Off Tests
Capillary Suction Tests
Effects of Chemical Composition on Drilling Fluid Invasion
Flow Properties of Aphron Drilling Fluids
Multi-Phase Flow
Fluid Rheology
Modeling of Drilling Fluid Invasion into Permeable Media
Radial Flow of Aphron Drilling Fluids
Wettability and Formation Damage Potential of Aphron Drilling Fluids

Aphron Visualization

Ambient Conditions:

Acoustic Bubble Spectrometry (ABS) was evaluated to determine its suitability for measuring bubble size distribution (BSD) in aphron drilling fluids. Three types of polymer-based (APHRON ICS^{TM}) drilling fluids were used in this Project. Their composition is given in Table 1.

Table 1. Composition and Mixing Procedure of APHRON ICS^{TM} Drilling Fluids

Component	Function	Unit	Quantity per 350 mL Standard	Quantity per 350 mL Enhanced	Quantity per 350 mL SuperEnhanced	Mixing Time (min)
Water		mL	338	337	337	
Soda Ash		g	3	3	3	5
X-CIDE	Biocide	mL	0.1	0.1	0.1	3
ACTIVATOR II	Alkalinity Control Agent	g	2	2	2	2
GO-DEVIL II	Viscosifier	g	5	5	5	2
ACTIVATOR I	Thermal Extender	g	5	5	5	2
ACTIGUARD	Shale Sabilizer/Conditioner	g	1	1	1	2
BLUE STREAK	Aphron Generator	mL	0.91	0.91	0.91	1
APHRONIZER A	Aphron Stabilizer	mL		0.5	0.5	1
APHRONIZER B		g		0.5	0.5	2
PLASTISIZER		mL			0.3	2

All capitalized products are trademarked by MASI Technologies LLC, except X-CIDE, which is trademarked by M-I SWACO. The reference aphron drilling fluid used in the visualization tests was the Enhanced APHRON ICS^{TM} mud system. Two conventional methods for measurement of BSD were used for comparison: photomicrography and laser granulometry (also called laser light scattering). Since these techniques require a transparent fluid medium, a "transparent" version of the Enhanced APHRON ICS^{TM} system was developed that does not contain any of the opaque components, yet possesses key properties, such as rheology and aphron stability, which are similar to the whole mud:

Table 2. Composition of Transparent Enhanced APHRON ICS^{TM} Fluid

Component	Unit	Quantity per 350 mL
Water	mL	347
50% NaOH		pH = 10
FLOVIS PLUS	g	3.5
BLUE STREAK	mL	0.91
APHRONIZER A	mL	0.5
APHRONIZER B	g	0.5

FLOVIS PLUS is a low-solids xanthan gum from M-I SWACO. The fluid samples examined were prepared with varying air concentration and shear history.

A schematic of the ABS system is shown in Figure 2, while the equipment used for photomicrography is shown in Figures 3 and 4 and for laser granulometry in Figure 5.

Figure 2. Configuration of Dynaflow Acoustic Bubble Spectrometer[15]

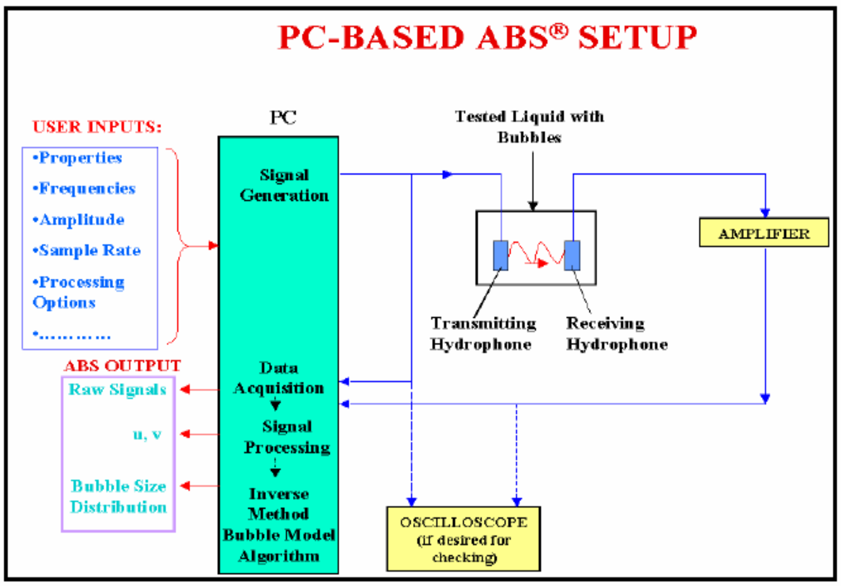

Figure 3. Stereo Microscope

Figure 4. Canty Glass Viewing Cell

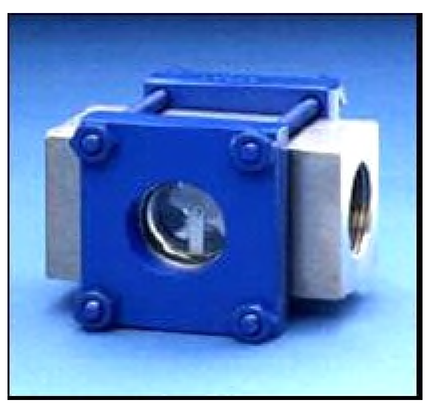

Figure 5. Coulter Laser Granulometer

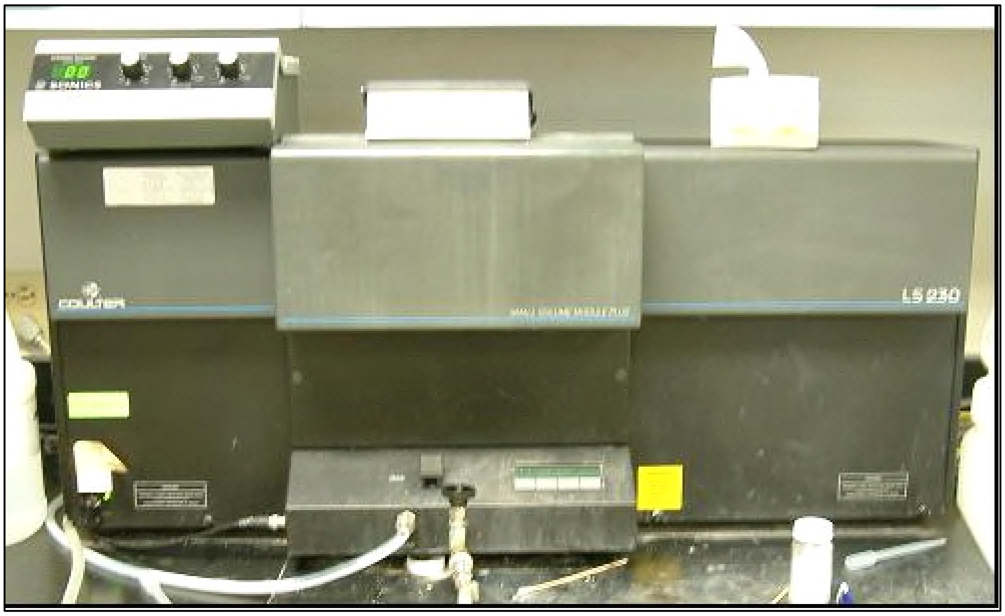

The Canty Viewing Cell is a glass sight-flow cell capable of withstanding 20.5 MPa (3000 psig). Photomicrographic analysis of bubble sizes was carried out manually using a standardized slide containing a 250 μm circle for size comparison. The laser granulometer is capable of measuring particle sizes in the range 1 to 700 μm diameter.[16]

The responsiveness of ABS to bubble size depends on the acoustic frequency: low frequencies are more responsive to large diameter bubbles, whereas high frequencies are more responsive to small diameter bubbles. However, no significant difference was observed when the window was varied from as wide as 50 – 250 kHz to as narrow as 140 – 150 kHz. Nevertheless, the frequency window was left as wide as possible to ensure maximum sensitivity to all bubble sizes. Additional tests were performed to determine if there was any effect of varying the sound spectrum analysis to adjust the bubble size range. Here again, the same pattern was observed whether using 0 – 1000μm or 0 – 500μm.

Elevated Pressure and Temperature:

An HTHP Circulating System was designed for the purpose of visualizing aphron drilling fluids under simulated downhole conditions. The system can sustain a target pressure of 20.5 MPa (3000 psia) and a temperature of 121 ^{o}C (250 ^{o}F). The HTHP cell can accommodate two hydrophones, each of which has a surface area of 58 cm^2 (9 in^2). The Canty Viewing Cell was added so that both ABS and optical imaging could be carried out at the same time. The HTHP Circulating System is shown in Figures 6 and 7.

Figure 6. HTHP Circulating System

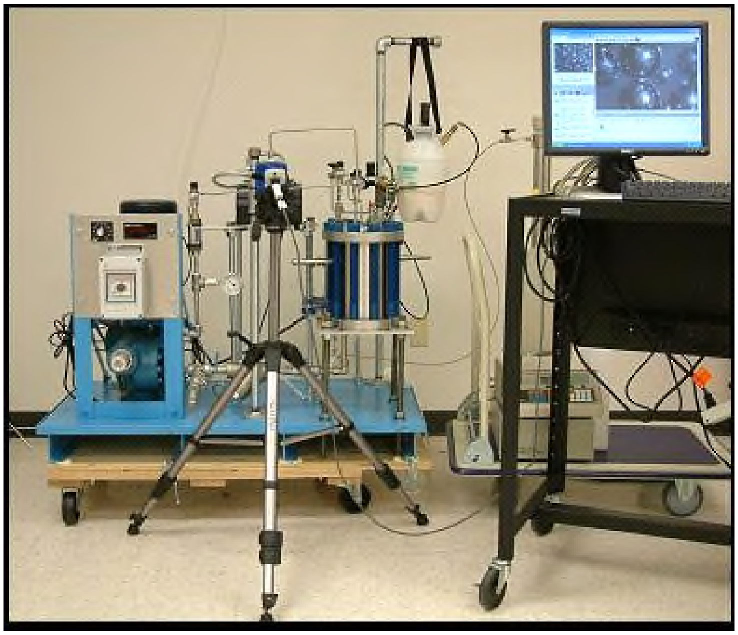

Figure 7. Close-Up View of HTHP Circulating System & Viewing Cell

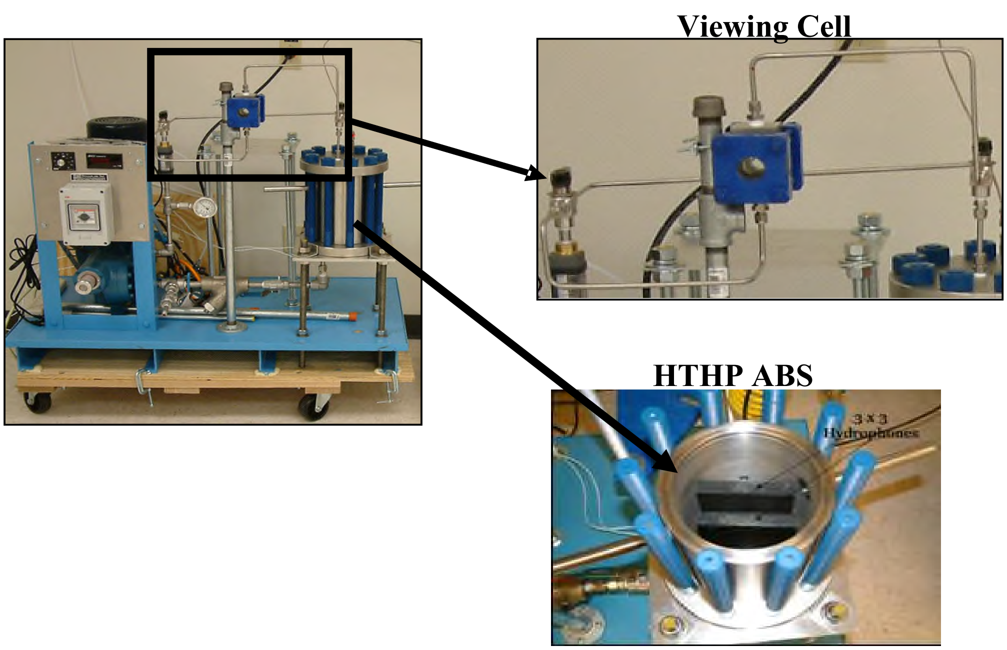

This system has several major drawbacks for the study of aphron drilling fluids. First, it requires a volume of about 5.7 L (1½ gal). Second, it relies on ABS for measurement of the BSD in a fluid; although the hydrophones used in the HTHP ABS Cell are almost an order of magnitude more sensitive than those in the open air cell, preliminary tests indicated that it was prone to the same problems, i.e. a BSD skewed to very low values. Third, the reference optical imaging system possesses a very deep chamber that requires a transparent fluid system and creates much uncertainty about the viewing depth.

Consequently, an HTHP optical imaging system was designed without these limitations. A prototype of this system, dubbed the Variable Reservoir Depth Viewing Cell, is shown in Figure 8.

Figure 8. Variable-Reservoir-Depth (VRD) Polycarbonate Viewing Cell

Front View of Cell

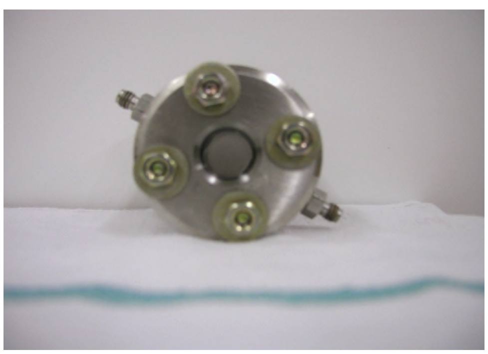

Side View of Cell

Disassembled Cell

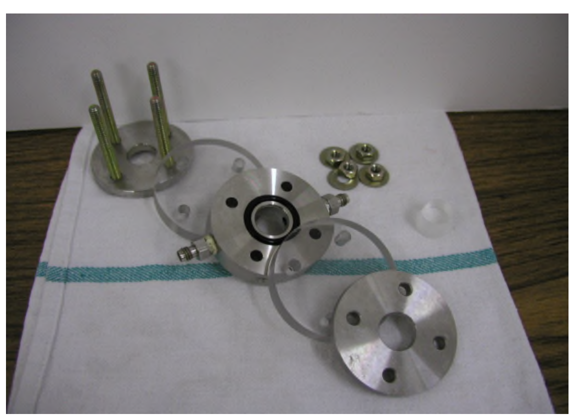

The chamber, made of steel with 1.2-cm (1/2”) polycarbonate windows, contains a polished polyacrylic plug that fits up against a lip that regulates the depth of the chamber (and path length of light). For most tests, the chamber depth was set at 1 or 2 mm. This new sample cell has been found to be useful for microscopic work to pressures of 27.3 MPa (4000 psig) at ambient temperature. Two of these cells were constructed for some of the work involving the effect of shear on aphron longevity.

A third cell of very similar design was constructed, but using ¼”-thick sapphire windows and high-strength bolts to enable working at elevated temperatures, as well as elevated pressures. This cell is shown in Figure 9.

Figure 9. HTHP VRD Viewing Cell with Sapphire Windows

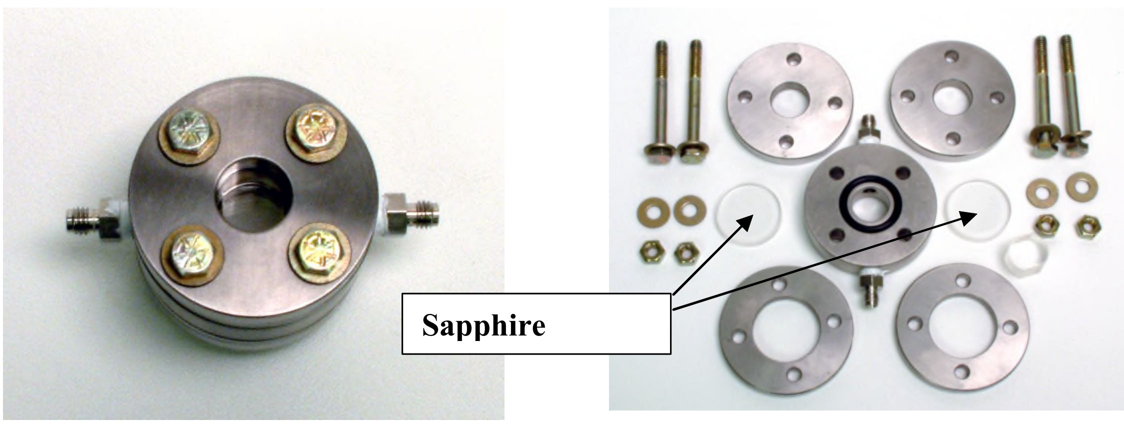

Cell **Exploded View**

A microscope camera was obtained along with Vision Assistant™, an optical imaging software package from National Instruments, to monitor the effects of environmental variables on bubble size distribution and track individual bubbles. Maximum magnification used with this Cell is approximately X60. Calibration of bubble sizes was accomplished using a precision microscope slide standard with disks of multiple sizes. The complete VRD Optical System, consisting of the VRD Viewing Cell, Microscope and Camera, is shown in Figure 10.

The Vision Assistant™ software consists of image functions that extract and alter the structure of objects in an image using transformations to delineate objects and prepare them for quantitative analysis. A photomicrographic image of a transparent APHRON ICS™ sample analyzed through

Vision Assistant™ is shown in Figure 11. Filling of the bubbles (shown in red), followed by compiling the surface areas or diameters of the filled circles, will generate a BSD.

Figure 10. VRD Optical System

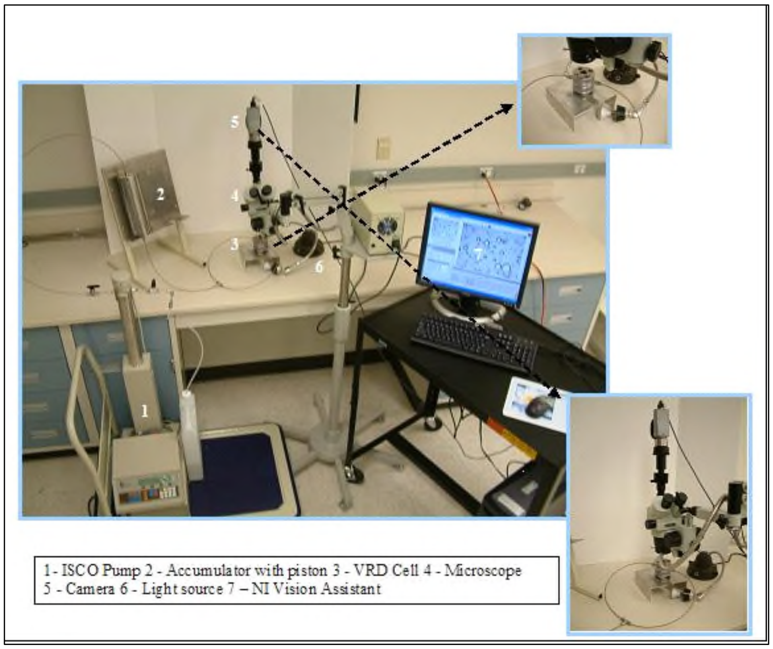

Figure 11. Example of Output Screen from Vision Assistant Software

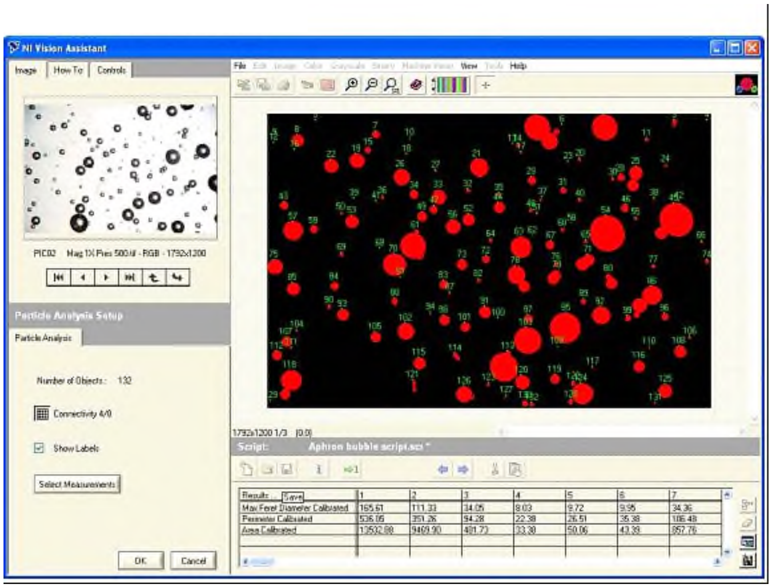

Most of the tests in the VRD Viewing Cells were conducted either with the transparent Enhanced APHRON ICS™ fluid or with one of the regular whole APHRON ICS™ drilling fluid systems shown in Table 2. Some times ACTIGUARD was omitted, depending on the experiment.

Additional microscopic methods include conventional high-powered microscopy, which enables visualizing aphron drilling fluids at magnifications up to X1000, and Environmental Scanning Electron Microscopy (E-SEM).

Aphron Longevity

Effect of Pressure:

To measure the rate of loss of air from aphrons at elevated pressures and temperatures, it was proposed to monitor the concentration of Dissolved Oxygen (DO) in the surrounding aqueous medium as a function of time. A vessel was constructed to accommodate a suitable DO probe and enable measurements of DO at HTHP.

Figure 12. FOXY Dissolved Oxygen System for Air Diffusivity Tests

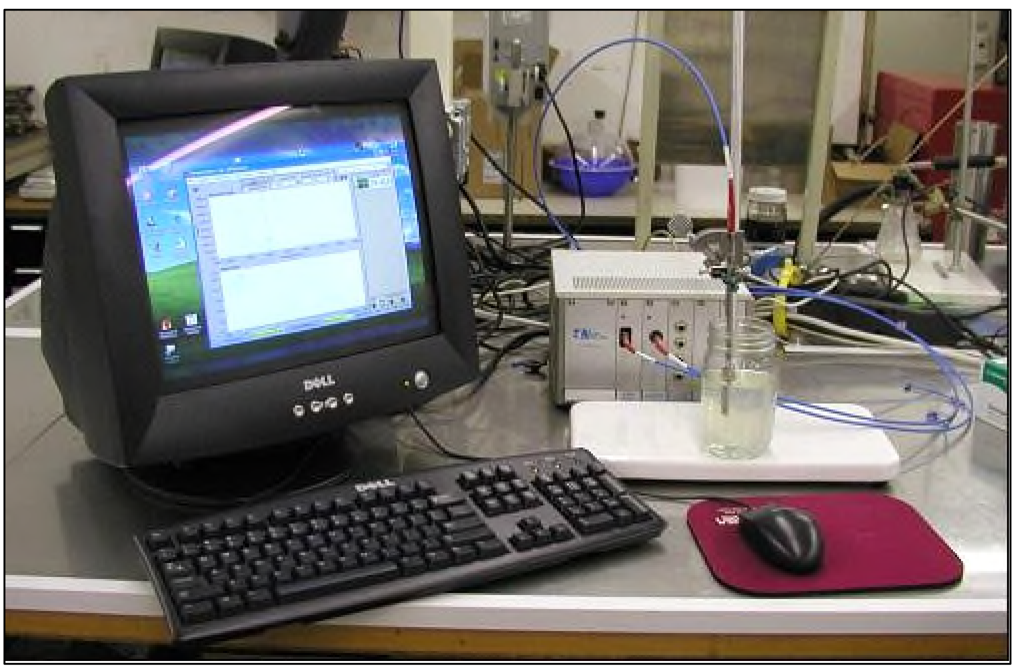

Initial experiments were conducted at ambient pressure and slightly above to evaluate the potential for DO to serve as an indicator of air loss from aphrons. Unfortunately, all of the DO probes tested during those initial tests proved inadequate for technical or mechanical reasons: poor accuracy and reproducibility, slow response time, deterioration or destruction by high pressure and/or temperature. Of these, the FOXY probe (OceanOptics), shown in Figure 12, was found to be the best candidate and perhaps could still be used at moderate temperatures.

Unfortunately, it was learned during the course of the tests that DO itself was being affected by components in the drilling fluid, independent of diffusion from the aphrons. Indeed, DO depletes very rapidly (within just a few hours at ambient temperature and pressure) as a result of chemical reaction with some of the components in APHRON ICS™ drilling fluids. Consequently, it was decided to monitor the rate of loss of air from aphrons through optical imaging, i.e. by monitoring bubble size as a function of time in a VRD cell.

Effect of Compression/Decompression:

The ability of aphrons to withstand compression and decompression is an important facet of the ability of aphrons to control fluid invasion. With this in mind, experiments were set up to measure BSD (using the Canty and VRD Viewing Cells) and fluid density after repeated pressurization/depressurization. For the latter, an Isco pump -- used to generate pressure and monitor volume changes of the fluid -- was employed to drive a floating piston in a 500-mL cylinder to which was connected a piston-less 500-mL cylinder. The volume of mud was almost 1000 mL. Later, the apparatus was re-designed to reduce the error introduced by air in the plumbing system. However, tests of deaerated mud samples still showed, at best, 1 to 2 % undissolved air.

The original intent of this project was to determine if aphrons can survive repeated cycling of pressures between 0.1 MPa (0 psig) and pressures up to at least 6.9 MPa (1000 psig). For a mud sample of 1000 mL which contains 15% air (aphrons), or 150 mL air, pressurization itself (with no loss of air to the surrounding mud) would reduce the volume of air to 2.25 mL (0.225%). The air that might be "lost" during pressurization is assumed to leak through the aphron shell and dissolve in the mud matrix. Thus, the experimental apparatus must be able to generate distinguishable results between the case where no air is lost vs all air is lost, i.e. ΔV_0 = 147.8 mL (no loss of air) vs ΔV_{100} = 150 mL (all air is lost). That should be feasible. However, the air trapped in the plumbing at the beginning of a test would generate a ΔV of 10 to 20 mL. Thus, ΔV_0^{Corr} = 157.8 to 167.8 mL and ΔV_{100}^{Corr} = 160 to 170 mL. Since the uncertainty in the trapped air volume (~ 10 mL) is more than four times the expected maximum volume difference ($\Delta V_{100} - \Delta V_0 = 2.25$ mL), the test was completely revamped.

First, rather than measure the volume change during compression, it was decided to investigate the hysteresis effect on the APHRON ICS™ mud after each compression/decompression cycle. Second, the system was modified by adding a vacuum pump (and the associated tubing, fittings and a valve) and replacing the piston-less accumulator cell with a second floating piston cell to serve as a filling station for the sample cell. This reduced the active mud volume to about 500 mL (the volume of the sample cell). The experimental set-up is shown in Figure 13.

The pressure was varied cyclically, by first increasing the pressure for 1.5 minute to the desired value (100 psig, 200 psig and so on up to 1000 psig, in increments of 100 psig, or 0.69 MPa), then decreasing the pressure after each step over a period of 1.5 minutes down to a nominal pressure of 0 psig (actually closer to 10 psig). We noticed that for each cycle, during the depressurizing step the air that was first compressed during the pressurizing step was not all coming back. We thought that this effect was probably due to the short time between the steps, so the time between the steps after that was increased to 10 minutes.

Although in most cases the volume readings at the end of each cycle were similar to the original volume, no systematic pattern emerged from the volume vs pressure readings. It was determined that the erratic nature of the readings was likely caused by stick/slip of the floating piston in the accumulator cell, perhaps exacerbated by blow-by of air. To minimize these problems, the piston was redesigned several times and ultimately was fitted with two polyurethane gaskets energized by Viton O-rings. Then the bore of the cylinder was honed, and powdered household lubricating graphite was used to reduce stick-slip further.

The results using that cell were significantly improved, generating relatively stable and monotonically changing volume vs pressure readings.

Figure 13. Fluid Density Apparatus

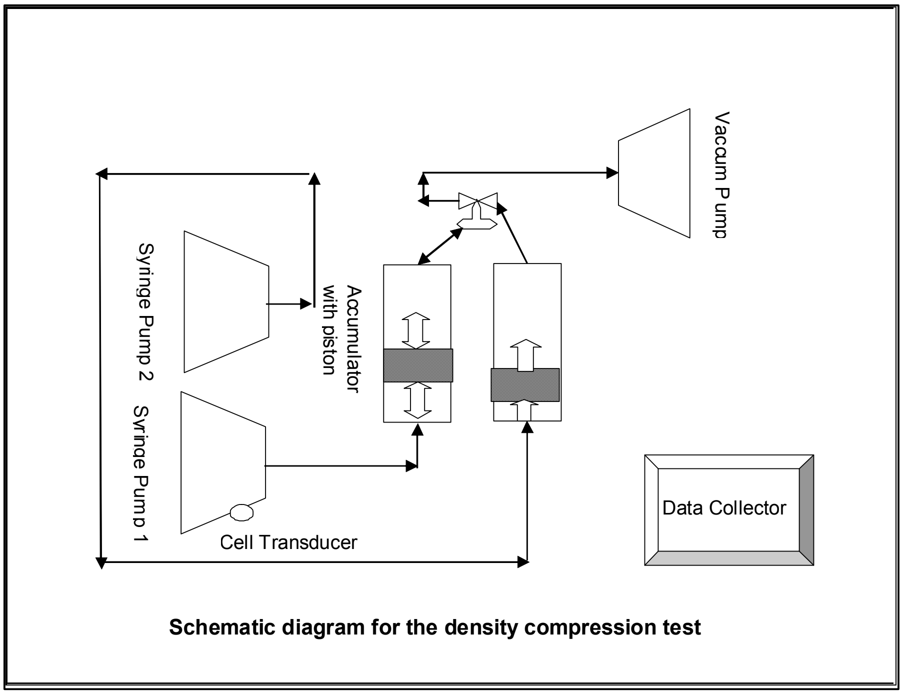

Effect of Shear:

Conventional bubbles can be easily comminuted (subdivided) by shearing them, e.g. via passage through a capillary or a permeable medium. Invasion of drilling fluid into a permeable formation downhole is expected to result in shearing of the aphron drilling fluid and comminution of the aphrons. The smaller size of the aphrons and the shearing process itself (at elevated pressure) may have important consequences for the stability of the aphrons. To investigate this, an apparatus was built to flow aphron drilling fluids through a short fritted filter at elevated pressure, after which the BSD is monitored. A schematic of the apparatus is shown in Figure 14.

One of the accumulators (#1) is filled with a test fluid, which is forced through a Swagelok filter/strainer of known opening size into a Variable Reservoir Depth (VRD) Viewing Cell and then into the other (empty) accumulator (#2). To avoid particulate matter that might clog the filter, a transparent (solids-free) version of the APHRON ICS™ test fluid is used.

Figure 14. Apparatus for Investigating Survivability of Bubbles under High Pressure

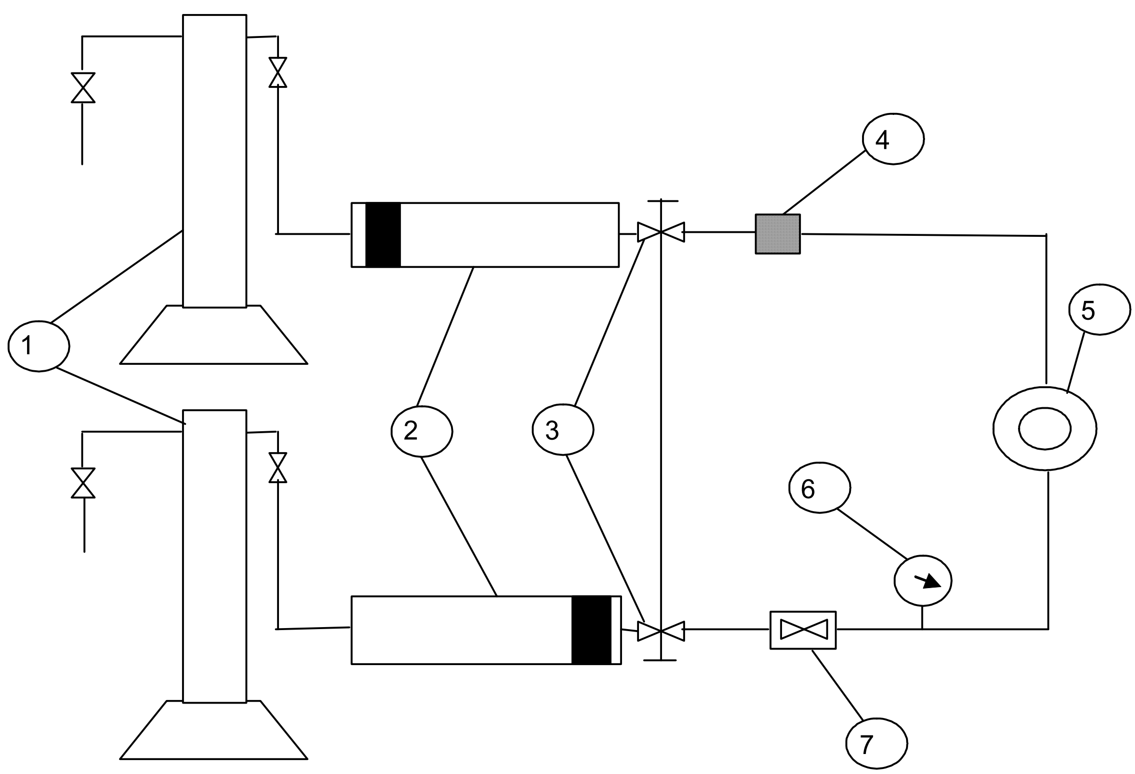

High Pressure Bubble Sizing System.

1 - ISCO pumps, 2 - accumulators with pistons, 3 - three ways valves, 4 - filter,
5 - variable reservoir depth cell, 6 - gauge, 7 - back pressure regulator.

A Swagelok sintered metal filter -- with an average opening of 15 µm and a thickness of about 2 mm -- and a strainer (for larger particles/bubbles) are shown in Figure 15. Images of the fluid passing through the Viewing Cell are acquired for determination of BSD. Fluid from accumulator #2 is then forced through a 5-ft (1.5 m) long section of 250-µm or 500-µm ID capillary tubing and collected back in accumulator #1 to determine the Pressure vs Flow Rate viscosity profile. Because this system is completely closed, the procedure described above can be repeated indefinitely without introducing additional air into the mud.

Figure 15. Swagelok Sintered Metal Filter and Strainer

To better define the roles of pore size and pressure on survivability of aphrons, the design of the apparatus was modified by adding a second VRD Viewing Cell to the system (see Figure 16). The two Viewing Cells simultaneously record size and concentration of bubbles before and after filtration. An ISCO syringe pump, set for a fixed flow rate, pushes the fluid through visualization cells VRD 1 and 2; between the cells is the frit. Photographs are taken with a microscope/camera system before and after passage of the fluid through the frit. These are analyzed with the Image Analysis software from National Instruments to determine the effect of shear on BSD. Initially, a 440-µm frit is used to ensure that particulate matter does not create a physical plug in the pores of the frit.

Figure 16. Apparatus for Investigating Survivability of Bubbles under High Pressure with Two VRD Viewing Cells

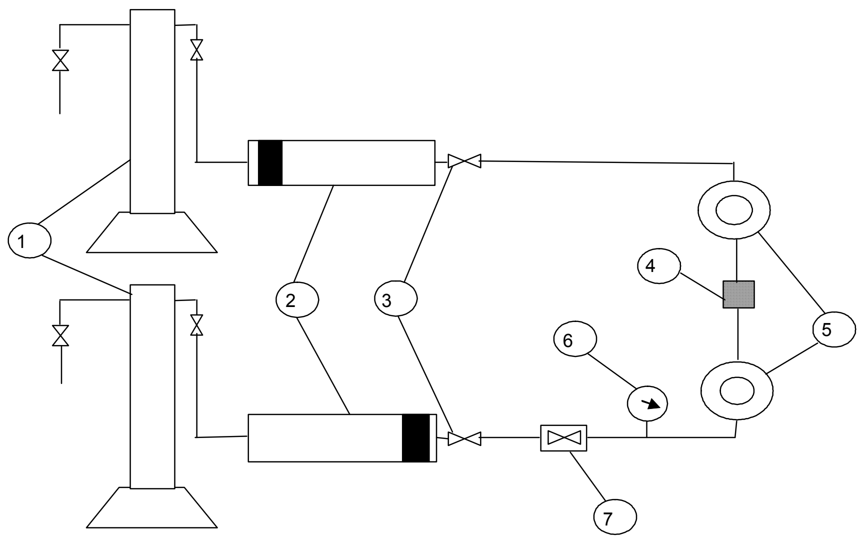

High Pressure Bubble Sizing System.
1 - ISCO pumps, 2 - accumulators with pistons, 3 - two ways valves, 4 - filter, 5 - variable reservoir depth cells, 6 - gauge, 7 - back pressure regulator.

Effect of Method of Generating Aphrons:

Various laboratory mixers and flow/pressure drop through an orifice were examined to determine if there is any effect of the method of generating aphrons on bubble stability, including the Prince Castle Mixer (see Figure 17), a Silverson L4RT and a GE kitchen blender. In addition, an APV Gaulin Homogenizer (Figure 18) was examined because of the high pressure drop imposed on the fluid being mixed; although this device is not generally used to mix drilling fluids, it is commonplace in the food and dairy industries. It pumps the fluid with a reciprocating piston that applies a pressure drop of 500 to 4500 psig (3.5 to 30.7 MPa) to the sample.

The effect of submitting aphron drilling fluids to a pressure drop was also investigated. The experiment was set up in the HTHP Circulating System. This was modified by replacing the ABS cell with an HTHP Fluid Loss Cell, adding a fluid reservoir and adding a by-pass containing a Viewing Cell. A garden sprayer was also attached to administer the required ½ gal of fluid for the apparatus, and the entire flow system is heated. This modified HTHP Circulating System is shown in Figure 19.

Figure 17. Prince Castle Mixer

Figure 18. APV Gaulin Homogenizer

Figure 19. Modified HTHP Circulating System

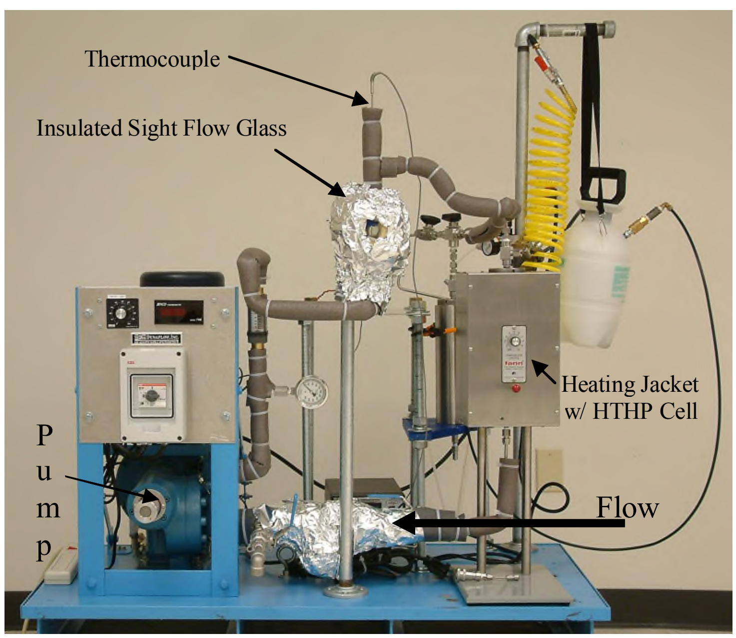

For running pressure-drop tests, the Canty Viewing Cell was modified by inserting a precision-bore capillary tube into the bottom port of the cell, as shown in Figure 20. Most tests were conducted with 0.5- or 1-mm ID tubes. A pressure drop is applied across the orifice while maintaining the pressure in the viewing chamber at a pressure of 500 to 2000 psig (3.5 to 13.7 MPa).

Figure 20. Set-Up for Pressure-Drop Tests in Canty Viewing Cell

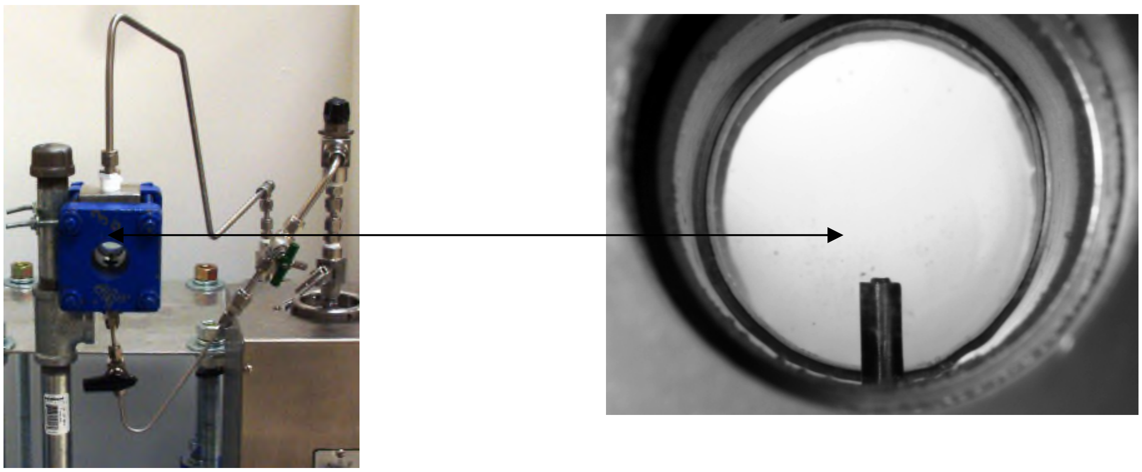

Pressure Transmissibility

Various hypotheses have been advanced for the mechanism by which aphrons and aphron drilling fluids control fluid invasion into permeable and fractured formations. One such idea envisions aphrons forming a cushion that makes the pressure profile more shallow and prevents full transmission of the pressure deep into the formation. To test this hypothesis as it might pertain to fractures, a 6.5-m (20-ft) length of 0.64 cm (¼ in) OD stainless steel tubing fitted with pressure transducers at opposite ends was used for the initial tests to simulate a long fracture. The apparatus is shown in Figure 21.

The rate, as well as the amplitude, of pressure transmission of aphron-based drilling fluids was monitored. Later the transient measurements were replaced with steady-state measurements of pressure drop and change in pressure drop through the system as functions of the concentration of air. Tests were conducted under both static and flow conditions. To simulate flow through permeable media, sintered metal filters with various sizes of pore throats were employed.

Figure 21. Pressure Transmissibility Apparatus

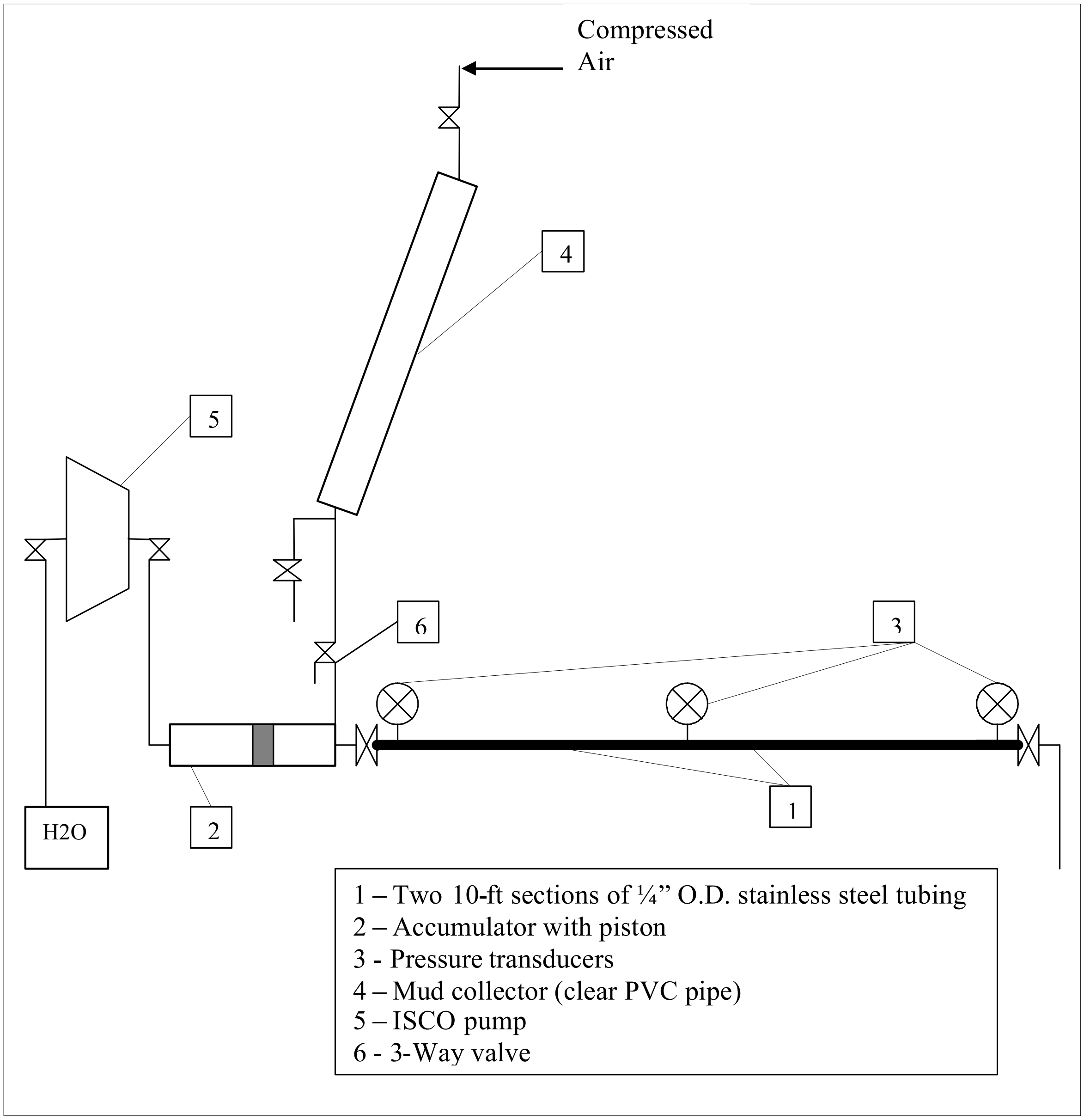

To enable flow visualization, a 2.3 m (7.7 ft) length x 2.54 cm (1 in) ID clear polyvinyl chloride (PVC) pipe was used in subsequent tests and was filled with sand (both wet and dry) of various grades and fitted with pressure transducers at the beginning and the end of pipe. Later, the PVC pipe was shortened to 0.97 m (3 ft). A photograph of the PVC apparatus is shown in Figure 22.

Figure 22. Clear PVC Pressure Transmissibility Apparatus

Sealing of Permeable Media by Aphron Drilling Fluids

Core Leak-Off Tests:

To measure the rate of fluid invasion into a core, a Core Leak-Off Test Apparatus was constructed from a Temco coreholder. The device enables radial and axial loading of cores up to 6 inches in length, pressures up to 17.3 MPa (2500 psi) and temperatures up to 177 ^{o}C (350 ^{o}F). A schematic of this apparatus is shown in Figure 23.

This apparatus is of a fairly conventional design for testing of typical filter-cake-producing drilling fluids. The core is a short (5 cm, or 2 in) fused Aloxite cylinder of well-defined permeability; flow into the core is linear (through the core) and there is no dynamic flow across the face of the core. The inlet cap of the coreholder was modified to provide a cone-shaped entry to the fluid, thereby minimizing channeling and problems arising from formation of a non-uniform filter cake. To prevent channeling of mud between a fresh core and walls of the tester, the core is tightly pre-wrapped in a sleeve of thermal shrinking plastic. The pre-wrapped core is evacuated under water to remove all air and to fill the pores with water, and then it is installed inside the coreholder.

Figure 23. Schematic of Leak-Off Tester (with BPR)

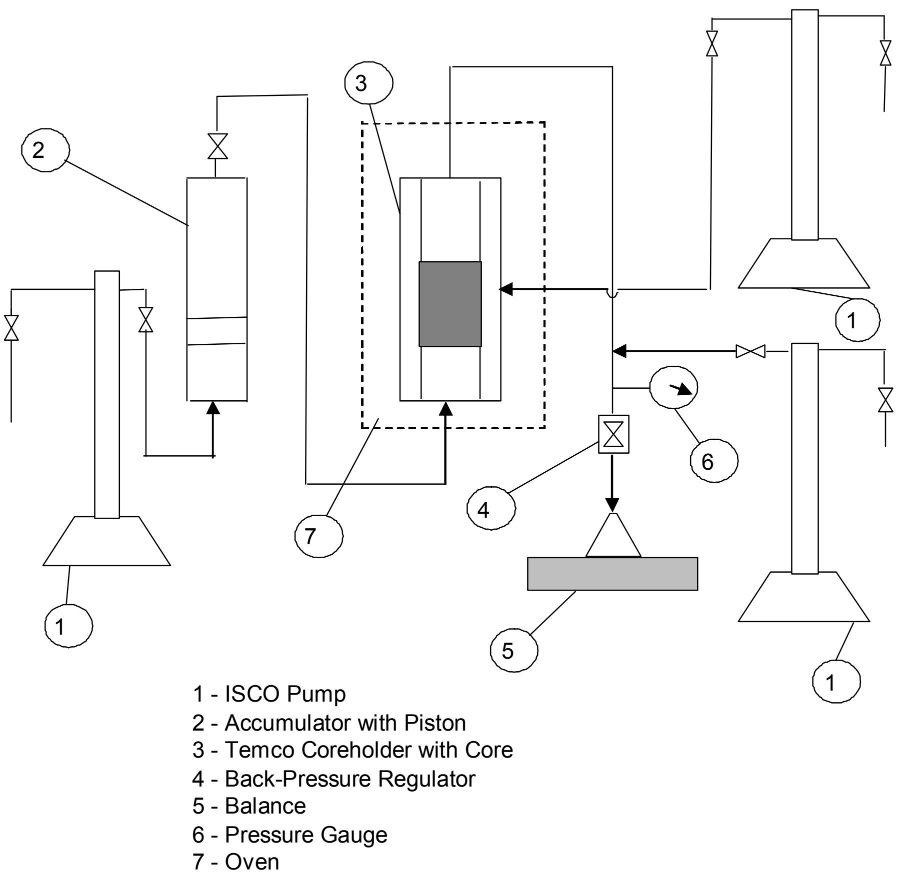

Confining (radial) pressure is applied to the cell with an Isco syringe pump, and the volume filled by water in the inlet space between the mud front and the bottom of the core – called the "dead volume" – is measured. Fore pressure is also applied with an Isco syringe pump. Net Leak-Off volume is calculated by subtracting the "dead volume" from the total volume of filtrate collected throughout the 30-minute test.

In all experiments, the confining pressure is maintained at a pressure 3.4 MPa (500 psi) higher than the fore pressure. To eliminate uncertainty in the amount of water trapped in the upstream tubing of the system at the beginning of experiments, a 1 psi check valve is installed on the back end of the tubing close to the filtrate collector. This check valve keeps the system completely filled with liquid during all stages of the experiments. Back pressure is applied with another Isco syringe pump, a precise back-pressure regulator (BPR) or a check valve, depending on the experiment.

Another Leak-Off Test apparatus was constructed for visualization of fluid flow in sand packs. This consists of a 2.5 cm (1 in) OD x 91.4 cm (3 ft) length polycarbonate tube, which permits visualization of the flow. Attached to the inlet is a 500-mL accumulator and an Isco syringe pump; no confining or back pressure is applied.

Disk Leak-Off Tests:

Simpler, faster fluid invasion tests were sought that would provide important clues about the nature of the invasion process and enable screening and optimization of drilling fluid formulations. A filtration test was devised using a "core" of reduced thickness, as shown in Figure 24. In these experiments, fluid is passed through an HTHP Fluid Loss cell fitted with a ¼-in thick Aloxite disk, collected in a container, and weighed continuously with a digital balance and recorded by computer. Weight and quality of the filter cakes on the Aloxite disks are also investigated. For these experiments, 10-µm and 35-µm disks are used, and the tests are usually run at ambient temperature for 30 min at 3.5 MPa (500 psig) inlet pressure and no back pressure.

Figure 24. Disk Leak-Off Tester

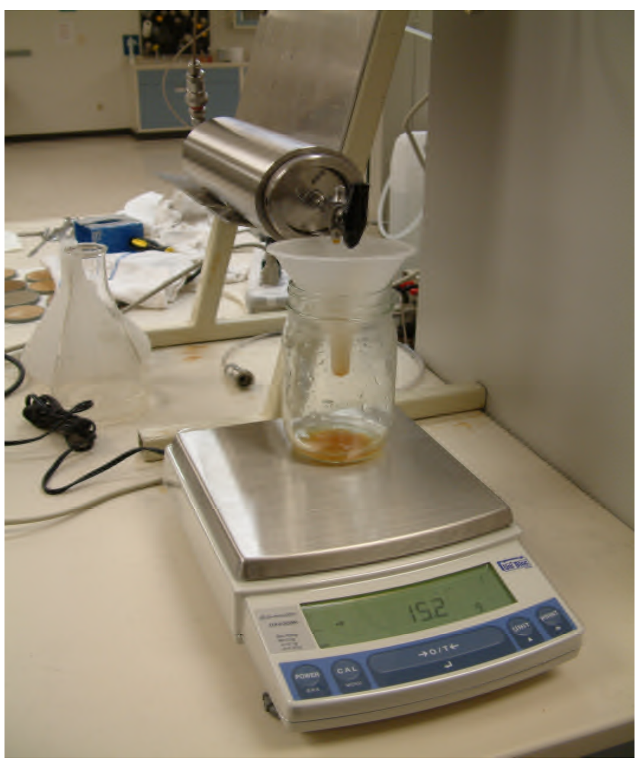

Syringe Sand Pack Leak-Off Tests:

Another test method was developed to quantify the effect of mud composition on performance of aphron drilling fluids. The Syringe Leak-Off test employs a 60-mL disposable, transparent syringe that is pre-packed about half-way with a sand, e.g. 20/40 or 70/100. This is done under water with a manual tamper to create a bed that is intended to simulate an unconsolidated, highly permeable sand formation. After the sand bed is packed, a minute amount of water is left remaining just above the top of the sand bed, a finger is kept over the syringe tip, and the remaining 30 mL of the bore of the syringe is filled with the test fluid, as shown in Figure 25. The plunger is inserted, and displacement of the water by the mud is attempted. The goal is to determine whether the test fluid will plug the sand and stop its invasion.

Figure 25. Syringe Sand Pack Leak-Off Test

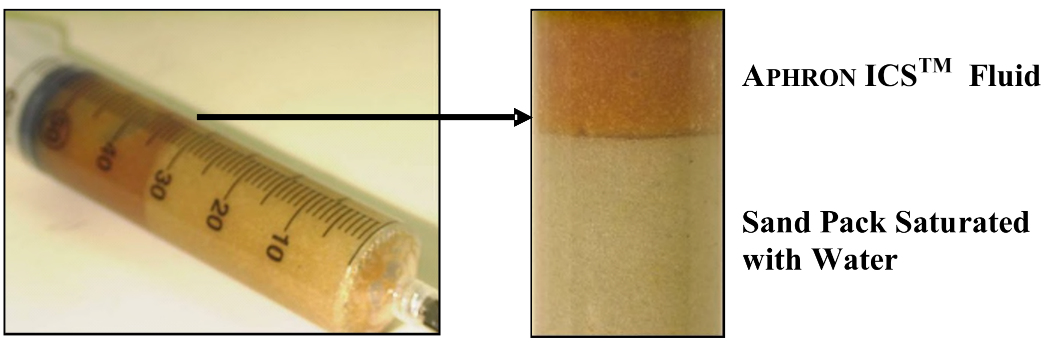

Leak-Off tests tend to be very sensitive to the sand-packing protocol. The Syringe Leak-Off Test is no exception. Consequently, this test method may present reproducibility problems, and we will need to pay very close attention to the way we pack the sand.

Capillary Suction Tests:

The Capillary Suction Time tester measures the speed of filtration of drilling fluid on a special thick piece of filter paper continuously wetted by the fluid. Figure 26 shows the hollow sample cylinder, which is placed on the paper and filled with fluid. Filtrate moves out along the paper; ring electrodes under the paper measure the travel time of the filtrate from the inner ring to the outer ring.[17]

Figure 26. Capillary Suction Time Test Apparatus

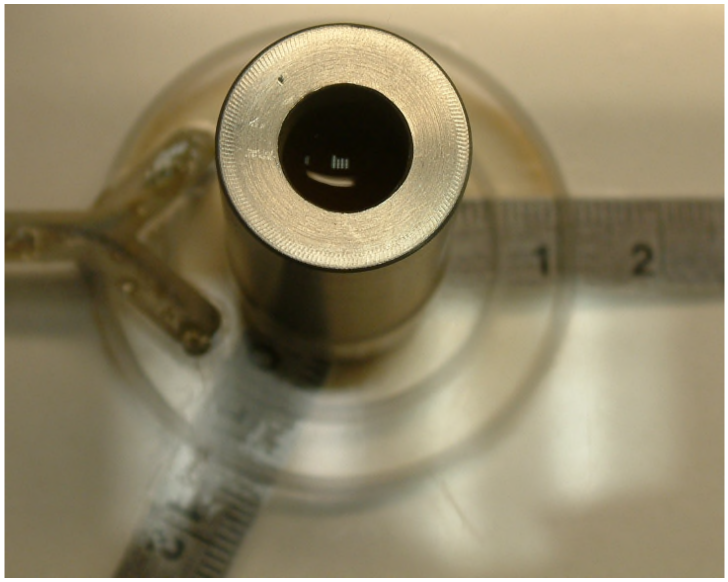

For fluids with very long CST's – typically more than a few minutes for the fluid to travel between the two conducting rings – artifacts such as dehydration of the paper make the CST values meaningless. An alternative CST method was developed, which involves measuring the distance travelled from the sample cup, CSD, within an arbitrary time period (30, 60, 90 and 120 min were used in this work). This appears to provide an accurate assessment of the relative permeability of the filter cake:

- Two 2-cm (20 mm) rules are attached to the top of the glass cover.
- The 1.8 cm opening of the test cylinder is placed against the filter paper.
- Five mL of the test mud is placed into the cylinder using a 5 mL syringe.
- The migration of the mud fluid is recorded every 30 minutes for 2 hours.
- The results are expressed in distance (mm) versus time (min). At least two readings from different points around the test cylinder are taken at each time and averaged.

Capillary Flow Tests:

Microbore stainless steel tubing of 1.5 m (5 ft) length and 3.2 mm (1/8 in) OD was used to simulate long, but not tortuous, pores in a reservoir. The experimental set up is shown in Figure 27.

Figure 27. Capillary Flow Test Apparatus

Two tubing ID's were used: 0.25 mm (0.01 in) and 0.127 mm (0.005 in). The APHRON ICS™ fluid was constructed from its individual components, rather than the branded products, and the effect of each component was determined by omitting it from the mix. The fluid is pumped through the tubing with an ISCO D500 syringe pump using a pressure ramp, and the flow rate is recorded as a function of pressure.

Flow Properties of Aphron Drilling Fluids

Multi-Phase Flow:

Imaging of the flow in a permeable medium was accomplished using a low-pressure clear acrylic pipe and a transparent Enhanced APHRON ICS™ fluid sample. The bed was packed with a clean, nearly transparent sand. Aphrons (or any bubbles, for that matter) are lighter in color than the base fluid, and the contrast is highest when the base fluid is colored and the aphrons are small. To record the phase behavior of the mud during flow, the transparent mud is saturated with RIT #6 blue dye. The front end of the acrylic pipe is connected to a valve and to an accumulator with a piston. The back end of the pipe is open to the atmosphere. At the beginning of the experiment, the valve is closed and a pressure of 100 psig is applied to the mud in the accumulator. The valve is opened, allowing the mud to begin moving through the sand pack. To limit the speed of mud movement through the sand, the pump flow rate is limited to 25 mL/min.

Fluid Rheology:

Shear viscosity of the aphron drilling fluids was measured with a Grace M3500 viscosimeter at ambient temperature and pressure over the shear rate range 0.01 to 1000 sec^{-1}. This covers the standard Fann 35 viscosimeter shear rate range of 5 to 1000 sec^{-1} (Fann Speed 3 to 600 rpm), as well as the Brookfield viscosimeter LSRV measurements at 0.06 sec^{-1} (Fann Speed 0.037 rpm). Samples were run periodically on these two instruments to confirm the results from the Grace viscosimeter.

To investigate the effects of bubble size on viscosity, it is much more accurate to measure the viscosity and bubble size simultaneously. For this purpose, a capillary tube viscosimeter was designed, as shown in Figure 28, which permits shearing a fluid to alter its BSD, measurement of the BSD in a VRD Viewing Cell and passing the fluid directly through a 5-ft (1.5 m) long precision bore capillary. This apparatus is a modification of the apparati shown schematically in Figures 14 and 16, which possess an added filter (for shearing tests) and, in Figure 16, a second VRD Viewing Cell.

Figure 28. Apparatus for Investigating the Effect of Bubble Size on Fluid Viscosity

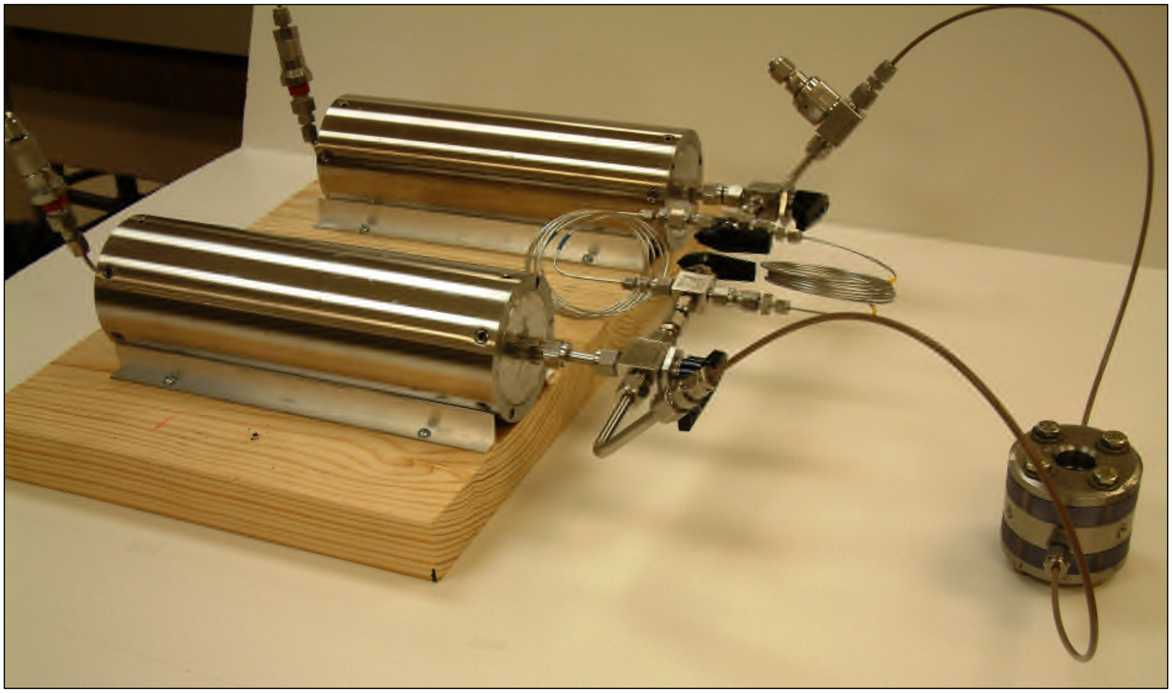

Modeling of Drilling Fluid Invasion in Permeable Formations:

Dr. Peter Popov of Texas A&M University led an effort to develop a mathematical model for invasion of aphron drilling fluids into drilled formations. Using experimental shear viscosity profiles of the base APHRON ICS™ fluid over the shear rate range 0.01 to 1000 sec^{-1}, along with capillary flow data, the model predicts fluid invasion profiles for low-viscosity (high shear rate) and high-viscosity (low shear rate) boundary cases, assuming Darcy flow, and includes Bubbly Flow of the aphrons. Validation of the model was carried out using the Radial Flow Apparatus.

Radial Flow of Aphron Drilling Fluids:

Conventional Leak-Off tests are generally carried out with a fixed fluid reservoir using cores only 2 to 6 in long and in a linear flow geometry. The transparent leak-off apparatus shown in Figure 22 and the shorter tube described above in the Multi-Phase Flow section were employed in initial tests to visualize the flow pattern under these conditions, using 20/40 and 70/100 sand-packs. However, these conditions are far removed from those experienced downhole, which entail dynamic flow of fluid past the formation (and with a continuous source of aphrons at constant concentration), a long path length and radial flow. To simulate these conditions, a Radial Flow Apparatus was designed, a schematic of which is shown in Figure 29.

Figure 29. Schematic of Radial Flow Apparatus

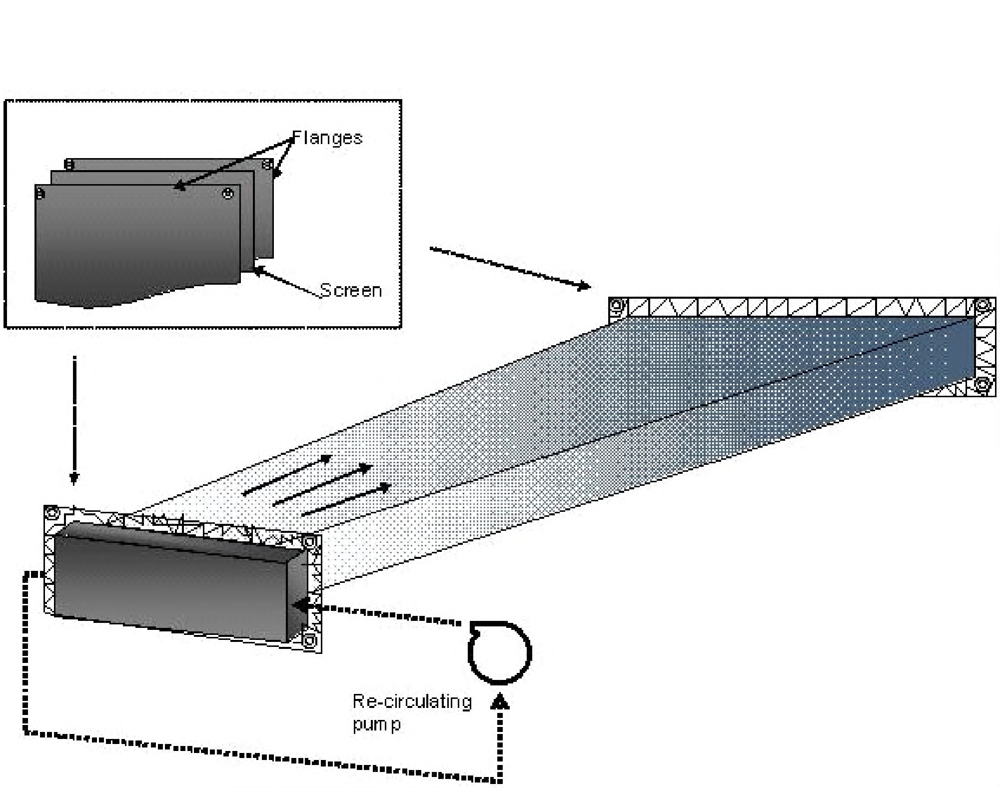

The Radial Flow Apparatus, shown in Figures 30 and 31, incorporates dynamic flow at the fluid inlet (wellbore side) and a long path length for the fluid (69 cm, or 27 in), along with radial flow. An Oberdorfer variable speed ¾ hp progressive cavity pump provides the required movement of all the fluids. The walls of the Apparatus are made of Lexan (polycarbonate plastic) glued together and supported with clamps that minimize swelling and bending of the plastic when subjected to pressure. The entire apparatus sits atop a light box of similar dimensions that contains several 7-W and 13-W 4100 ^{o}K fluorescent lights. The system is packed with sand or glass beads and is repeatedly filled and pressurized/depressurized with water to tighten the packing as much as possible. Prior to starting a test, the system is filled with water; during the course of a test, the water is displaced with mud. A Sony DCR-HC90 Digital MiniDV camcorder is attached to a rail that permits rack and pinion X-Y movement, thus enabling the camera to traverse the length and width of the apparatus without the need to re-focus.

Figure 30. Radial Flow Apparatus

Mud is circulated continuously across the inlet of the Radial Flow Cell to simulate the drilling process. When a pressure drop is imposed across the length of the Cell, mud invades the Cell and advances radially to the opposite end, where it is collected and measured regularly. Because the total stress on the walls rises dramatically with increasing depth of penetration, the inlet pressure has to be restricted to less than 15 psig. This, of course, also limits the tightness of the packing that can be used in the cell. Indeed, even 20/40 sand produces packing that is too tight. Experience indicates that glass beads no smaller than 1 or 2 mm diameter are the finest particles that can be run in the system with highly viscous fluids like the APHRON ICS™ mud.

Figure 31. Radial Flow Cell as seen from above

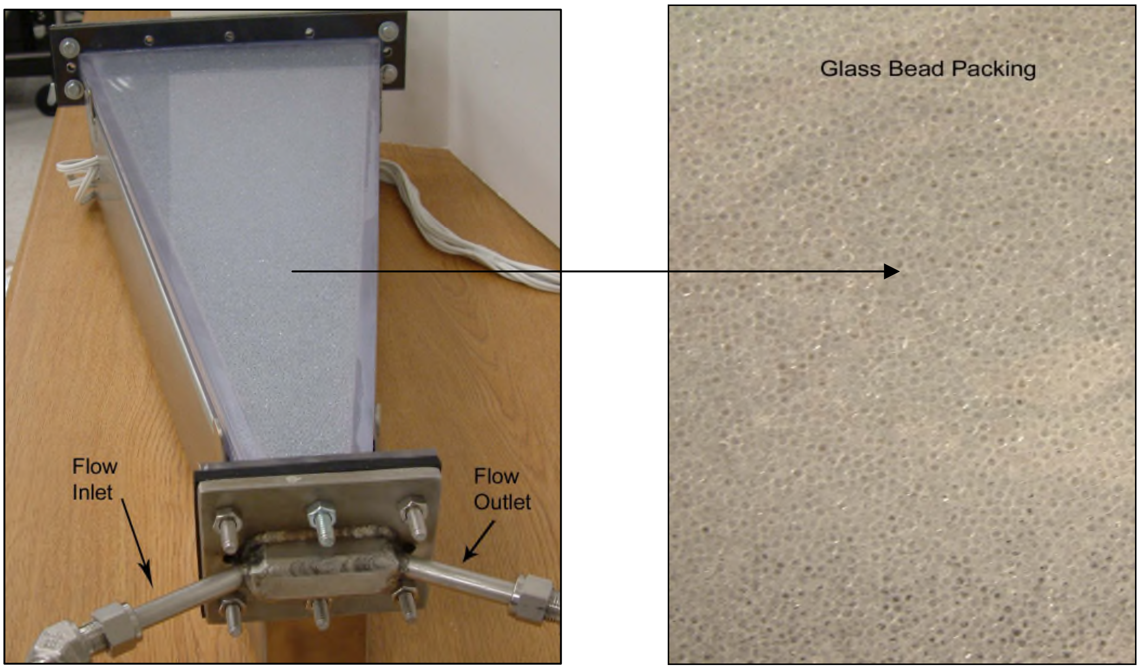

Wettability and Formation Damage Potential of Aphron Drilling Fluids

Base drilling fluid and aphrons interact with each other and with pore walls and produced fluid in various ways to determine the extent of drilling fluid invasion and formation damage and subsequent productivity of an oil or gas reservoir. During the course of this Project, we identified six such interactions. These are given below, along with the test methods employed to quantify them:

(1) Bubble-Bubble – Optical Imaging
(2) Bubble-Mineral Surface (pore wall) – Optical Imaging
(3) Drilling Fluid-Produced Fluid (connate water or oil) - Emulsion Compatibility
(4) Bubble-Drilling Fluid - Contact Angle and Surface Tension
(5) Drilling Fluid-Mineral Surface - Contact Angle
(6) Produced Fluid-Mineral Surface - Contact Angle and Emulsion Compatibility

The Optical Imaging work was carried out as 2-D visualization studies using various types of glass vessels, commercial ant farms and Hele-Shaw cells.[18] Contact Angle Goniometry was carried out with the Sessile Drop method, and Surface Tension measurements were made with a duNouy Tensiometer (ring method).[19] Emulsion Compatibility tests were carried out using a modified version of the Chevron procedure.[20]

Several Optical Imaging test methods were tried to measure the stickiness of bubbles. A schematic of one of the first devices is shown in Figure 32. A transparent APHRON ICS™ mud sample is placed in the chamber of a syringe. The aphrons are filtered and compressed while driving the bulk fluid through a fine glass filter that prevents passage of the aphrons. The syringe is then back-filled with the same aphron-free fluid to its initial volume and the bubbles that have agglomerated, coalesced and/or stuck to the walls of the chamber are counted.

A modification of the apparatus shown above employs two glass syringes connected with a disposable filter of pore size much smaller than the average bubble size. A photograph of this apparatus, fitted with a syringe pump, is shown in Figure 33.

Figure 32. Aphron Hydrophobicity Apparatus

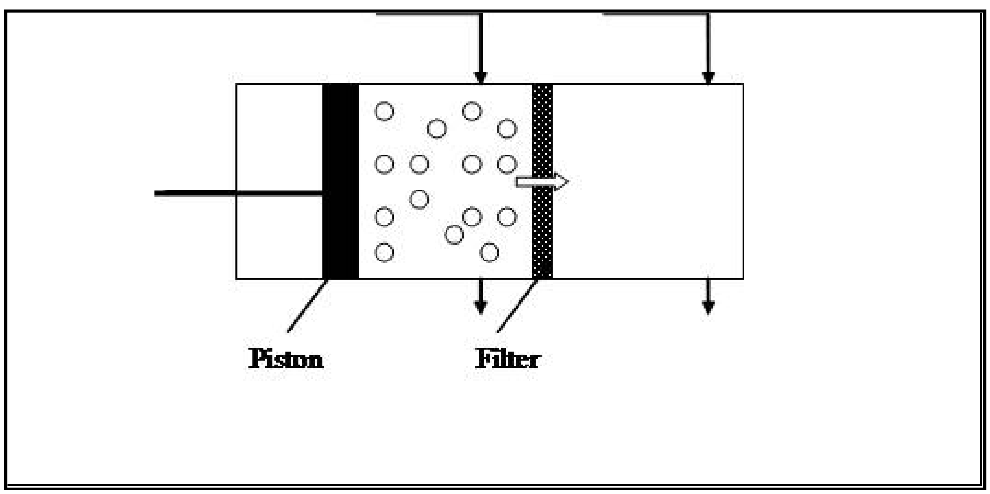

To better observe how bubbles move through beds of glass beads and sand, various commercial ant farms were tried, and a Hele-Shaw cell[18] was constructed from two plates of glass with a spacing of about 5 mm. This cell was originally developed to examine flow of bubbles in water at ambient pressure. In our version, the cell is packed with a bed of particles and water, and a very shear-thinning fluid is pumped into the bed, creating a significant pressure gradient across the permeable bed. Whole SuperEnhanced APHRON ICS™ Mud was run in this cell, and close-up photos were taken of the mud as it passed through the bed of beads. Some photos of the cell with mud are shown in Figure 34.

Figure 33. Dual Syringe Hydrophobicity Apparatus Fitted with Syringe Pump

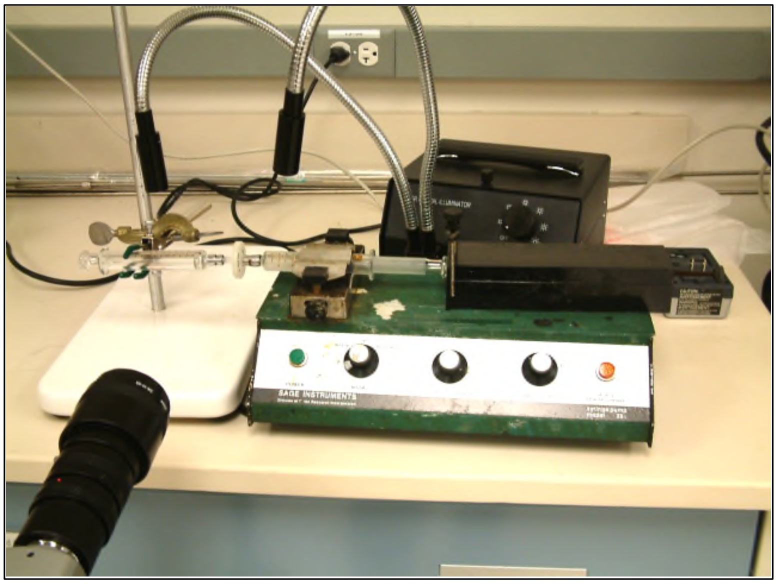

Figure 34. APHRON ICS™ Drilling Fluid in Hele-Shaw Cell Packed with 5-mm Glass Beads

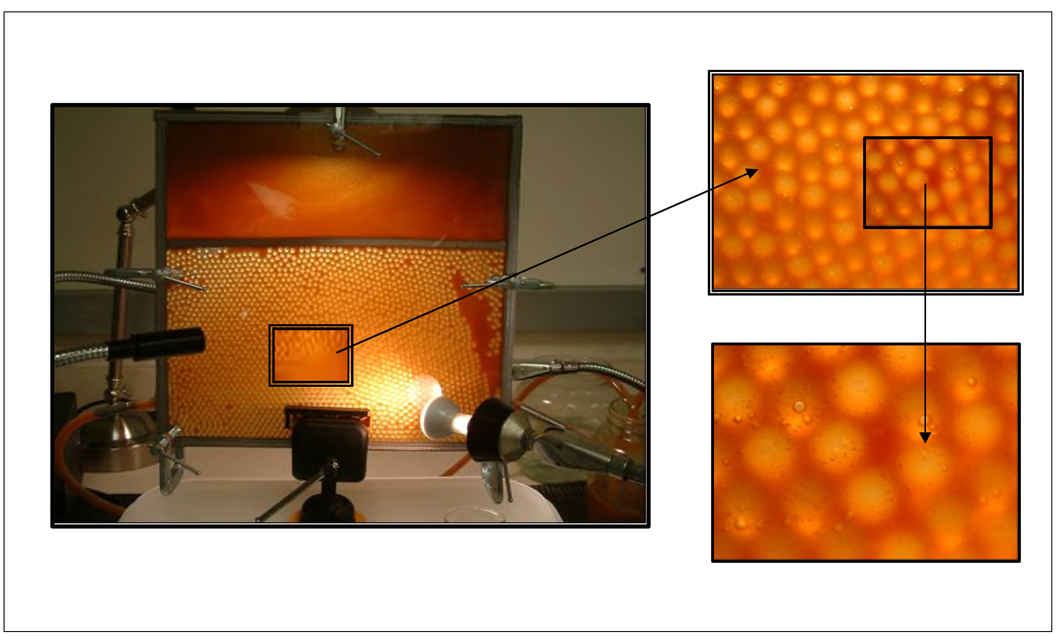

Unfortunately, for both the ant farms and the Hele-Shaw cell, as soon as a pressure drop was administered to the system, the beads shifted in attempts to pack more tightly, and ultimately channels developed in the bed (see photo at left in Figure 34). To minimize this problem, a new cell was constructed (see Figure 35) with very thick walls of Lexan (polycarbonate) using a fixed gap of 10 mm. For most tests, the cell was packed with 2-mm or 5-mm glass beads and filled initially with water. This new cell is smaller, sturdier, easier to clean and more transparent than the Hele-Shaw cell and various "ant farm" devices that had been used previously.

Figure 35. Modified Hele-Shaw Cell Packed with 5-mm glass beads

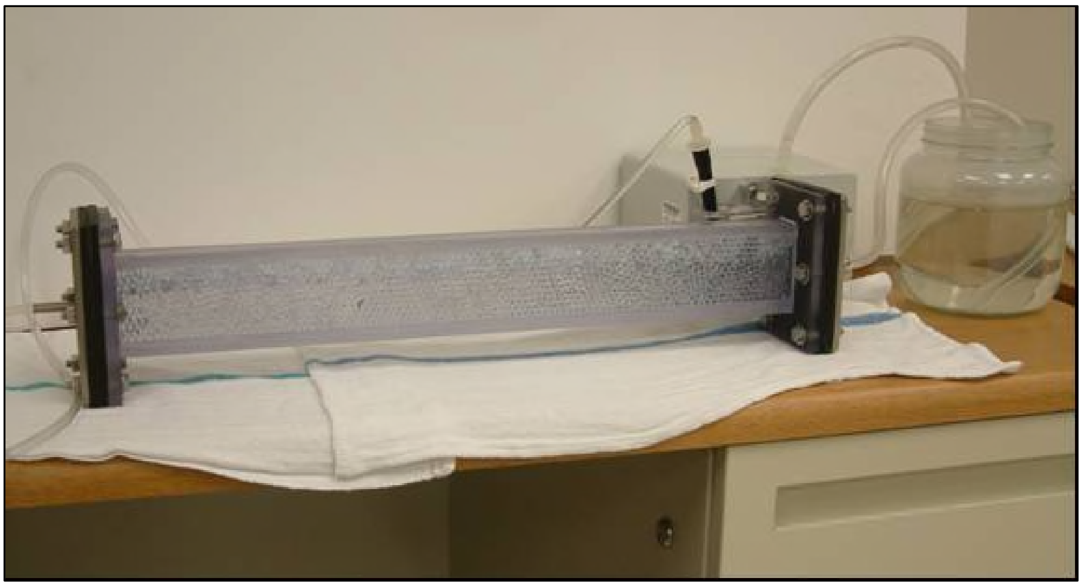

For Contact Angle measurements, the Sessile Drop technique described in Reference 19 was adopted initially. A preliminary set-up of the apparatus containing a sample of SuperEnhanced APHRON ICS™ fluid is shown in Figure 36.

The clamp holds a microscope slide, which the orange Level ensures is positioned horizontally. The tube coming down into the mud is actually a syringe needle, which is bent upward and is used to dispense a drop of a low-density fluid, e.g. oil, to the underside of the microscope slide. As it stands, the Sessile Drop Apparatus does not permit looking through opaque fluids. Consequently, a transparent version of the APHRON ICS™ fluid system was used, and this was centrifuged to remove aphrons. In addition, a darker oil supplanted the nearly colorless oil used before, thus providing sufficient contrast between the oil droplet and the drilling fluid. A couple of photos of the Sessile Drop Apparatus with these modifications are shown in Figure 37.

Figure 36. Sessile Drop Contact Angle Apparatus

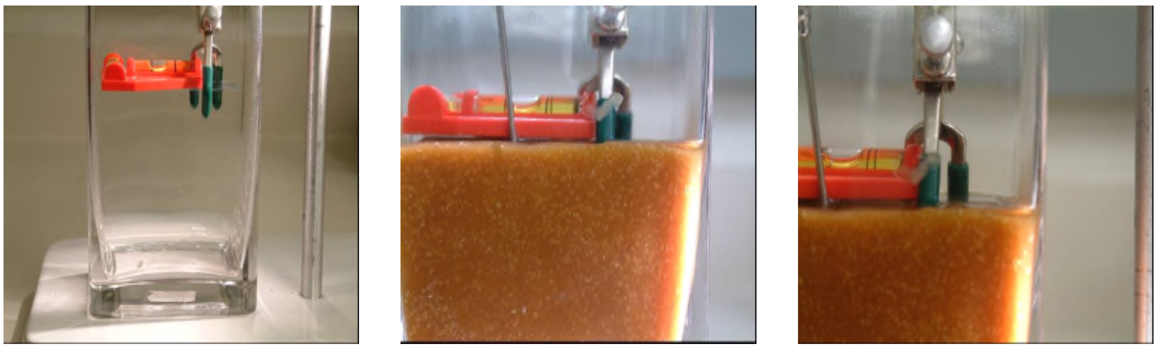

Figure 37. Sessile Drop Apparatus: Dark Oil and Transparent APHRON ICS^{TM} Mud

Due to the high viscosity of the oil and of the mud, it was very difficult for the oil droplet to assume its equilibrium circular shape and enable accurate measurement of the contact angle. Here the oil droplets on the underside of the microscope slide appear to be "comma"-shaped. Thus, an additional modification was made: The viscosities of both the mud and oil were decreased. The mud was diluted 50:50 by volume with water, and a less viscous crude oil was substituted for the dark crude. The photos in Figure 38 show what happened.

Figure 38. Sessile Drop Apparatus with Light Oil and Diluted APHRON ICS™ mud

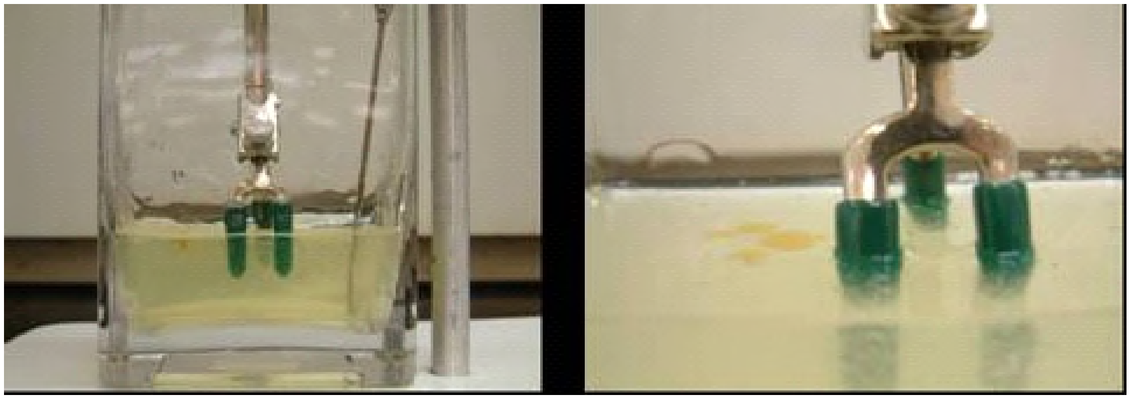

Although the oil droplet produced a fine, nearly circular pattern on the slide, absence of a suitable optical train made it very difficult to quantify the contact angle. Consequently, the Sessile Drop method was abandoned in favor of a Microscope Slide Smear test. The slide is pre-wetted with the whole SuperEnhanced APHRON ICS™ mud, and a drop of the oil of interest is placed on its surface. The slide is examined edge-on with a microscope and a rough estimate of the contact angle is made using a protractor on a photographic print of the image. The converse appears to work well, too, i.e. pre-wetting the slide with the oil and placing a drop of the mud on its surface.

For the Emulsion Compatibility test, a modified API RP 42 Emulsion Test Method[20] was used as the primary test for compatibility between the APHRON ICS™ drilling fluid and various oils. Mixtures of the oil and APHRON ICS™ mud are prepared in different volume ratios adding up to 100 mL (sometimes more). These are blended at a high shear rate for one minute on a Prince Castle single-spindle mixer, after which the mixture is decanted rapidly into a 100-mL glass graduated cylinder. The decanted mixture is observed for a total of 3 hr for any signs of separation. The condition of the mixture is noted every 2 min for the first 30 min and every 30 min thereafter. A sample of the decanted mixture is pulled with a syringe from the bottom of the cylinder and examined under the microscope (conventional microscope slide with a cover slip) at a magnification of 10X to ascertain with certainty which phase is external and which internal. For confirmation, a few drops of the drilling fluid-oil blend are added to a beaker of water and gently swirled to determine whether the mixture disperses in the water.

RESULTS AND DISCUSSION

Aphron Visualization

Ambient Conditions:

The focus of this task was to "prove" the utility of Acoustic Bubble Spectrometry (ABS) for measuring the bubble size distribution (BSD) in aphron drilling fluids. Two transparent APHRON ICS^{TM} formulations were examined, one with a high concentration of bubbles (> 20% air) and one with only a few bubbles (< 1% air). The high-bubble-concentration sample was prepared in the amount of 1 Lab Equivalent Barrel (350 mL) and mixed with a Silverson L4R mixer running at 7000 rpm for 6 minutes. The low-bubble-concentration sample was prepared by careful blending of a small aliquot (0.2 ml) of the high-bubble-concentration sample, using a spatula, into 50 mL of deaerated APHRON ICS^{TM} fluid. Deaeration was carried out using a centrifuge running at 4000 rpm for 20 minutes. The high-bubble-concentration sample is labeled "Aphron Sample;" the low-bubble-concentration sample is labeled "Diluted Aphron Sample."

The Bubble Size Distributions (BSD) measured for the Aphron Sample using the Acoustic Bubble Spectrometry (ABS), photomicrography and laser granulometry are shown in Figure 39. The BSD ranges measured on the (undiluted) Aphron Sample for the three techniques are as follows:

- ABS 30 - 90 µm
- Photomicrography 170 - 350 µm
- Laser Granulometry 130 - 270 µm

Figure 40 shows the major BSD micron ranges measured on the Diluted Aphron Sample:

- ABS 50 - 110 µm
- Photomicrography 110 - 290 µm
- Laser Granulometry 170 - 330 µm

The results for both the Aphron Sample and Diluted Aphron Sample demonstrate that photomicrography and laser granulometry produce similar BSD data ranges, whereas ABS yields a BSD that is shifted to a much lower range.

Figure 39. Comparison of BSD Methodologies for (undiluted) Aphron Sample

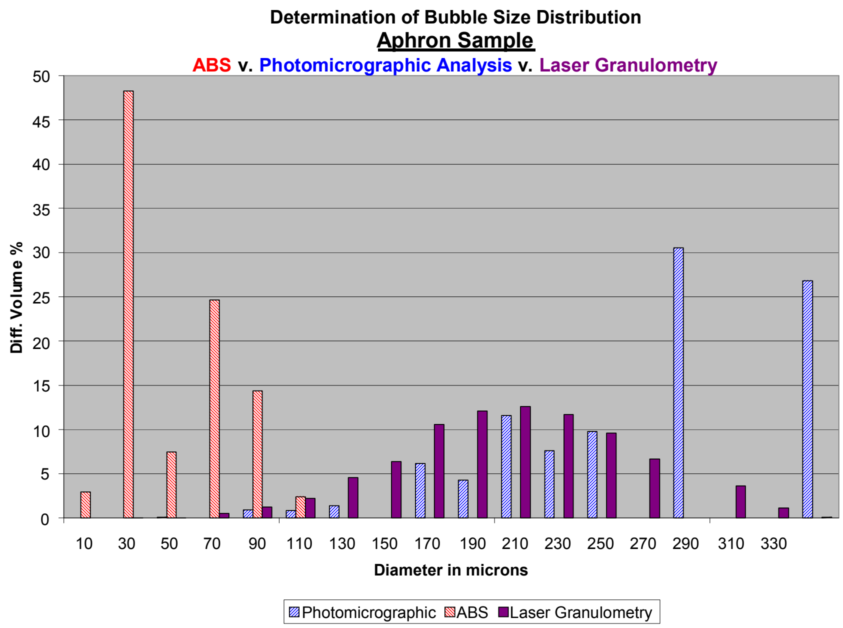

The disparate results in the BSD obtained with ABS versus laser granulometry and photomicrography suggest that there is something about the properties of the APHRON ICS™ sample that skews the BSD from ABS measurements to very low values. Discussions with the ABS developer, Dynaflow, indicate that the very high low-shear-rate viscosity of the APHRON ICS™ fluids is most likely responsible: the algorithm incorporated into the analysis software assumes Newtonian behavior, which is grossly inadequate. Another problem with the ABS software is that it has never yielded bubble diameters less than 10 µm. In tests involving very fine bubbles (in the range 1-50 µm diameter), ABS was not able to recognize any bubbles smaller than 10 µm.

A comment about the laser granulometry test results. The fluid samples were tested first with the ABS and then immediately evaluated using photomicrography, so that the condition of the samples was similar for both tests. The laser granulometer measurement was made by George McMennamy in the M-I SWACO Analytical Group as soon as possible thereafter, generally within 2 hours. Some deterioration of the samples might have occurred during this period. It was for this reason that photomicrography was used as a reference test method. Deterioration of a laser granulometry sample will occur partly as a result of the natural lifetime of the bubbles under static conditions, but the effect may be exacerbated by sample manipulation during introduction of the sample into the viewing cell. Bubble coalescence during that 2-hr period is expected to result in loss of a small portion of the smaller bubbles, an increase in intermediate-sized bubbles and loss of very large bubbles to the atmosphere.

Figure 40. Comparison of BSD Methodologies for Diluted Aphron Sample

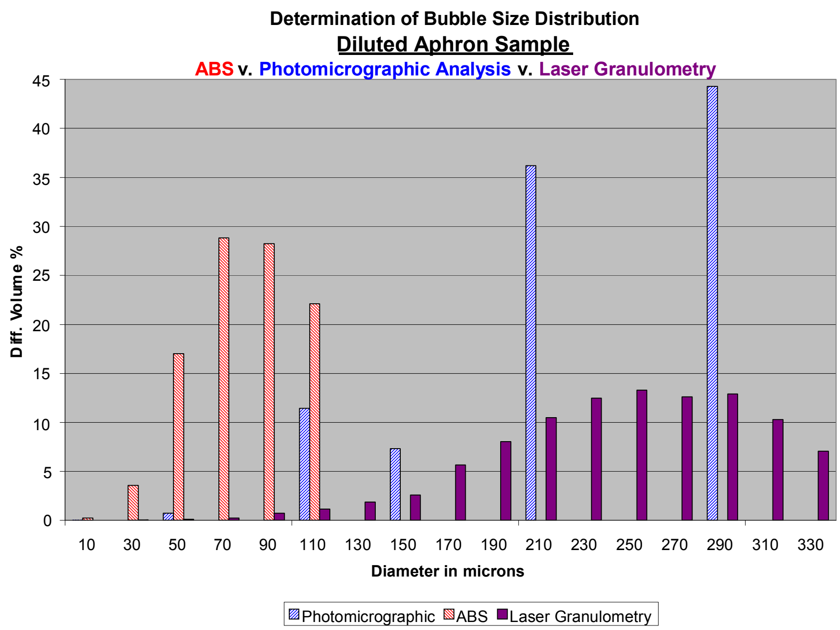

Elevated Pressure and Temperature:

Although the ABS did not look very promising in the evaluation conducted at ambient pressure, it was deemed worthwhile to re-examine the technology in the HTHP Circulating System, partly because the hydrophones employed in the high-pressure ABS Cell have nine times the surface area of those used in the ambient-pressure cell, thereby giving the ABS nine times the sensitivity. Initial tests were carried out at room temperature. Static ABS measurements of a transparent Enhanced APHRON ICS™ system containing ~ 40% v/v air were made at 0.1 MPa, 6.9 MPa, 13.7 MPa, 2nd 0.1 MPa, and 2nd 0.1 MPa + 15 min (0 psig, 1000 psig, 2000 psig, 2nd 0 psig, and 2nd 0 psig + 15 min, respectively). Dynamic ABS readings with the pump running at 0.5 gal/min were also recorded at 13.7 MPa (2000 psig) and at 2nd 0.1 MPa (0 psig) + 15 minutes. Digital photos of the aphrons in the Canty Viewing Cell were also collected at each of the above static pressures. An example of the static images taken at 0.1 MPa, 13.7 MPa and 2nd 0.1 MPa + 15 min (0 psig, 2000 psig and 0 psig + 15 min) is shown in Figure 41. Some 500-μm glass beads were also introduced into the mud for reference.

Figure 41. Optical Images of Transparent APHRON ICS™ Mud

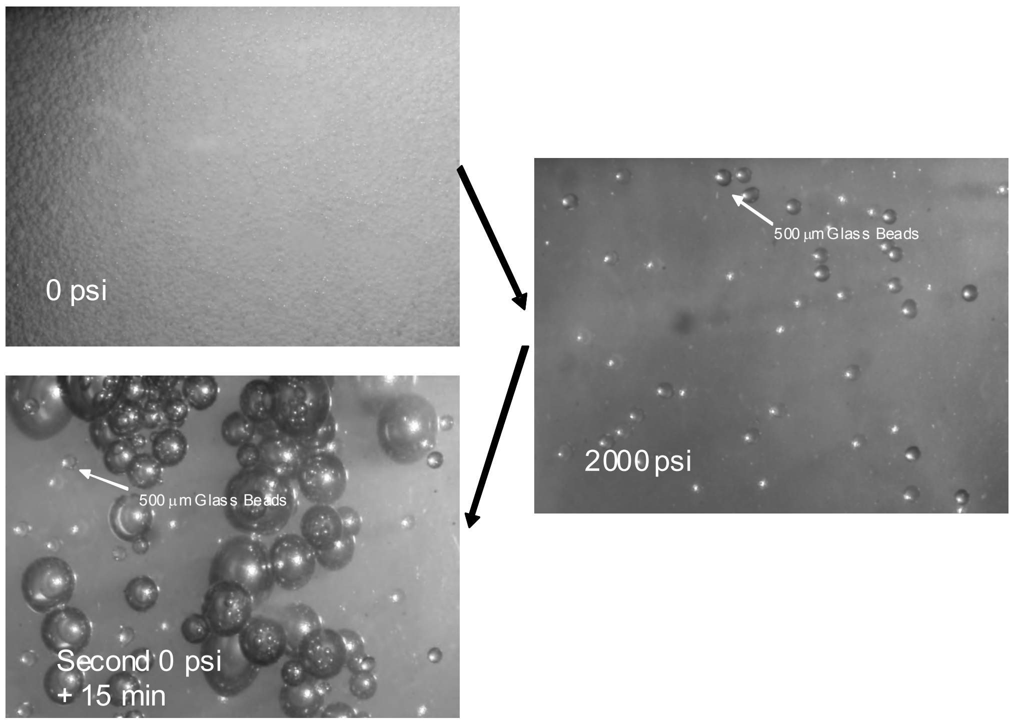

At 0.1 MPa (0 psig) most of the bubbles are less than 500 μm diameter and appear to average a few hundred μm. After pressurizing to 13.7 MPa (2000 psig), a few bubbles remain; these appear to be mainly out-of-focus spheres of a few tens of microns diameter. Finally, after decompressing back to 0.1 MPa, the bubbles are much larger than they were initially, though perhaps similar in number to those that survived 13.7 MPa (2000 psig). There are a number of other small bubbles that are attached to these larger ones. It is thought that many of the aphrons do not survive compression to 13.7 MPa (2000 psig), although previous tests have shown that some aphrons – if they are large enough to begin with – can survive to 27.3 MPa (4000 psig). The air from non-surviving aphrons dissolves in the base fluid, only to be released when the system is depressurized sufficiently to form a supersaturated solution. This air can enter existing aphrons or can form other aphrons that serve to feed the larger aphrons.

Under static conditions, ABS yielded a bubble size distribution (BSD) at 6.9 MPa (1000 psig) with average bubble size around 50 µm diameter, compared with an estimated value from optical image analysis of 250 µm (see Figure 42).

Figure 42. Comparison of ABS and Photomicrographic BSD: 6.9 MPa (1000 psig)

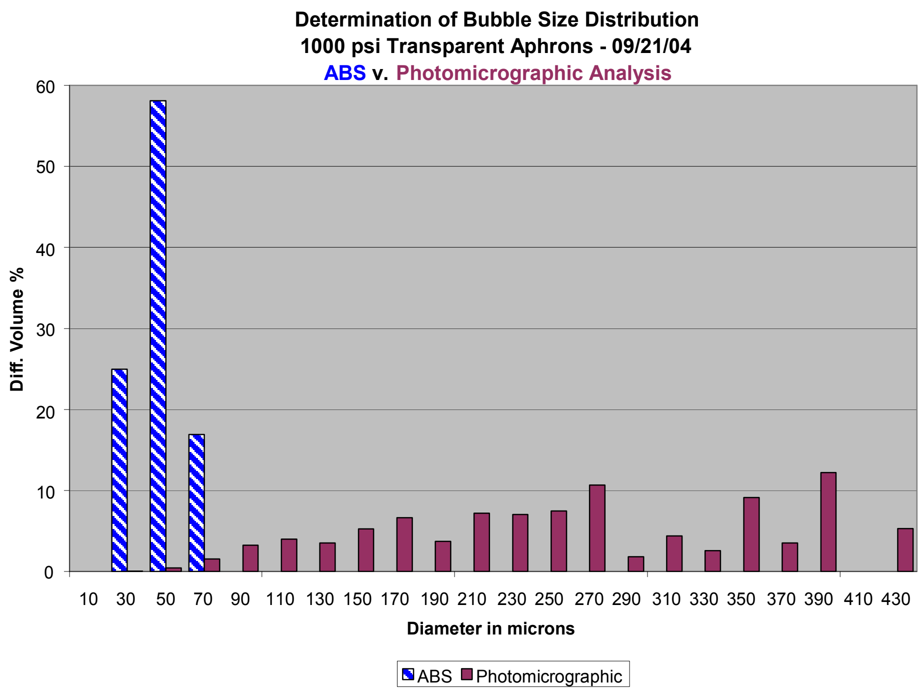

At 13.7 MPa (2000 psig), sensitivity of ABS was too low, and no bubbles were observed. At 2nd 0.1 kPa (0 psig), ABS showed an average bubble size of about 250 µm, whereas photomicrography gave an average bubble size of 650 µm (see Figure 43). Generally, the larger the bubble, the better the agreement between ABS and photomicrography. However, for moderately sized or small bubbles, the BSD generated by ABS can be too low by as much as an order of magnitude.

Under dynamic conditions, the ABS output is even more problematic. As shown in Figure 44, very similar BSD's were obtained at 2000 psig and at 2nd 0.1 kPa (0 psig) + 15 min, whereas the average bubble size for this sample under these conditions is estimated from photomicrography to be < 20 µm at 13.7 MPa (2000 psig) and > 1000 µm at 2nd 0.1 MPa (0 psig) + 15 min.

Figure 43. Comparison of ABS and Photomicrographic BSD: 2^{nd} 0.1 MPa (0 psig)

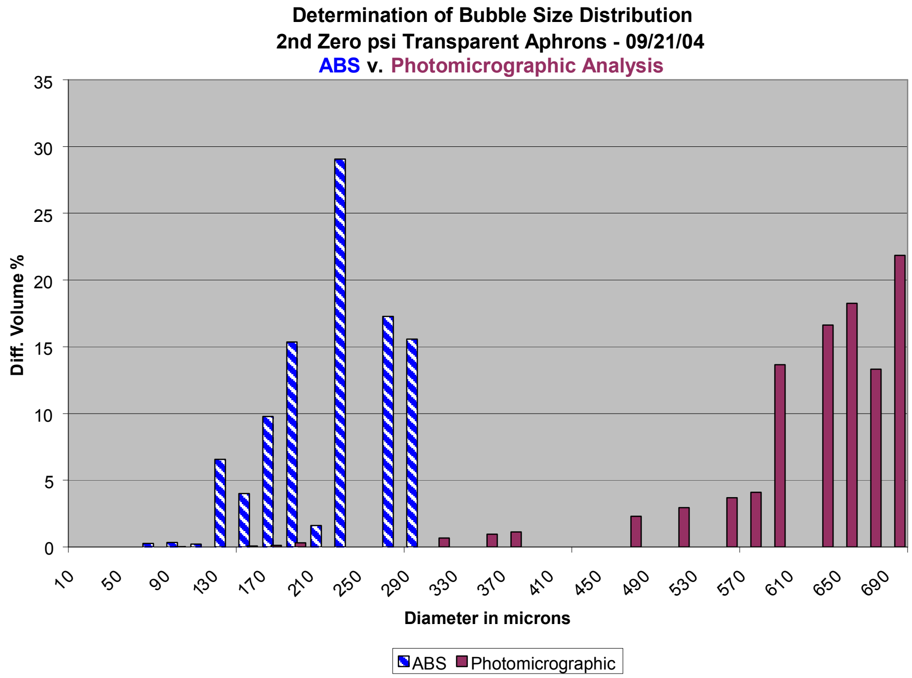

Figure 44. ABS Output for Dynamic Tests at 13.7 MPa (2000 psig) and 0.1 MPa (0 psig)

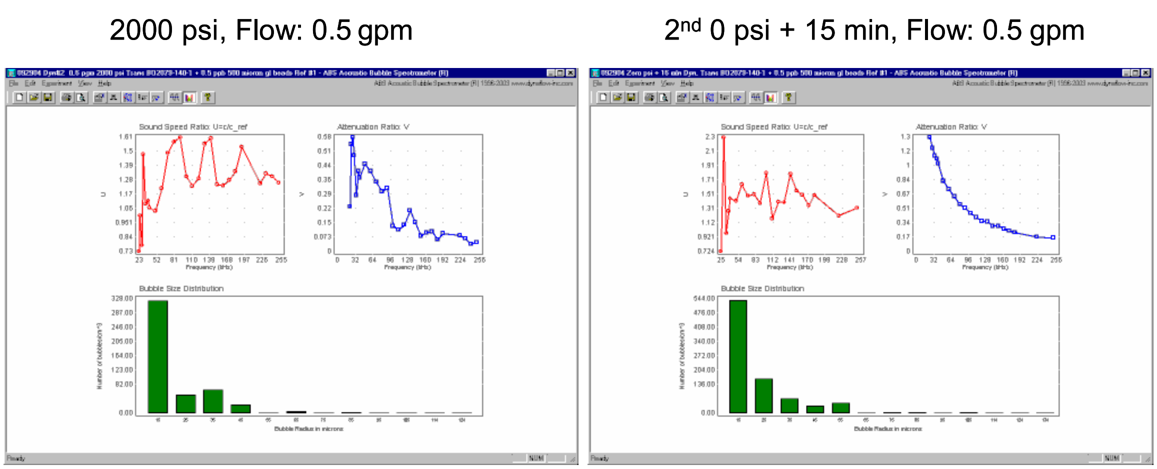

Thus, ABS does not appear to be a suitable method for monitoring the BSD in APHRON ICS™ drilling fluids at any pressure under either static or dynamic conditions. As a result, optical imaging became the method of choice for visualization of aphrons. Although the Canty Viewing Cell provided what appears to be fairly good quantitative BSD's, the Cell requires use of a transparent fluid, BSD must be analyzed manually, and there is considerable uncertainty associated with the depth of field within which aphrons are counted and measured. As a result, the ultra-thin VRD Viewing Cell, coupled with the NI Image Analysis software was used for most BSD determinations. With this system, aphrons have been able to be viewed at pressures as high as 27.3 MPa (4000 psig). Figure 45 shows room temperature images of a transparent Enhanced APHRON ICS™ fluid at 0.1, 6.9, 13.7 and 27.3 MPa (0, 1000, 2000 and 4000 psig) pressurized in increments of 3.4 MPa (500 psi) and holding the pressure at each step for about 15 sec.

Figure 45. Trans. APHRON ICS™ Fluid at 27.3 MPa (4000 psig) in VRD Viewing Cell

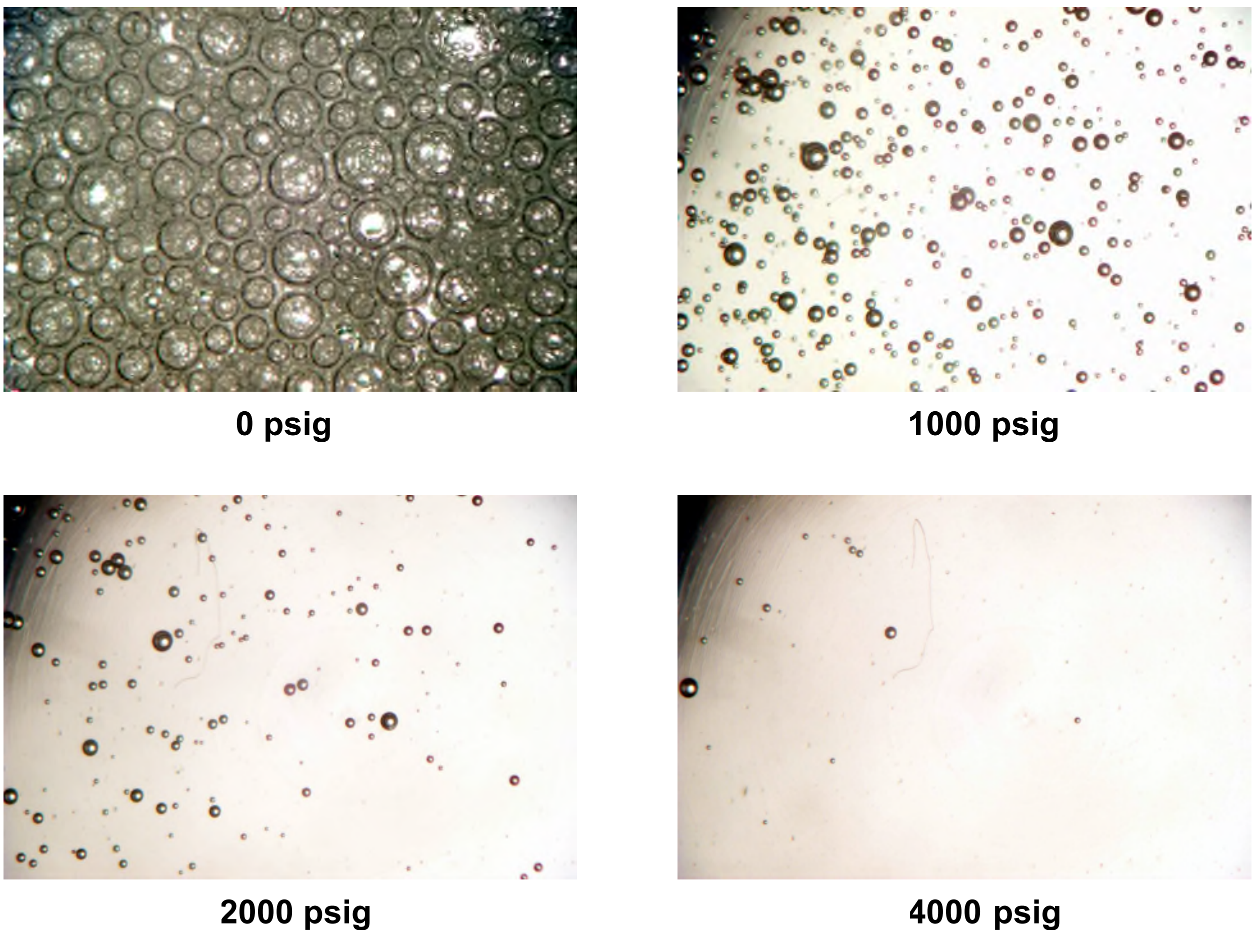

Only a few bubbles survive to 27.3 MPa (4000 psig). This was confirmed during depressurization, which did not regenerate any other bubbles until the pressure was below 3.5 MPa (500 psig). However, aphrons have never been observed at pressures above 20.5 MPa (3000 psig), and it is expected that the whole mud, especially in SuperEnhanced form, would generate a greater fraction of surviving aphrons than the transparent Enhanced APHRON ICS™ fluid.

Aphron Longevity

Measurement of Aphron Stability:

Monitoring Dissolved Oxygen

Various dissolved oxygen (DO) probes were examined. The FOXY T-1000 fluorescence quenching probe (Ocean Optics) was shown to be unacceptably delicate (the manufacturer was not able to keep the silicone coating from peeling off) and gave incorrect values of DO in high-viscosity fluids, such as the APHRON ICS™ drilling fluid. Of the other probes examined, the one that proved to be the most reliable was a Hach SC100 (see Figure 46). This particular probe is a break-through technology that relies on a timed response to an LED signal. Although the Hach probe cannot be used at pressures above 20 psig and is limited to moderate temperatures, initial tests showed it to be rugged and to give a fast response time.

Tests were run with the Hach SC100 under ambient conditions to determine the effects of (a) type of drilling fluid, (b) low-shear-rate viscosity and (c) aerobic biodegradation. Several drilling fluids, some with varying amounts of viscosifier and biocide, were tested to ascertain whether the rate of loss of air from aphrons could be obtained by monitoring DO concentration.

Figure 46. The Hach SC100 Dissolved Oxygen Probe

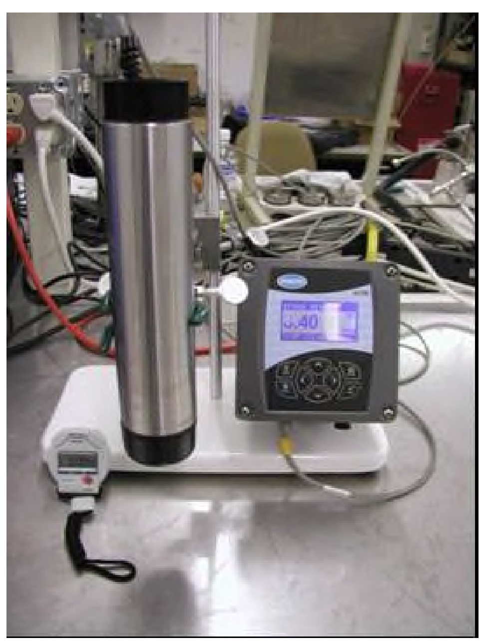

The Hach SC100 showed very encouraging results. Response time was rapid, generally giving a steady-state value of DO within 15 to 30 min, depending on viscosity and how the probe was introduced into the sample. As shown in Figure 47, the steady-state DO values recorded for the SuperEnhanced (SE) APHRON ICS™ mud dropped very quickly. Indeed over the initial 3-hr period between mixing the mud and getting a steady-state DO reading, the concentration of DO had already dropped by more than 50%. Initial readings were approximately 8.5 ppm (parts per million). As shown in Figure 47, a 30-ppb slurry of Black Hills bentonite retained that value indefinitely. Apparently the "Transparent APHRON ICS™" (transparent Enhanced APHRON ICS™) mud, which lacks the hemicellulose, starch, MgO and EMI-802 of the regular SE APHRON ICS™ mud, also remained high, at least for the first couple of days. But the regular SE APHRON ICS™ mud depleted DO very rapidly, so that within a day the concentration of DO was negligible. This system contains a low level of X-CIDE™, a powerful biocide.

Xanthan gum, one of the main components of the APHRON ICS™ mud system, can undergo aerobic biodegradation, but the process is thought to be relatively slow. Tests here indicate that when long-term DO monitoring tests were conducted of a pH-adjusted solution of xanthan gum, here in the form of a premium grade called FLOVIS PLUS™, DO did indeed fall, though not as rapidly as it did in the SE APHRON ICS™ mud system. The FLOVIS PLUS™ solution did not contain any biocide. Thinking that aerobic biodegradation might be involved in the depletion of DO in the SE APHRON ICS™ mud, the level of X-CIDE™ was increased from 0.1 to 5 ppb. As is apparent in Figure 47, even with 5 ppb X-CIDE™, the depletion rate of DO was not affected significantly. It appears, therefore, that some of the other components in the SE APHRON ICS™ system cited above, namely the hemicellulose and starch, are very likely reacting directly with dissolved O_2. This process is so rapid -- and in all likelihood is even more rapid at elevated pressures and temperatures -- that it is not possible to use DO as an indicator of the rate of transport of air from aphrons into solution.

Similar long-term exposure tests were run with other fluids, as shown in Figure 48. While the HYSSTER™ (nee EMS-2100, a clay-based aphron drilling fluid) and 3% KCl FLOPRO NT™ systems (with biocide) did not show any indication of a drop in DO over time, DRILPLEXTM™ did exhibit a steady drop in DO, though not as rapid as FloVis Plus™ without biocide. The DRILPLEXTM™ system contains an organic fluid loss control agent that is thought to react easily with oxygen.

Figure 47. Effect of Time on DO Concentration in Various Drilling Fluids

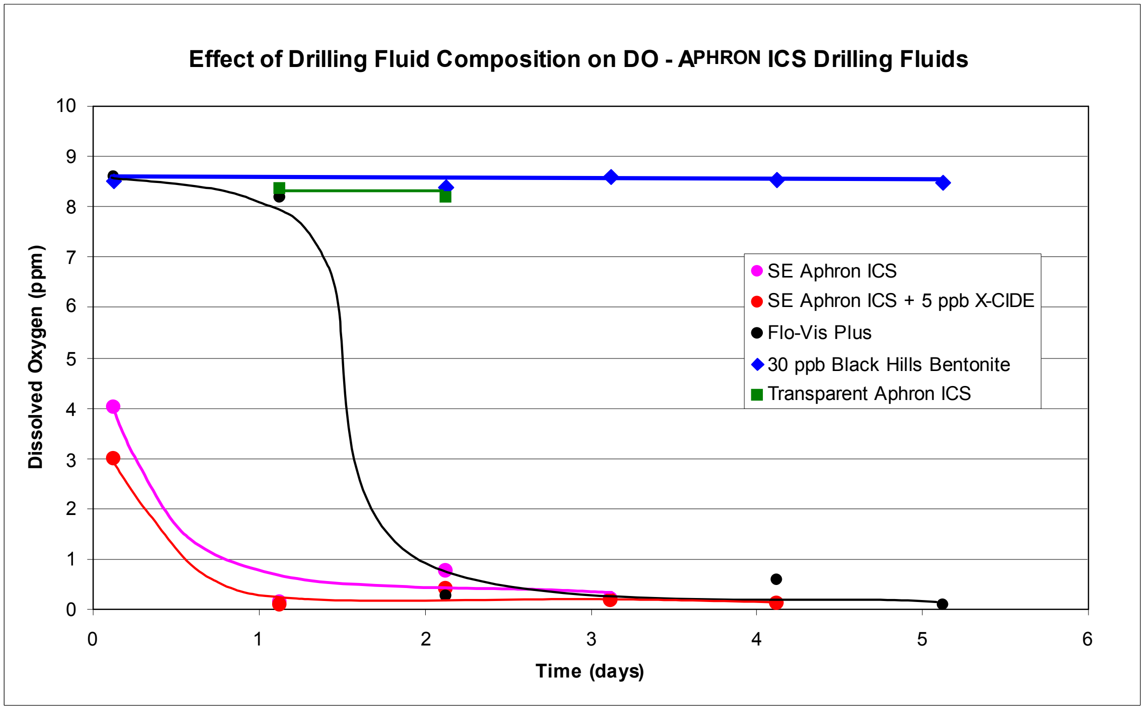

Figure 48. Effect of Time on DO Concentration in Miscellaneous Fluids

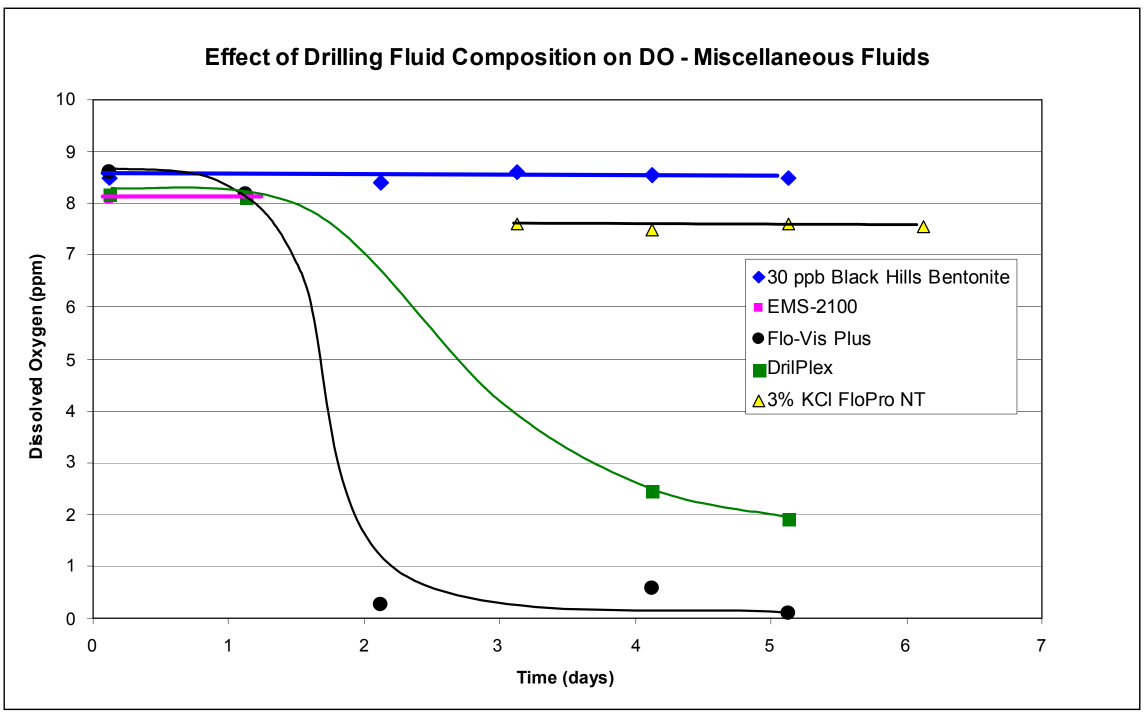

Another issue that was of concern for the measurement of DO was the effect of viscosity -- especially LSRV -- on the rate of attainment of steady-state values of DO. The effect of LSRV on steady-state DO was determined using freshly prepared solutions of FloVis Plus™ (with different concentrations of the polymer) that ranged in viscosity from 97 kcP to 156 kcP. The steady state DO in all cases ranged from 8 to 8.5 ppm (parts per million). Thus, there appears to be little or no effect of viscosity on the steady-state value of DO; even the rate of attainment of the steady-state value of DO was not slowed much by high viscosity.

Thus, although viscosity is not a problem and aerobic biodegradation can be controlled, some components of the SuperEnhanced APHRON ICS™ mud serve as substrates for direct oxidation. This leads to the inescapable conclusion that, even at ambient pressure and temperature, DO reacts with these components so rapidly that monitoring of DO is <u>not</u> an acceptable method of measuring the rate of loss of air from aphrons.

During the measurements of DO of closed systems, it was noted that the bubbles shrank a little. Indeed, one would expect that loss of O_2 from the aphrons would result in a reduction in bubble volume of 21% when the system is fully depleted of O_2. Although this is not an insignificant amount, the change in bubble "size" (diameter or radius) is only about 7.5%. Since sealing of pores and microfractures is governed by particle size, the loss of O_2 from the aphrons is not expected to play a major role in their performance. An advantage of losing the O_2, of course, is decrease in corrosivity of the drilling fluid. About 3 vol% O_2 (15 vol% air) is entrained at ambient conditions. This is 10.5 mL/Lab Equivalent Barrel, or 0.015 lb/bbl (1.3 x 10^{-3} mol/L). If all of the O_2 were to dissolve, its concentration in the fluid would reach about 43 ppm. Although this amount of O_2 is relatively low (compared to energized or foamed fluids), tubulars downhole would be expected to suffer some corrosion from continued exposure. Consequently, elimination of the O_2 is preferable, and it removes any doubt about the corrosivity of the drilling fluid.

<u>Monitoring Bubble Size</u>

Since O_2 proved to be too reactive a component to maintain in the system, and ABS gave very inaccurate values of the BSD, a more direct method was sought to measure the rate of air loss from aphrons. With direct optical imaging, rate of loss of air can be determined from the rate of shrinkage of the bubbles. This had been the method of choice originally, but at the time opaque fluids could not be monitored optically and there were issues with making observations at elevated pressures and quantifying the BSD. Development of the transparent VRD Viewing Cell (see Figures 8 - 10) removed these issues: bubble size can be monitored in opaque drilling fluids containing a few bubbles, observations can be made at elevated pressure and temperature and an image analysis software package is now available to facilitate measurements of the bubble size.

A systematic series of tests was begun to determine the effects of pressure, pressurization protocol, shear rate, method of aphron generation and fluid composition on BSD. Initial tests indicated that some aphrons are more stable than others. Indeed, significant differences in bubble stability were noted for bubbles of different sizes, as well as different treatments: pressurized to different pressures or at different rates, sheared at different rates, created in different ways and prepared with different components.

Effect of Pressure:

The sizes of seven well-defined bubbles in a normally prepared SuperEnhanced (SE) APHRON ICS^{TM} fluid were measured after initially pressurizing the system to 3.5 MPa (500 psig).

Figure 49. Effect of Bubble Size on Aphron Stability

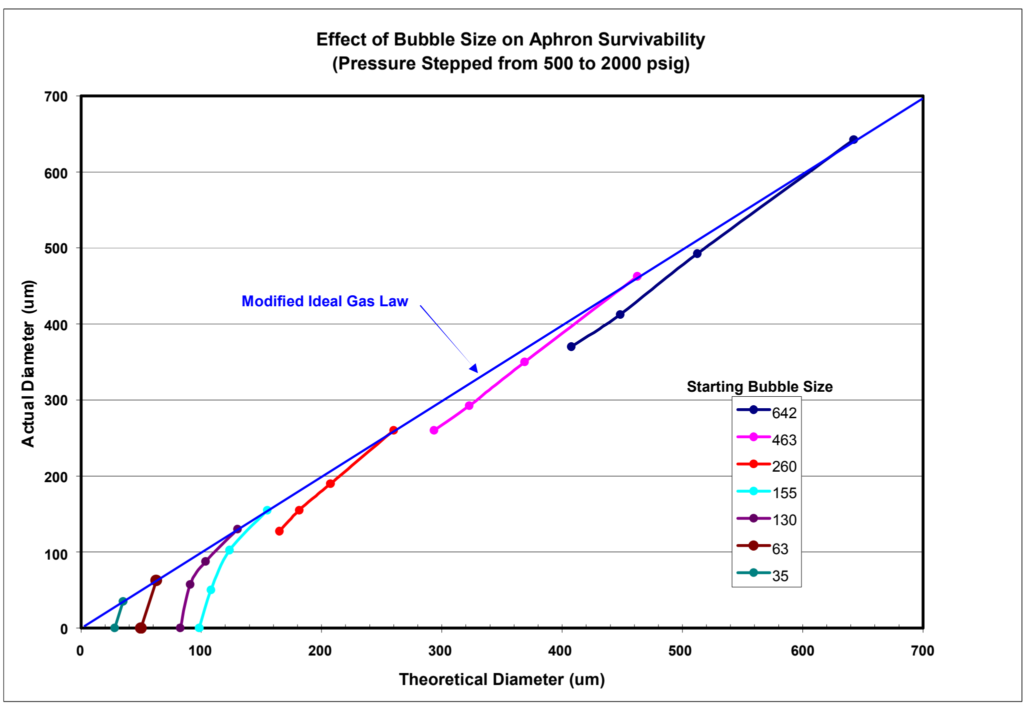

These are plotted on the graph in Figure 49 in the form of Actual (measured) Diameter vs Theoretical (modified Ideal Gas Law) Diameter, and they are made to fall on a line with a slope of 1. When the system was pressurized sequentially to 6.9, 10.3 and 13.7 MPa (1000, 1500 and 2000 psig), each bubble shrank as shown in Figure 49. The Theoretical Diameter is given by the expected size obtained using the Modified Ideal Gas Law,

$$P_1V_1/z_1 = P_2V_2/z_2 \tag{1}$$

where P is the Pressure (the subscript 1 is for the 500 psig case, 2 is for each of the other cases), V the volume, and z the compressibility factor for air (obtained from tables in standard chemical engineering handbooks[21]). Figure 49 shows that, under these conditions, the bubbles follow the Modified Ideal Gas Law rather closely (but not perfectly) for bubble sizes in excess of 100 µm diameter, though they deviate markedly below that critical size. Indeed, when the size of a bubble is in the range 25 to 50 µm, the bubble disappears after the next increase in pressure.

The primary mechanism for destabilization of aphrons is thought to be loss of air through the bubble shell, which is likely via diffusion through the aphron shell into the surrounding fluid. Indeed, the deviation in measured bubble size from that predicted by the Modified Ideal Gas Law for bubbles larger than 100 µm diameter may be attributable to diffusion of air during the pressure ramp. Taking into account some thickness for the aphron shell causes the deviation to be even greater. Non-interacting bubbles larger than 100 µm diameter may be expected to lose air with increasing bubble size according to the following expression:[22]

$$\text{Rate of Escape of Air} = \text{Driving Force x Leakage Rate} \tag{2}$$

or

$$\text{Rate of Escape of Air} = (k_1/r) \text{ x } (k_2r^2) = k_1k_2r \tag{3}$$

The Driving Force (the excess pressure between the bubble and the medium) is inversely proportional to the radius of the bubble, and the Leakage Rate is proportional to its surface area. Here k_1 and k_2 are coefficients that depend on how the fluid is prepared and on environmental variables such as pressure and temperature. Thus, the Rate of Escape of Air is expected to be proportional to the bubble size (radius or diameter). However, if the Rate of Escape of Air for the bubbles described in Figure 49 is calculated from the bubble diameters, it is found that for bubbles greater than 100 µm diameter, the actual loss in volume vs the theoretical loss in volume (upon increasing the pressure from 3.5 MPa, or 500 psig to 13.7 MPa, or 2000 psig) appears to be proportional to the Leakage Rate, i.e. it is proportional to the surface area of the bubble. For aphrons, the increase in Driving Force that generally accompanies a decrease in size of the bubble may be nullified by compaction of the shell. Conversely, the larger the bubble, the more permeable the aphron shell. Thus, we take the liberty of modifying expression (3) as follows:

$$\text{Rate of Escape of Air} = \text{Driving Force} \times \text{Permeability} \times \text{Leakage Rate} \qquad (4)$$

or

$$\text{Rate of Escape of Air} = (k_1/r) \times (k_2 r) \times (k_3 r^2) = k_1 k_2 k_3 r^2 \qquad (5)$$

where k_3 is related to the permeability of the aphron shell.

When aphrons become smaller than about 50 µm diameter, they become <u>less</u> stable and suffer catastrophic loss of air. Clearly, the mechanism for air loss changes below this critical size and does not follow expression (5).

Sebba[5] hypothesized that aphrons smaller than 25 µm diameter may not be able to survive. This agrees very well with our own observation, as demonstrated in Figure 49, that when an aphron is squeezed to a size less than 25 to 50 µm, it will disappear when pressurized further, though the rate of disappearance is expected to be a function of variables such as composition, pressure and rate of pressurization. On the other hand, Sebba declared that maybe aphrons smaller than 25 µm do survive and speculated that perhaps they simply cannot be seen. If that were the case, however, reducing the pressure should make them visible again. When the pressure on the fluid described in Figure 49 was reduced from 13.7 MPa (2000 psig) to 3.5 MPa (500 psig), the aphrons that had shrunk to less than 50 µm during the pressure ramp did not re-appear.

Effect of Compression/Decompression:

In addition to pressure itself, the <u>rate</u> at which pressure is applied or removed appears to have a significant impact on the survivability of aphrons. It has been hypothesized that a slow pressure ramp would allow the surfactants in the aphron shell to rearrange themselves into a tight, low-permeability membrane, whereas a fast pressure ramp might not give the surfactants sufficient time to do so. The results of pressurization tests demonstrate that this is not the case.

Tests in VRD Viewing Cell

Tests were carried out with the transparent Enhanced APHRON ICS™ drilling fluid in the VRD Viewing Cell to determine the effect of rate of pressurization on the shrinkage rate of aphrons:

- Slow Pressurization – 0.1, 3.5, 6.9, 10.3 and 13.7 MPa (0, 500, 1000, 1500 and 2000 psig), waiting 15 seconds at each pressure. The system was then depressurized in the same manner down to 0.1 MPa (0 psig), and photos were taken at 0, 5, 10, 20 and 30 min.

- Fast Pressurization – 0.1 and 13.7 MPa (0 and 2000 psig), waiting 15 seconds after reaching 13.7 MPa (2000 psig). The system was then depressurized rapidly to 0.1 MPa (0 psig) and photos were taken at 0, 5, 10, 20 and 30 min.

Figure 50 shows first that aphrons do not recover their initial size very quickly; indeed, it appears that 30 minutes is a minimum amount of time necessary for full recovery. Secondly, aphrons recover at a rate and to a steady state size that depends on the rate of pressurization. In Figure 50, two bubbles of similar size were exposed to the two pressurization protocols described above.

Figure 50. Effect of Rate of Pressurization Rate on Aphron Size

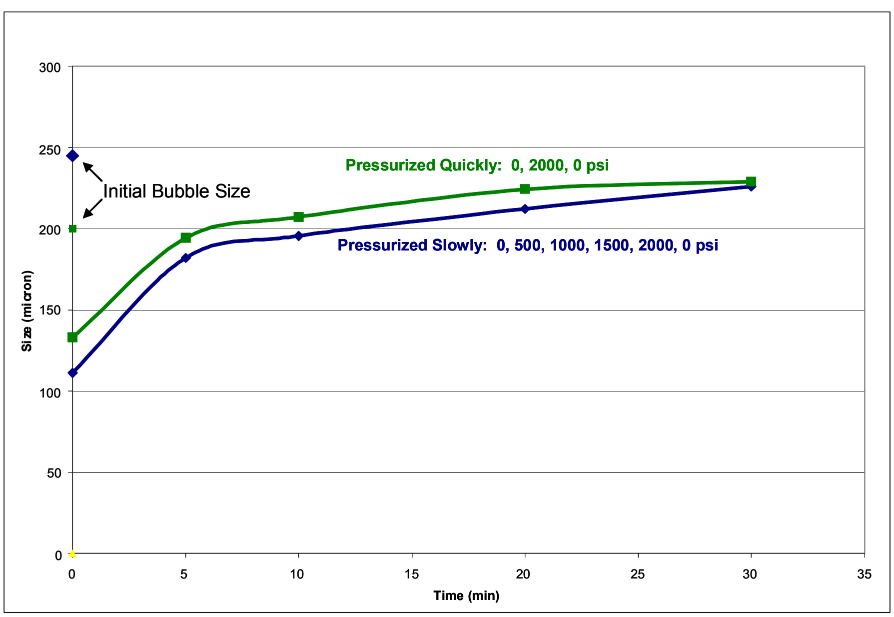

The aphron that was pressurized slowly began with an initial diameter of 245 µm, but 30 min after depressurization it had only reached 226 µm, a deficiency of 8%. However, the aphron that was pressurized quickly recovered its initial size of 200 µm within 5 min, and in 30 min surpassed its initial size to reach 229 µm, a surplus of 13%. With more time, the aphron that was pressurized slowly might have reached its initial size.

The aphron that was pressurized quickly, however, appears to have gained some air. The 13% increase in diameter of that bubble translates to a 44% increase in volume. Indeed, the photographs show that there are fewer small aphrons in the vicinity of this aphron after depressurization than were evident at the beginning of the test. This is consistent with the view that the small aphrons were destroyed during pressurization and the lost air went into solution, only to emerge later when the system was at 0.1 MPa (0 psig) and the system was supersaturated. Some of that air may serve to form new aphrons, but it appears that a larger fraction becomes incorporated into existing aphrons. Thus, the aphron shell not only is permeable and susceptible to loss of air, it also appears equally capable of absorbing air from solution.

<u>Tests in Canty Viewing Cell</u>

Compression/Decompression tests were also conducted in the Canty Viewing Cell, using a syringe pump to apply pressure through a 500-mL accumulator, which contains a floating piston that separates the hydraulic fluid (water) from the mud sample. Although the glass cell is rated at 20.5 MPa (3000 psig), the experiments were restricted to a pressure of 13.7 MPa (2000 psig), the rating of the accumulator. A streaming video digital camera was used to capture the images of the mud as it underwent changes in pressure.

In the first test (Figure 51), without magnification, the transparent APHRON ICS™ mud was pressurized very quickly (<15 seconds) to 13.7 MPa (2000 psig).

The 2000 psig pressure was maintained for 30 to 40 seconds and then reduced to zero. In the first photo in Figure 51, it can be seen that the aphrons block much of the fiber-optic light applied to the rear of the cell. The second photo shows transmission of a large amount of light due to the aphrons being compressed. The final photo of the series at the second zero psig indicates that the aphrons have returned to their original state.

The second set of photos (Figure 52) was recorded at 6X magnification using the same apparatus and protocol as used in the first set. An additional photo appears at the second zero plus 2.2 min. The sight glass was facing up, so that bubbles tended to accumulate under the viewing window. This test was the fourth pressurization of the same sample of transparent Enhanced APHRON ICS™ mud.

Figure 51. Transparent APHRON ICS™ Pressurized to 13.7 MPa (2000 psig): 1st Pressurization

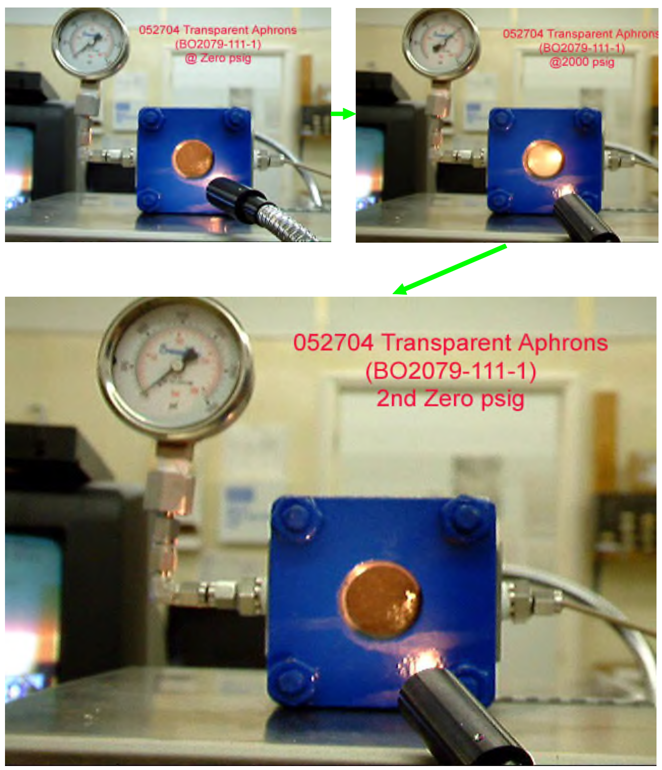

These tests indicate that aphrons are stable to at least 13.7 MPa (2000 psig) at ambient temperature. Immediately after depressurization (2^{nd} Zero psig), the bubbles appear to be smaller than in their initial state (Initial Zero psig). However, after a couple of minutes (2^{nd} Zero + 2.22 minutes), they have grown and appear to be <u>larger</u> than in their initial state. Evidently some bubbles have been lost, very likely due to escape of air from the bubbles and dissolution of that air into the surrounding bulk fluid. When decompressed, the supersaturated fluid yields up its air into existing aphrons or forms new ones. Thus, it appears that there is a stability distribution among the aphrons: some remain stable to 13.7 MPa (2000 psig), while others do not. Modification of the formulation may reduce the incidence of poorly stable aphrons.

Figure 52. Transparent APHRON ICS™, Pressurized to 13.7 MPa (2000 psig): 4th Pressurization

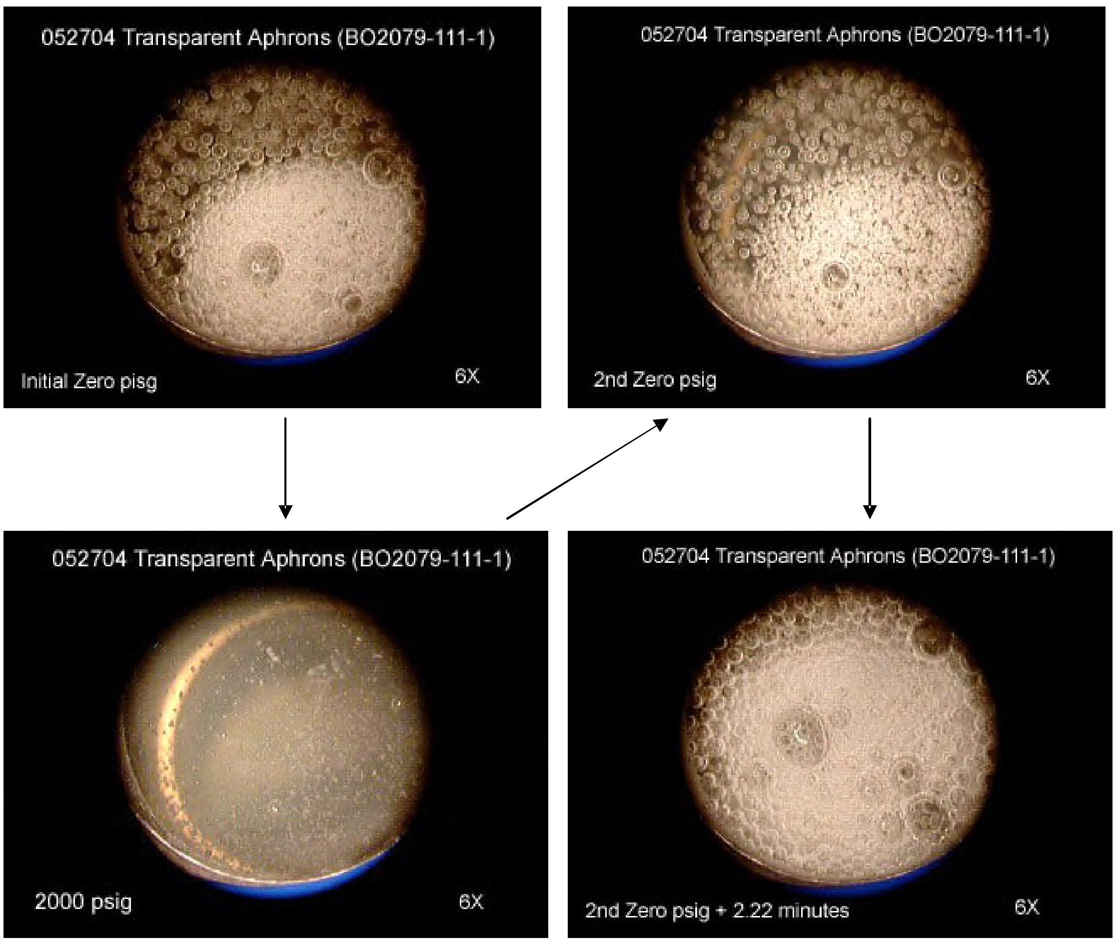

A second series of tests was conducted with the transparent APHRON ICS™ mud, but this time up to a pressure of 20.5 MPa (3000 psig). Here the Sight Flow Glass Viewing Cell was configured horizontally, with light entering only from the front, so as to avoid "creaming" of the aphrons. In the first test (Figure 53), the first photo shows the bubbles at ambient pressure, which appear as a white "foam." When the mud was quickly pressurized to 20.5 MPa (3000 psig) -- second photo -- the fluid turned quite dark, inasmuch as the volume fraction of bubbles was greatly reduced. The pressure was maintained for 30 seconds, then reduced to zero, and the sample was allowed to rest for a few minutes (third photo); this final photo at the second zero psig indicates that the bubbles have been regenerated, as indicated by the re-appearance of the white foam.

Figure 53. Transparent APHRON ICS™ Pressurized to 20.5 MPa (3000 psig): 1st Pressurization

Another test was carried out to 20.5 MPa (3000 psig) using a microscope, the same glass viewing cell as in the previous set (mounted horizontally) and the same mud sample. The first photo in Figure 54 is of the sample at 0 psig, using a magnification of 15X. In the second photo, 20.5 MPa (3000 psig) was applied to the sample, and the magnification was increased to 40X. Faint outlines of the bubbles can be observed at this pressure. The bubbles are faint because they have been driven deeper into the fluid and a good focus is not possible. The sample was depressurized

30 seconds later and the aphrons began to expand (third photo), and a few minutes later another photo was taken (fourth photo), still at 40X. The last photo shows the same view a few seconds later, but at a magnification of 15X. A comparison of the first and last photos makes it clear that most of the bubbles (aphrons) survived pressurization to 20.5 MPa (3000 psig) and, consequently, they are regenerated essentially intact when depressurized to 0 psig.

Figure 54. Transparent APHRON ICS™ Pressurized to 20.5 MPa (3000 psig): 2nd Pressurization

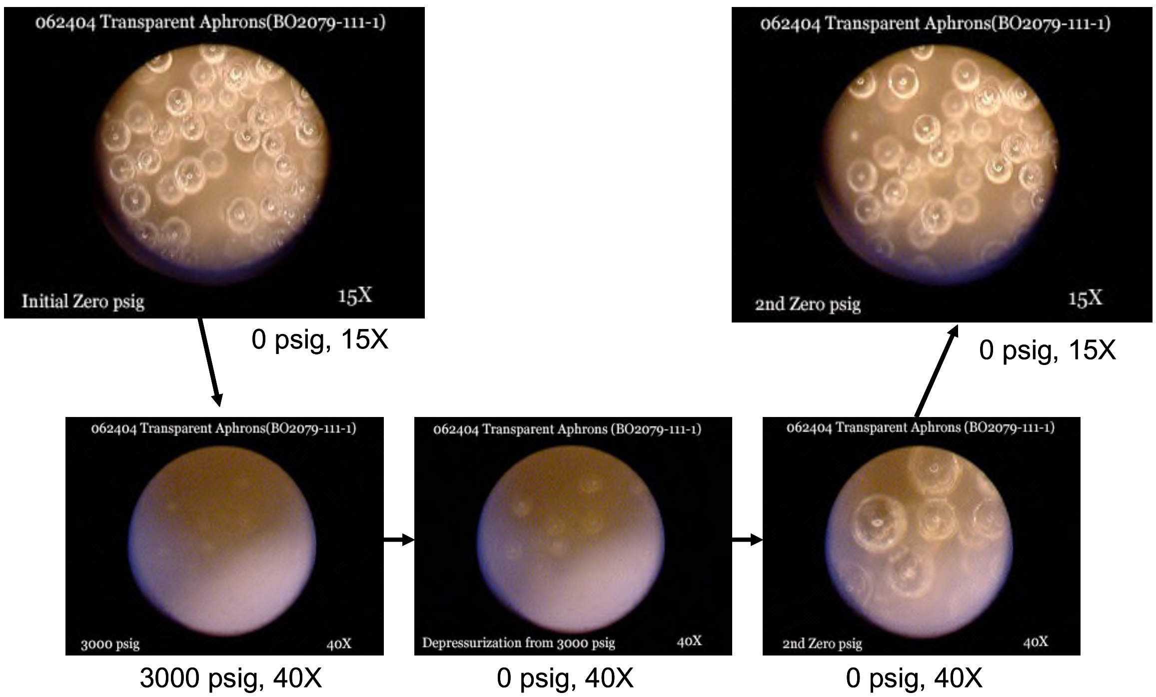

This series of tests indicates that most of the aphrons in this sample are stable to at least 20.5 MPa (3000 psig) at ambient temperature. When taken back down in pressure, they simply expand to their original size. Since the chemical composition of this fluid and the compression/decompression protocol was the same as in the previous series of tests, one must conclude that after the first compression/decompression cycle, i.e. after the first test series, the bubbles had acquired a more stable configuration. Thus, the method by which the aphrons are generated is probably as important to the stability of the bubbles as is the absolute chemical composition.

Fluid Density Tests

Measurements of the recovery of fluid density were made on samples that were cycled between ambient pressure and increasingly higher pressure up to 6.9 MPa (1000 psig). A couple of examples of those data gathered with the SuperEnhanced APHRON ICS™ mud formulation are shown in Figures 55 and 56.

Figure 55. Fluid Density Test with SuperEnhanced APHRON ICS™ Mud Sample #1

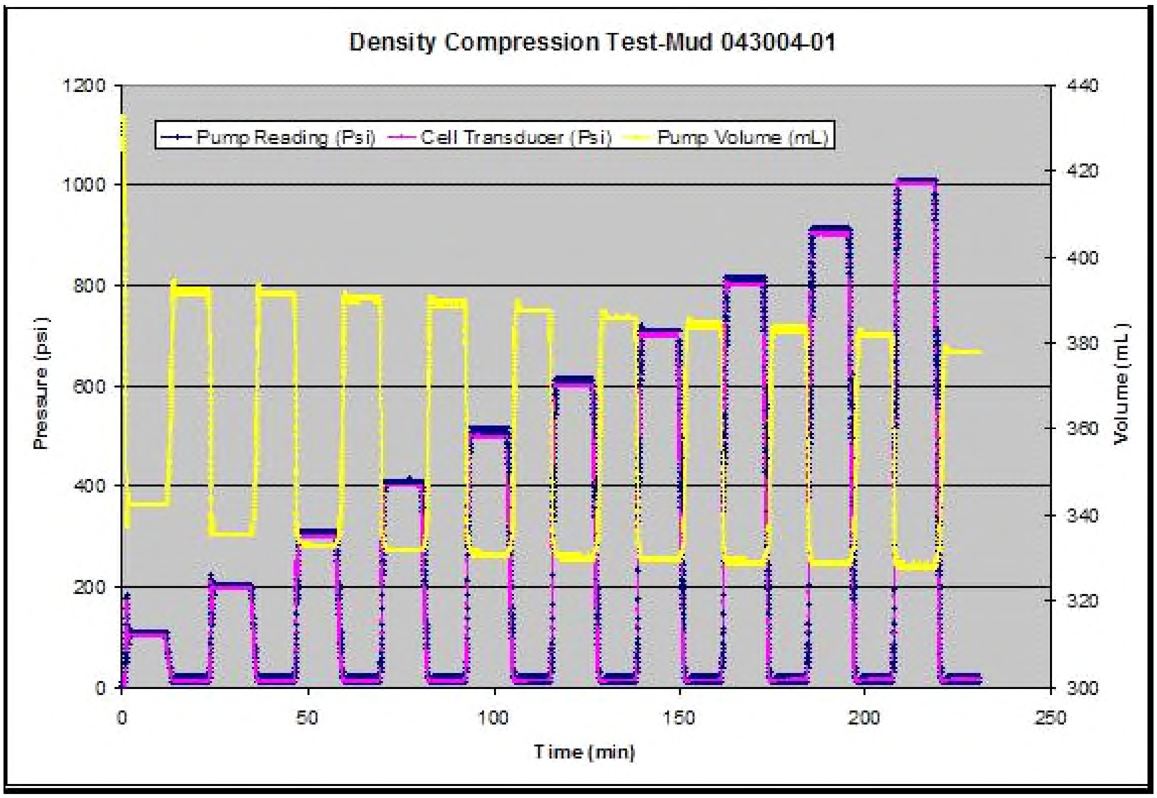

When the system is depressurized, it is assumed that air that was solubilized during a previous pressurization step requires significantly more time to come out of solution than air trapped within aphrons. Thus, the steady-state volume recovered after each depressurization step represents aphrons that retained their integrity during the previous pressurization step. Since there is some uncertainty in the position of the piston during the initial application of pressure to the system, the reference point is chosen to be the first depressurization step, i.e. after the 0.69 MPa (100 psi) step in Figure 55 and after the 25-psi step in Figure 56; this is assumed to represent 100% volume recovered (100% of the aphrons survive). All subsequent recovered volumes are compared to this volume. It should be noted that the pump pressure during the depressurization step does not drop to 0.10 MPa (0 psig), rather about 0.17 MPa (10 psig), again due to the stick-slip phenomenon mentioned in the Experimental Approach. Each post-pressurization volume measurement was made at that same pressure of 0.17 MPa (10 psig).

Figure 56. Fluid Density Test with SuperEnhanced APHRON ICS™ Mud Sample #2

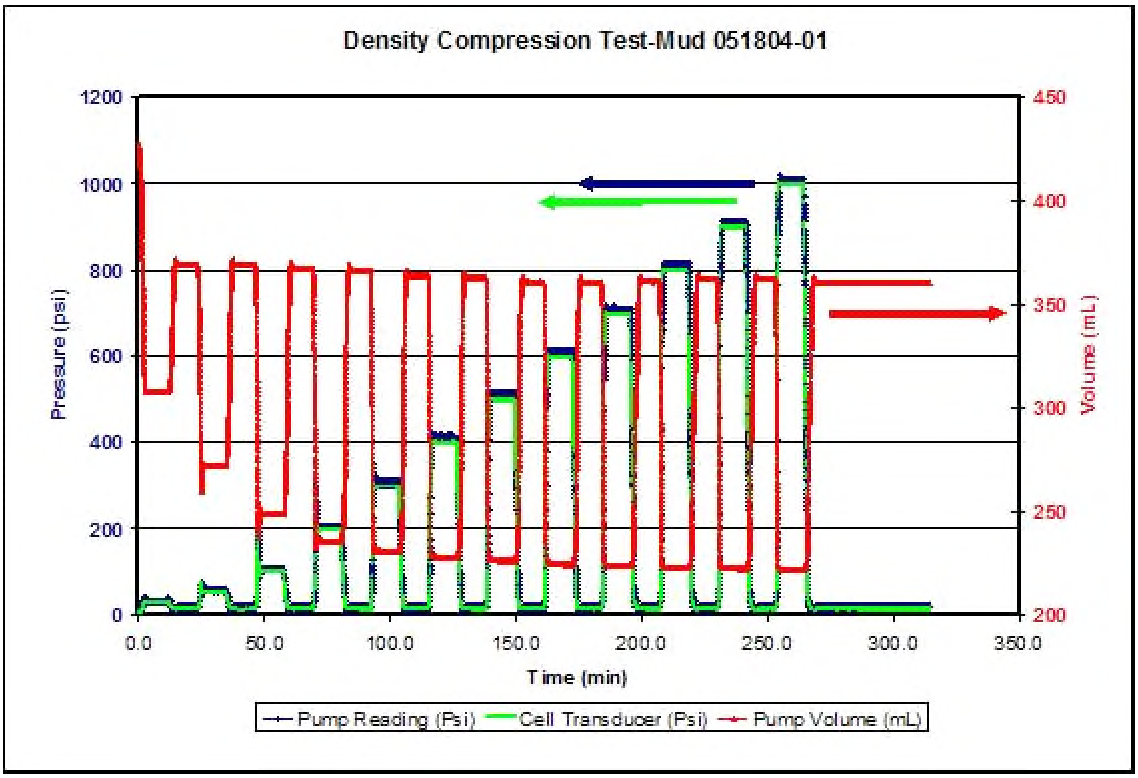

In the examples above, the amount of entrained air in the mud initially had been calculated from density measurements. However, this can be determined more accurately from the compressibility data. From the modified Ideal Gas Law, expression (1), when a gas is compressed from P_1 to P_2, the change in volume from V_1 to V_2 should compensate almost exactly (since the compressibility factor at these pressures is close to 1) to give $P_1V_1 = P_2V_2$ This is illustrated in Figure 57 by the horizontal red line. The mud sample used in the data presented in Figure 55 nominally contained 55 vol% air. However, one can see that with 55% v/v air, PV increases with increasing pressure. Through trial and error, one can determine that if the initial amount of air had actually been 49 vol%, PV would remain constant throughout the test. Thus, it is concluded that 49 vol% air is a more accurate value for the initial concentration of air in the mud at ambient pressure.

Figure 57. Determination of % Entrained Air in Fluid

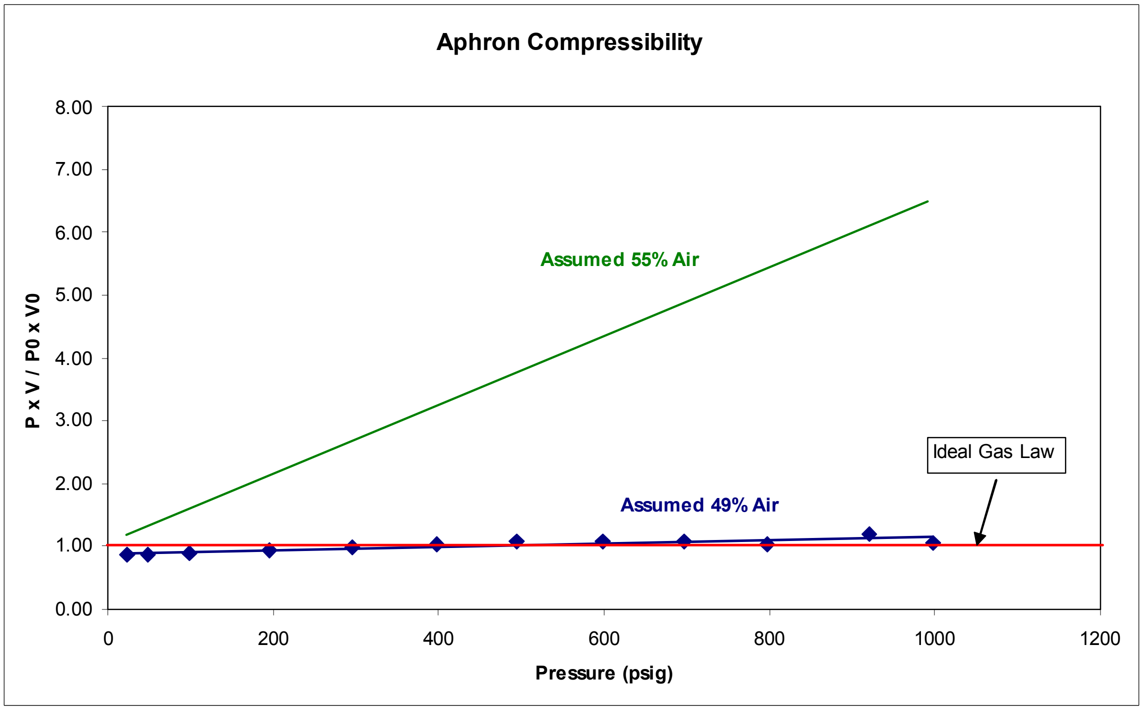

Analysis of Figures 55 and 56 indicates that, with increasing pressure, less and less volume is recovered when the system is depressurized, which we interpret as air which is lost from the aphrons and has gone into solution. However, the fraction of aphrons that is lost is relatively low, as shown in Figure 58. Here the data used was the set shown in Figure 56. The fraction of aphrons that survive after each depressurization step is given by

$$P^*(V_{cell} - V_{0fluidcell})/P_0{}^*V_{0aircell} \tag{6}$$

where P_0 is the absolute pressure and $V_{0aircell}$ the volume of air at the beginning of the test series; P is the absolute pressure and $V_{cell} - V_{0fluidcell}$ is the volume of air after each subsequent pressurization/depressurization step. $V_{0aircell}$ was 49 vol%, as determined from the procedure described above. As shown in Figure 58, it is evident that essentially all of the aphrons (> 95%) survived pressurization up to 6.9 MPa (1000 psig). This is consistent with the aphron visualization tests described in the previous section.

Figure 58. Effect of Pressure on Aphron Survival

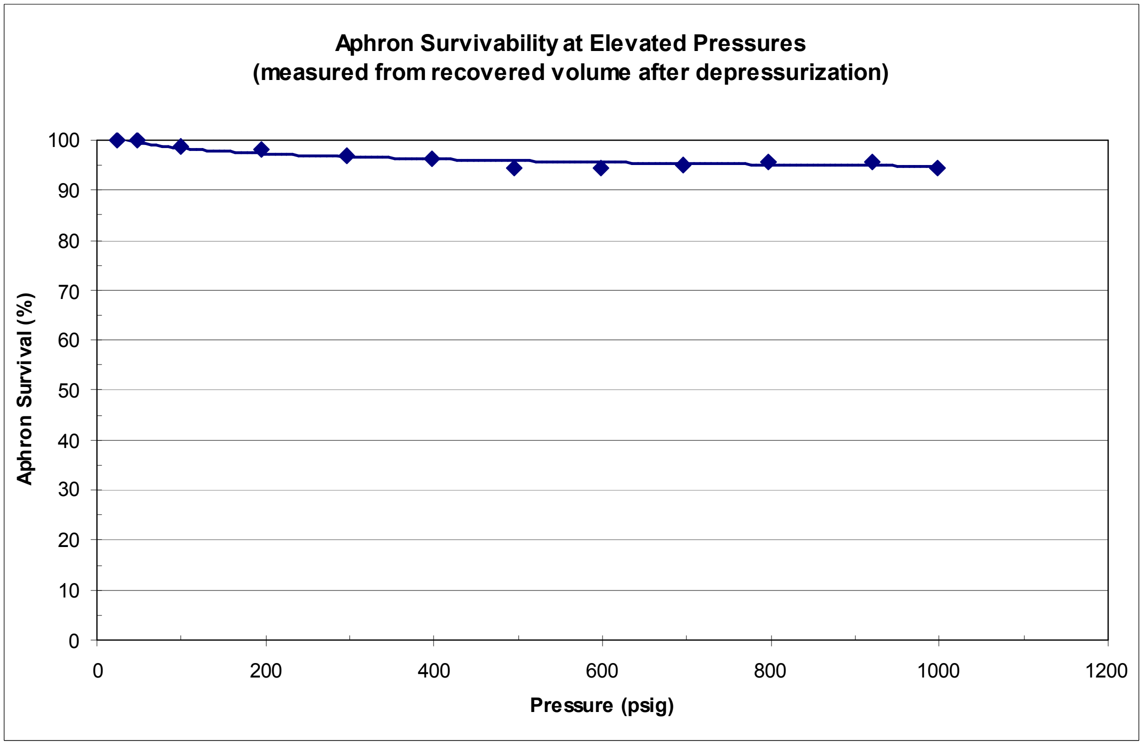

Effect of Shear:

Shearing of Aphrons at Ambient Pressure

In tests that were conducted with the Dual Syringe Hydrophobicity Apparatus (Figure 33) at ambient pressure, it was noted that when an aphron-laden fluid was passed back and forth through a 5-µm filter disk, the aphrons not only were easily comminuted (broken up into smaller bubbles), but eventually they approached a size and were so great in number that it became increasingly difficult to push the fluid through the filter. Eventually, it was not possible to do so, without breaking the syringe. It was also observed that, for a constant volume concentration of air, a fluid with smaller bubbles requires higher pressure to push it through the filter than a fluid with larger bubbles. Does comminution of the aphrons increase bulk viscosity of the fluid, or are the finer bubbles able to seal fine pores better, as is the case for typical solid lost circulation materials?

The apparatus used for determining the effect of flow of aphrons through permeable media on BSD and the corresponding effect of BSD on viscosity of fluid is shown in Figure 14, using a 15-μm filter between the VRD Viewing Cell and l. To eliminate plugging effects by the particulates in the fluid, a transparent Enhanced APHRON ICS™ fluid was used for all tests. On the first pass through the filter, air bubbles become smaller and possess a narrower BSD. Pictures of the original fluid and the same fluid after one and two passes through the 15-μm filter are shown in Figure 59.

Figure 59. Aphrons in Transparent APHRON ICS™ Fluid before and after passage through 15-μm Filter

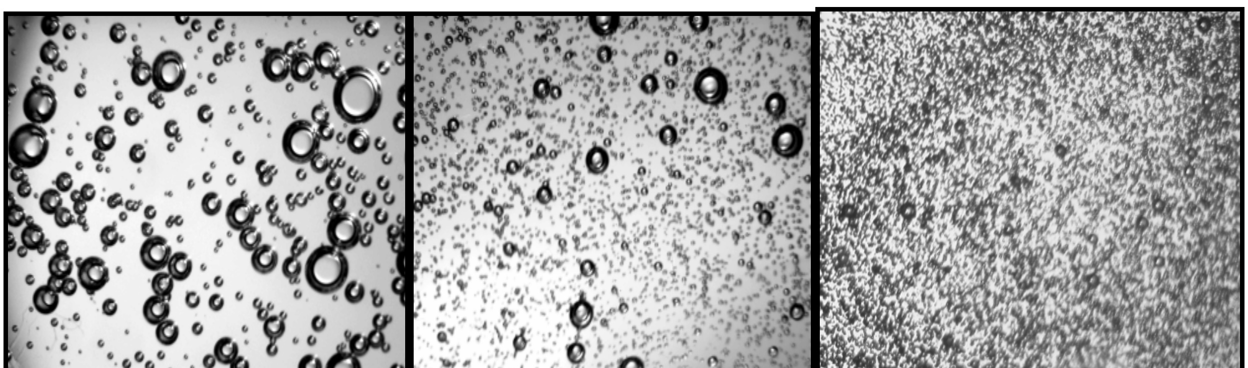

Original Fluid

After First Pass through the Filter

After Second Pass through the Filter

Clearly, each pass of the mud through the filter reduced the concentration of large bubbles significantly, but at the same time it greatly increased the concentration of small bubbles.

Viscosity of fluid samples containing different initial BSD's was measured in 250- and 500-μm steel capillary tubing (see apparatus in Figure 31) and was compared with the viscosity of that same mud deaerated by centrifugation. The results of these experiments are presented in Table 3, which shows that – at the air concentrations used in this work (ranging from 18 to 30 vol %)— the pressure vs flow rate relationships of the fluid in the two capillary tubes are affected neither by entrained air nor by the BSD of the air, i.e. viscosity of the fluid is <u>not</u> affected by aphrons, regardless of their size.

Although a shift of the BSD in the direction of smaller bubbles does not change the bulk viscosity of the fluid, it does appear to increase its resistance to flow in media with smaller openings, such as the 15-µm filter. The relationship between pressure and flow rate as a function of number of passes through the 15-µm filter is presented in Figure 60.

Table 3. Pressure (psig) Required to Pass Fluid Through Capillary Tubing.

Flow rate, mL/min	Without air		With Air After first filter pass		With Air After second filter pass	
	250 µm	500 µm	250 µm	500 µm	250 µm	500 µm
0.25	139		140		142	
0.5	187	46	186	50	184	51
1	270	59	269	59	262	58
2.5	456	79	453	79	452	77
5	710	105	703	105	705	104
7.5	934	128	928	128	930	128
10		148		146		146
20		216		215		215
25		248		247		247

The greater resistance to flow in the filter vs the long capillary tubes may be explained in two ways: (a) the force that is required to change the curvature of small bubbles during forced entry into small openings is greater than the force required to change the curvature of larger bubbles; and (b) high concentrations of small bubbles can physically block openings more effectively than lower concentrations of large bubbles. The latter is thought to be the more likely possibility and is analogous to conventional bridging of permeable media by particulates.

Figure 60. Pressure vs. Flow Rate for APHRON ICS™ Fluid after Passage through 15-µm Filter

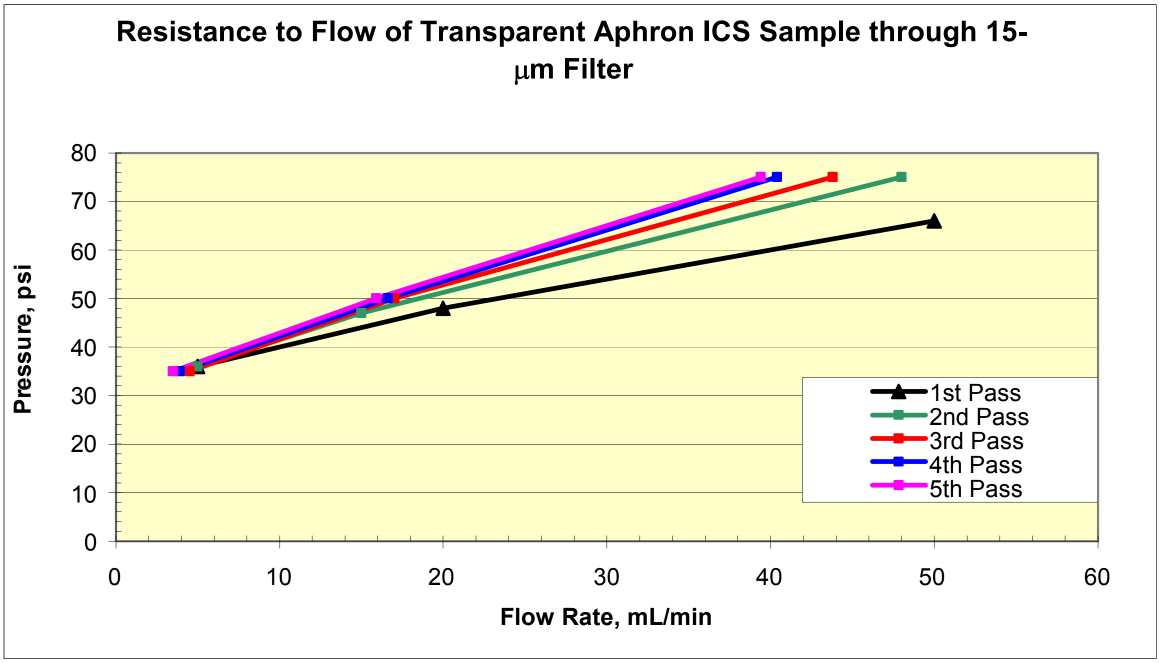

Shearing of Aphrons at Elevated Pressure

In these experiments, which were carried out in the apparatus shown in Figure 14, fluid from one accumulator was passed through the filter, then through the VRD Viewing Cell and BPR, and finally into the second accumulator. BSD in the Viewing Cell was recorded, and pressure was regulated with the BPR.

A 2-µm filter was used with a transparent APHRON ICS™ mud, and a 90-µm filter was used with an SE APHRON ICS™ fluid. The large-pore filter was used for the whole mud to avoid plugging by particulates. Both fluids contained 15-18 vol % air before the experiments were begun. At 500 psig (3.5 MPa) after passing through the filters, the aphrons were no longer visible under 40X magnification: evidently they disintegrated and the air dissolved in the fluid. The images of SE APHRON ICS™ acquired at 500 psig (3.5 MPa) before and after passage through the 90-µm filter are shown in Figure 61.

Figure 61. SE APHRON ICS™ Fluid before and after Passage through 90-μm Filter

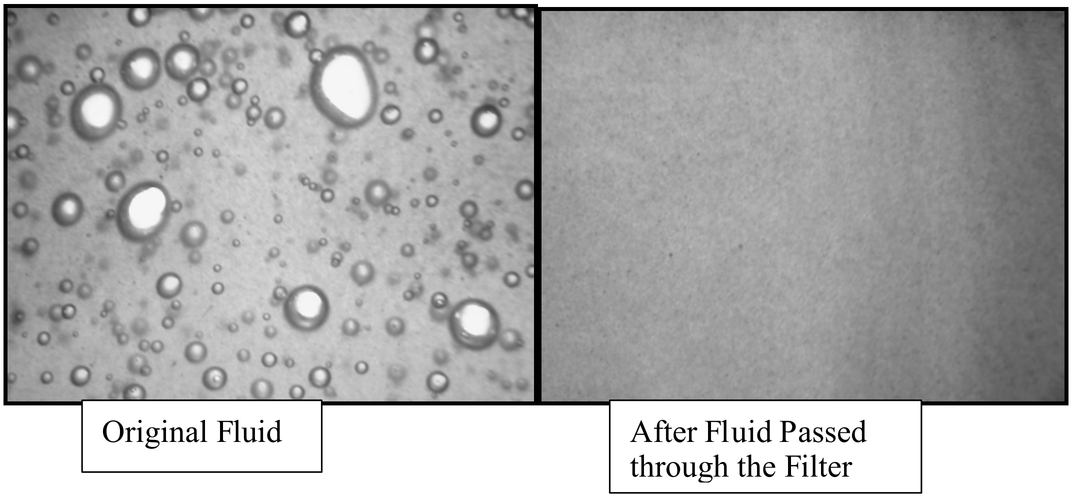

To better define the roles of pore size and pressure on survivability of aphrons, the design of the apparatus was modified by adding a second VRD Viewing Cell to the system. The two Viewing Cells simultaneously record size and concentration of bubbles before and after filtration. A diagram of the modified apparatus is shown in Figure 16.

The SE APHRON ICS™ fluid with 18% air was pumped through a 440-μm strainer (see Figure 15) and images of the fluid were recorded before and after filtration at 1.8, 3.5 and 5.2 MPa (250 psig, 500 psig and 750 psig). The images of the mud acquired before and after filtration at each pressure are shown in Figure 62.

These images show that a filter with openings as large as 440 μm can create enough shear to comminute the bubbles to a very small, almost invisible size. As shown previously, all bubbles (including aphrons) decrease in size with increasing pressure according to Boyle's Law; in addition, at elevated pressure there is a substantial driving force for air to diffuse out of the bubbles, which causes them to shrink continuously. Eventually the bubbles shrink to a critical size below which the bubble membrane cannot be sustained, and the bubbles collapse into submicroscopic swollen micelles. Evidently the stabilizing shell of an aphron is fairly sensitive to shear and the aphrons can be comminuted with relative ease; it is likely that, as the aphron is changing shape and size from being sheared, it becomes highly permeable (leaky) and less able to contain the gas within.

Figure 62. SE APHRON ICS^{TM} Fluid before and after Passage through 440-µm Strainer

250 psi

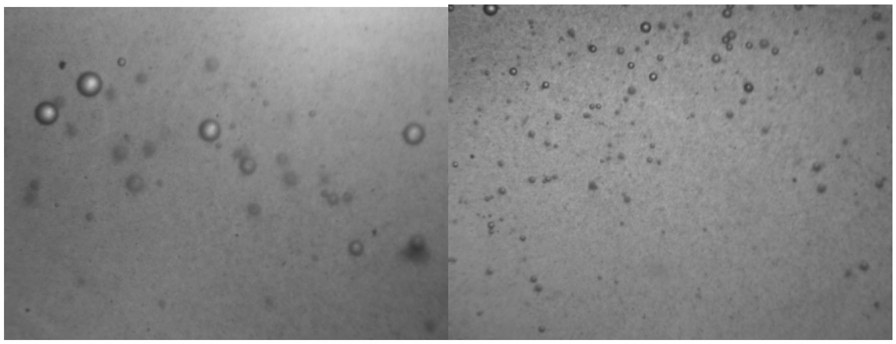

Before After

500 psi

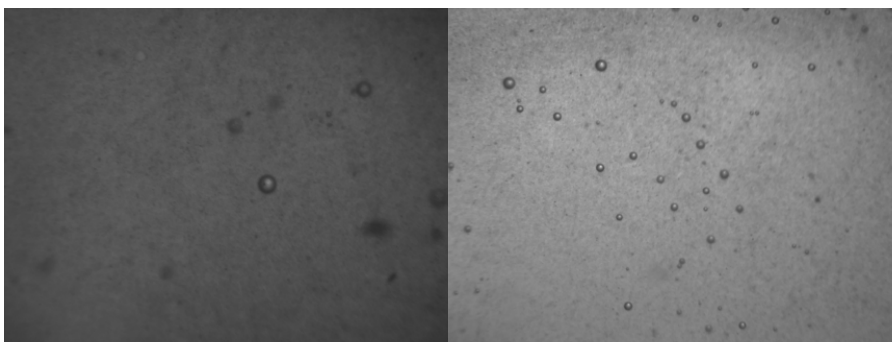

Before After

750 psi

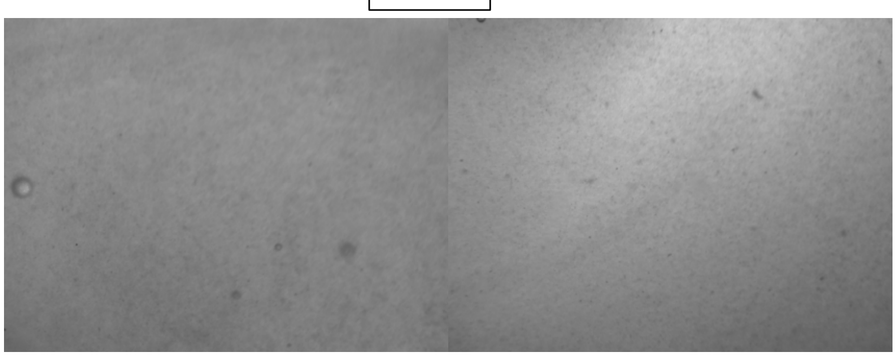

Before After

Effect of Method of Generating Aphrons:

Air was entrained in an APHRON ICS™ drilling fluid using the three types of mixers. Bubble stability was measured using the standard Density Change method and Bubble Compression Resistance. The results indicate that, while there is some difference in generation of the aphrons with a kitchen blender, the samples mixed with the the Silverson L4RT and Prince Castle mixers produced SuperEnhanced APHRON ICS™ drilling fluids with similar physical properties, BSD and aphron stability; these were superior to the drilling fluids produced with a General Electric kitchen blender. Although larger bubbles have been shown to withstand compression better than do smaller bubbles, they also tend to coalesce faster and separate from the body of the liquid at a more rapid rate.[19]

Next was tested the APV Gaulin Homogenizer, i.e. shear with a single spindle mixer versus shear / cavitation / extension with a pressure-drop pump. The following operating parameters were used: (a) the Prince Castle mixer at 7,000 rpm for 6 min (control sample), (b) the Gaulin Homogenizer with one pass (fluid pumped through once) at 27.4 MPa (4,000 psi) and (c) the Gaulin Homogenizer with recirculation for 2 minutes at 27.4 MPa (4000 psi). Some significantly different mud properties were observed from these three treatments, particularly with regard to Brookfield viscosity and BSD. After only one pass, the Gaulin Homogenizer reduced the LSRV of the fluid significantly and produced a smaller BSD than the Prince Castle mixer; with multiple passes, the LSRV dropped by an order of magnitude. This is explained by the very high shear rate that the Gaulin Homogenizer imparts to the fluid, which can result in fragmentation of the viscosifying polymer.

Nevertheless, it was considered instructive to examine in closer detail the effects of subjecting the APHRON ICS™ mud to a pressure drop, since in the past it was thought necessary to subject an aphron drilling fluid to a pressure drop in order to generate aphrons.[1] For this purpose, tests were designed to simulate downhole conditions. A simple 1-mm orifice was installed in the Canty Viewing Cell of the HTHP Circulating System; a pressure drop was imposed across the orifice by maintaining the inlet pressure at 13.7 MPa (2000 psig) in all cases, while the Viewing Cell was maintained at 0.1 or 10.3 MPa (0 or 1500 psig), i.e. ΔP = 3.4 or 13.7 MPa (500 or 2000 psi) instead of the 27.4 MPa (4000 psi) of the Gaulin Homogenizer. The specifications of the tests were as follows:

- Test #1: Injection of <u>aerated</u> mud at 13.7 MPa (2000 psig) through a 1000-µm orifice into the Viewing Cell filled with <u>de-aerated</u> mud at <u>ambient pressure</u>. Results are shown in Figure 63.
- Test #2: Injection of <u>de-aerated</u> mud at 13.7 MPa (2000 psig) through a 500-µm orifice into the Viewing Cell filled with <u>de-aerated</u> mud at 10.3 MPa (1500 psig). See Figure 64.
- Test #3: Injection of <u>aerated</u> mud, <u>held at 13.7 MPa (2000 psig) for 2 min,</u> through a 500-µm orifice into the Viewing Cell filled with <u>de-aerated</u> mud at 10.3 MPa (1500 psig). See Figure 65.

Figure 63. Injection of Aerated Mud at 13.7 MPa (2000 psig) into De-Aerated Mud at 0.1 MPa (0 psig)

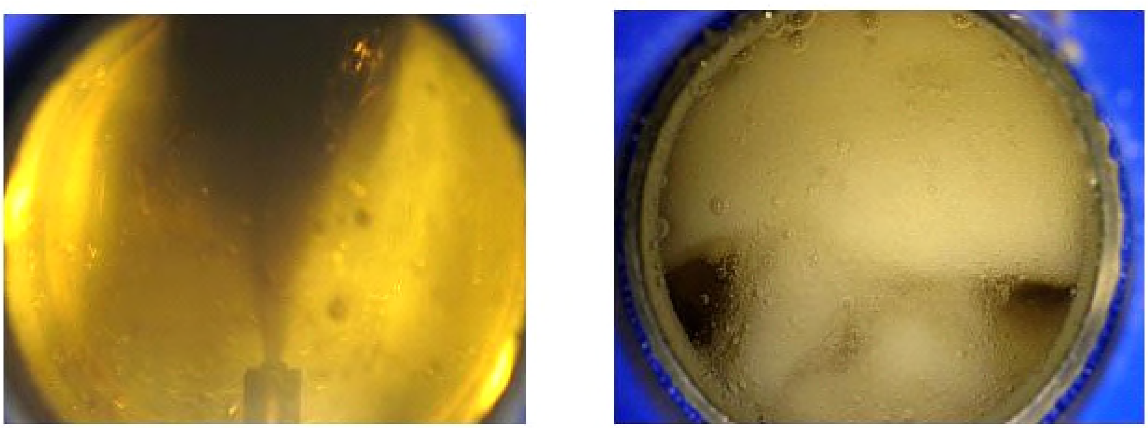

Initial Injection

End of Test

These photos indicate that, if the mud system already contains undissolved air (aphrons), a pressure drop can induce the aphrons to expand and perhaps form new ones (Test #3, Figure 65). However, when the mud is de-aerated via centrifugation and injected at 13.7 MPa (2000 psig) into de-aerated mud at 10.3 MPa (1500 psig), aphrons are <u>not</u> formed (see Test #2, Figure 64).

Figure 64. Injection of Deaerated Mud at 13.7 MPa (2000 psig) into Deaerated Mud at 10.3 MPa (1500 psig)

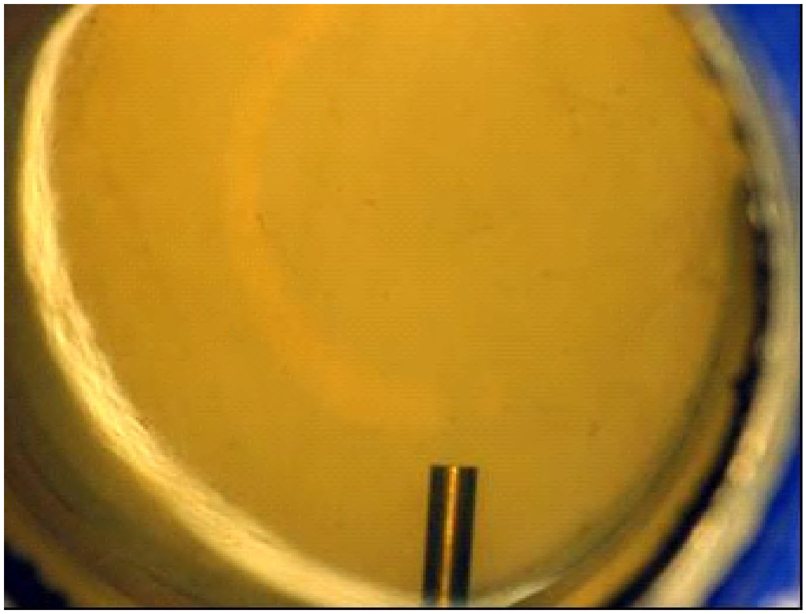

Figure 65. Injection of Aerated Mud Held at 13.7 MPa (2000 psig) for 2 min into De-aerated Mud at 10.3 MPa (1500 psig)

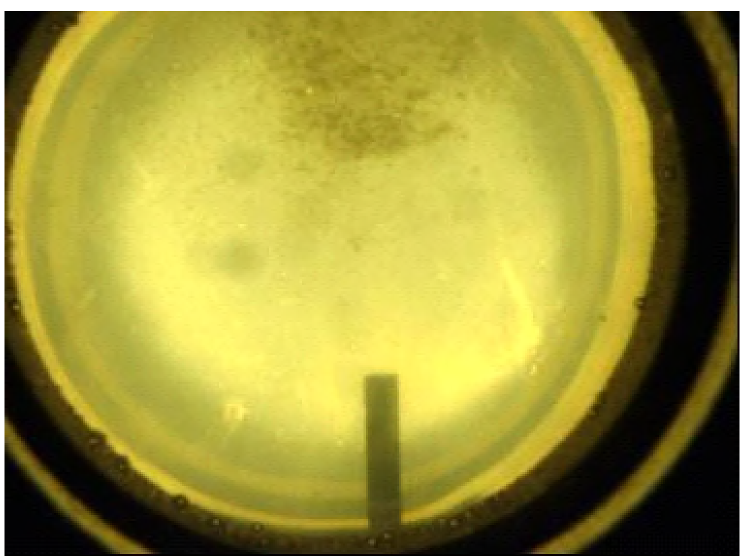

A modification of Test #3 was carried out, the difference being that the mud was held at 13.7 MPa (2000 psig) for 15 min instead of 2 min. Within that time frame, most of the aphrons were expected to have degraded to such an extent that very few of them would still be around. The results are shown in Figure 66.

Figure 66. Injection of Aerated Mud Held at 13.7 MPa (2000 psig) for 15 min into De-aerated Mud at 10.3 MPa (1500 psig)

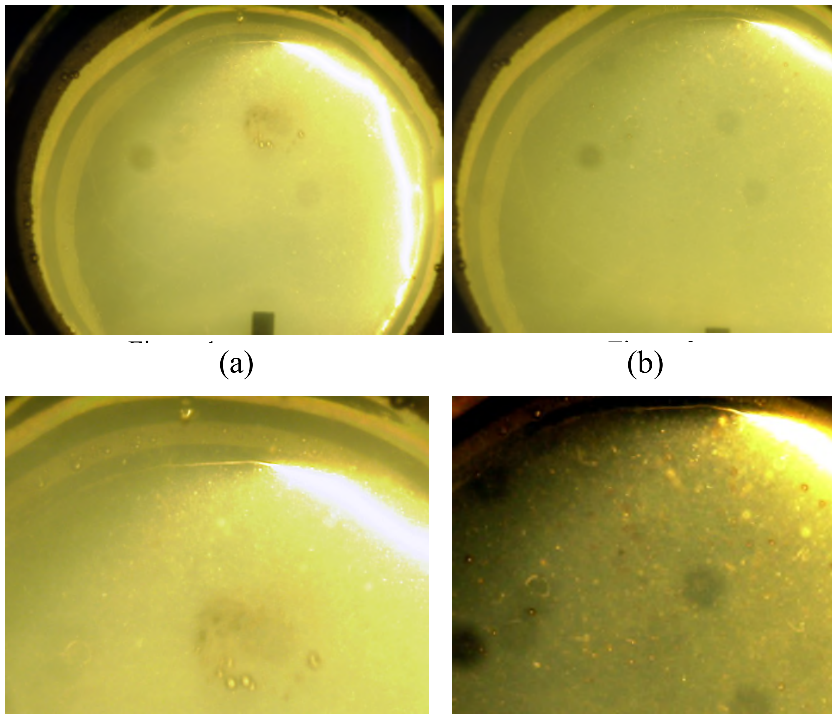

(a) (b)

Enlargement of (a) Enlargement of (b)

Very few aphrons were observed exiting the orifice, indicating that aphrons cannot be created from dissolved air if the pressure on the low side (10.3 MPa, or 1500 psig, in this case) is sufficiently high that the system is under-saturated with air. Indeed, the system pressure must drop below the point where the concentration of air in solution exceeds the solubility limit.

Verification tests were conducted by passing the SE Aphron ICS™ fluid through a 500-µm nozzle from a constant pressure of 13.7 MPa (2000 psig) into a chamber maintained at 10.3 MPa (1500 psig). In previous tests using an SE Aphron ICS™ drilling fluid that was maintained at 13.7 MPa (2000 psig) for 1 hr, no aphrons appeared to form. For SE Aphron ICS™ Mud that was maintained at 13.7 MPa (2000 psig) for only 15 min prior to the start of a test, the number of visible bubbles emanating from the orifice also was insignificant, but waves of lighter mud were again expelled and these appeared to show more contrast in light intensity.

This wave phenomenon is generally interpreted as a density gradient in the fluid, but it is not at all clear whether it arises from variation in the density of the liquid phase or from the presence of very small bubbles. Further testing was performed using the Transparent APHRON ICS™ formulation with distilled water (to eliminate optical interference) and at higher magnification (~60X). Figure 67 shows a lighter wave of material moving down the viewing area; this was followed by some distinctly visible bubbles. Due to low available light, the "Night Shot" camera mode was used, giving the pictures a green cast. The nature of the wave pattern is still not known. Many small aphrons that are not distinguishable with our optical system <u>may</u> be present in the wave pattern. Further investigation is required to determine the nature of these waves.

Figure 67. Transparent APHRON ICS™ Mud Shot through 500-μm Nozzle with P_{inlet} = 2000 psig and P_{outlet} = 1500 psig

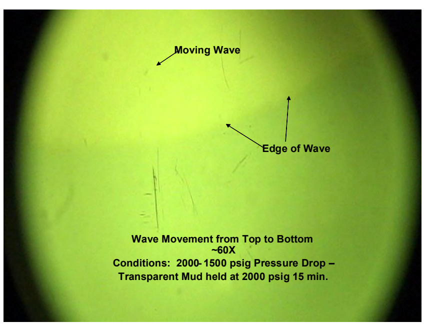

Wave Photo #1

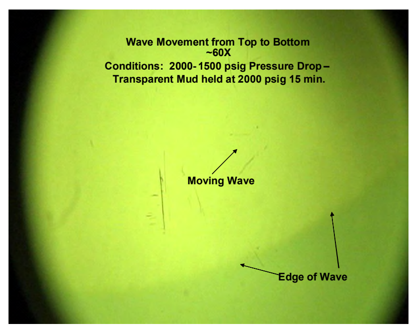

Wave Photo #2

Effect of Fluid Composition:

The effect of chemical composition on bubble stability was examined using a soap solution, a Standard APHRON ICS™ mud and a SuperEnhanced (SE) APHRON ICS™ mud. Figure 68 shows how aphrons from these three fluids withstand an applied pressure of 500 psig over a period of time. Initially, the bubbles used in this comparison were of similar size (about 950 μm).

Figure 68. Effect of Fluid Composition on Aphron Stability

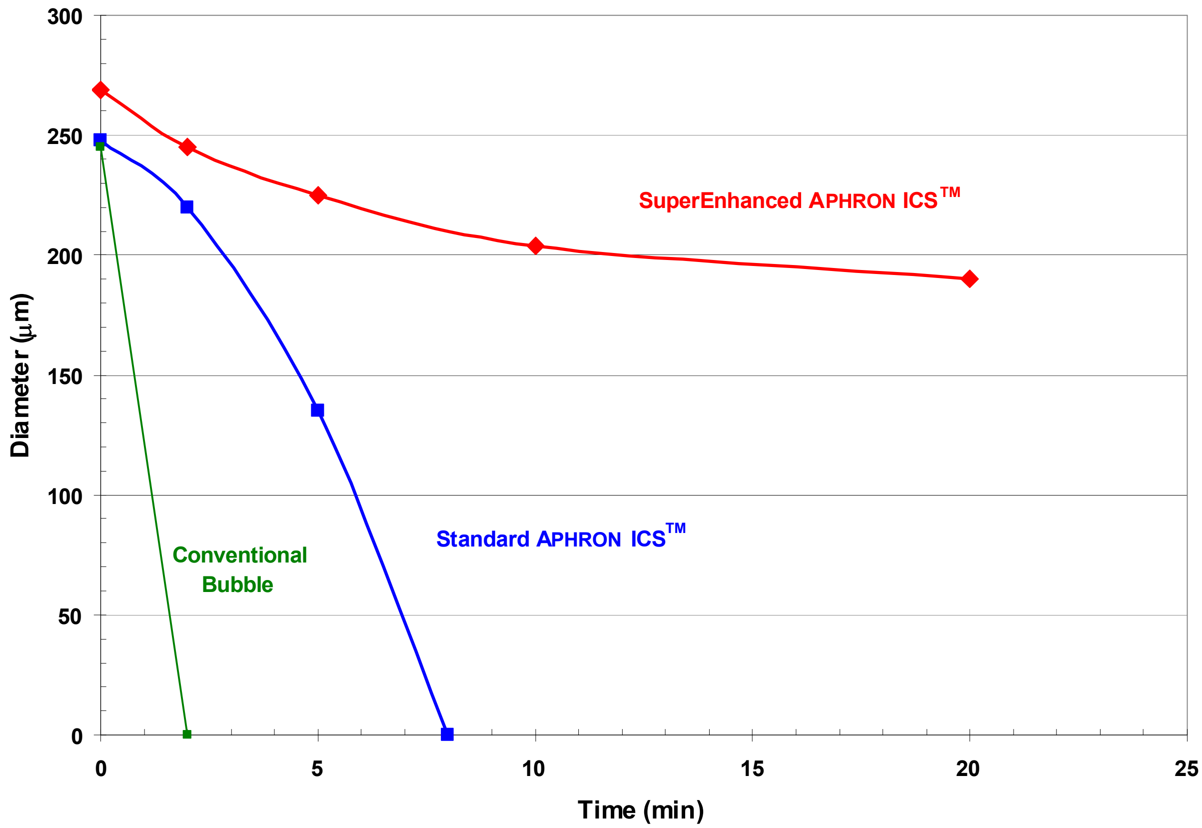

Immediately after pressurizing to 500 psig, all three bubbles – according to the Ideal Gas Law – should have been compressed to about 290 µm; instead, they shrank to 250 - 270 µm. It is clear that even immediately after pressurization, the bubbles from the soap solution ("Conventional Bubble") and the standard APHRON ICS™ mud deviate from ideal behavior by almost twice as much (14%) as the aphron from the SE APHRON ICS™ mud (7%). With time, the bubbles from both muds continued to shrink, but the SE aphron shrank significantly more slowly than the standard aphron and considerably more slowly than the conventional bubble. Equation (5) may be used to treat the rate of loss of nitrogen from aphrons. Thus,

$$dV/dt \propto S^2 \tag{7}$$

where *dV/dt* represents the change in bubble volume and *S* the bubble size (diameter). By making appropriate substitutions and rearranging (7), we obtain

$$dS/dt = g \tag{8}$$

where g is a constant. Integration of (8) gives

$$S_t = S_0 - 2gt/\pi \qquad (9)$$

Where S_t and S_0 are the bubble diameters at time t and time 0, respectively. For the SE mud, S_0 = 270 μm, and S = 190 μm at 20 min. This gives $g = 6.28\ \text{min}^{-1}$. For the Standard mud, the only measurement we have besides S_0 = 270 μm is S = 135 μm at 5 min, which gives $g = 42.4\ \text{min}^{-1}$, while for the soap solution g is so large that it is not calculable. Thus, the rate of loss of air is almost an order of magnitude greater in aphrons from the Standard mud than from the SE mud. This conclusion is probably conservative, as it appears from Figure 64 that the rate of air loss from the Standard mud accelerates after 5 min. Even for the aphron from the APHRON ICS™ mud, Expression (9) is probably not quite correct. In deriving it, it was assumed that aphron stability was not impacted by the compression process itself. As shown in the following section, the rate of compression and decompression can affect aphron stability; during the compression process, surfactant and polymer molecules in the shell must rearrange and very likely lose nitrogen at a faster rate during that process.

Figure 69. Structural Schematic of Aphron Structure (after Sebba[5])

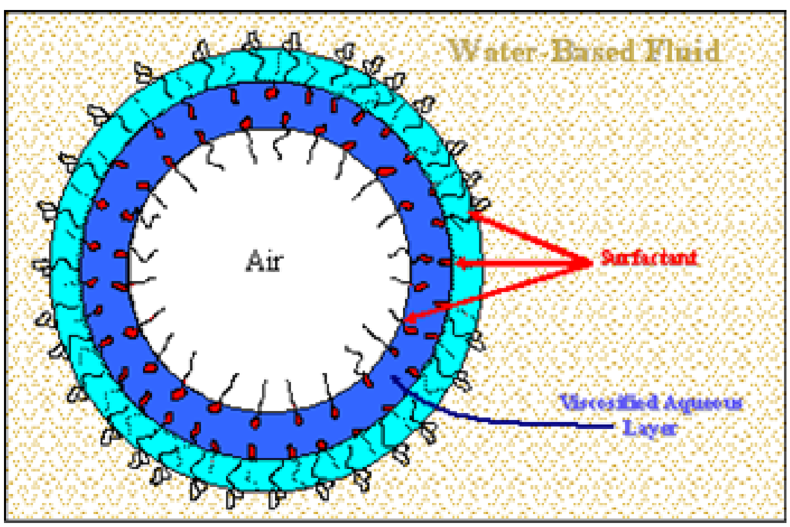

If the fit of the data from the SE APHRON ICS™ fluid is only fair, it is much worse for the other two fluids. The downward turn of the curve for the aphron from the Standard APHRON ICS™ mud is consistent with a second mechanism that involves rapid shrinkage and ultimate destruction of the aphron below some threshold size, which is consistent with previous data which indicate that at elevated pressure aphrons do not survive long after attaining a size less than 100 µm.

Aphrons are thought to possess a tri-layer of surfactants, as shown in Figure 69. Photographs of an SE APHRON ICS™ system at high magnification (400X) are shown in Figures 70 and 71.

Figure 70. APHRON ICS™ Fluid containing 10 lb/bbl of ACTIGUARD

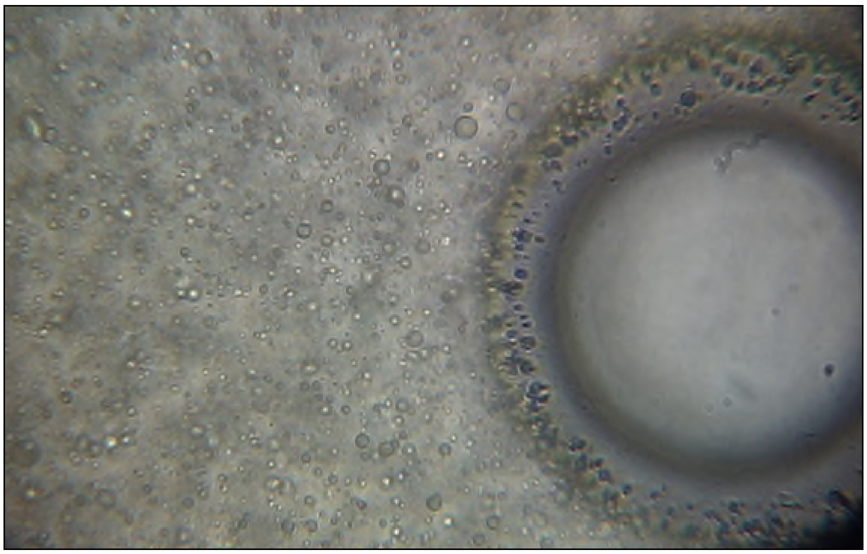

Figure 71. SE APHRON ICS™ Fluid Containing 10 lb/bbl ACTIGUARD

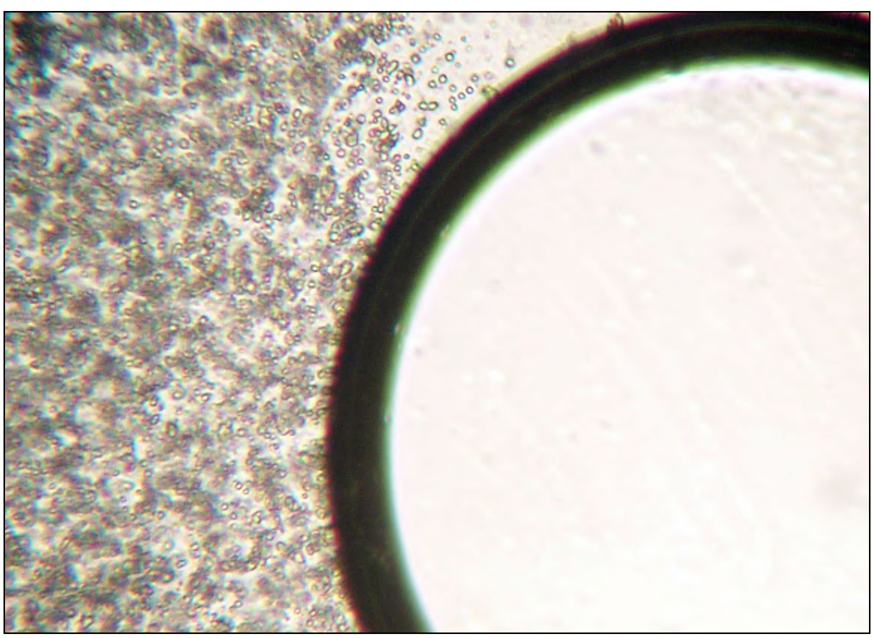

The large structure on the right in both photographs is an aphron several hundred microns in diameter, whereas the smaller lightly dyed globules of a few microns diameter are primarily ACTIGUARD. Cover slips were used in both cases. Figure 70 was taken with a higher-resolution microscope, and the sample was back-lit to bring out the 3-D character of the structures. It seems to suggest that there is a significant membrane, perhaps a few tens of microns in thickness, surrounding the aphron, but it is difficult to conclude anything else from these photos. Environmental SEM photos were also taken of these samples, an example of which is shown in Figure 72, but the polymer/surfactant residue that is left after the explosive loss of air during vacuum exposure seems to have no identifiable structure that can be associated only with the aphrons.

Figure 72. E-SEM Photo of SE APHRON ICS™ Fluid

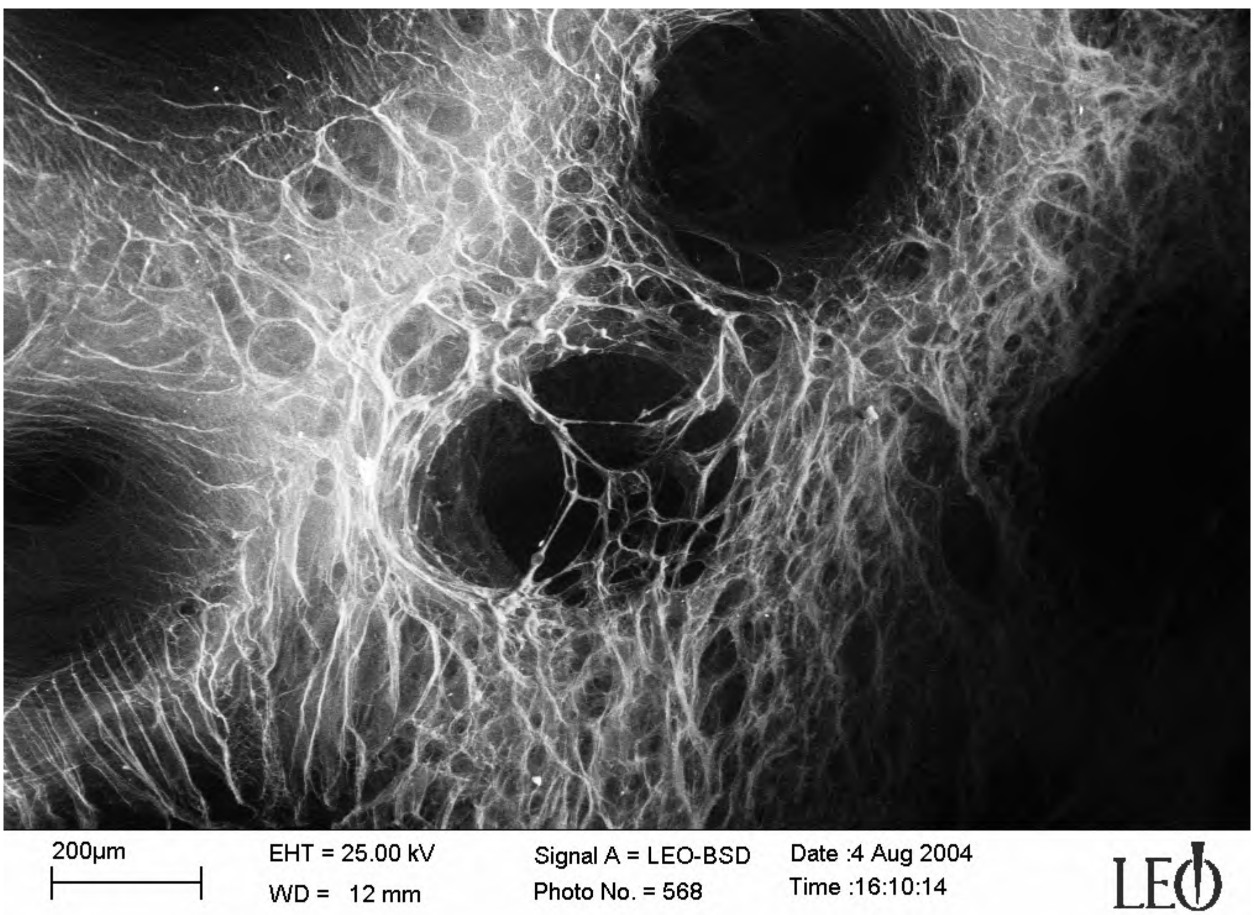

Given the sensitivity of aphrons to pressure, shear and method of entraining air, perhaps modification of the chemical composition of the drilling fluid can improve the resistance of the aphrons to these stresses. With this in mind, tests were devised to vary the concentrations of key components in the SE APHRON ICS™ drilling fluid. A test matrix was devised consisting of 16 formulations with varying concentrations of GO-DEVIL II and the three aphron stabilizers APHRONIZER A, APHRONIZER B and PLASTISIZER, as shown in Table 4. Aphron survivability was determined by monitoring the full bubble size distribution (BSD) after pressurizing the fluid to 500 psig and maintaining it at that pressure under static conditions; complementing these measurements were measurements of the rate of shrinkage of individual aphrons at that pressure.

Table 4. Test Matrix for Optimization of APHRON ICS™ Drilling Fluid Composition

Formulation	Soda Ash (ppb)	X-Cide (ppb)	Activator II (ppb)	Go-Devil (ppb)	Activator I (ppb)	Blue Streak (ppb)	Aphronizer A (ppb)	Aphronizer B (ppb)	Plasticizer (ppb)
1	3	0.1	2	3.5	5	1	0.25	0.25	0.2
2	3	0.1	2	5	5	1	0.25	0.25	0.2
3	3	0.1	2	3.5	5	1	0.25	0.25	0.4
4	3	0.1	2	5	5	1	0.25	0.25	0.4
5	3	0.1	2	3.5	5	1	0.25	0.6	0.2
6	3	0.1	2	5	5	1	0.25	0.6	0.2
7	3	0.1	2	3.5	5	1	0.25	0.6	0.4
8	3	0.1	2	5	5	1	0.25	0.6	0.4
9	3	0.1	2	3.5	5	1	0.75	0.25	0.2
10	3	0.1	2	5	5	1	0.75	0.25	0.2
11	3	0.1	2	3.5	5	1	0.75	0.25	0.4
12	3	0.1	2	5	5	1	0.75	0.25	0.4
13	3	0.1	2	3.5	5	1	0.75	0.6	0.2
14	3	0.1	2	5	5	1	0.75	0.6	0.2
15	3	0.1	2	3.5	5	1	0.75	0.6	0.4
16	3	0.1	2	5	5	1	0.75	0.6	0.4

A typical example is Formulation #8, with 0.25 ppb APHRONIZER A, 0.6 ppb APHRONIZER B and 0.4 ppb PLASTISIZER (compared to the SE formulation which contains 0.5, 0.5 and 0.3 ppb, respectively, of these products). Figure 73 shows the effect of pressurizing this sample to 500 psig. Through the application of the image analysis software NI Vision Assistant, BSD's can be generated in the form of Differential Volume, Cumulative Volume or # Bubbles vs Size. The Total Volume of Air in the sample can be obtained by integrating the Differential Volume curve. For example, in Formulation #8 at 500 psig, the Total Volume of Air calculated via image analysis is 0.45 vol %. This compares quite favorably with the volume of air predicted from application of the modified Ideal Gas Law to the measured initial volume of air: $V_{final} = P_{initial}V_{initial}/V_{final}$, i.e. 15 vol % at ambient pressure (14.7 psia) is reduced to 0.42 vol % at 500 psig (514.7 psia).

Shown in Figures 74 and 75 are BSD's that were determined for Formulations #8 and #15, respectively, at 500 psig immediately after pressurization and 10 minutes later.

Figure 73. Image of APHRON ICS™ Formulation #8 Compressed to 500 psig

P = Ambient, T = Ambient

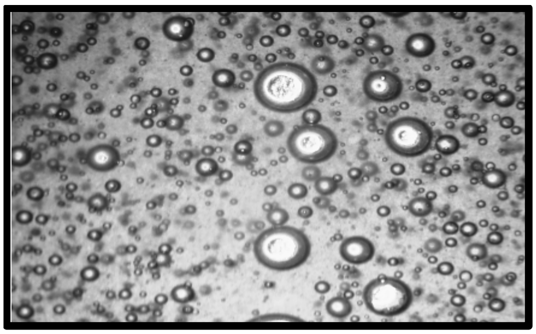

P = 500 psig, T = Ambient

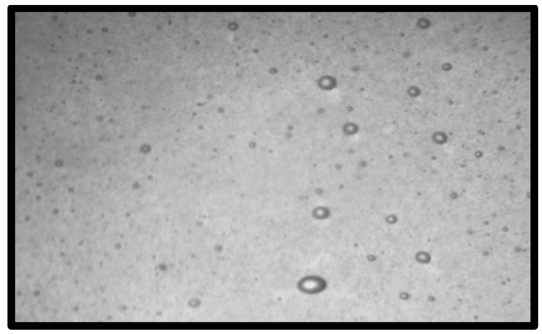

Figure 74. Survivability of Aphrons in Formulation #8

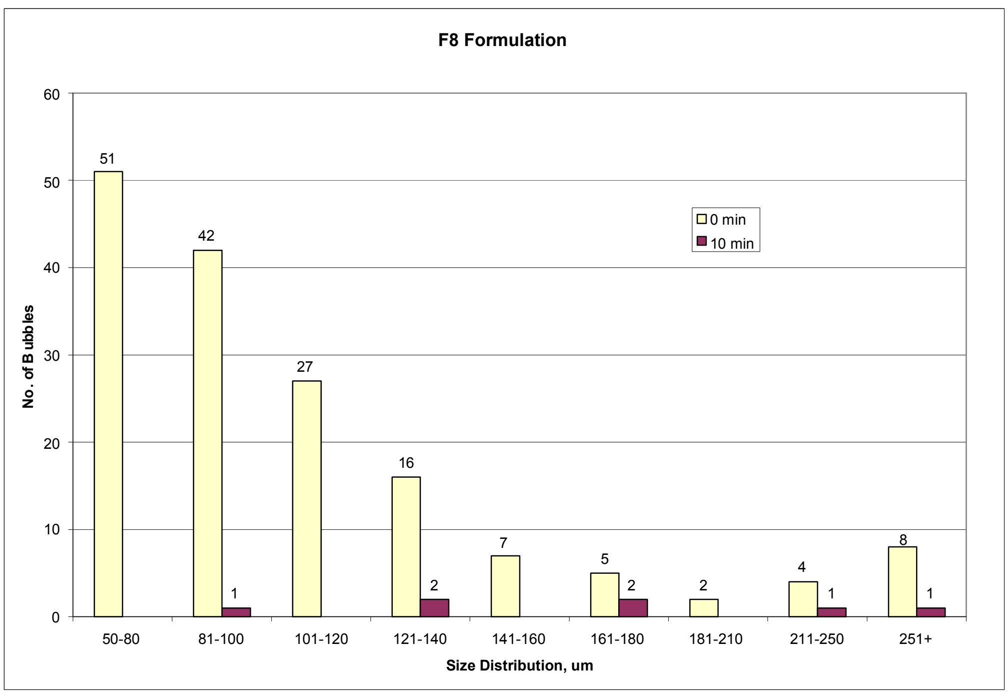

One can clearly see how many aphrons survived and how they shrunk over the 10-min period. It will be noted that no aphrons were observed that were smaller than 50 μm diameter, consistent with our previous observations and those of Sebba.[5]

Figure 75. Survivability of Aphrons in Formulation # 15

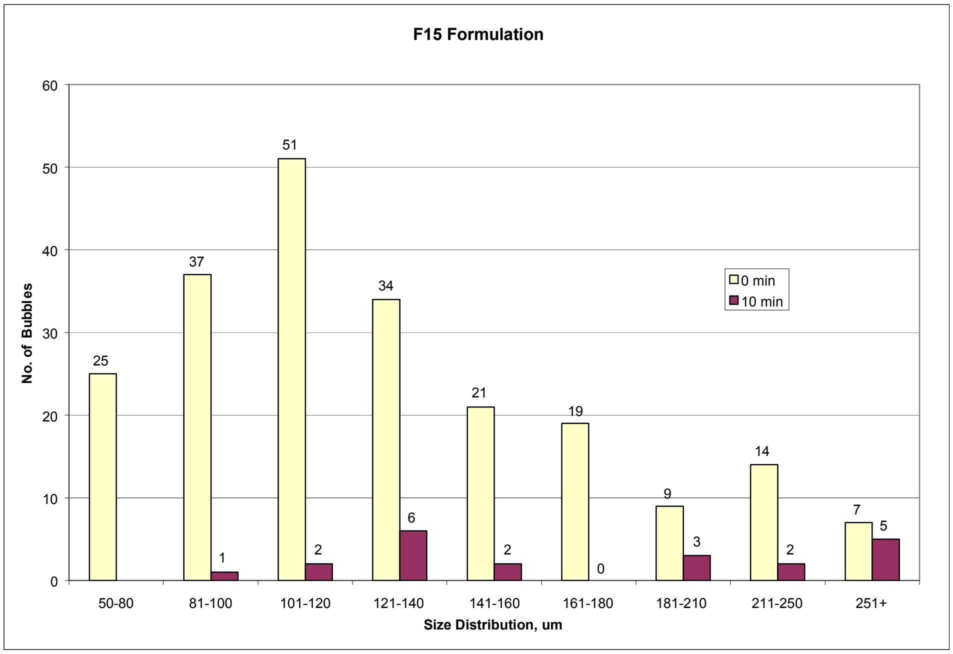

The outcome of the analysis is that formulations such as # 15 which have a reduced concentration of GO-DEVIL II (3.5 vs 5.0 lb/bbl) and a raised concentration of PLASTISIZER (0.4 vs 0.3 lb/bbl) generally yielded longer lasting bubbles than the SE APHRON ICS™ Mud (not shown). However, as stable as the aphrons may be in the "best" of these fluids (such as formulation # 15), even greater stability is highly desirable.

Other components, such as BLUE STREAK, were also varied. In the case of BLUE STREAK, it was found that the amount of air entrained in a fluid generally increases with increasing amount of BLUE STREAK up to 4 lb/bbl. Conversely, increasing the concentration of ACTIGUARD tends to suppress the amount of entrained air. In neither case, however, were any effects observed on bulk mud properties, such as viscosity. For example the effect of increasing the concentration of BLUE STREAK from 0.5 to 3 ppb on LSRV is shown in Figure 76. No apparent change in LSRV was noted for deaerated samples of the mud. When air was introduced, however, LSRV appeared to drop a little between 1 and 3 ppb BLUE STREAK, but the effect is not considered very significant.

Figure 76. Effect of [Blue Streak] on LSRV

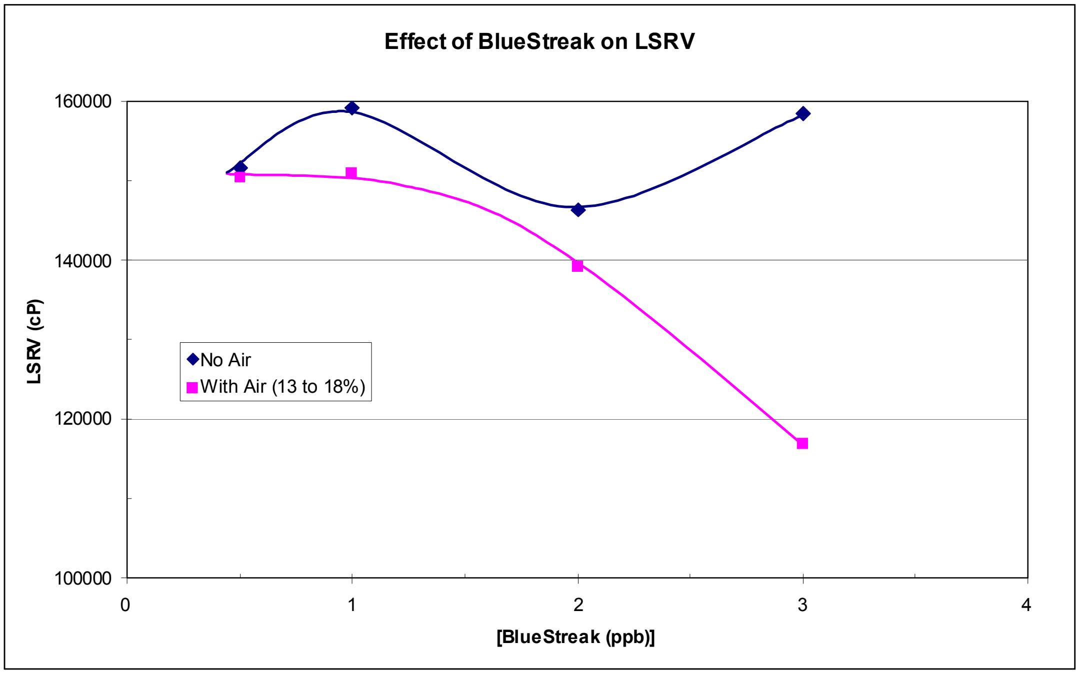

Additional modifications were made to the SE APHRON ICS™ fluid in an effort to improve aphron longevity. Rather than modify the levels of current components, alternative additives to the aphron stabilization package were considered. These included some conventional crosslinking agents and plasticizers, but none showed any improvement in aphron longevity.

In previous tests designed to optimize the current SE APHRON ICS™ formulation, aphron survivability (longevity) has been determined primarily by monitoring the rate of change in bubble size distribution (BSD) and size of individual aphrons at 500 psig (3.5 MPa) under static conditions. However, it was learned from flow studies in capillary tubes and permeable cores that bubble stability is greatly affected by passage through these media, presumably due to the shear forces involved (see Section on Effect of Shear on Aphron Longevity); similar phenomena may occur downhole during invasion of aphron drilling fluids into permeable formations. These findings begged for a new test procedure to optimize the aphron drilling fluid formulation. The Dual VRD Shear Test (see Figure 16) was employed for this purpose, using (a) ambient pressure and (b) a pressure sufficiently high that the fluid is below the solubility limit for air (or nitrogen), thus ensuring that there is sufficient driving force to permit all of the air entrained in an APHRON ICS™ mud to go into solution if the aphrons are leaky enough.

Will the aphrons be chopped into finer bubbles, will they coalesce or will they simply vanish? Initial tests were carried out at ambient pressure with the SuperEnhanced (SE) APHRON ICS™ drilling fluid. The results from four tests carried out at different flow rates are shown in Figure 77. Because the overall BSD did not appear to generate any differences among different fluids, analysis was carried out on only the five largest bubbles in the field of view before and after passing the frit, and the smallest and largest of these five are recorded in Figure 77. It is evident from these results that the maximum bubble size increased by as much as a factor of 2, i.e. some coalescence occurred.

Figure 77. Bubble Size Distribution in APHRON ICS™ Fluid Before and After Passing through Frit at Ambient Pressure

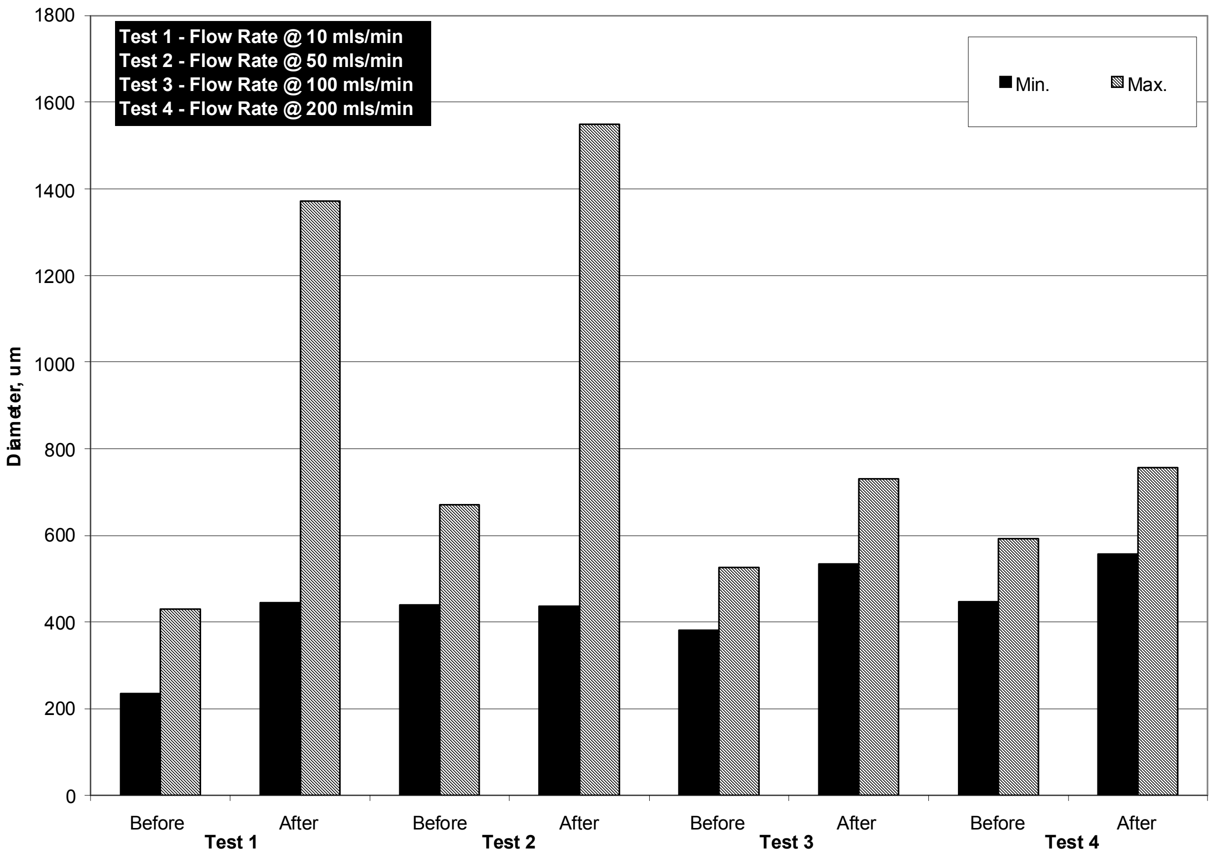

A back-pressure regulator was added to the Dual VRD Shear Test Apparatus for tests at elevated pressure, and the tests were repeated at constant pressure, rather than constant flow rate. Initial tests at several hundred psi with a 440-µm frit confirmed what was shown earlier, namely that shear influences the survivability of aphrons as much as pressure and time. Aphrons do not survive passage through a permeable medium at elevated pressure (even a thin frit) unless the fluid system has become saturated with air (nitrogen); although the average concentration of air or nitrogen in aphron drilling fluids will never reach that level downhole, in principle Bubbly Flow can produce such an environment, though only at the fluid front.

To analyze properly how fluid composition affects aphron survivability, any test method for a benchmark fluid must generate a significant population of bubbles that can be analyzed. Therefore, it was decided to repeat the Dual VRD Shear Tests at a reduced pressure of 100 psig, which, according to Henry's Law, should yield a supersaturated solution of air if all of the aphrons fail, i.e. the total amount of air in the fluid is above the solubility limit. Thus, a greater percentage of aphrons is expected to survive flow through the 440-µm frit at 100 psig than at 300 psig. Indeed, a large number of aphrons did survive at this reduced pressure. However, the BSD's for the Standard and SE APHRON ICS™ fluids were so similar as to be indistinguishable. Even conducting statistics only on the largest bubbles, as shown in Figure 78, did not yield much – if any – difference between the mud systems. Only at a flow rate of 100 mL/min did the SE APHRON ICS™ fluid demonstrate a significantly larger average bubble size (for the five largest bubbles) than the Standard APHRON ICS™ fluid.

Thus, it was concluded that the Dual VRD Shear Test does not provide sufficient differentiation between the Standard and SE APHRON ICS™ muds to make this a suitable test method for correlating aphron stability with mud composition.

It should be noted, however, that although modifications of the components did not appear to affect aphron longevity significantly, the same cannot be said for the performance of the aphron drilling fluid in sealing permeable formations and its interaction with producing formations. This is particularly true for the surface active components (such as BLUE STREAK) and particulates (such as MgO). Some of these effects are described in the sections on Sealing of Permeable Formations and Wettability.

Figure 78. Comparison of the five largest surviving aphrons in the Standard APHRON ICS™ vs SE APHRON ICS™ fluids after passage through a 440-µm frit at 100 psig

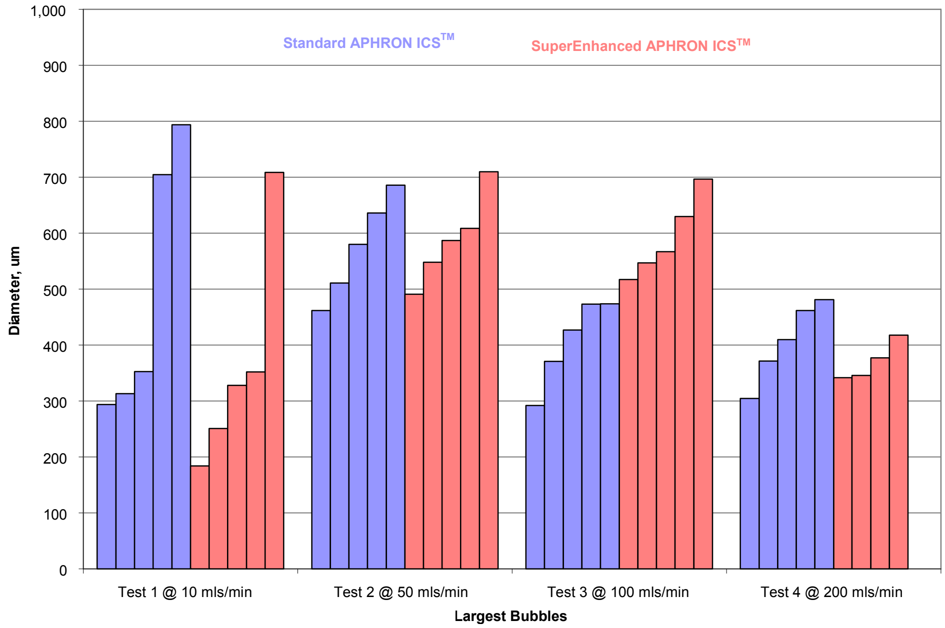

Pressure Transmissibility:

Pressure Transmission in 6.1-m (20-ft) 0.64-cm (¼-in) OD Tube

In these tests, the outlet port of the apparatus shown in Figure 21 was closed, and the inlet pressure (P_1) was raised to 2000 psig very quickly by opening the valve between the accumulator and the test section. The response at the outlet (P_3), which was 6.1 m (20 ft) away, was essentially instantaneous. Indeed, even with millisecond response of the data acquisition system, very little difference was observed among all of the fluids tested. Furthermore, reflection of the acoustic signal from the end of tubing produced complicated results which made it very difficult to extract the rate of propagation of the initial signal.

The test protocol was changed and consistent steady-state pressure differences between the pressure transducers ($\Delta P = P_1 - P_3$) was observed. Steady-state pressure differences were measured initially by applying a stepped pressure ramp from ambient to 2000 psig in the closed tube, holding for several minutes, then depressurizing at the same rate. Consistent pressure-differences ($\Delta P = P_1 - P_3$) were observed. Two aphron drilling fluids containing 5% and 38% air by volume were used. Both muds produced essentially the same results, indicating that the observed behaviors were the result of the base fluid and not related to the aphrons. On the other hand, ΔP appeared to decrease with increasing pressure, e.g. at P_{pump} = 644 kPa (80 psig), ΔP = 115 kPa (17 psi), whereas at P_{pump} = 6.9 MPa (1000 psig), ΔP = 34 kPa (5 psi). See Figure 79.

Figure 79. Pressure Transmissibility in Enhanced APHRON ICS™ Mud

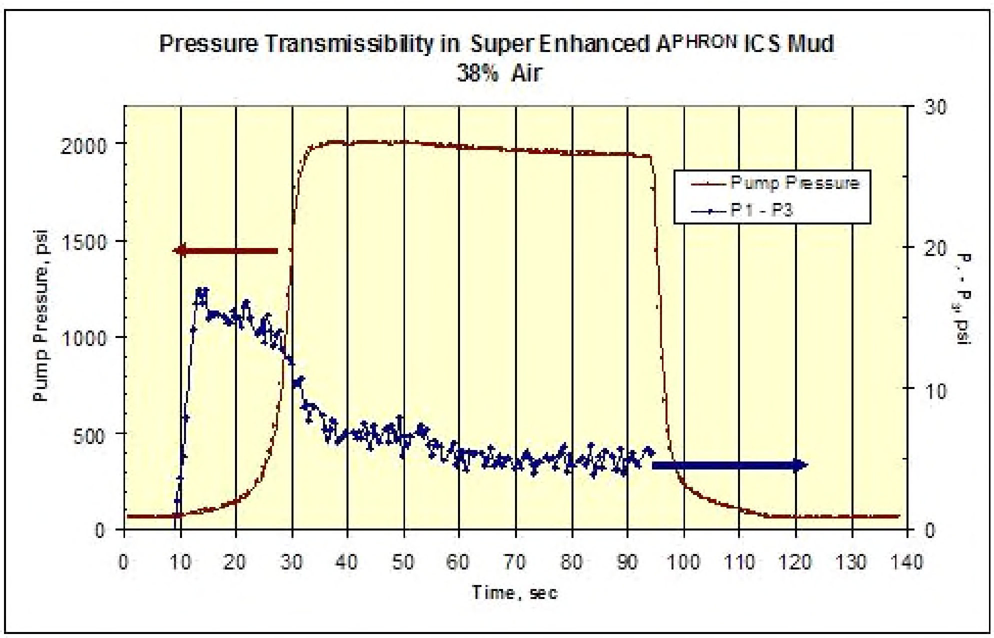

Immediately after decompression, some small bubbles (aphron-size) appeared, but some big air bubbles also formed gradually and continuously. This indicates that some of the aphrons survived pressurization to 13.7 MPa (2000 psig), in agreement with visualization tests. When the fluid was depressurized, the air simply came out of solution, much of it going into existing bubbles; the bubbles grew much like crystals growing from a supersaturated salt solution.

Because of the lower ΔP values observed at higher pressures and the belief that any effects of aphrons would most likely be manifested at lower pressures, subsequent testing, such as that shown in Figures 80 and 81, was carried at very low pump pressure: < 1.1 MPa (150 psig).

Figure 80. Press. Transmission of DRILPLEX™ Mud in 6.1-m (20-ft) x 0.64-cm (¼-in) Tube

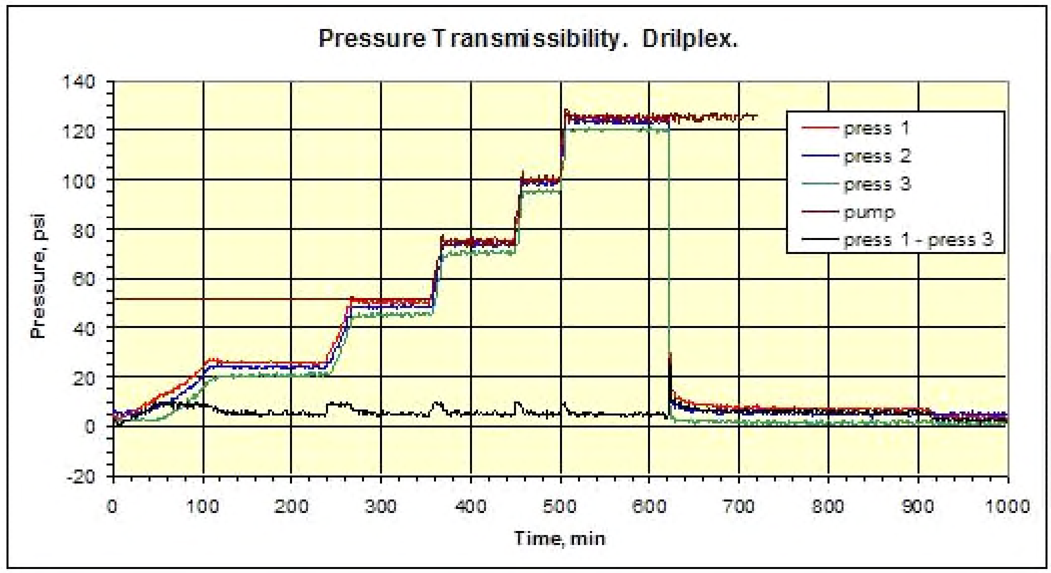

Figure 81. Press. Transmission of HYSSTER™ Mud in 6.1-m (20-ft) x 0.64-cm (¼-in) Tube

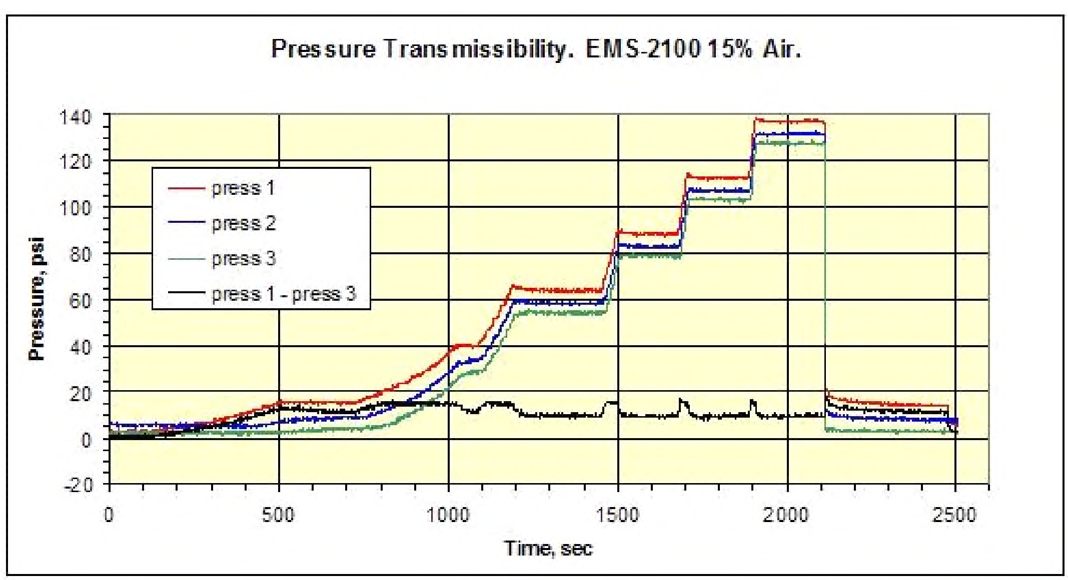

Two Enhanced APHRON ICS™ drilling fluids containing 5% and 38% air by volume and two conventional muds used for drilling in depleted fields (DRILPLEX™ and FLOPRO NT™) were used. Also, the new clay-based aphron drilling fluid, HYSSTER (nee EMS-2100), was used for comparison. Both APHRON ICS™ tests produced essentially the same results. The result for HYSSTER™ was close to those obtained for the APHRON ICS™ fluids (Figure 81). The DRIL-PLEX™ mud showed a lower pressure drop than the APHRON ICS™ muds (Figure 80), while the FLOPRO NT™ mud behaved like water and produced an almost negligible pressure drop. The results indicate that the APHRON ICS™ mud produces a greater pressure drop than the reference muds, but that the results are due to properties of the base fluid and are not related to the presence of aphrons. The pressure drops recorded between 0 and 6.1 m (20 ft) from the pump ("Press 1 – Press 3" in the figures above) were as follows:

Drilling Fluid System	Pressure Drop
APHRON ICS™ (5% and 38% Air)	0.068 – 0.082 MPa (10 - 12 psi)
HYSSTER™ (nee EMS-2100)	0.068 MPa (10 psi)
DRILPLEX™	0.034 – 0.041 MPa (5 – 6 psi)
FLOPRO NT™	0.007 – 0.014 MPa (1 – 2 psi)

Enhanced APHRON ICS™ muds with low LSRV and 15% and 45% air were also prepared to investigate the relationship between viscosity of base fluid and pressure drop. These muds contained 3 ppb, rather than 5 ppb, of Go-Devil and gave LSRV in the range of 104,000 -118,000 cP, which is almost 2/3 the LSRV of regular APHRON ICS™ fluids in the lab.

The result of one of these tests is shown in Figure 82. Pressure transmission experiments with these muds showed pressure drops in the 20 ft. tube in the range 0.034 to 0.054 MPa (5 to 8 psi) for both concentrations of air, which is consistent with the 0.068 – 0.082 MPa (10 – 12 psi) pressure drop observed with the regular high-LSRV APHRON ICS™ system.

Figure 82. Pressure Transmission of Low-LSRV Enhanced APHRON ICS™ Mud

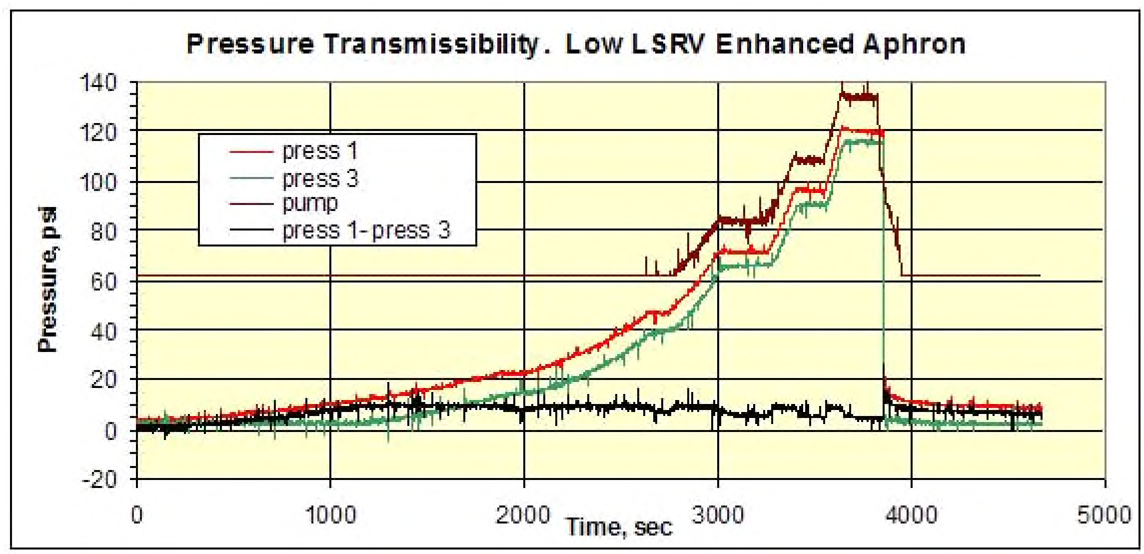

Pressure Transmission in Sand Packs

The flow tests were carried out in the apparatus shown in Figure 22, using 20/40 and 70/100 mesh sand.

Water permeability of both sand packs was estimated using the Darcy equation, as shown below, which relates volumetric flow and pressure drop with properties of the fluid and media. An ISCO pump connected to a floating-piston accumulator and a hydrostatically driven water column were used for creating a constant water flow rate. The permeability equation is as follows:

$$Q = -\frac{kA}{\mu}\left(\frac{dP}{dx}\right) \tag{10}$$

where Q = Volumetric Flow (cm^3/sec)

k = permeability (darcy, or (cm^2-cP)/(sec-atm), where 1 darcy = 9.869233×10^{-13} m^2)

A = cross-sectional area, 4.37 (cm^2)

μ = viscosity, 0.89 at 26 °C (cP)

P = pressure (atm)

x = length, 91.44 (cm)

Rearranging Equation (10) and incorporating the data provided here yields

$$k = 18.6 \frac{Q}{\Delta P} \tag{11}$$

Thus, the permeabilities of the 20/40 and 70/100 sand packs were determined to be 100 and 8 darcy, respectively.

Two series of experiments with Enhanced APHRON ICS™ muds were conducted with each mesh size of sand. In the first series, the pipe was filled with dry sand or with wet sand which was blown dry with air or N_2. In the second series, the sand packs were filled with water at the beginning of each experiment and tested in that state.

The results of both series of experiments are shown in Figures 83-87. As indicated in Figures 83 and 84, the APHRON ICS™ mud effectively sealed both sizes of dry sand packs, and no filtrate was collected after 30 minutes in the Leak-Off test. But the pressure drop for both the centrifuged muds (no air) and the muds containing aphrons was 0.69 MPa (100 psi) for 70/100 mesh sand, while for the 20/40 mesh sand it varied from 0.53 MPa, or 78 psi (no air) to 0.68 MPa, or 100 psi (with air). The procedure for preparing the dry sand pack did not change the character of pressure transmission, but it did change the depth of penetration of the mud.

One experiment was conducted by filling the pipe with wet slurry of 70/100 mesh sand, followed by complete drying using air and nitrogen. The differential pressure established across this sand pack was 0.69 MPa (100 psi) for the mud containing 18% air (about the same as for the sand pack filled directly with dry sand), but invasion of mud inside the previously wetted sand pack was about 3 times higher. This difference in the behavior of the two types of dry sand packs could be explained by a difference in the water-wet state of the sand pack; for the previously wetted sand pack, a water film covering the surface of the sand might very well have survived the air/nitrogen drying process.

Figure 83. Pressure Transmission Across Dry and Water-Filled 20/40 Sand

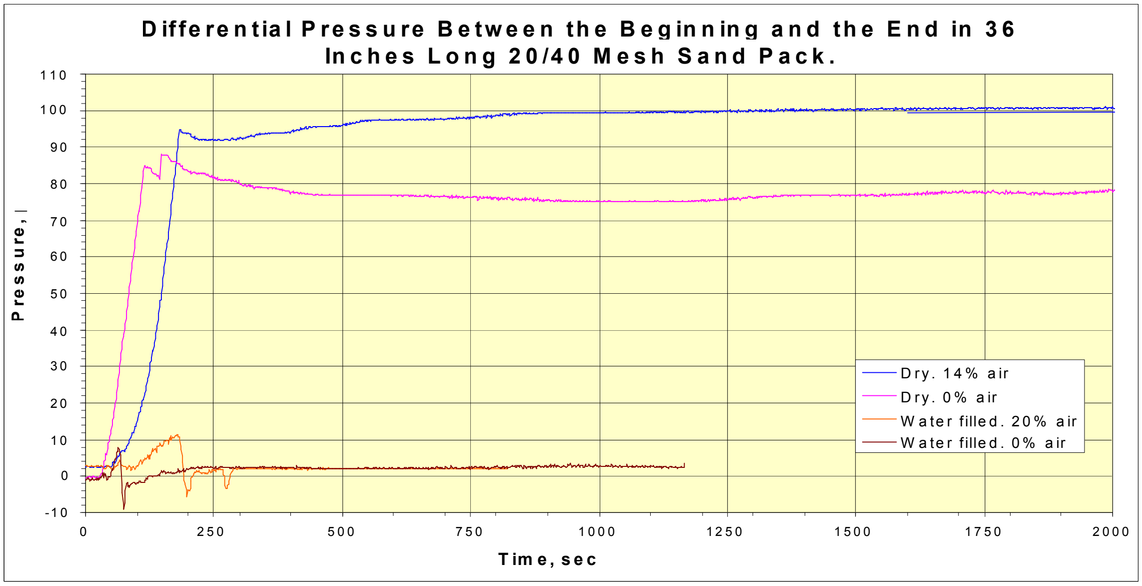

Figure 84. Pressure Transmission Across Dry and Water-Filled 70/100 Sand

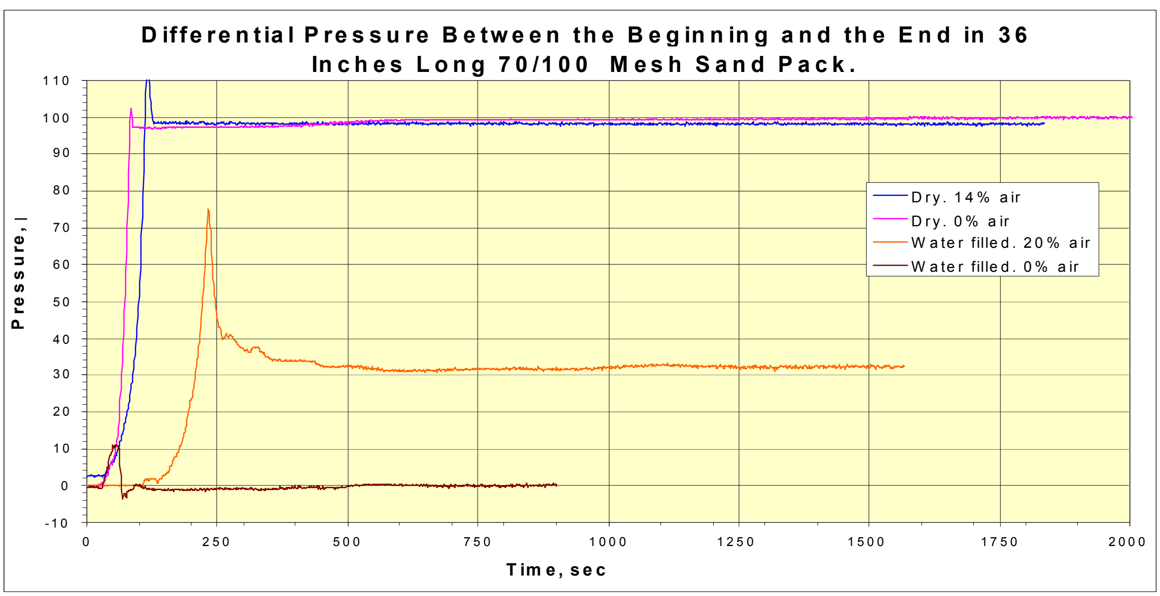

When the sand packs were completely filled with water at the commencement of the tests, pressure transmission took on a different character. These results are shown in Figures 83 and 84, with additional results shown in Figure 85. High pressure from the pump propagated very fast in sand packs filled with water. The differential pressure established across 20/40 sand packs was almost nil in muds containing 0% and 20% air. For the 70/100 sand packs, however, a consistent difference was observed for aerated muds compared to deaerated muds. As indicated in Figure 85, muds with 0% air showed 0.069 – 0.20 MPa (10-30 psi) less pressure drop than muds containing 13 to 22% air.

Figure 85. Press. Trans. of Enhanced APHRON ICS™ Across Water-Filled 70/100 Sand

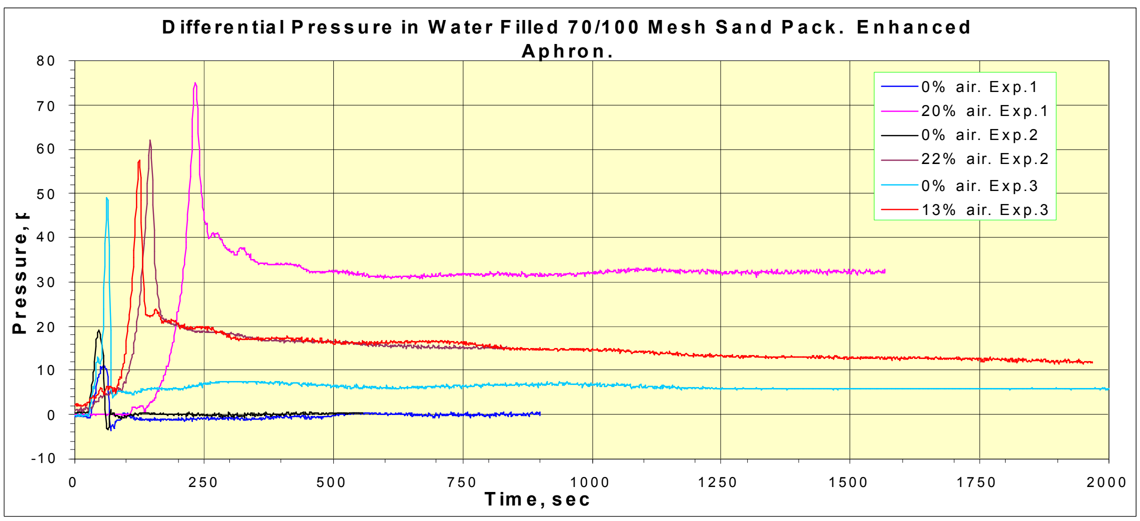

In addition, both the filtration rate and the rate of change of the filtration rate were lower for aerated muds than for deaerated muds, as shown in Figures 86 and 87. Invasion of mud in sand packs filled with water was very small in all cases compared to dry sand packs, as one might expect from the high void volume of the dry packs.

These experiments show that the difference in permeability of 20/40 and 70/100 sand packs (100 vs 8 darcy) strongly affects the ability of bubbles (presumably aphrons) to reduce depth of fluid invasion and pressure transmissibility. While aphrons appear to be effective in the water-filled 70/100 sand, this is not the case in the 20/40 sand. In addition, both pressure transmissibility and invasion of aphron muds in a sand pack depend heavily on the packing method and the presence of water in the sand pack. Since sands downhole are generally considered to be water-wet, the water-filled sand pack tests probably reflect downhole conditions best.

Figure 86. Leak-Off of Enhanced APHRON ICS™ in Water-Filled 70/100 Sand

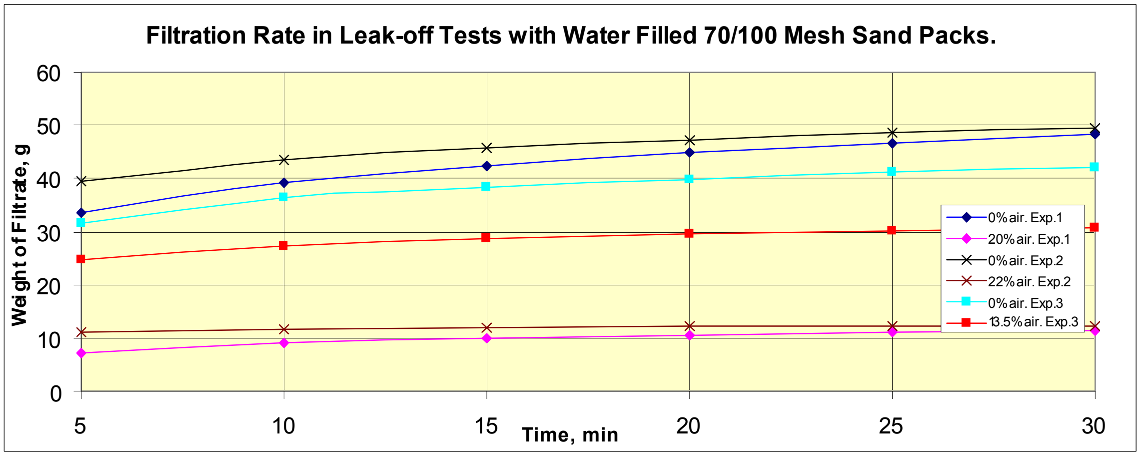

Figure 87. Leak-Off Rate of Enhanced APHRON ICS™ in Water-Filled 70/100 Sand

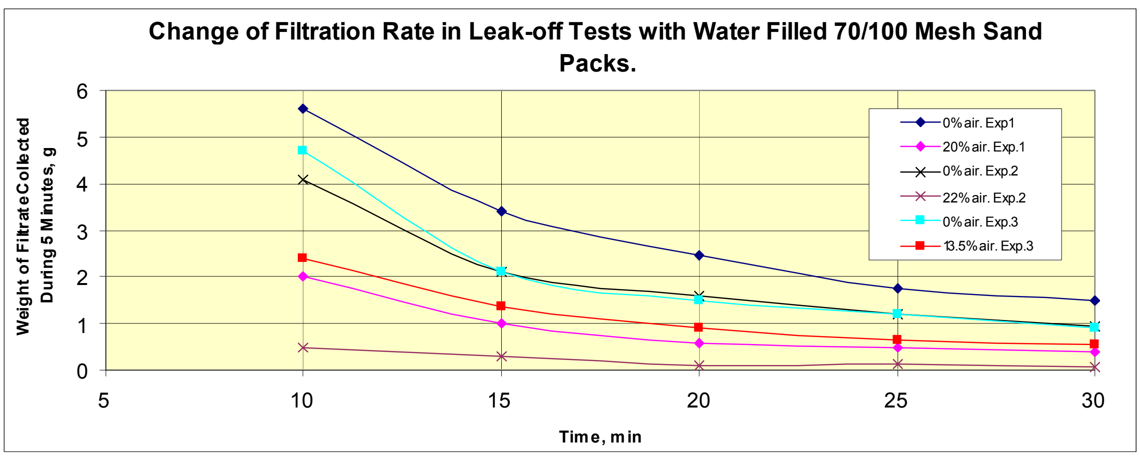

Sealing of Permeable and Fractured Media

Core Leak-Off Tests:

The tests were conducted with FAO-5 (nominal air permeability 5 darcy) Aloxite cores 3.8 cm (1-1/2 in) diameter x 5.1 cm (2 in) length, using 3.5 MPa (500 psig) and 7.0 MPa (1000 psig) fore pressure. SuperEnhanced APHRON ICS™ mud was used in all cases, and the effect of aphrons on leak-off was determined with back-to-back tests with samples containing air and samples that had been deaerated by centrifugation.

All tests resulted in plugging of the cores and collection of clear filtrate. Figure 88 shows the results obtained at the two fore pressures comparing deaerated mud with mud containing 21% air. As Figure 88 reveals, Leak-Off increased with increasing fore pressure and no air. These effects appear to be associated solely with the spurt loss at the beginning of the run.

Figure 88. Leak-Off Tests with 5-Darcy Aloxite Cores at Various Inlet Pressures

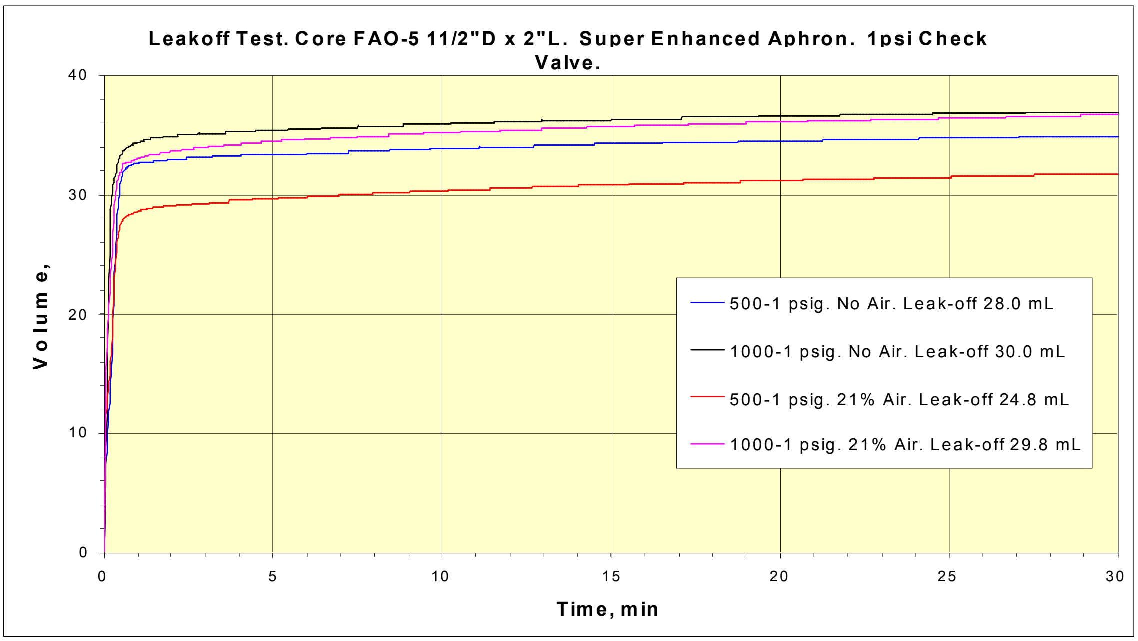

To determine the effect of core permeability on Leak-Off, tests were conducted at 3.5 MPa (500 psig) fore pressure with Aloxite cores WFAO-A (nominal air permeability 0.75 darcy) and FAO-10 (nominal air permeability 10 darcy) of 3.8 cm (1-1/2 in) diameter x 5.1 cm (2 in) length. The results are compared with those using FAO-5 in Figure 89.

Figure 89. Effect of Aloxite Core Permeability on Leak-Off

3.5 MPa (500) psig Fore Pressure

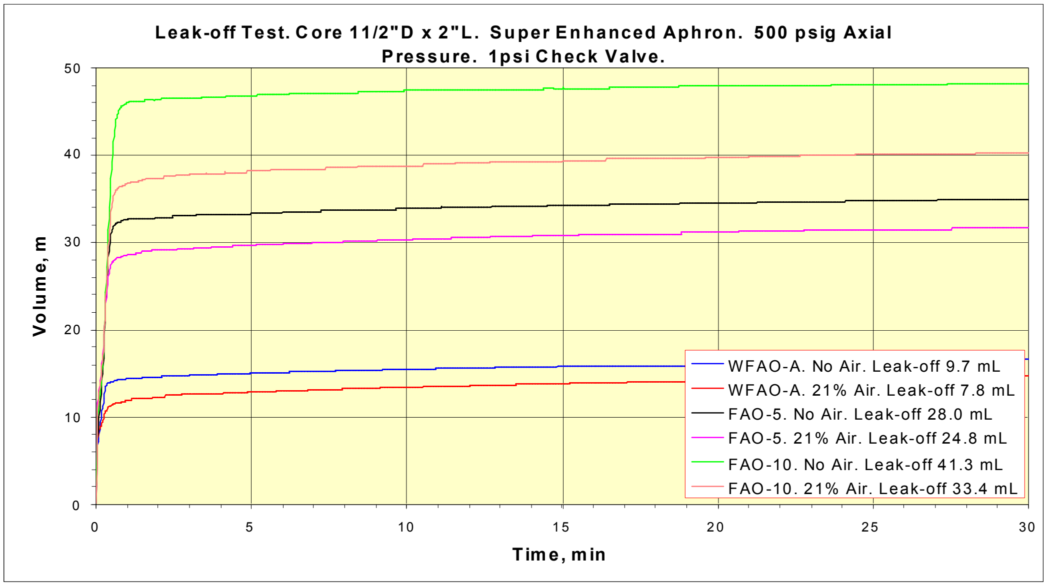

It is clear that Leak-Off increases with increasing permeability of the core, and again it is the spurt loss which is primarily affected. It is also clear that the muds containing air gave consistently lower Leak-Off than the deaerated samples, and the differential in Leak-Off appears to increase with increasing core permeability. This differential between deaerated mud and mud containing 21% was 2.1 mL, 3.2 mL and 7.9 mL for WFAO-A, FAO-5 and FAO-10 cores, respectively.

Finally, the effect of core length on Leak-Off was determined using two FAO-10 cores in series, which resulted in an effective core length of 10.2 cm (4 in) instead of the standard length of 5.1 cm (2 in). The result of this experiment is shown in Figure 90.

Leak-Off for the deaerated mud in the 4-in core was a few mL less than that observed for the 5.1-cm (2-in) core (see Fig. 89), and, although the Leak-Off when air (14% v/v) was introduced into the sample was a little lower than for the deaerated mud, it is probably within experimental error. Other than normal scatter, it is speculated that the effect of air on Leak-Off may be non-linear, i.e. 21% air (see Fig. 89 again) may have a significantly larger affect on Leak-Off than expected from the simple ratio of air volumes.

Figure 90. Leak-Off Tests with Two 10-Darcy Aloxite Cores of 4 in (10.2 cm) Total Length

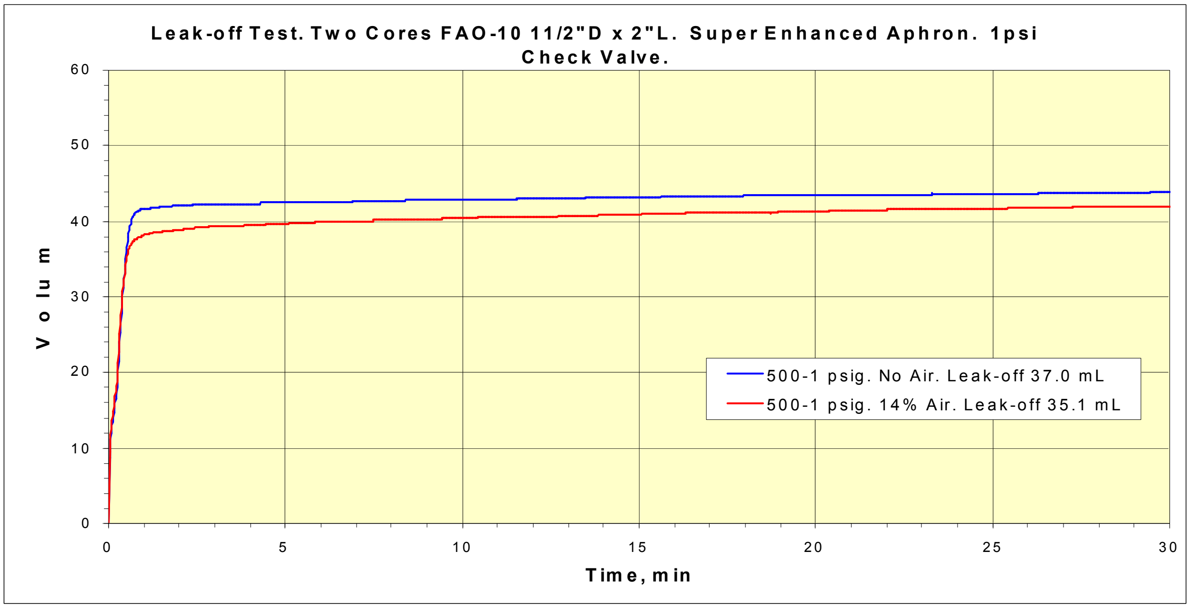

The Aloxite cores included FAO-00, FAO-5, FAO-10 and FAO-40 with nominal air permeability of 2, 5, 10 and 80 Darcy, respectively. The composition of the two "Solids-Free" mud samples is given in Table 5.

Table 5. Composition of APHRON ICS™ and FLOPRO NT™ Samples*

APHRON ICS™	
Component	**Concentration (lb/bbl)**
Water or 10% NaCl	337 mL
Soda Ash	3.0
X-CIDE	0.1
ACTIVATOR II	2.0
GO-DEVIL II	5.0
ACTIVATOR I	5.0
ACTIGUARD	0.5
BLUE STREAK	1.0
APHRONIZER A	0.5
APHRONIZER B	0.5
PLASTISIZER	0.3

FLOPRO NT™	
Component	**Concentration (lb/bbl)**
Water or 10% NaCl	316 mL
FLO-VIS PLUS	2.3
FLO-TROL	4.5

*For the $CaCO_3$-treated mud samples, the volume of Water or 10% NaCl is reduced by 14 mL.

In addition, the APHRON ICS™ mud contained 17 to 20% air, which was dispersed in the fluid with a Silverson L4RT mixer at 7,000 rpm for 6 min. Both fluids were also treated with 30 lb/bbl $CaCO_3$ of nominal diameter 40 μm; particle size analysis of the sample actually used showed it to possess D_{10} = 0.8 μm, D_{50} = 9 μm and D_{90} = 114 μm. Initially the APHRON ICS™ fluids were all prepared with fresh water, while the FLOPRO NT™ fluids were prepared with 10% NaCl; these are common diluents used in field formulations of the two muds. However, for a fair test of the two fluids, it was determined to prepare both muds using both diluents and perform Leak-Off tests on as many samples as time permitted.

Some bulk rheological properties of the four fluids are shown in Table 6. The FLOPRO NT™ system is usually run with a LSRV (Low Shear Rate Viscosity) at ambient conditions of 20,000 to 40,000 cP. For these tests, it was determined to optimize the fluid viscosity of the FLOPRO NT™ system so as to compete well with the APHRON ICS™ mud. Consequently, the viscosifier concentration was raised to the maximum level provided in the engineering guidelines, which elevated the LSRV of the brine-based FLOPRO NT™ system to ~ 110,000 cP.

The effects of Back-Pressure and core permeability on Leak-Off were determined first with the "Solids-Free" fresh water-based and 10% NaCl-based drilling fluids. A summary of the results obtained with the Solids-Free fresh-water-based fluids is given in Table 7.

Net Leak-Off is obtained after 30 minutes by subtracting the Dead Volume of water between the mud and the face of the core at the beginning of each test. Dead Volume was approximately 33 mL in all cases. All of the APHRON ICS™ tests resulted in plugging of the cores and production of clear filtrate. Not so for the FLOPRO NT™ system, which was not able to seal even the core with the lowest permeability (FAO-00).

When the fresh water used to prepare the mud samples was replaced with 10% NaCl, Leak-Off of the APHRON ICS™ system was markedly reduced, e.g. for FAO-10 with 1000 psi back-pressure, Leak-Off was 9.3 mL/30 min. Meanwhile, FLOPRO NT™ provided no control at all with fresh water or 10% NaCl as the base fluid. Thus, for the Solids-Free fluids, the APHRON ICS™ drilling fluid system yielded good control of Leak-Off, while the FLOPRO NT™ system did not.

Table 6. Rheology of APHRON ICS™ and FLOPRO NT™ Drilling Fluids

	Fresh Water			10% NaCl			
Test	AphronICS	AphronICS + $CaCO_3$	FloPro NT + $CaCO_3$	AphronICS	Aphron ICS + CaCO3	FloPro NT	Flo-Pro NT + CaCO3
Brookfield LVDV-II+, 3L, 0.06 sec^{-1}, 77 F	158000	173000	148000	198000	210000	111000	126000
Grace 3500, 77 F							
600 rpm	92	118	85	114	148	84	90
300 rpm	77	95	72	94	113	68	70
200 rpm	69	84	65	82	108	60	60
100 rpm	59	71	55	67	89	49	49
6 rpm	50	59	34	40	50	26	42
3 rpm	41	46	32	36	45	24	26
Gel Strength - 10 sec	38	41	30	34	39	22	24
Gel Strength - 10 min	47	46	31	38	42	24	29
Gel Strength - 30 min	51	47	31	39	43	24	30
Grace 3500, 150 F							
600 rpm	73	114	62	83	103	62	67
300 rpm	64	89	56	72	87	52	54
200 rpm	59	85	52	65	77	46	48
100 rpm	53	76	45	56	66	39	40
6 rpm	45	63	25	35	40	21	35
3 rpm	35	47	21	32	36	19	23
Gel Strength - 10 sec	33	39		31	33	18	20
Gel Strength - 10 min	42	42		35	36	21	25
Gel Strength - 30 min	44	42		33	37	21	25

Figure 91 shows the relationship between filtrate volume and the square root of time for the Solids-Free fresh water-based APHRON ICS™ and FLOPRO NT™ fluids. This type of graph is used for evaluation of the filtration rate of a drilling fluid after creation of a filter cake.[24] As shown in Figure 91, even with the lowest permeability core, the experiment with FLOPRO NT™ had to be stopped after 8 minutes, because the fluid reservoir was nearly emptied; indeed, the fluid flowed through the core at the maximum flow rate set for the pump, and the pressure drop on the core fell significantly below the pre-set level of 1000 psig.

Both drilling fluids generated similar slopes during the initial phase of the Leak-off, as would be expected for fluids possessing similar rheological characteristics. However, the APHRON ICS™ plot bends after 20 sec and ultimately produces a linear Leak-Off vs $t^{1/2}$ plot, which is strong evidence for static formation of some type of filter cake. The FLOPRO NT™ curve did not change slope throughout the 8-min period of that test, which is consistent for a system that does not form a filter cake at all.

Figure 92 shows the Gross Leak-Off obtained with the fresh water-based APHRON ICS™ mud in FAO-5 cores at the three designated Back-Pressures. The results are quite similar and suggest little effect of Back-Pressure, at least in the range 500 to 1500 psig. This is to be expected for incompressible fluids or fluids with a low concentration of a compressible phase. Only when the Back-Pressure was reduced to 0 psig (not shown here) was some effect noted. Note: Here Back-Pressure is reported as Pressure Drop, i.e. Fore-Pressure – Back-Pressure.

Table 7. Net Leak-Off of Solids-Free APHRON ICS™ and FLOPRO NT™ Drilling Fluids

Base Fluid: Fresh Water

Sample	Core	Nominal Gas Permeability (darcy)	Mean Pore Diameter (μm)	Axial Pressure Drop (psi)	Net Leak-Off after 30 min (mL)
APHRON ICS™	FAO-00	2	10	1000	7.0
APHRON ICS™	FAO-5	5	20	1500	10.2
APHRON ICS™	FAO-5	5	20	1000	11.2
APHRON ICS™	FAO-5	5	20	500	11.9
APHRON ICS™	FAO-10	10	35	1500	36.3
APHRON ICS™	FAO-10	10	35	1000	30.8
APHRON ICS™	FAO-10	10	35	500	29.6
FLOPRO NT™	FAO-00	2	10	1000	380*

* Test stopped after 8 minutes

Although Back-Pressure does not affect Leak-Off significantly, Table 7 makes it clear that permeability affects Leak-Off. Indeed, it appears that Leak-Off is roughly proportional to permeability; this is consistent with Darcy Flow, which is typical for flow of fluids through porous media before establishment of a filter cake.

With incorporation of 30 lb/bbl $CaCO_3$ in the APHRON ICS™ and FLOPRO NT™ formulations, Leak-Off was reduced considerably. Table 8 shows the results obtained with the fresh water-based drilling fluids.

Figure 91. Leak-Off vs Time$^{1/2}$ for Solids-Free APHRON ICS™ and FLOPRO NT™

Base Fluid: Fresh Water

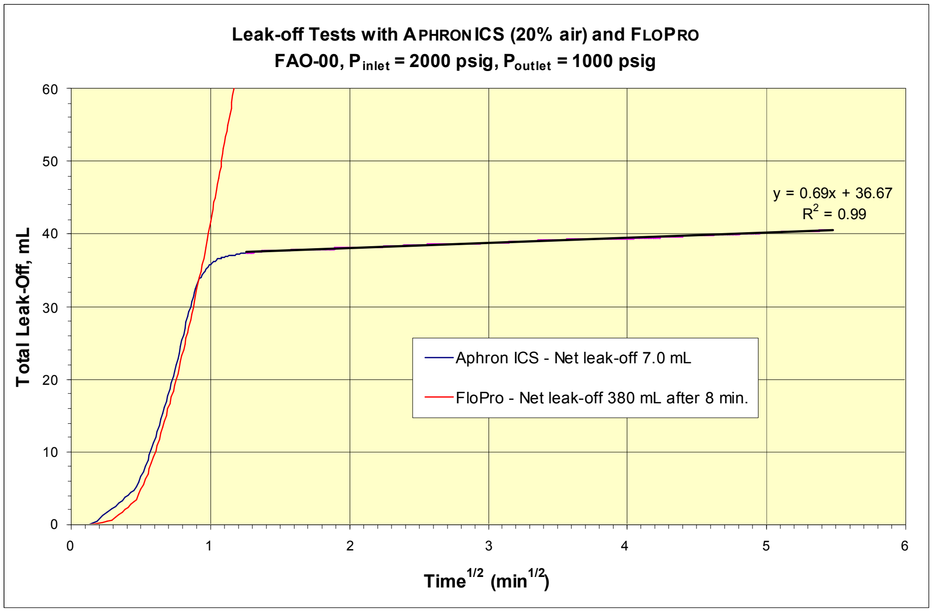

Figure 92. Effect of Back-Pressure on Leak-Off of Solids-Free APHRON ICS™ Mud

Base Fluid: Fresh Water

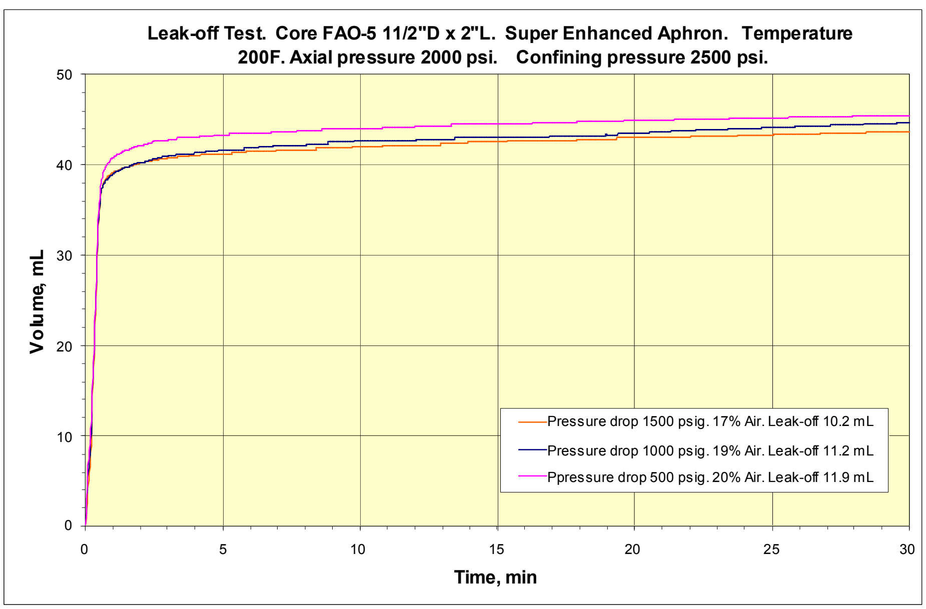

Table 8. Net Leak-Off of $CaCO_3$-Laden APHRON ICS™ and FLOPRO NT™

Base Fluid: Fresh Water

Sample	Core	Nominal Gas Permeability	Mean Pore Diameter	Axial Pressure Drop	Net Leak-Off after 30 min (mL)
APHRON ICS™ + 30ppb $CaCO_3$	FAO-5	5	20	1000	8.1
APHRON ICS™ + 30ppb $CaCO_3$	FAO-10	10	35	1000	8.4
APHRON ICS™ + 30ppb $CaCO_3$	FAO-40	80	80	1000	8.0
FLOPRO NT™ + 30ppb $CaCO_3$	FAO-10	10	35	1000	2.9

It is clear that $CaCO_3$ lowered the Leak-Off of both fluids significantly, but it lowered the Leak-Off of the FLOPRO NT™ more, producing a Net Leak-Off of the $CaCO_3$-treated FLOPRO NT™ fluid that was consistently lower than that of the $CaCO_3$-treated APHRON ICS™ fluid. [Note: the Leak-Off curves show the Total Leak-Off, before correcting for the Dead Volume].

Comparison of Figures 93 and 94 shows that the fresh water-based APHRON ICS™ system yields both higher spurt lost and higher filtration rate than fresh water-based FLOPRO NT™. Filter cake formed from APHRON ICS™ + $CaCO_3$ appears to be somewhat thicker and gelatinous compared to that formed from FLOPRO NT™ + $CaCO_3$. Indeed, particle size analysis suggests that the $CaCO_3$ possesses an erodible coating that may affect the manner in which it bridges on the surface of the core.

In 10% NaCl, on the other hand, the $CaCO_3$-laden APHRON ICS™ test results look quite different. As shown in Table 9, the two brine-based drilling fluids produce essentially identical Leak-Offs, within experimental error. This Leak-Off value is independent of permeability and is about the same as that observed for FLOPRO NT™ in fresh water. In this case, all of the filter cakes appeared compact and relatively hard, and the APHRON ICS™ formulation generated a particle size distribution that was similar to that of uncoated $CaCO_3$.

Figure 93. Leak-Off of APHRON ICS™ + 30 lb/bbl $CaCO_3$ in Fresh Water

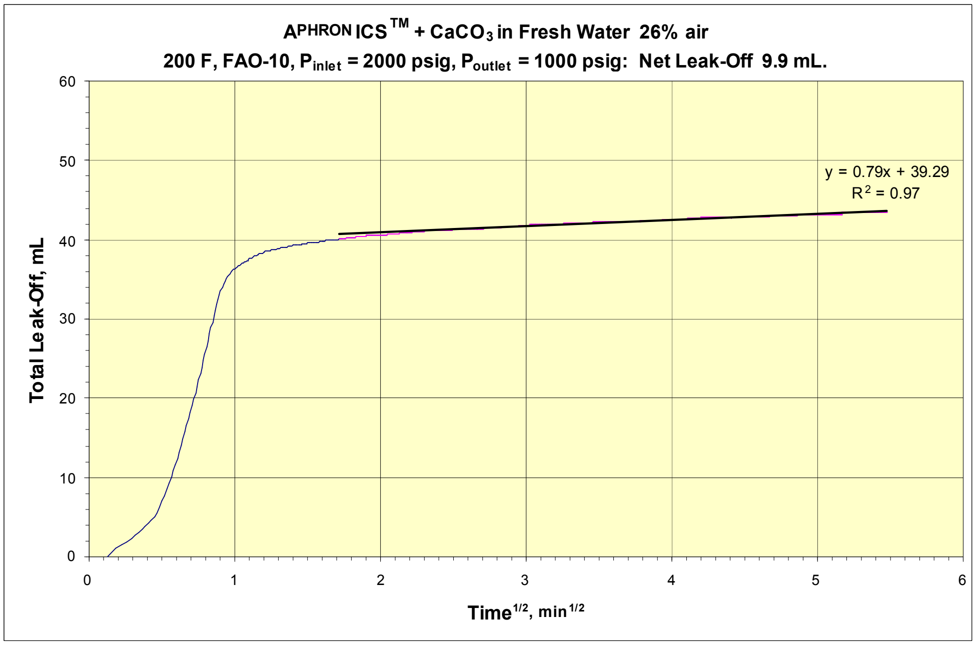

Figure 94. Leak-Off of FLOPRO NT™ + 30 lb/bbl $CaCO_3$ in Fresh Water

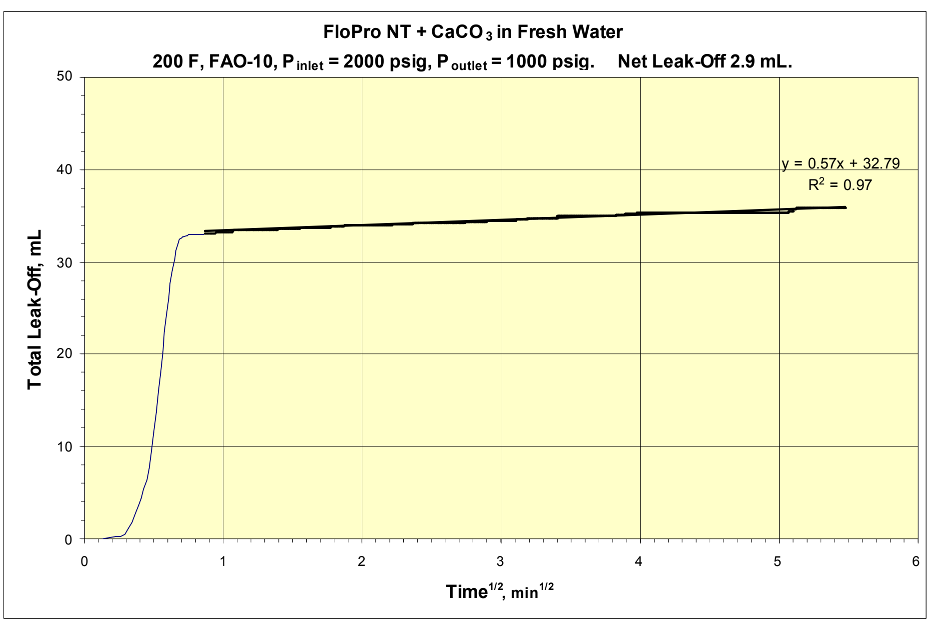

Table 9. Net Leak-Off of CaCO3-Laden APHRON ICS™ and FLOPRO NT™

Base Fluid: 10% NaCl

Sample	Core	Nominal Gas Permeability (Darcy)	Mean Pore Diameter (μm)	Axial Pressure Drop (psi)	Net Leak-Off after 30 min (mL)
APHRON ICS™ + 30ppb $CaCO_3$	FAO-5	5	20	1000	3.2
APHRON ICS™ + 30ppb $CaCO_3$	FAO-10	10	35	1000	3.2
APHRON ICS™ + 30ppb $CaCO_3$	FAO-40	80	80	1000	2.9
FLOPRO NT™ + 30ppb $CaCO_3$	FAO-5	5	20	1000	2.1
FLOPRO NT™ + 30ppb $CaCO_3$	FAO-10	10	35	1000	1.7
FLOPRO NT™ + 30ppb $CaCO_3$	FAO-40	80	80	1000	3.3

Figure 95. Leak-Off of APHRON ICS™ + 30 lb/bbl $CaCO_3$ in 10% NaCl

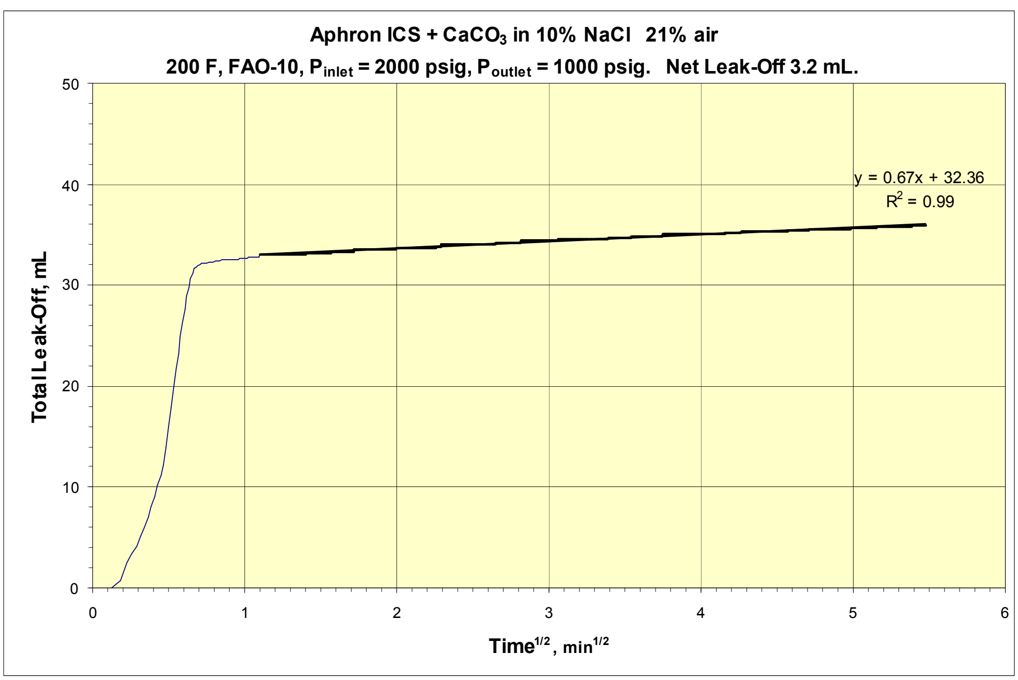

Figure 95 shows the Leak-Off curve obtained for the $CaCO_3$-laden APHRON ICS™ system in 10% NaCl. The shape of the spurt loss phase of the curve is essentially the same as that observed for the $CaCO_3$-laden FLOPRO NT™ system in either fluid medium. The filtration rate, given by the slope of the linear part of the plot (linear with respect to $t^{1/2}$) is only a little higher than that obtained with the FLOPRO NT™ system.

Thus, the Solids-Free APHRON ICS™ system is able to control Leak-Off in these permeable cores relatively well, which is in keeping with its intended application as a Solids-Free drilling fluid. The FLOPRO NT™ system cannot control Leak-Off without the addition of $CaCO_3$. When treated with $CaCO_3$, the FLOPRO NT™ system can control Leak-Off very well, though the brine-based APHRON ICS™ system can match its performance.

Disk Leak-Off Tests:

The apparatus used for the filtration tests is shown in Figure 24. In these experiments, fluid is passed through an HTHP cell fitted with a ¼ -in (0.64 cm) thick Aloxite disk, collected in a container, and weighed continuously with a digital balance and recorded by computer. Weight and quality of the filter cakes on the Aloxite disks were also investigated. For these experiments, 10-μm disks were used, and the tests were run for 30 min at 500 psig (3.5 MPa) and ambient temperature.

To investigate the effect of the components of SE APHRON ICS™ on the invasion control of mud and filtrate into permeable media, samples of this drilling fluid were prepared from the original chemical components (rather than the brand-name products), including (a) the standard complement of mud and no magnesium oxide, (b) the standard complement of mud and no hemicellulose and (c) the standard complement of mud and no starch. The compositions of the prepared muds are given in Table 10.

After preparation, all samples were hot rolled 16 hr at 150 ^{o}F (65.5 ^{o}C). To compare the base characteristics of these fluids and exclude any effects of aphrons, the samples were deaerated by centrifugation for 1 min at 2000 rpm and then thoroughly mixed with a spatula to prevent formation of additional bubbles.

Table 10. Composition of Drilling Fluids (in ppb) Used in Filtration Tests

Component	SE APHRON ICS™	No MgO	No Hemicellulose	No Starch
Water	338	339	333	339
Soda Ash	3	3	3	3
Starch	1	1	1	
MgO	2.35		2.35	2.35
DUOVIS	3.5	3.5	3.5	3.5
Hemicellulose	5.15	5.15		5.15
APHRONIZER	0.5	0.5	0.5	0.5
APHRONIZER	0.5	0.5	0.5	0.5
PLASTISIZER	0.3	0.3	0.3	0.3
ACTIGUARD	0.5	0.5	0.5	0.5

The results of the filtration experiments are shown in Figure 96 and Table 11. The linear portions of the Leak-Off (V) vs $t^{1/2}$ curves (after about 1 min) were analyzed assuming standard static filtration theory:[24, 25]

$$V = S + F\,t^{1/2} \qquad (12)$$

Before the filter cake is established, the fluid that leaks through the 10-μm disk is whole mud, whose volume increases directly with time. S is the total volume of whole mud, or Spurt, that passes through during this period. After the filter cake is established, only liquid passes through, and V increases with $t^{1/2}$ at a rate given by F, the Filtration. Thus, S is the ordinate intercept and F is the slope of the filtration portion of the Leak-Off curve.

Figure 96. Effect of Fluid Composition on Total Filtrate vs Time$^{1/2}$

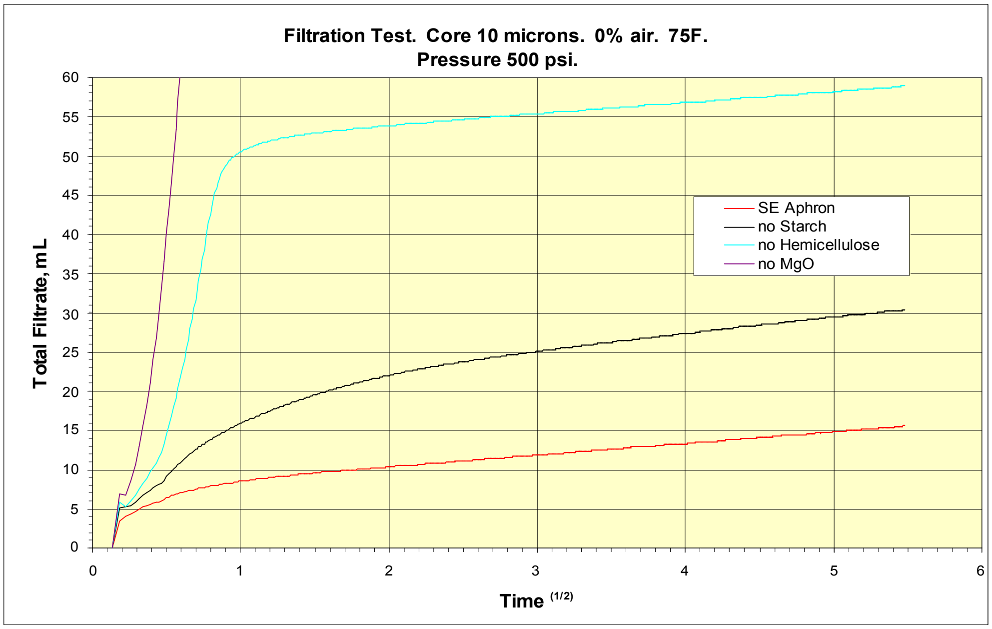

Table 11. Total Filtrate, Spurt Loss and Rate of Filtration

Sample	Total Filtrate (mL)	Spurt loss (mL)	Rate of Filtration (mL/min$^{1/2}$)
SE APHRON ICS™	15.6	7.3	1.48
SE APHRON ICS™ w/o Starch	30	18	2.22
SE APHRON ICS™ w/o Hemicellulose	59	51	1.43
SE APHRON ICS™ w/o MgO	200 after 1 min		

All three solid components of the SE APHRON ICS™ system play important roles in controlling invasion of the drilling fluid. The fluid without magnesium oxide did not create any significant external filter cake and passed through the10-μm filter at the maximum flow rate supplied by the pump. Removal of starch or hemicellulose did not cause such a catastrophic change, but in both cases the total amount of collected filtrate increased. The effects on spurt loss were dominant, though absence of starch increased the filtration rate as well as the spurt loss. Omission of each of these particulates also changed the appearance of the filter cake, but in the case of MgO, no filter cake was evident. Photographs of the air-dried filter cakes are shown on Figure 97.

Figure 97. Dried Filter cakes from SE APHRON ICS™ Fluid on Aloxite Disks: 1- Complete Formulation, 2 – w/o Starch, 3 - w/o Hemicellulose, 4 – w/o Magnesium Oxide

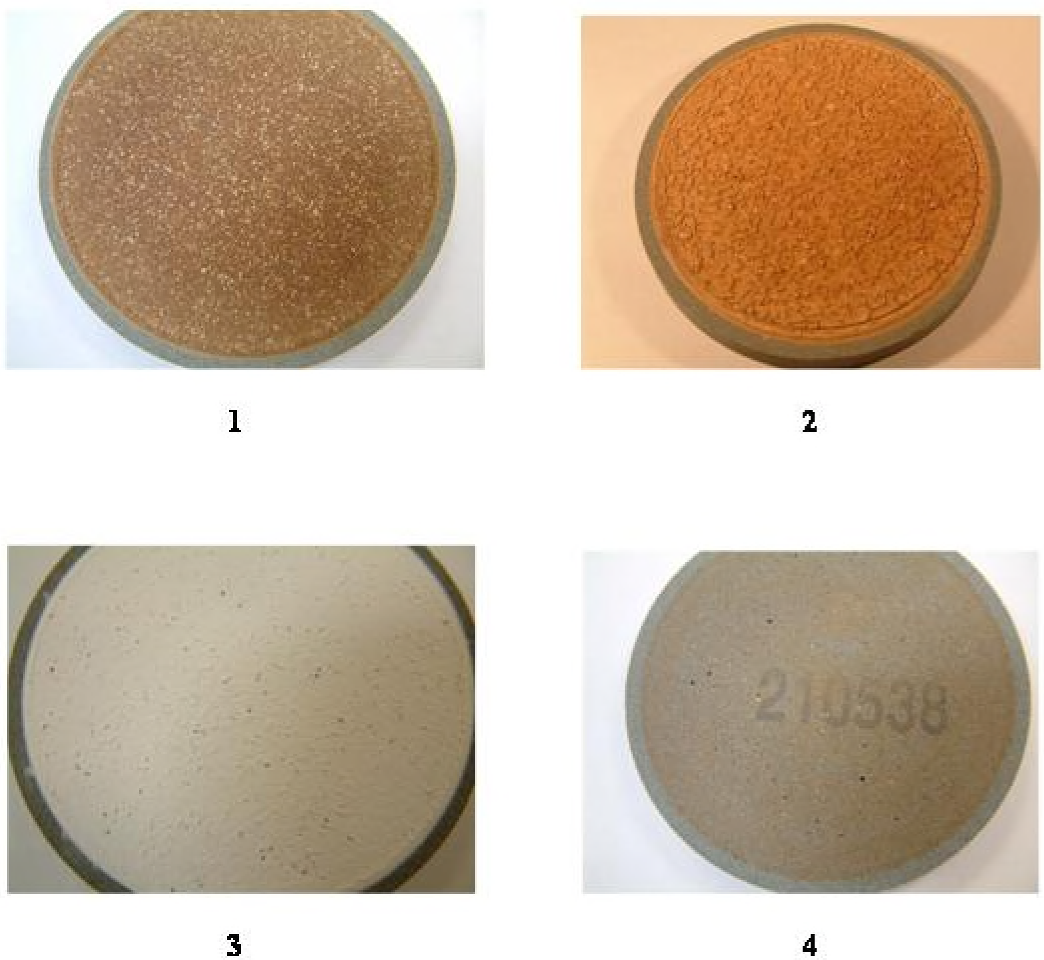

Syringe Sand Pack Leak-Off Tests:

With the realization that shear affects the stability and longevity of aphrons every bit as much as pressure itself, some Syringe Sand Pack Leak-Off screening tests were carried out using the

Standard APHRON ICS™ system as the base fluid. To it was added 1 ppb of a candidate stabilizer, and the sample was hot-rolled overnight at 150 °F before entraining air with the Prince Castle mixer and testing.

Below is a list of some of the fluid compositions that were run:

- SuperEnhanced APHRON ICS™
- Standard APHRON ICS™
- Air Free - SuperEnhanced APHRON ICS™
- Air Free - Standard APHRON ICS™
- Transparent SuperEnhanced APHRON ICS™
- Transparent Enhanced APHRON ICS™
- Standard APHRON ICS™ + Urea
- Standard APHRON ICS™ + FORM-A-SET™ (M-I SWACO) + CrossLinker
- Standard APHRON ICS™ + EMI-770 (M-I SWACO)
- Standard APHRON ICS™ + RHEOSYN™ 250 (Rheosyn)
- Standard APHRON ICS™ + PLIOTEC™ LS1 (Eliokem)

All of the above samples were run in both the 20/40 and 70/100 sand packs. The openings in the former may be thought of as simulated microfractures. Initially, every sample containing air was run with 12 to 15 vol% air. Later, these samples were run with at least 20 vol% to simulate the band of aphrons that accumulates at the fluid front during Bubbly Flow.

In the 20/40 sand pack, every fluid tested went through the sand with little resistance and did not form a seal, i.e. no plugging occurred. The results were quite opposite in the 70/100 sand pack. Every fluid tested, save one, demonstrated resistance to flow and plugging. When a seal was effected in the 70/100 sand, phase separation was usually evident, giving rise to the "spectrum" shown in Figure 98. These apparent phases are thought to arise from a combination of phenomena: initial spurt loss (whole mud) accompanied by Bubbly Flow and subsequently filter cake formation and passage only of liquid (filtrate).

Figure 98. Typical Phase Separation Observed in Syringe Sand Pack Leak-Off Test

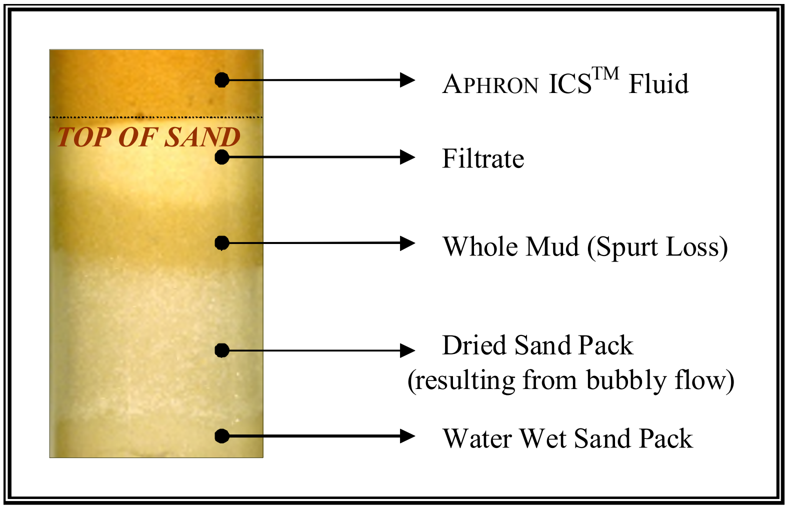

As instructive as these tests appeared to be, it was not possible to differentiate among the samples insofar as how rapidly and tightly they sealed, and no conclusions were forthcoming.

Capillary Suction Tests:

The CST apparatus is shown in Figure 26, and its normal application is discussed in Reference 17. The Modified CST test procedure developed in this Project is described in the Experimental Approach. In all cases, the fluid samples were blended with a Prince Castle mixer and hot-rolled for 16 hours at 150°F. Initial tests were performed using the standard CST method.[1] Various mud types were evaluated, and the results are given in Figure 99.

The fluids with very long CST values cannot be very clearly differentiated, and artifacts such as evaporation of water from the blotting paper control the rate of advance of the filtrate. It was determined that CST values higher than a few thousand seconds are fraught with unacceptably high error. For these fluids, the Modified CST test appears to provide a much more precise and accurate way to monitor relative filtration rates. The Modified CST test involves measuring CSD, the distance in mm traveled by the fluid in a given time period, usually 30 or 60 min.

Figure 99. CST Results using Standard CST Procedure

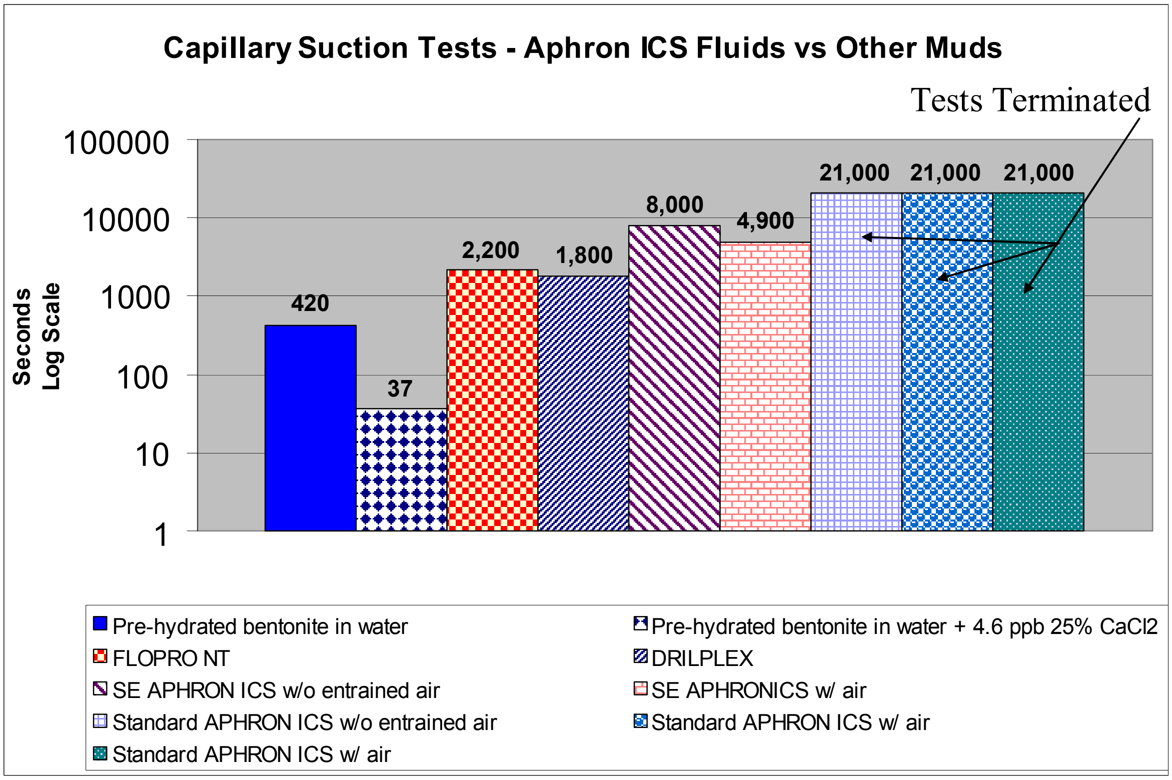

Once the CSD test procedure was established, four samples of each system were blended, and the concentration of viscosifier specific to each system was varied. The systems utilized were: Standard APHRON ICS™, SE APHRON ICS™, FLOPRO NT™ and DRILPLEX™. These samples were run as "solids free" systems, but some tests were also run with samples containing 30 lb/bbl of $CaCO_3$ having a nominal particle diameter of 40 µm. The corresponding Low-Shear-Rate Viscosity (LSRV), Leak Off, and CSD were measured for each one of these samples. All of the tests were run at room temperature. LSRV was measured with a Brookfield LV-II+ Viscosimeter at 0.06 sec^{-1} using a L3 spindle. The Core Leak-Off tests were run with 1,000 psi confining pressure, 500 psi inlet pressure and no back pressure, using 2-in. long Aloxite cores of about 5-Darcy air permeability.

In all cases, the CSD values used for the correlations were those measured at 60 min (half of the total testing time). The CSD vs Leak-Off correlations obtained with the 30-min CSD data were similar to these, but the CSD data appeared to be somewhat less precise. The correlations obtained with the 90-min and 120-min data were also similar to those obtained with the 60-min data and did not appear to provide any greater precision. Consequently, the 60-min CSD values were used for all of the correlations.

Filtration in the Modified CST (CSD) Test

If a unit volume of a stable suspension of solids is filtered against a permeable substrate (paper or core in our case), and x volumes of filtrate are expressed at time t, then $1-x$ volumes of cake will be deposited on the substrate. As a simplifying approximation, the rate of growth of the filter cake is assumed to be proportional to the rate of growth of filtrate. Therefore, if Q_c represents the volume of the cake, and Q_f the volume of the filtrate:[24]

$$\frac{Q_c}{Q_f} = \frac{1-x}{x} = R \tag{13}$$

where R is a constant ratio of filter cake to filtrate. The area of the filter cake, A, is constant in linear static filtration, such as API Fluid Loss and Core Leak-Off tests. It is also constant in a CSD test, though the filtrate itself expands radially along the plane of the paper. Q_c is given by the product of A and the thickness of the filter cake:

$$Q_c = A \cdot h \tag{14}$$

Thus,

$$h = \frac{R \cdot Q_f}{A} \tag{15}$$

Now, Darcy's law states

$$\frac{dq}{dt} = \frac{k \cdot \Delta P \cdot A}{\mu \cdot h} \tag{16}$$

Where k = permeability of the filter cake (Darcy), ΔP = differential pressure across the cake (atm), μ = viscosity of the filtrate (cP), h = thickness (cm), q = volume of filtrate (cm^3), and t = time (sec).

Therefore,

$$\frac{dq}{dt} = \frac{k \cdot \Delta P \cdot A^2}{\mu \cdot R \cdot Q_f} \tag{17}$$

Integrating,

$$Q_f{}^2 = \frac{2k \cdot \Delta P \cdot A^2 \cdot t}{\mu \cdot R} \tag{18}$$

Unifying the constant terms results in

$$Q_f{}^2 = K \cdot t \tag{19}$$

or,

$$Q_f = K' \cdot t^{1/2} \tag{20}$$

Where K and K' are proportionality constants. This last equation governs filtration under static conditions.[23]

In the Modified CST method (CSD), the distance that the fluid travels, d, is proportional to Q_f. Thus,

$$d = K'' \cdot t^{1/2} \tag{21}$$

Some results for two types of Aphron Drilling Fluids are plotted in this fashion (d vs $t^{1/2}$) in Figure 100. The closeness of the data for the two samples of Deaerated SE APHRON ICS™ fluid demonstrate the reproducibility of the Modified CST test.

Figure 100. CSD vs Square Root of Time

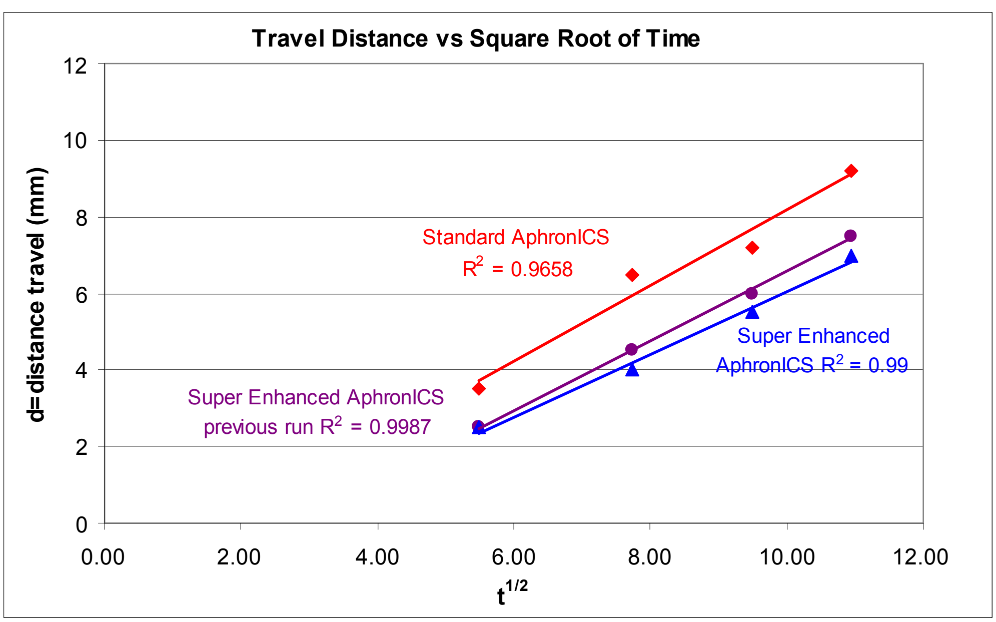

The linearity of the $t^{1/2}$ plots shows that CSD follows static filtration theory. It does not necessarily follow, however, that CSD will correlate with core Leak-Off behavior. Key differences between core Leak-Off and Modified CST tests include saturation of the pore network (wet vs dry), the nature of the filter medium (core vs paper), differential pressure (elevated inlet pressure vs ambient pressure), and possibly temperature. The effect of saturation of the pore network with the base fluid is manifested as a displacement in the apparent Spurt (see Equation (12)). Spurt is generally defined as the loss of whole mud that occurs initially during fluid invasion, i.e. prior to formation of a fully established filter cake. This is given approximately by the y-axis intercept on the $t^{1/2}$ plot. In the mathematical treatment of static filtration given above, Spurt is assumed to be negligible. However, Spurt is known to be significant in permeable rocks. Furthermore, "a low fluid loss and a dry cell with high hold up volume will cause a negative y-axis intercept".[24] To prove this, two CSD tests were run, one using dry filter paper and one using wet filter paper. The system used was Deaerated SE APHRON ICS™ fluid. The results are shown in Figure 101.

Figure 101. CSD for Wet vs. Dry Filter Paper with Deaerated SE APHRON ICS™ Fluid

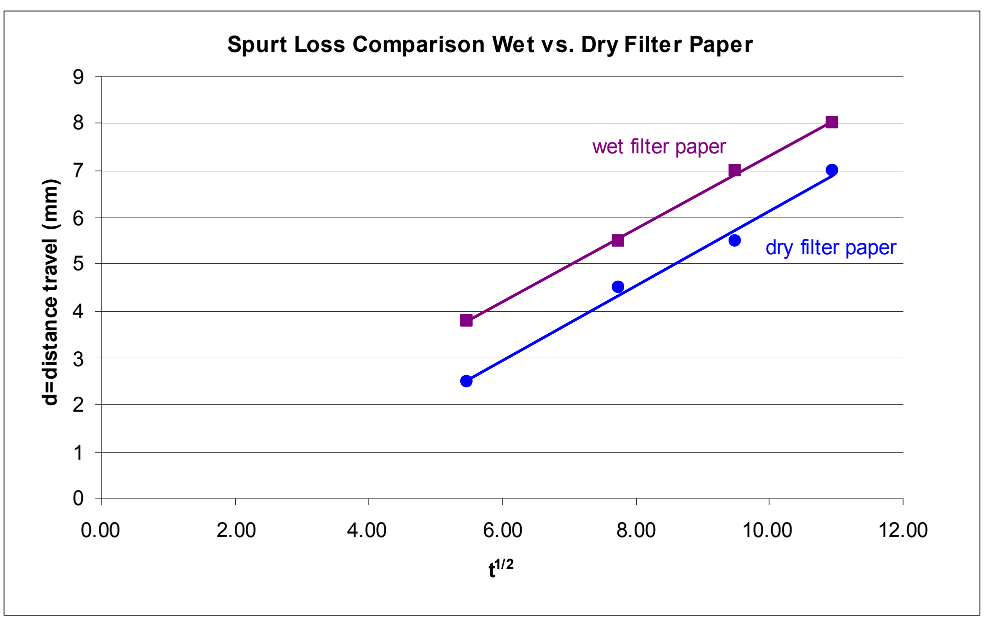

It is evident from Fig. 101 that, when the paper is saturated with water at the start of the test, the straight line plot for the dry filter paper is displaced upwards about one unit. The Spurt changes from negative to approximately zero, thus confirming the role played by the interstitial fluid in the paper.

The effects of the nature of the filter medium and differential pressure are more complex. Once a filter cake is well established on a filter medium, the filtration rate is not expected to be affected very much by the nature of the filter medium (paper vs core), since fluid flow is controlled entirely by the permeability of the cake. Conversely, Spurt is dominated by Darcy flow, where k and h are the permeability and thickness of the filter medium, respectively, and μ is the viscosity of the whole mud. Each mud system has a different viscosity profile, which will in turn produce a different rate of Spurt. In addition, different concentrations and size distributions of particulate matter in the mud will affect the Spurt period (the length of time of the Spurt phase). Thus, total Spurt, as given by the product of the Spurt rate and Spurt period, will vary from mud to mud. The higher the permeability of the filter medium, the greater will be the Spurt and the variability in Spurt from mud to mud. Thus, the effects of the nature of the filter medium and pressure differential are expected to be manifested in a higher Spurt for the Core Leak-Off tests vs the CSD tests. This will undoubtedly lead to different correlations of Core Leak-Off vs CSD for each mud system,[25, 26] as shown below.

Correlations of CSD and Core Leak-Off vs. LSRV

The effect of LSRV on CSD is shown in Figure 102. All of the curves in Figure 100 follow power law trends fairly well, though it appears that the curves cannot be unified into a single model, *i.e.* each fluid system appears to follow a different power law expression. The APHRON ICS™ systems give lower CSD values than the DRILPLEX™ and FLOPRO NT™ systems. Aerating the Enhanced ADF system lowers the CSD even more. This is likely the result of the air (aphrons) acting as a bridging agent.[27]

Figure 103 shows the correlation of Core Leak-Off vs. LSRV for all the data. As was the case for the CSD correlations, Core Leak-Off appears to follow a power law trend with respect to LSRV. Again, it does not seem possible to be able to unify the curves; indeed, the curves appear to be considerably more scattered than were the CSD vs LSRV curves (Figure 102). As discussed in the previous section, this is likely the result of Spurt being more variable for invasion into a core than for invasion into blotter paper. This is especially evident for DRILPLEX™, which exhibits the lowest Core Leak-Off, yet the highest CSD. The sealing mechanism of this fluid involves a special polymer-clay network that is very effective at reducing Spurt.[28]

Figure 102. CSD vs LSRV for All Fluid Systems Tested

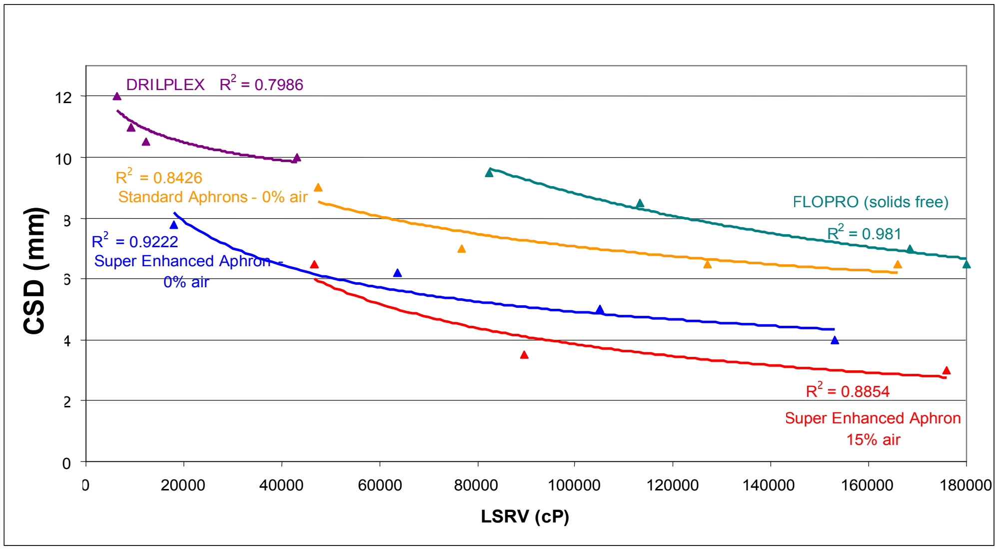

Figure 103. Core Leak-Off vs LSRV

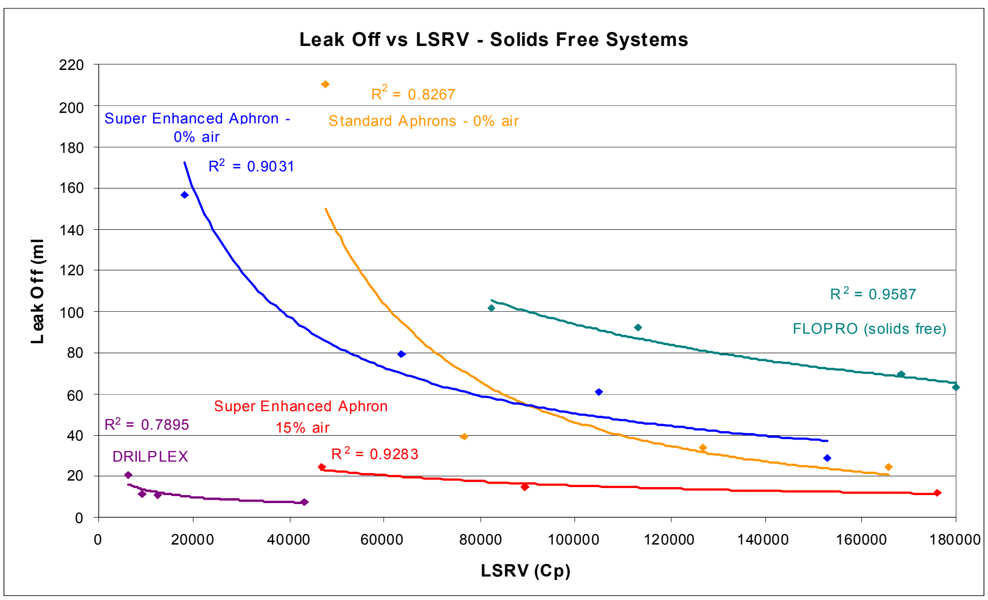

Core Leak-Off vs. CSD

Fig. 104 shows the correlation of Core Leak-Off vs. CSD for all the systems. As expected from previous discussions and borne out by these data, there is a fair correlation between CSD and Core Leak-Off for individual fluid systems, but there is no unifying correlation for all of them.

Figure 104. Correlation of Core Leak-Off with CSD for Several Drilling Fluids

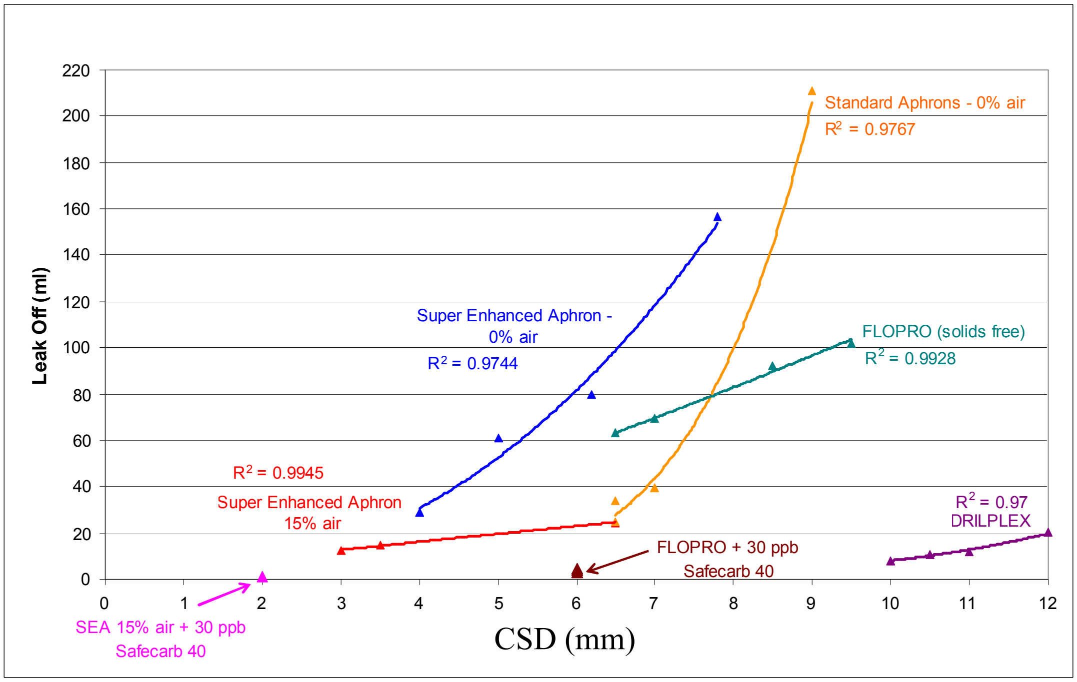

Addition of $CaCO_3$ to the DRILPLEX™ and the SE APHRON ICS™ systems reduces both Leak-Off and CSD. Likewise addition of air to the SE APHRON ICS™ system reduces both Leak-Off and CSD. From the results shown in Fig. 104, it appears that CSD and Core Leak-Off for any given fluid system correlate well enough to approximate the value of the Leak-Off of a particular system based on its CSD value. Thus, the value of CSD measurements is expected to lie in monitoring of fluid invasion trends and evaluation of potential additive treatments.

Effects of Chemical Composition on Drilling Fluid Invasion:

Particulates

To determine the effects of the solid components in the APHRON ICS™ system on Leak-Off, capillary flow experiments were carried out with four APHRON ICS™ fluids prepared from chemical components rather than branded products. Composition of the fluids is shown in Table 12, and the rheological properties at room temperature of Samples #2 - #4 are given in Table13.

The results of the capillary flow experiments are shown in Figures 105 and 106; water serves as a reference fluid.

Sample 1, which is not shown, plugged the 0.01 in ID tubing after an essentially negligible amount of fluid was pumped through the tubing. This shows that the hemicellulose (HC) in that fluid is of sufficient size and quantity to bridge an opening of 0.01 in. The PSD (Particle Size Distribution) of HC in a solution similar to that of an APHRON ICS™ mud shows it to have a very broad range of effective spherical particle size: D_{10} = 1 µm (0.00004 in), D_{50} = 20 µm (0.0008 in) and D_{90} = 103 µm (0.004 in).

Sample 4 contains MgO, but no HC. MgO has a much narrower PSD that is skewed to lower values: D_{10} = 2 µm (0.00008 in), D_{50} = 10 µm (0.0004 in) and D_{90} = 38 µm (0.0015 in). Having a smaller effective particle size, the MgO passed through the 0.01 in ID tubing, yet it was able to plug the 0.005-in ID tubing.

Table 12. Composition of APHRON ICS™ Test Fluids*

Component	Sample 1	Sample 2	Sample 3	Sample 4
Water	339.	342.	340.	340.
Soda Ash	3.00	3.00	3.00	3.00
Hemicellulose	5.15			
Starch	1.00	1.00	1.00	1.00
Xanthan Polymer	3.50	3.50	5.00	3.50
BLUE STREAK	1.00	1.00	1.00	1.00
APHRONIZER A	0.50	0.50	0.50	0.50
APHRONIZER B	0.50	0.50	0.50	0.50
PLASTISIZER	0.30	0.30	0.30	0.30
ACTIGUARD	0.50	0.50	0.50	0.50
MgO				2.35

* Concentrations are in lb/bbl

Samples 2 and 3, neither one of which contains particulates (HC or MgO), did not plug either of the capillary tubes. Indeed, the Pressure vs Flow Rate curves appear to correlate with the fluid viscosity, as expected, and with the amount of Viscosifying Polymer. Sample 4, which is identical in composition to Sample 2 save for the MgO, generates a higher Pressure at any Flow Rate, indicating that solids like MgO not only can serve as plugging agents in a sufficiently small orifice, but they also raise the viscosity of the base fluid.

Table 13. Rheology of Test Fluids

Test	Sample 2	Sample 3	Sample 4
Brookfield LVDV-II+, 3L Spindle, 0.06 sec^{-1}, 70 ^oF	100000 cP	208000 cP	132000 cP
Grace M3500, 70 ^oF			
600 rpm	68	102	82
300 rpm	58	90	69
200 rpm	54	83	62
100 rpm	47	74	53
6 rpm	30	52	35
3 rpm	27	48	33
Gel Strength -10 sec	27	48	32
Gel Strength – 10 min	30	51	34
Gel Strength – 30 min	30	52	35

Figure 105. Pressure vs. Flow Rate in 0.01-in ID Tubing for APHRON ICS™ Samples

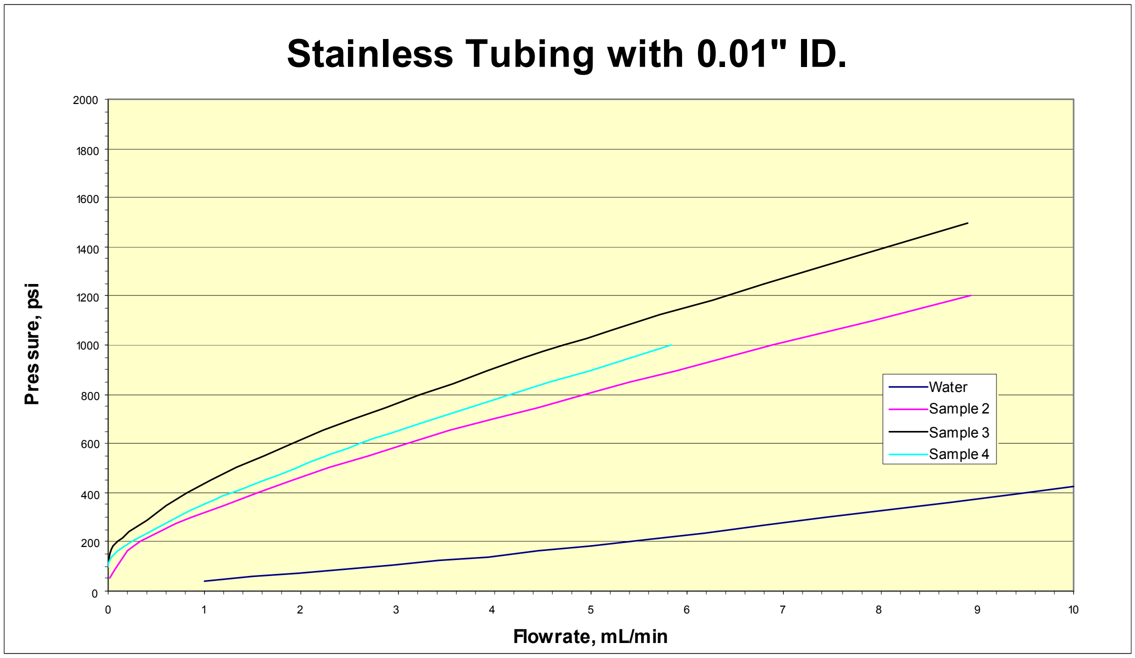

Figure 106. Pressure vs. Flow Rate in 0.005-in ID Tubing for APHRON ICS™ Samples

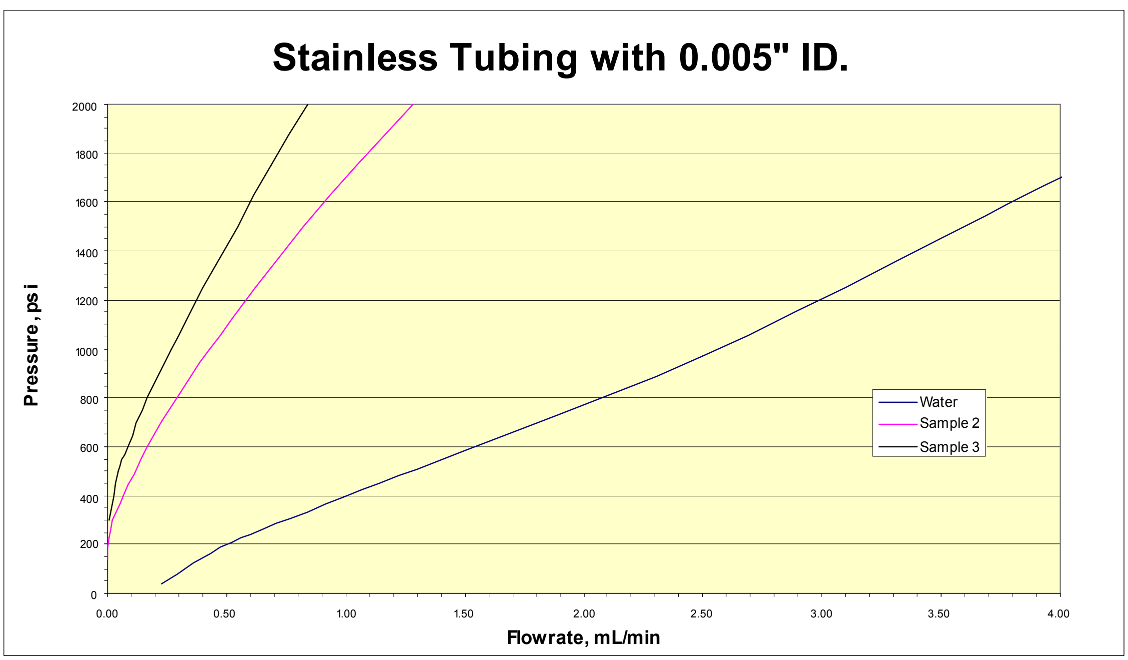

Surfactants and Air

To better understand the roles that air and surfactants play in controlling invasion of whole mud and filtrate into permeable media, samples of the SE APHRON ICS™ system were prepared containing (a) the standard complement of surfactants and air, (b) the standard complement of surfactants and no air and (c) neither surfactants nor air. The composition of the two mud samples (one with and one without surfactants) is given in Table 14. Three types of mud invasion tests were performed to better understand the roles played by the surfactants and air: Modified Capillary Suction Time, Core Leak-Off and Capillary Flow.

After they were mixed, both samples were hot rolled 16 hours at 150 °F. Because the stability of air bubbles in the fluid without surfactants was much lower than in the standard fluid, the former lost all of its entrained air during heat aging. To compare the base characteristics of these fluids and exclude any effects from aphrons, both samples were deaerated by centrifugation. As made clear by the results in Table 15, the surfactants had a negligible effect on the rheological profile of the SE APHRON ICS™ system. When air (aphrons) was added to the full SE APHRON ICS™ system, it, too, appeared to have no significant effect on the rheology.

Table 14. Composition of SE APHRON ICS™ with and without Surfactants

Component (lb/bbl)	SE APHRON ICS™	SE APHRON ICS™ w/o surfactants
Water	337.0	339.0
Soda Ash	3.0	3.0
ACTIVATOR II	2.0	2.0
GO DEVIL II	5.0	5.0
ACTIVATOR I	5.0	5.0
ACTIGUARD	0.5	0.5
BLUE STREAK	1.0	
APHRONIZER A	0.5	
APHRONIZER B	0.5	0.5
PLASTISIZER	0.3	0.3

Table 15. Rheology of SE APHRON ICS™ and SE APHRON ICS™ without Surfactants

	SE APHRON ICS™	**SE APHRON ICS™ w/o surfactants & Air**
Brookfield LVDV-II+, 3L Spindle, 0.06 sec^{-1}, 70 °F	193000	193000
Grace M3500, 70 °F		
600 rpm	93	90
300 rpm	78	75
200 rpm	69	67
100 rpm	59	57
6 rpm	39	39
3 rpm	36	36
Gel Strength – 10 sec	36	35
Gel Strength – 10 min	38	37
Gel Strength – 30 min	38	38

On the other hand, both surfactants and air appeared to have a strong effect on filtration rate of the fluid. The Modified Capillary Suction Time test was run on all three fluids; this test generates a Capillary Suction Distance, or CSD, which is a measure of the filtration rate of the fluid. As shown in Table 16, CSD increased upon removal of air from the SE APHRON ICS™ drilling fluid, and it increased further when the surfactants in the drilling fluid were omitted. It is clear that the surfactants, as well as the aphrons, reduce the filtration rate. What is not clear is why the surfactants should play such a strong role. The surface tensions of the full SE APHRON ICS™ fluid and of the SE APHRON ICS™ fluid without BLUE STREAK and APHRONIZER A were determined with a Du Nouy tensiometer to be 34 dyn/cm and 63 dyn/cm, respectively. The low surface tension of the full SE APHRON ICS™ fluid is consistent with surfactant concentrations that are high enough to form micelles. These micelles may be of sufficient size to be incorporated into the filter cake and reduce the filtration rate.

Table 16. Modified Capillary Suction Time (CSD) of APHRON ICS™ with and without Air and without Surfactants

	CSD (mm)			
Fluid	**30 min**	**60 min**	**90 min**	**120 min**
SE APHRON ICS™ 16% air	1.5	3.0	4	4.5
SE APHRON ICS™ 0% air	2.5	4	5.5	7
SE APHRON ICS™ without surfactants	4	6	8	10

Core Leak-Off tests were carried out with the full SE APHRON ICS™ drilling fluid and the SE APHRON ICS™ fluid without BLUE STREAK and APHRONIZER A. All Core Leak-Off tests were carried out at 200 °F, 2000 psig fore pressure and 1000 psi pressure drop across the 2-in Aloxite cores, using the apparatus shown in Figure 23. When core permeability was low (FAO-00 and FAO-5), the Leak-Off for fluid with surfactants/air was a little lower, as expected, than the Leak-Off for fluids with no surfactants/no air. For cores of higher permeability (FAO-10), the Leak-Off of fluid with surfactants/air was greater than the Leak-Off for fluid with no surfactants/no air. The results of the Leak-Off experiments are given in Table 17; replicate tests were run with the FAO-5 and FAO-10 cores. The initial FAO-10 Leak-Off curves are shown in Figure 107.

It is helpful to divide Total Leak-Off into its two components, as in Equation (12): Total Core Leak-Off = Spurt + Filtration, where Spurt is the initial invasion of whole fluid before a filter cake is fully established, and Filtration is the invasion of filtrate after a filter cake is formed. Spurt is obtained by extrapolation of the Filtration portion of the curve back to time = 0, and Filtration is given by the balance of the Leak-Off.

Table 17. Effect of Core Permeability and Surfactants on Leak-Off of SE APHRON ICS™

200° F, P_{fore} = 2000 psig, P_{back} = 1000 psig, $P_{confining}$ = 2500 psig

Core	Mean Pore Diameter (µm)	SE APHRON ICS™ w/o Surfactants and Air			SE APHRON ICS™ 13% Air		
		Spurt	Filtration	Total	Spurt	Filtration	Total
FAO-00	10	3.8	4.2	8.0	3.1	3.9	7.0
FAO-5	20	8.8	4.0	12.8	6.0	5.2	11.2
		11.4	5.0	16.4			
FAO-10	35	11.6	5.9	17.5	22.5	3.8	26.3
		13.0	5.2	18.2	32.1	3.1	35.2

As expected, both Filtration and Spurt in the FAO-00 and FAO-5 cores appear to be a little lower for the full APHRON ICS™ system than for the system without surfactants and to increase only a little with increasing core permeability. The same is true for Filtration in the FAO-10 core. The Spurt in the FAO-10 core, on the other hand, is anomalously high for the full APHRON ICS™ system.

Results of the Capillary Flow experiments with the two fluids are shown in Figures 108 and 109. In both sizes of tubing, resistance to flow was a little higher for the fluid without surfactants (and no air) than for the fluids with surfactants. All of the fluids had similar viscosity profiles (see Table 15), showing that neither the surfactants nor the air affect viscosity. One explanation for the slight difference in the Capillary Flow curves is the difference in time required to establish steady-state pressures at any given flow rate. Upon incrementing the flow rate, the pressure generated by the fluid without surfactants reached a steady state value very quickly, whereas the pressure generated by both fluids with surfactants took a long time to stabilize and may not have actually reached a constant (steady state) value. We do not have a reasonable explanation for that temporal behavior but the result is that the reported pressure readings for the fluids with surfactants may have been a little low.

Figure 107. Effect of Surfactants on Leak-Off vs Time$^{1/2}$ of APHRON ICS^{TM} Drilling Fluids

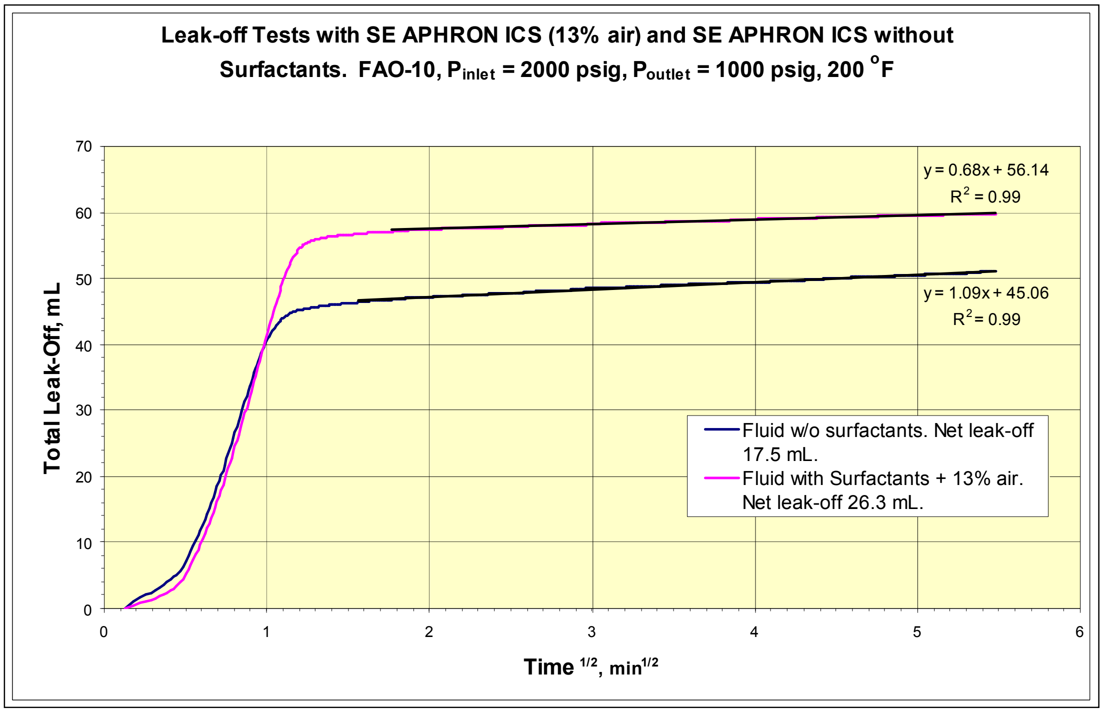

Figure 108. Effects of Surfactants and Air on Flow Curves in 0.02-in (0.5-mm) ID Tubing

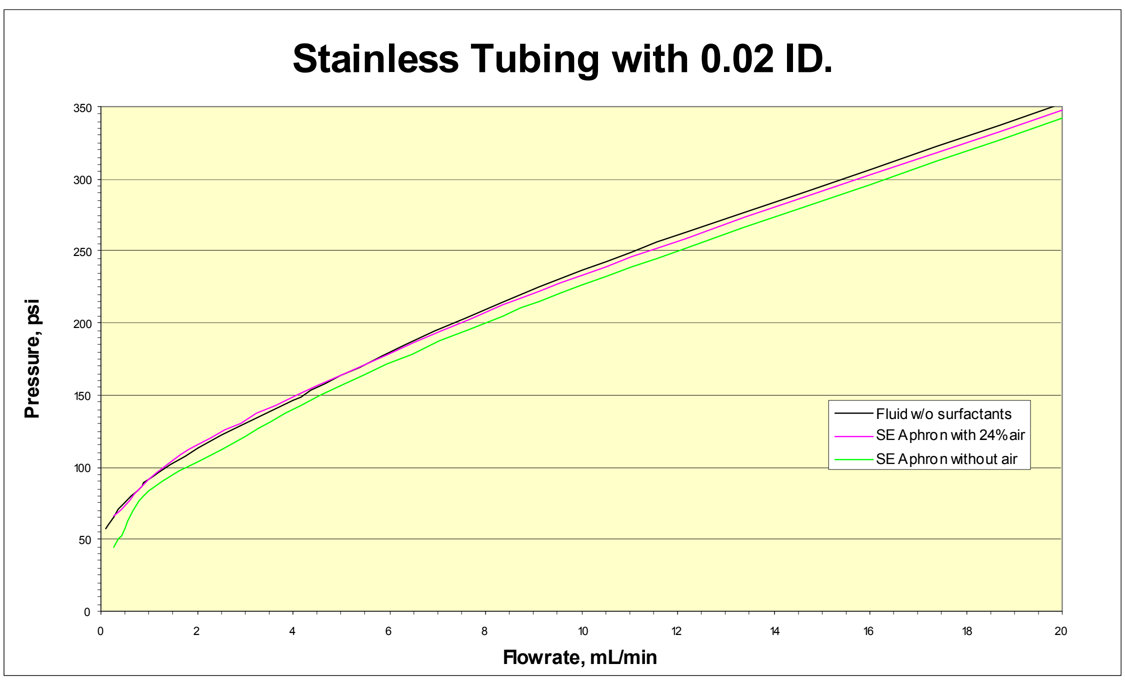

Figure 109. Effects of Surfactants and Air on Flow Curves in 0.03-in (0.76-mm) ID Tubing

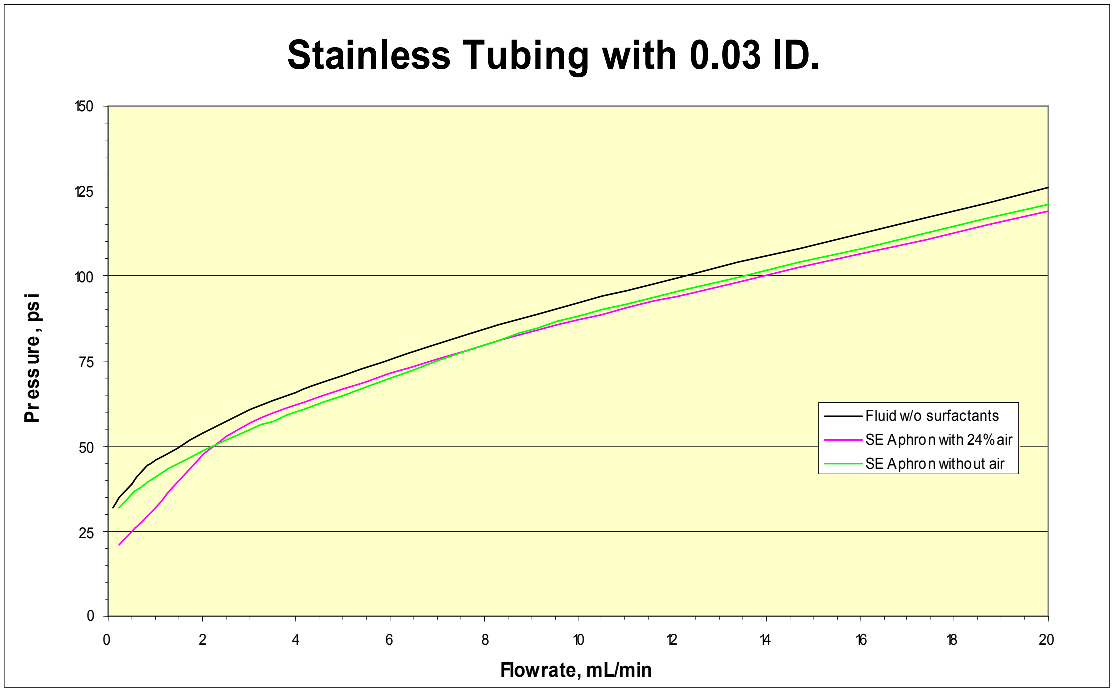

While surfactants in the SE APHRON ICS™ formulation serve to stabilize air and other non-polar internal phases, they are not expected to affect processes that are determined by bulk properties of the fluid, e.g. laminar flow, which is controlled by fluid rheology. Indeed, we have noted no effects of surfactants on rheology as measured via flow in large conduits or concentric cylinder viscosimeters. However, the slow rise of the pressure gradient in the Capillary Flow experiments reported above suggests that surfactants affect flow through capillaries and perhaps other vessels with a high Surface Area / Volume ratio. Surfactants do, of course, affect many processes that involve surface or interfacial properties, such as emulsion stability and wettability. It may be argued that the high surface areas of the filtration media used in Core Leak-Off and Capillary Suction may be influenced by surfactants as well. Thus, not only would aphrons be expected to reduce the rates of fluid invasion in all three tests – Capillary Flow, Leak-Off and Capillary Suction – so would the surfactants themselves. The influence of surfactants on Capillary Flow is reminiscent of the thixotropic effects one observes in concentric cylinder viscosimetry of clay and polymer suspensions. Surfactant micelles could play a role in all three types of tests, as might interaction of the surfactants with other components in the drilling fluid.

Flow Properties of Aphron Drilling Fluids

Multi-Phase Flow:

In initial tests conducted with sand packs in the transparent tube shown in Figure 22, flow of the SuperEnhanced APHRON ICS™ mud gave rise to an unusual phenomenon: the bubbles appeared to move faster than the bulk fluid and to concentrate at the front of the moving mud. This was initially thought to be related to a "jump" effect that viscoelastic fluids are known to impart to bubbles.[30] Another phenomenon sometimes seen in two-phase flow with a low-density internal phase, namely congregation of the bubbles near the pipe wall, was not observed. The anomalous behavior of the bubbles was observed with both 20/40 and 70/100 mesh sand packs, as long as there was a pressure difference along the length of the sand pack. The most pronounced effect was observed with the 20/40 sand pack filled with water. Unfortunately, the brown color of both the sand and the APHRON ICS™ mud made for difficult viewing of this phenomenon.

Low-pressure flow tests were conducted in a short, clear acrylic pipe using water-saturated 20/40 sand and blue-dyed transparent Enhanced APHRON ICS™ fluid. Figure 110 shows one exposure from the video stream of the test. The colored mud is moving from right to left, and the leading edge of the fluid has passed the middle of the pipe. At the leading edge, the fluid is much lighter in color, and microscopic examination reveals that region to be composed primarily of bubbles. The highest color intensity is at the entrance to the tube, and few bubbles are apparent. One may argue that the loss of color while traversing the sand pack was due to depletion of the dye, but it was evident both from examination during and after the test, that little or no dye had adsorbed onto the sand grains.

Figure 110. Dyed Transparent APHRON ICS™ Mud Flowing through 20/40 Sand Pack

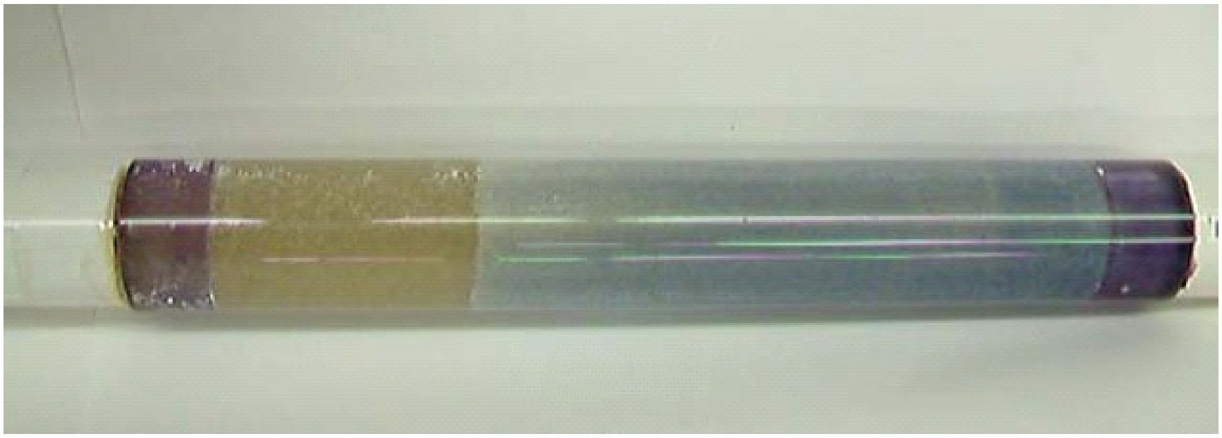

Researchers at Texas A&M University dub this phenomenon "Bubbly Flow," a type of flow that is observed for dispersed low-density internal phases.[29] The Navier-Stokes expression, which is commonly used in the drilling fluid industry to describe settling of high-density particles through a liquid, applies equally well to creaming or buoyancy of low-density "particles." When the force is a pressure differential, rather than gravity, a similar effect occurs and transport of the internal phase is in the direction of the pressure drop.[30] Various aspects of this Bubbly Flow phenomenon – system geometry (pore network, radial flow), compressibility of the bubbles and interaction of the bubbles with the liquid medium and with other bubbles -- are discussed in the section on Modeling of Drilling Fluid Invasion in Permeable Media.

Fluid Rheology:

The shear rheology of the base fluid in the APHRON ICS™ system is compared to that of the FLOPRO NT™ system in Figure 111. As indicated in the log-log plot, both fluids follow the Power Law model very well, and the APHRON ICS™ system shows a viscosity that is several times higher than the FLOPRO NT™ system throughout this shear-rate range. A consequence of this is that in a permeable medium, as the fluid velocity slows due to radial flow expansion (and, for the APHRON ICS™ system, additional decelaration induced by the aphrons and microgel), the higher viscosity of the APHRON ICS™ system will cause a greater deceleration and a greater drop of the shear rate, leading to a much faster increase in viscosity.

Although the solid components (such as MgO) in the Aphron ICS system appear to contribute a little to the viscosity of the drilling fluid throughout the shear rate range of interest, neither the surfactants nor aphrons affect the viscosity profile significantly (see Figure 76 and Table 15). Thus, the viscosities of the Standard and SE APHRON ICS™ fluids are essentially identical. Optional additives, such as ACTIGUARD, also appear to have a negligible effect on the viscosity profile, as shown in Figure 112.

Figure 111. Viscosity Profiles of SE APHRON ICS™ and FLOPRO NT™ Fluids

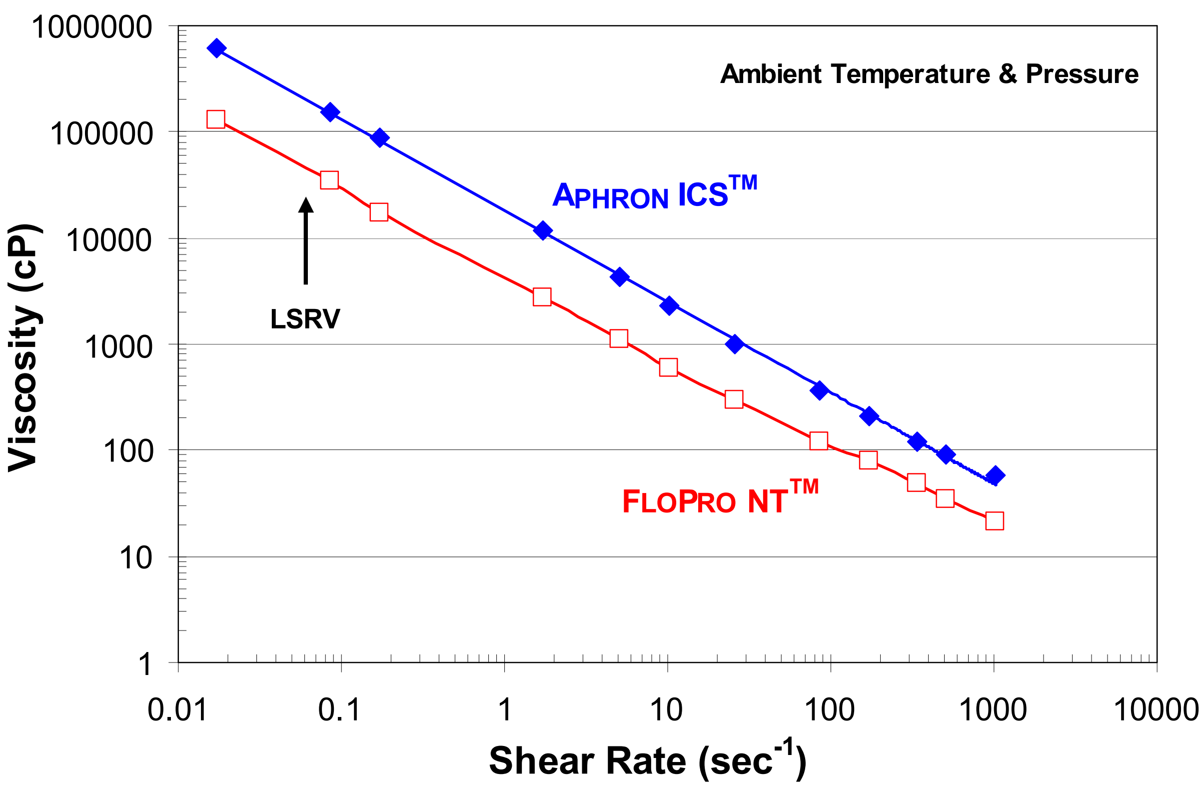

On the other hand, elevated concentrations of the additives can affect the viscosity profile significantly. Of particular interest is the concentration of air (nitrogen). As shown in Figure 113, for concentrations of air exceeding the typical amount that is entrained in an APHRON ICS™ fluid (12 to 15 vol % at ambient pressure), the bulk viscosity of the fluid at high shear rates increases with increasing amount of air. As is shown in the next section, when an APHRON ICS™ fluid invades permeable or microfractured rock, aphrons move rapidly to the fluid front, where they form a zone that is heavily populated with aphrons. It is expected that the viscosity of the fluid in this zone will rise and contribute to the decline in shear rate brought about by radial expansion of fluid as it moves away from the wellbore, thereby accelerating the increase in viscosity that accompanies a drop in shear rate for this highly shear-thinning fluid.

Figure 112. Effect of ACTIGUARD on Viscosity Profile of SE APHRON ICS™ System

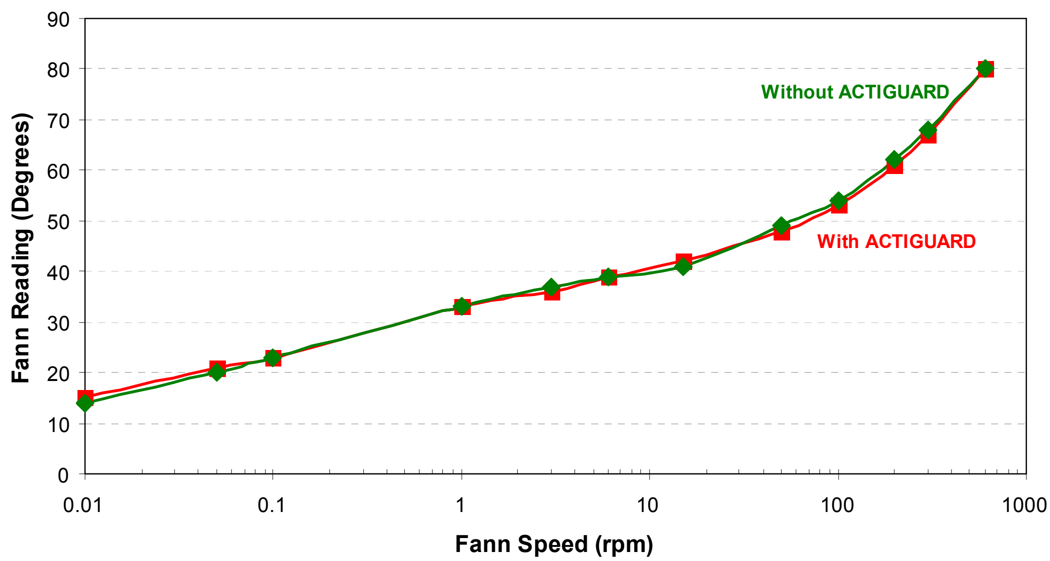

Figure 113. Effect of Air Concentration on Viscosity of the SE APHRON ICS™ Fluid

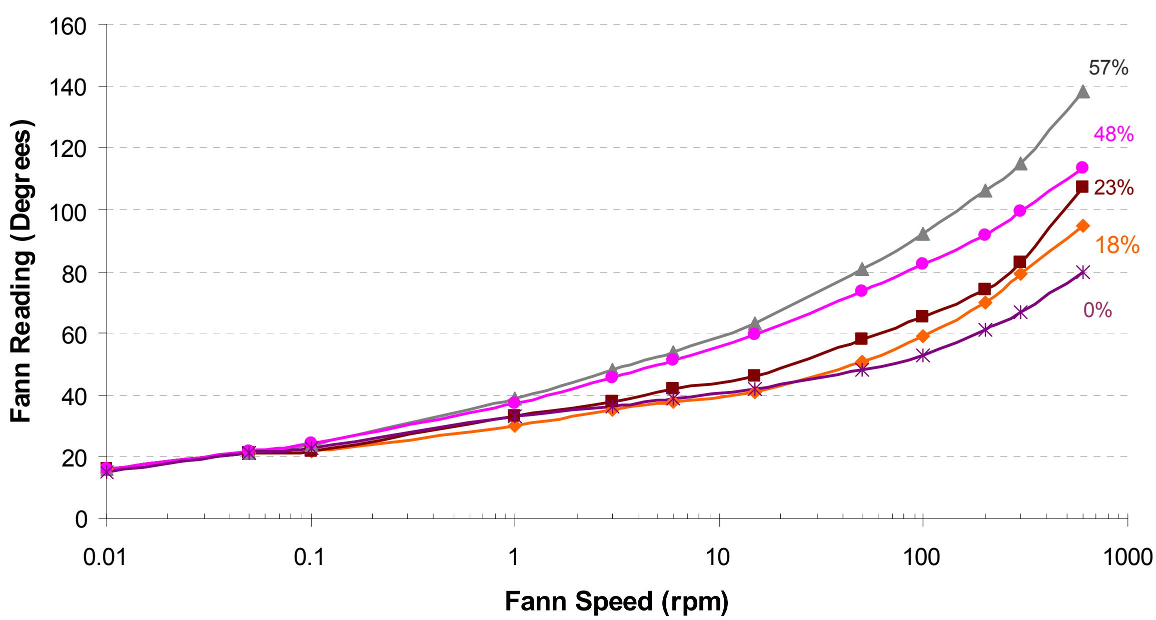

Modeling of Drilling Fluid Invasion in Permeable Media:

For a typical aphron drilling fluid, aphrons are present at such a low concentration that they have a negligible effect on fluid rheology in the wellbore. The base fluid is highly shear-thinning and roughly follows a Power Law model even down to a shear rate as low as 0.01 sec^{-1}. At the same time, steady-state values of shear stress are reached within seconds after changing shear rate; thus, aphron drilling fluids exhibit very low thixotropy. As shown in Figure 114 and detailed in Table 18, the Herschel-Bulkley model (also known as the "Yield Power Law" model) fits even better, but the best simple model fits are a Carreau[31] model and a Dual Power Law model ($\tau = k_1\gamma^{n1} + k_2\gamma^{n2}$, where τ is the shear stress, k_i is the consistency, γ is the shear rate and n_i is the power-law index). Based on these comparisons, the Carreau model with Yield was incorporated into a Fluid Invasion Model for the drilling fluid in the annulus and loss zone. The main characteristic of this model is that it predicts a constant viscosity μ_0 at very low shear rate and a constant viscosity μ_∞ at high shear rates. For intermediate values of the shear rate, it exhibits a power-law like, highly nonlinear relationship.

Figure 114. Comparisons of Viscosimetry Data and Several Rheological Models Ambient Temperature and Pressure

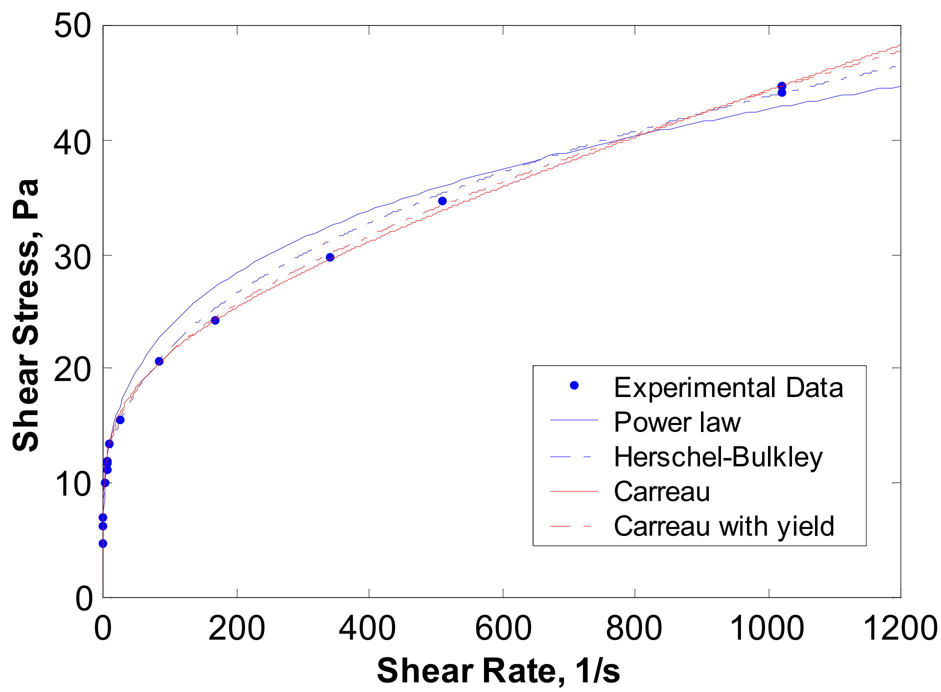

Table 18. Least Squares Residuals for Various Rheological Models

Model	Least-Squares Residual
Power Law	0.0778
Herschel-Bulkley	0.0418
Carreau	0.0291
Dual Power Law	0.0217
Carreau – With Yield	0.0206

Suppose that an axially symmetric wellbore of radius 0.15 m is drilled in a uniform, isotropic reservoir with 2.5 Darcy permeability. The pressure at the wellbore is 2500 psi (17.3 MPa), and the pressure at a distance of 10 m into the reservoir is 500 psi (3.5 MPa). Darcy flow through the formation and the conservation of mass govern the invasion process. In an annulus, the equation for conservation of mass takes the simple form:

$$\frac{1}{r}\frac{\partial}{\partial r}\left(r\frac{\partial p}{\partial r}\right)=0 \tag{22}$$

In the fast flow regime, $\mu = \mu_{\infty} = 0.0136 Pa \cdot s$; in the slow flow regime, $\mu = \mu_0 = 50.68 Pa \cdot s$. After 24 hours, the aphron fluid has invaded the reservoir to a distance of 10.7 m from the wellbore if the fast flow mode is assumed. If, however, the slow flow mode is assumed, the fluid has invaded only 0.43 m of the reservoir. These two numbers give the bounds in which the invasion of the aphron fluid can happen. The difference is significant, and there is a clear need to establish if and when the regime changes from fast to slow. Note that this drastic change in the invasion depth is only due to a change in the viscosity of the fluid from high to low shear rates.

Simulations using a base fluid with aphrons show that in the presence of a pressure gradient, a bubble will experience unbalanced forces on its surface and experience "bubbly flow." As a result, it will move relative to the fluid and in the direction of the pressure gradient. The relative velocity V of a bubble subjected in a pressure gradient can be related to the Stokes Equation,[29] which is often invoked for gravity-driven settling of weighting material or separation of bubbles.

For a rigid sphere in a fluid under the influence of a one-dimensional pressure gradient, $\Delta P/L$, the relative velocity of the bubble in an infinitely wide conduit is given by

$$V = (2/9)(r^2/\mu) * \Delta P/L \tag{23}$$

where r is the bubble radius and μ is the fluid viscosity.

In permeable rock under downhole conditions, accumulation of aphrons at the fluid front can create a barrier to flow of liquid or increase the viscosity of the fluid. In either case, increasing the concentration of aphrons slows invasion of the fluid. In modeling this, a constant concentration of about 0.15 vol % of the bubbles was assumed at the wellbore. As the bubbles are released for the first time at the wellbore, they form a front, which starts moving away from the wellbore. Their velocity is a sum of both the fluid velocity and their relative velocity -- Equation (23) -- with respect to the fluid. Since at different distances from the wellbore the fluid velocity and pressure gradients are different, the bubbles change speed, generally slowing down as they move away. Furthermore, as the pressure decreases, they expand and increase the volumetric concentration of gas. To simulate this, the volumetric bubble concentration was computed using a first-order upwind finite difference scheme for bubbles with initial radius 100 μm at several instances of time. The bubble concentration away from the wellbore increases very slowly. However, the bubble profile travels away from the wellbore very quickly, with a speed on the order of meters per second, as shown in Figure 115. This high speed appears to be due to the large pressure gradient, which is of about 10^7 Pa/m near the wellbore. Consequently, as soon as fluid penetrates the permeable rock, bubbles move to the fluid front and concentrate there to form a soft seal.

Since the volume ratio of liquid/air entering the reservoir is constant with time, the thickness of this highly concentrated bubble layer relative to the fluid invasion depth is also nearly constant. For an invasion depth of 10 m, the bubble layer has a thickness of 2-10 cm, depending on the concentration of bubbles in the layer. This bubble layer serves as a barrier to flow of the liquid and effectively slows the rate of invasion of drilling fluid.

Figure 115. Volumetric Bubble Concentration after Release of Aphrons at the Wellbore

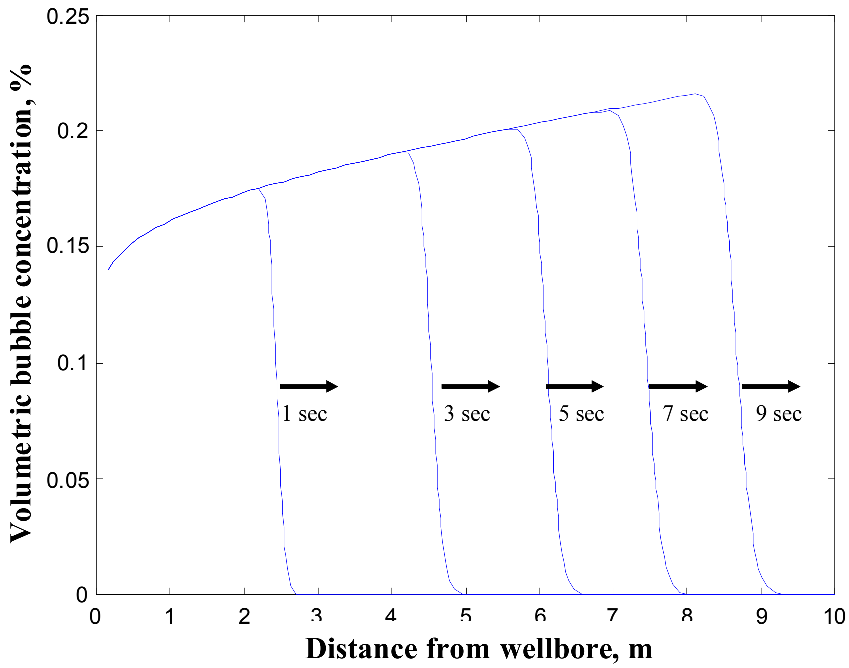

The Fluid Invasion Model was fitted to viscosity profiles for the base fluid, i.e. no aphrons and no particulates. It was found to match closely low-shear-rate viscosity profiles of a 3.5 ppb DUOVIS (xanthan gum) fluid in 5-ft (1.5 m) long 0.005 in (0.127 mm) and 0.01 in (0.254 mm) ID capillary tubes. Water was used as a reference fluid: experimental data were compared with the flow profile calculated using the very accurate Hagen-Pouiselle model for water.[29] The results indicated that the value of 0.01 in for the internal diameter of the larger capillary tube was accurate, but that the ID of the smaller capillary tube was probably closer to 0.00539 in (0.137 mm). The latter was used in all subsequent calculations.

Using the tube geometries verified above, it was determined that the Fluid Invasion Model did <u>not</u> simulate the high-shear-rate viscosity profiles of the polymer fluid very well. Since the Model currently incorporates a number of approximations that yield analytical solutions, it was decided to discard these and solve the flow equations numerically. The exact solutions that were obtained provided very good fits for the 3.5 ppb DUOVIS fluid in both capillary tubes, as shown in Figure 116.

Figure 116. Experimental and (Exact) Numerical Flow Curves for Fluid Invasion Model

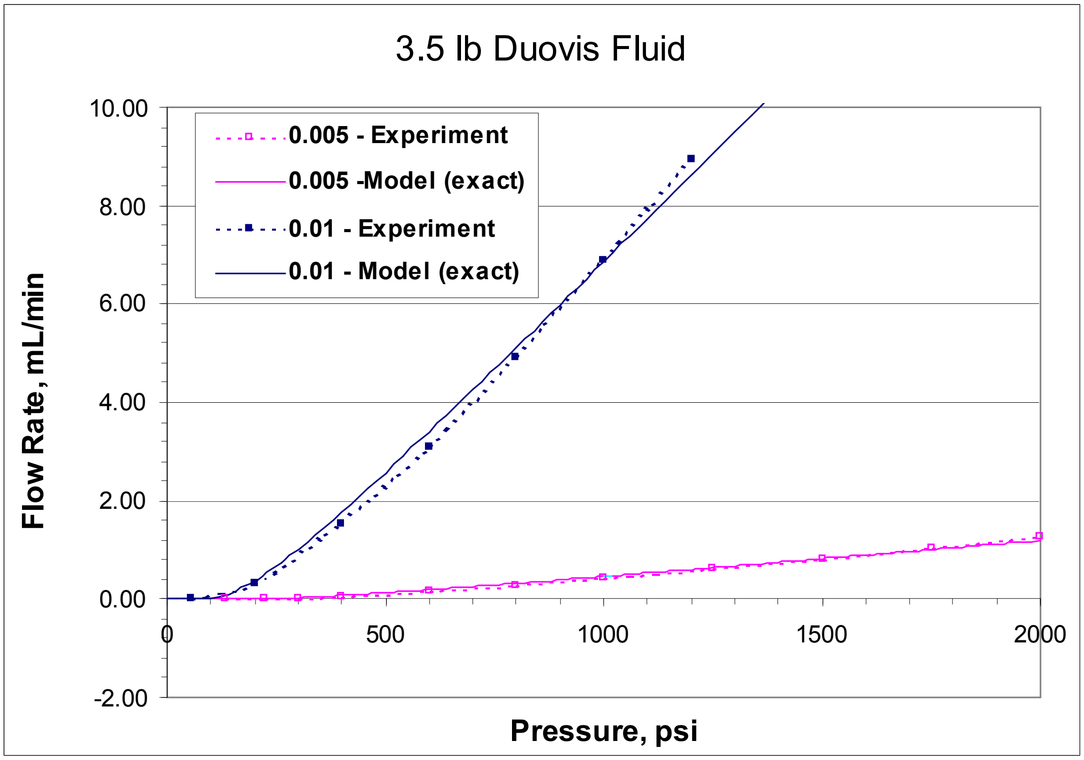

The first working version of the Pipe Flow Model for measurement of fluid invasion of APHRON ICS™ drilling fluids into permeable formations incorporates flow of the liquid and gaseous phases, but it omits a number of important variables. Among the most important are rock pore geometry, bubble population and size distribution in the aphron band, particulates and temperature. Findings from this study indicate that there is a window of rock pore geometry within which bubbly flow can occur. In addition, the high-shear-rate viscosity increases with increasing amount of air (nitrogen). Furthermore, as aphrons are sheared during passage through the loss zones, they are comminuted to the point where they are of a size similar to that of the openings and they form a soft bridge or seal. These effects will need to be incorporated into the next version of the Pipe Flow Model.

Radial Flow of Aphron Drilling Fluids:

Radial Flow Tests were performed to observe the presence of "bubbly flow" in the APHRON ICS™ system and validate the Fluid Invasion Model in radial permeable formations. The Radial

Flow Cell was filled with 2-mm glass beads and red-dyed water. Transparent Enhanced APHRON ICS™ Mud containing blue dye was pumped by the "bore hole" of the cell at a pressure of 10 psig, allowing invasion of the mud into the cell. As shown in Figure 117, a white band of bubbles formed almost immediately between the two fluids, as predicted by the Bubbly Flow Fluid Invasion model.

Figure 117. Flow of Transparent APHRON ICS™ Fluid in Radial Flow Apparatus

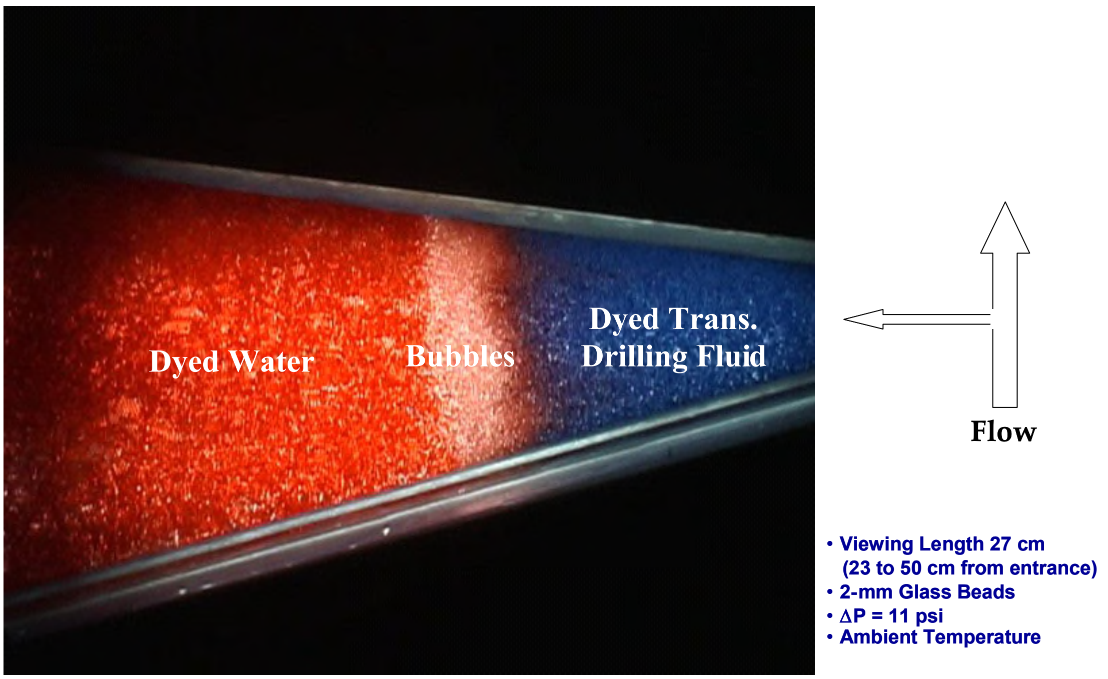

As the mud progressed through the cell (see Figures 118 and 119), the aphron bandwidth remained fairly constant (about 3 cm), again as predicted by the Fluid Invasion model for the APHRON ICS™ drilling fluid. The trailing end of the aphron band becomes increasingly difficult to discern, because the dyes mix more and more – to form a purple region -- as the fluid traverses the length of the flow apparatus.

The test above was repeated with SE APHRON ICS™ fluid in place of the dyed Transparent APHRON ICS™ Mud. Again a band of bubbles was formed at the fluid front (shown below in Figure 120), and it possessed a similar width as had been observed with the Transparent APHRON ICS™ mud.

Figure 118. Continuation from Fig. 117

Figure 119. Continuation from Fig. 118

Figure 120. Flow of SE APHRON ICS™ Mud in Radial Flow Apparatus

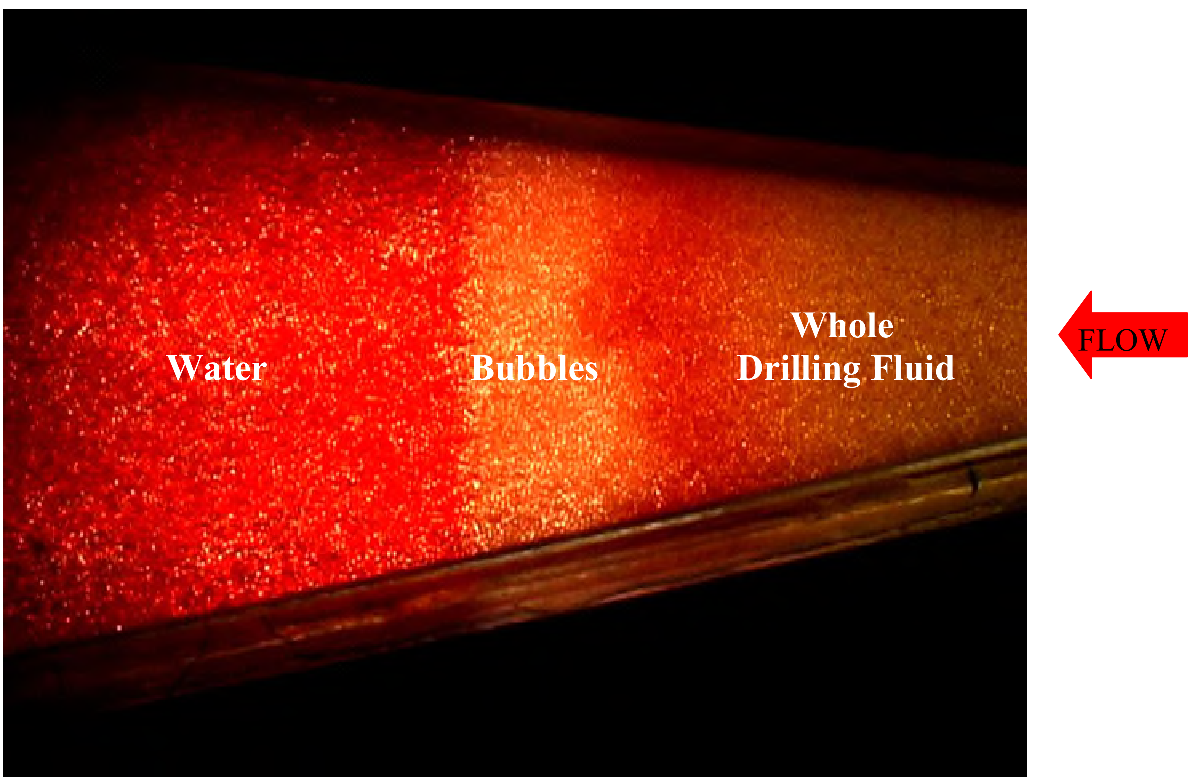

The rate of invasion of the SE APHRON ICS™ Mud was recorded and plotted in Figure 121. As the mud entered the viewing area, the linear flow rate was in excess 11 cm/sec, but it dropped off rapidly to a relatively constant value of less than 1 cm/sec.

Figure 121. Progress of SE APHRON ICS™ Fluid in Radial Flow Apparatus

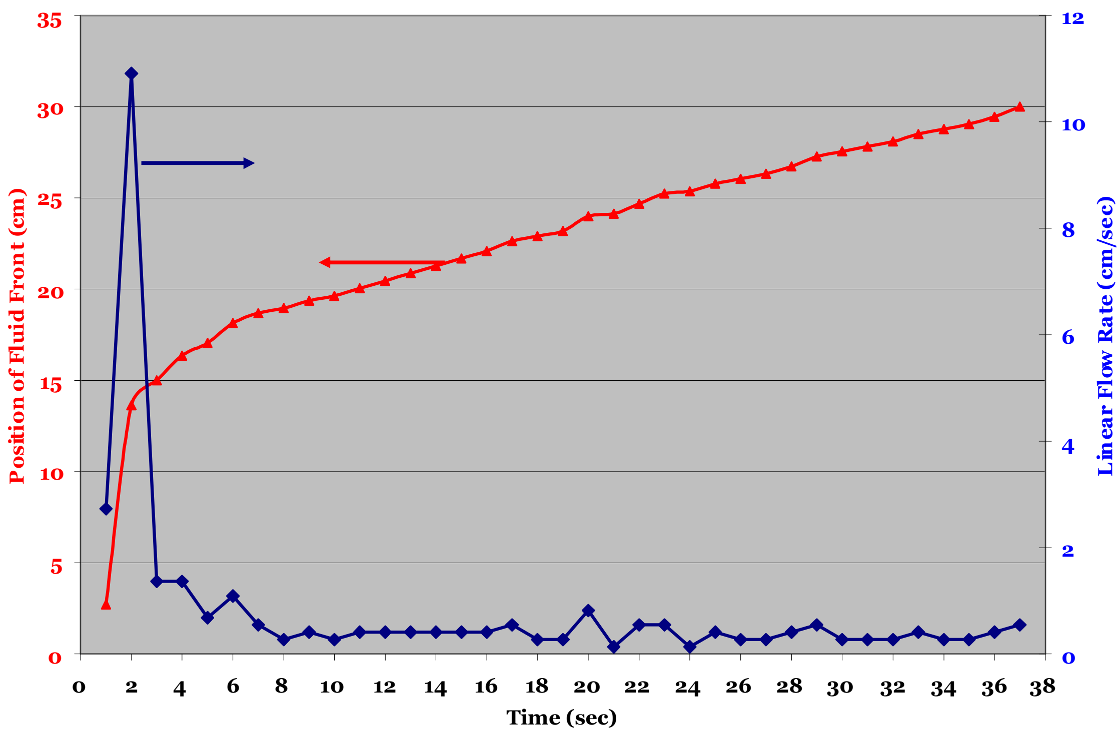

This low linear flow rate is consistent with what was observed with the Transparent Enhanced APHRON ICS™ fluid. For comparison, a solids-free reservoir drilling fluid, FLOPRO NT™, was run in similar fashion. The results, which are plotted in Figure 122, show that the average velocity of the FLOPRO NT™ fluid is about an order of magnitude greater than that of the full (aphron-laden) APHRON ICS™ fluid, although the LSRV of the FLOPRO NT™ fluid is only a little less than half that of the APHRON ICS™ fluid.

Figure 122. Invasion Rates of APHRON ICS™ and FLOPRO NT™ Fluids in Radial Flow Apparatus

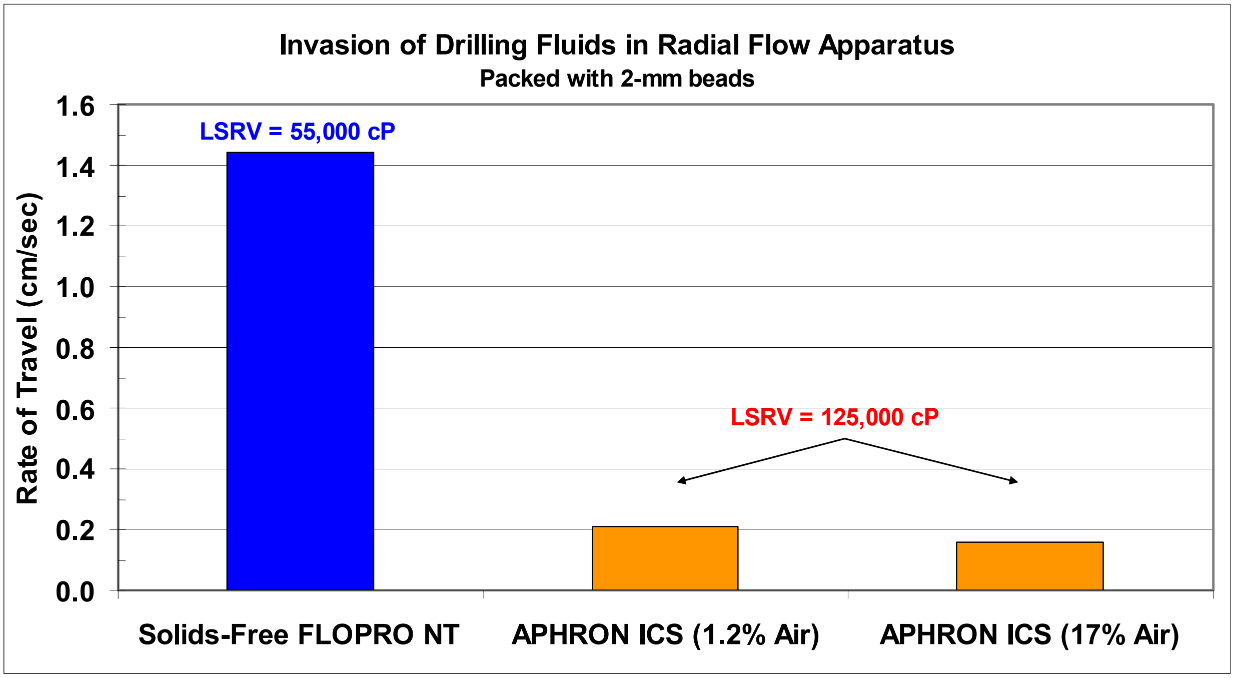

Wettability of Aphron Drilling Fluids

In the apparatus shown in Figure 33, the disposable filter connecting the two glass syringes has a pore size much smaller than the average size of the aphrons. However, very little force was required to squeeze over-size bubbles through the filter; indeed, repeated cycling of the fluid between chambers "polished" the bubbles to produce a relatively narrow bubble size distribution of ever decreasing average bubble size. Not only did the bubbles go through the pores with no problem, they also did not appear to stick to anything, including each other. The notable absence of aphrons on the glass walls of the syringes suggested that other mineral surfaces be tried. In a previous study, APHRON ICS™ muds were spread on Berea sandstone and Aloxite cores. When the cores were swirled gently in deaerated mud, none of the aphrons were found to be visibly attached to the mineral surfaces.

To get a better idea of the surface character of the aphrons, an alternative technique was devised to better evaluate the tendency for aphrons to aggregate. The idea was to generate a bubble aggregate (through collision or initial formation a bubble cluster) and observe whether the bubbles would continue to remain attached. If they moved as an aggregate, it meant that the bubbles had some affinity for each other. If they traveled on different paths, that meant that the bubbles did not stick together and, therefore, had little affinity for each other. Several techniques were tried, but the most promising (see Figure 123) involved a glass vessel through which the transparent Enhanced (TE) APHRON ICS^{TM} mud moved vertically and the bubbles were injected through two open tubes capped with septa and positioned opposite each other at angles of 45 degrees to the vertical.

It was learned that injection of air through a single syringe resulted in a string of bubbles that would flow as an aggregate. However, the fluid traveled in plug flow and did not give the bubbles an opportunity to separate. So, another method was developed to investigate how the bubbles act when some mechanical force is applied on them. For this, some centrifuged TE APHRON ICS^{TM} Mud was spread as a thin layer (a smear) on a standard microscope slide.

The set-up for this is shown in Figure 124. A string of aphrons was created, as above, by injection of air through a syringe. Then the fluid around the aphrons was moved around by swirling it using the syringe needle. It was clear from this simple procedure that the bubbles did not stay together. An example of this is shown in Figures 125 and 126.

Repeated tests showed the same result. An example of an aggregate that was created by the same technique with the needle abutting a quartz surface is shown in Figure 127. Here, not only do the bubbles separate after gently swirling the fluid near the aggregate, they also come away easily from the quartz surface. Thus, it appears that aphrons have little or no affinity for each other, nor for silica or alumina surfaces.

Figure 123. Air Injection Test Set-Up

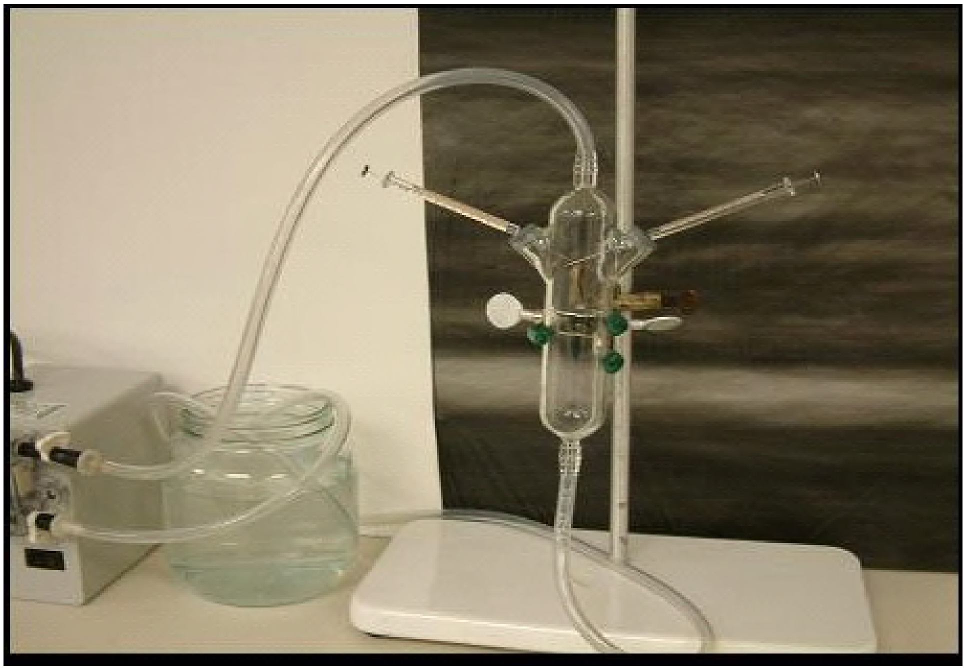

Figure 124. Set-Up for Microscope Slide Smear Test

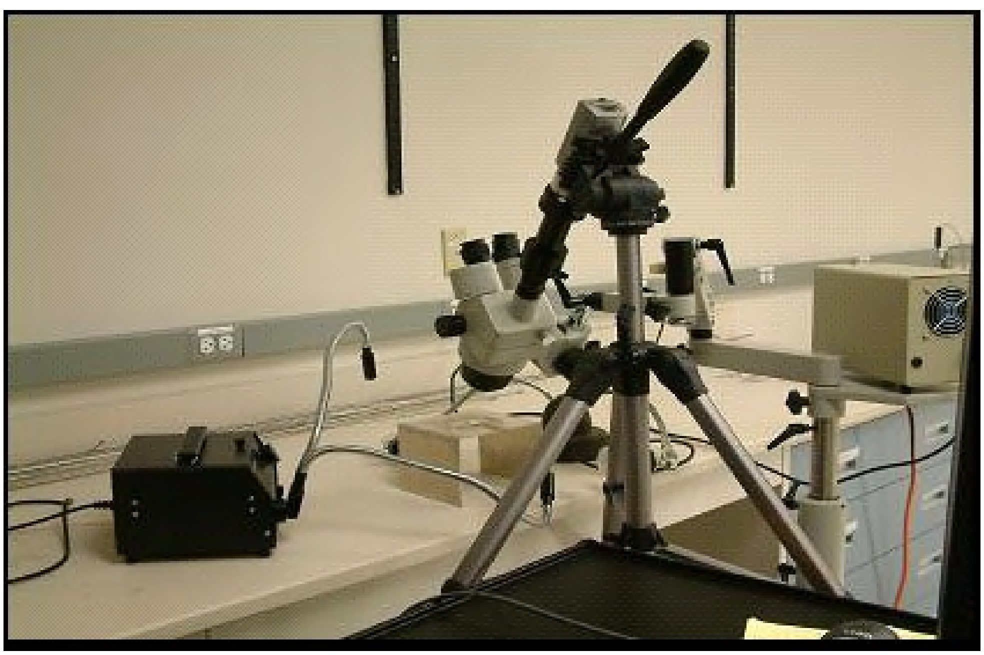

Figure 125. An Aggregate of Aphrons Formed during Bubble Creation

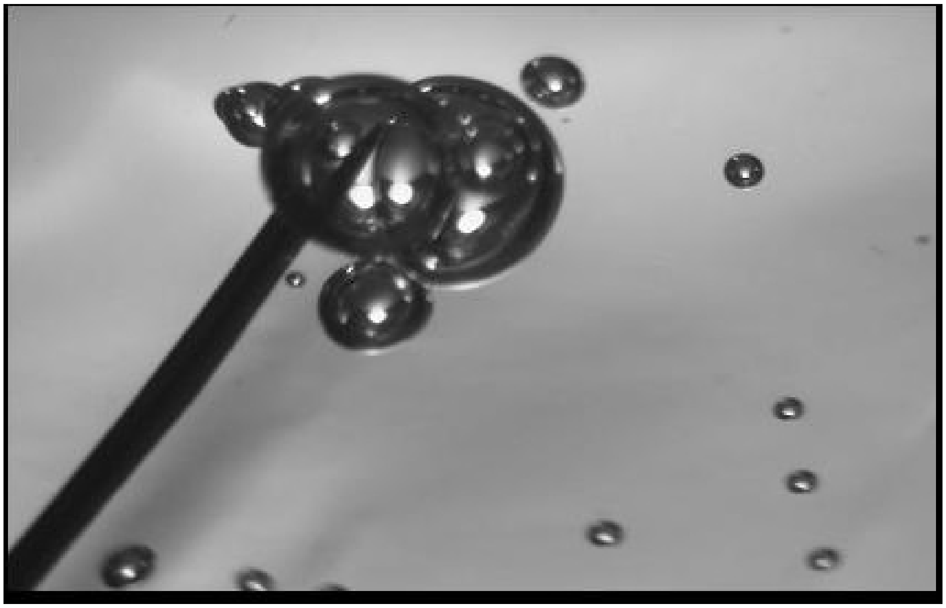

Figure 126. The Aphron Aggregate Breaks Up When Mild Swirling Force Is Applied

Figure 127. Aphron Aggregate on a Quartz Surface

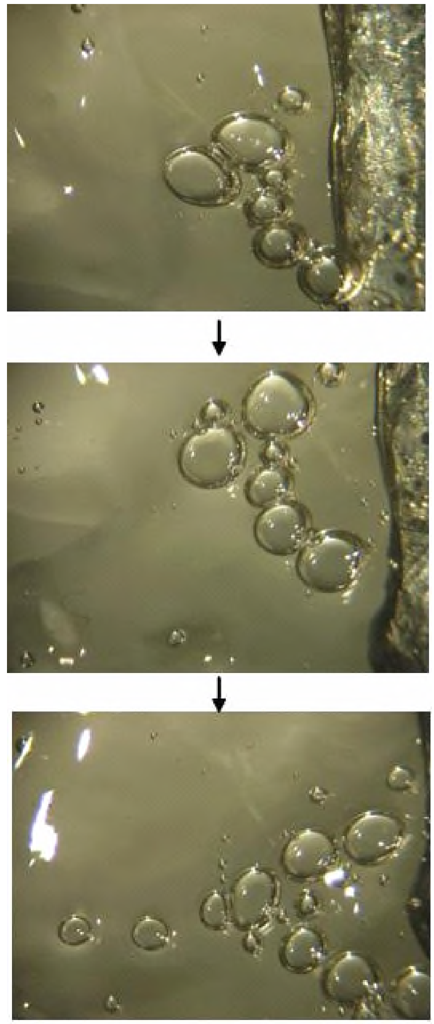

Emulsion Compatibility and Microscope Slide Smear Tests were carried out between APHRON ICS™ fluids and simulated produced fluids to determine whether any barriers might exist for producing fluids through an APHRON ICS™ invasion zone. A variety of oils were tested, including three base oils/synthetic fluids and four crude oils: LVT-200 (ConocoPhillips), BIOBASE 866 (Shrieve), IO 1618 (BP Amoco Chemical), crude oil from the GOM BP Pompano Well, crude from a Chevron well (Tengiz, Khazastan), a Husky crude oil, and a crude oil from an Overseas Limited well (Bogota, Colombia). Three volume ratios of oil vs SuperEnhanced APHRON ICS™ (SEA) Mud were tested: 50% oil/50% SEA, 25 % oil/75% SEA and 90% oil/10% SEA.

Some representative pictures of the blends obtained with the crude oil, IO 1618 and BIOBASE 866, respectively in the 90% oil/10% SEA are shown in Figure 128.

Figure 128. 90% Oil / 10% SEA after blending per API RP 42

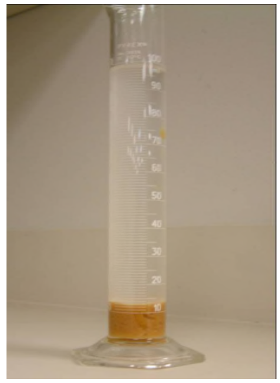

BP Pompano Crude Oil **IO 1618** **BIOBASE 866**

With the 50/50 the mixtures, in every case a uniform emulsion was generated which did not break even after 3 hours. The mixtures were creamy and contained very large globules. A photograph of the 50% BIOBASE 866/50% SEA mixture, which is representative of all the mixtures, is shown in Figure 129.

Figure 129. 50% BIOBASE 866 / 50% SEA Mixture after blending per API RP 42

To determine the wetting characteristics of the oil/mud mixtures, a few drops of each mixture were dropped into a glass beaker filled with water. If the mixture clung together, it was deemed to be oil-wetting; if it dispersed, it was deemed to be water-wetting. Figure 130 shows the results obtained for the mixture shown in Figure 129; the mixture spread, albeit slowly, indicating that it was water-wet.

Figure 130. Dispersion of 50% BIOBASE 866 / 50% SEA Mixture

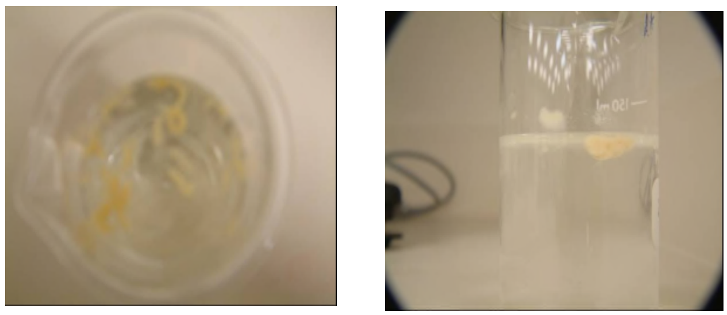

Microscopic examination of the mixture on a slide verified this. As shown in Figure 131, the bubbles, which have to be dispersed in an aqueous medium. This is obviously the continuous phase. Thus, the fluid is water-wet.

Figure 131. Photomicrographs of 50% BIOBASE 866 / 50% SEA Mixture

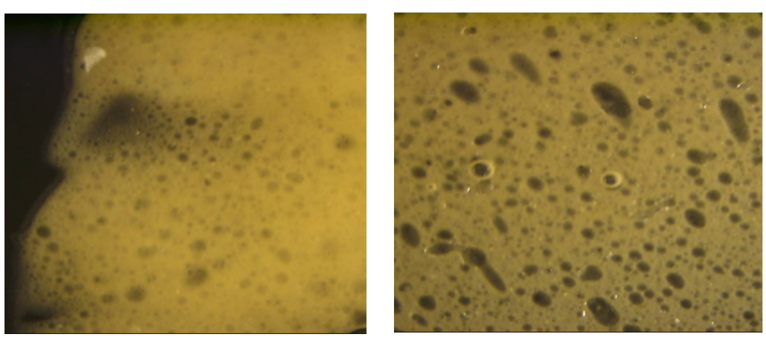

With the 75% oil / 25% SEA mud and 90% oil / 10% SEA mud mixtures, the oils separated from the SEA mud almost immediately. This strongly suggests that the mud did not contain sufficient surfactant to emulsify the mixtures with larger amounts of oil. Indeed, the question arose about what would happen if the SEA mud contained no surfactant. To test this, two 50%/50% mixtures were prepared from BIOBASE 866 and the SEA mud. In one mixture, the regular SEA mud was used; in the other, an SEA mud without BLUE STREAK and APHRONIZER A was used. The results are shown in Figure 132.

Figure 132. 50% BIOBASE 866 / 50% SEA Mixtures with and without Surfactants

With Surfactants

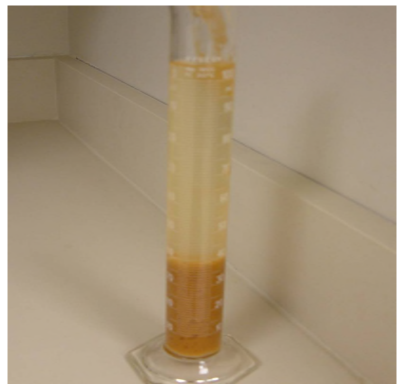

Without Surfactants

From these photographs, it is clear that the observed emulsification is dominated by the surfactant(s) in the APHRON ICS™ muds.

For the Chevron crude oil, all of the fluid mixtures separated almost immediately. Figure 133 shows the separations achieved for the 50/50 and 90/10 mixtures after 30 min.

Figure 133. 50/50 and 90/10 Chevron Crude Oil/ SE APHRON ICS™ Blends after 30 min

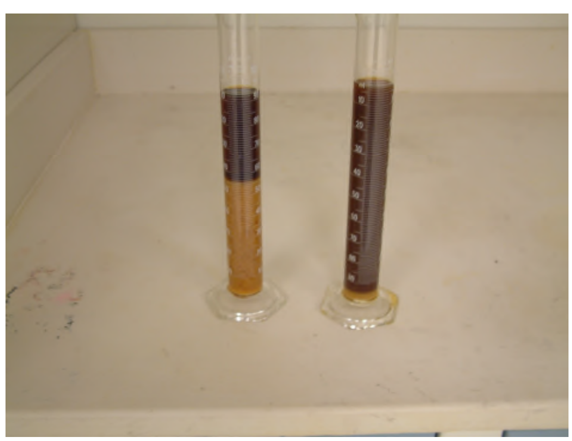

The other Crude Oils did not separate very easily, as shown in Figures 134 and 135.

Figure 134. 50/50 and 75/25 Husky Crude Oil/ SE APHRON ICS^{TM} Blends after 30 min

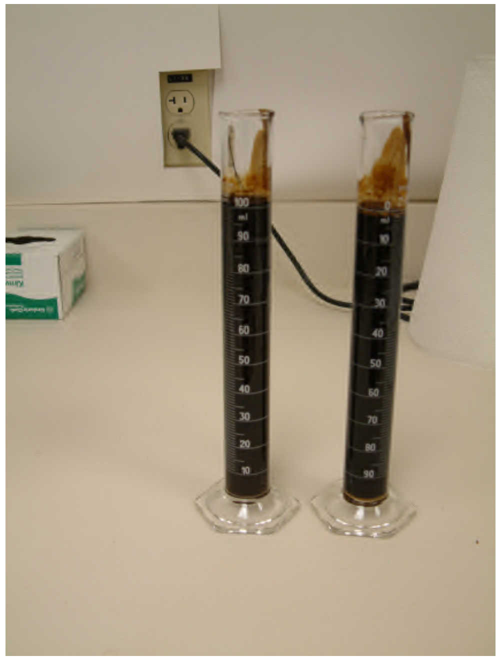

Figure 135. 75/25 and 50/50 Overseas Limited Crude Oil/ SE APHRON ICS^{TM} Blends after 30 min

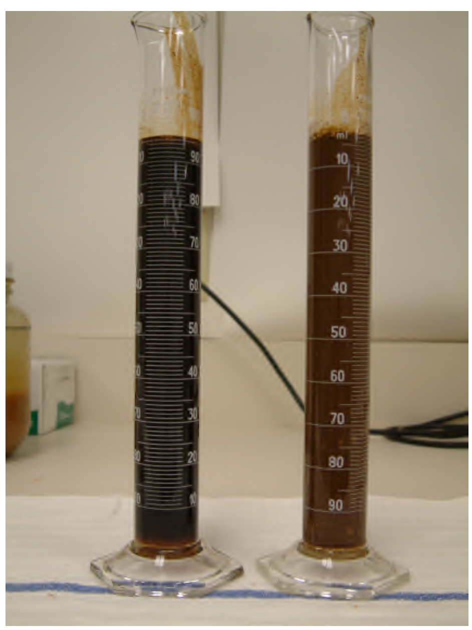

Consistent with the four oils tested previously, 50/50 mixtures of the Husky and Overseas Limited crude oils with the SE APHRON ICS™ fluid generated what appear to be uniform emulsions of similar viscosity to the SE APHRON ICS™ system which did not break even after 3 hours. The mixtures were creamy and contained a broad size distribution of bubbles.

The Chevron crude oil is the only one of the seven oils tested which demonstrated significant phase separation in the 50/50 mixture, and that occurred rapidly. Of all the crude oils, it was the only one to have a low viscosity, which may contribute to the rapidity of the phase separation. To examine the interaction of the oil and mud phases more closely, Microscope Slide Smear Tests were run to estimate contact angles of mud on an oil-covered slide and of oil on a mud-covered slide. As shown in Figures 136-138, for the Chevron, Husky and Overseas Limited crude oils, the oil and mud appeared to nearly spread over each other.

Figure 136. Displacement of Chevron Crude Oil by SE APHRON ICS™ Fluid

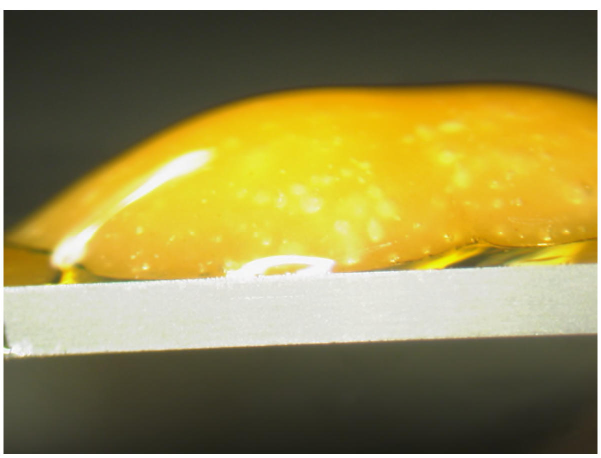

(a) Displacement of Oil by Mud

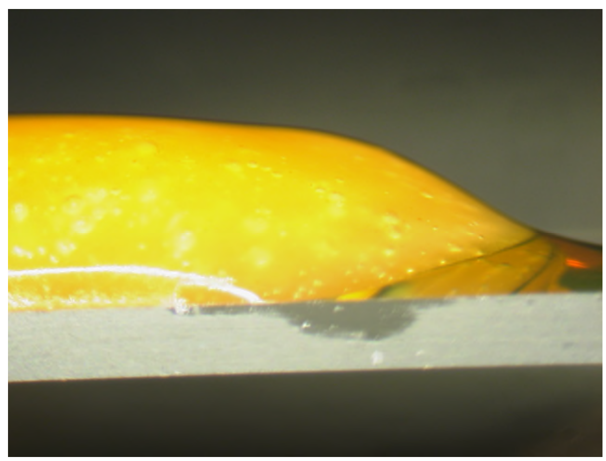

(b) Displacement of Mud by Oil

Figure 137. Displacement of Husky Crude Oil by SE APHRON ICS^{TM} Fluid

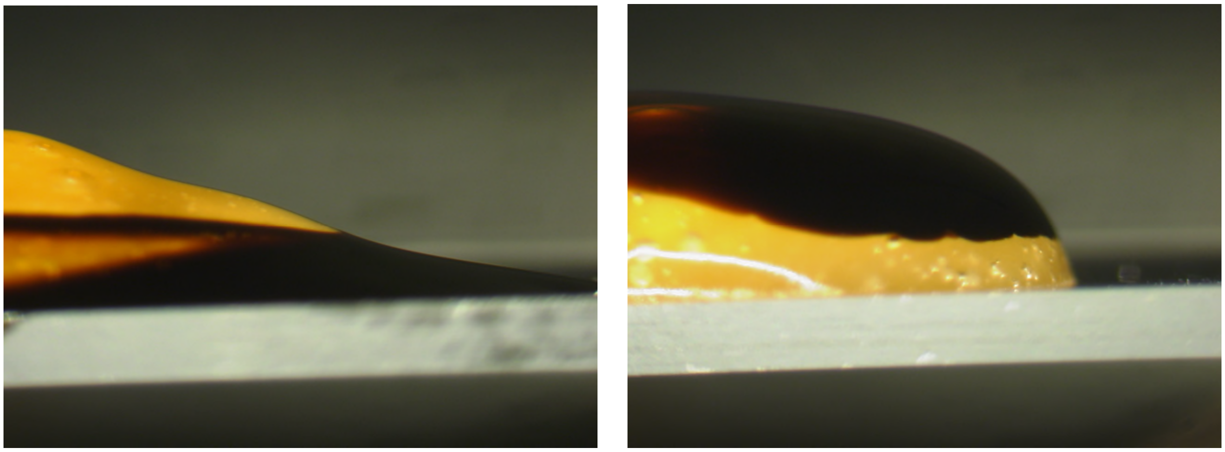

(a) Displacement of Oil by Mud (b) Displacement of Mud by Oil

Figure 138. Displacement of Overseas Limited Crude Oil by SE APHRON ICS^{TM} Fluid

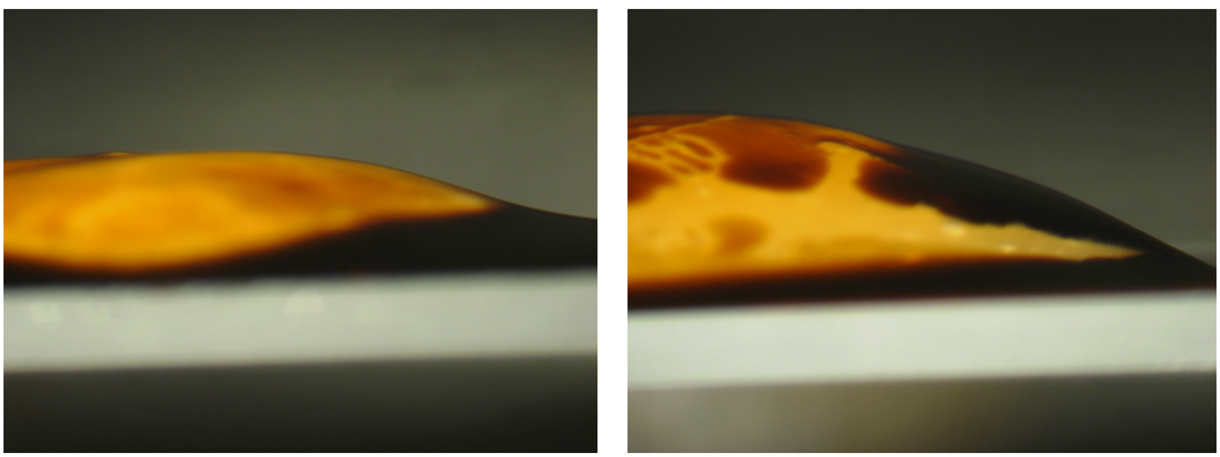

(a) Displacement of Oil by Mud (b) Displacement of Mud by Oil

The Husky crude oil was so viscous, however, that when a drop of the oil was placed atop the mud-covered slide, the oil remained floating on the pool of mud. The Overseas Limited crude oil did almost the same thing, but enough of it ran down to generate a visible mud/oil interface on the slide. In any case, contact angles in all cases (including the Chevron crude oil) were very low, indicating that the phases are nearly miscible. Microscopic examination of the sheared 50/50 mixtures of these oils with the SE APHRON ICS^{TM} mud (Figure 139) revealed the Husky oil mixture to be water-continuous (water-wetting), as evidenced by the presence of aphrons, while the Overseas Limited oil mixture appears to be at the nexus between water-wetting and oil-wetting. The Chevron mud phase (not shown) was obviously water-wetting.

Figure 139. Microphotographs of 50/50 Mixtures of Crude Oils and SE APHRON ICS™ Fluid

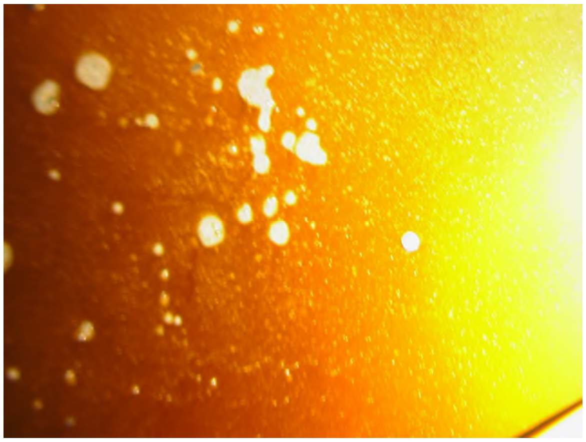

(a) Husky Crude Oil

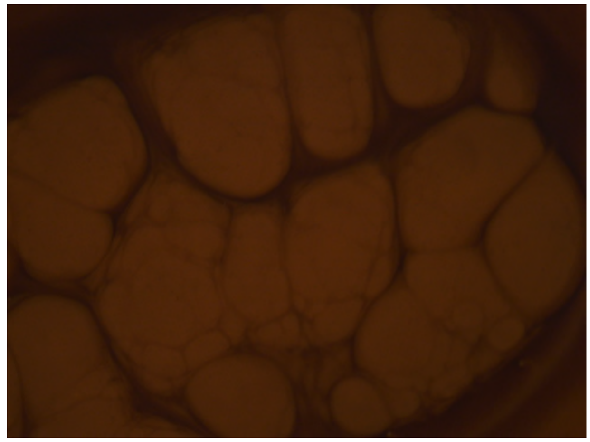

(b) Overseas Limited Crude Oil

These results indicate that the surfactant in the SE APHRON ICS™ fluid is sufficient to emulsify a 50/50 mixture of all the oils and the mud, though the Chevron crude oil appears to separate quickly from the mud. For 90/10 mixtures of oil and mud, the base oils and synthetic fluids, as well as the Chevron crude oil showed relatively rapid phase separation (less than 30 min), whereas the other three crude oils remained emulsified. In no cases, however, was any high-viscosity emulsion phase formed; indeed, in every case where a slowly-separating emulsion phase was formed, the viscosity appeared to be approximately that of the continuous phase.

Inasmuch as no high-viscosity phase was formed between oil and mud, and the contact angles between pure oil and mud were very low, it may be concluded that APHRON ICS™ muds are very compatible with produced oils.

CONCLUSIONS

Aphrons are generated by natural entrainment at the surface of 12 to 15 vol % air in a surfactant-stabilized, highly shear-thinning fluid. Very soon after they are created, the oxygen is scavenged by one of the components in the fluid, leaving the aphrons with a core of nitrogen. Some of these aphrons can survive downhole pressures of at least 27.3 MPa (4000 psig), though the number of visible aphrons at that pressure may be small, and the survivors may have a limited life. Compression of aphrons initially results in volume reduction that is inversely proportional to the absolute pressure. Over time, they shrink further at a rate that depends on the surface area of the bubble, the rate at which the fluid was compressed, the level of shear (if the fluid is flowing), the concentration of nitrogen in solution and the chemical composition of the fluid. Maximum longevity at a given pressure is obtained with bubbles several hundred microns in diameter that are compressed rapidly and subjected to minimum shear. When the bubbles reach a critical minimum size -- 25 to 50 μm diameter -- they undergo a structural change that leads to their collapse (if the fluid is not saturated with nitrogen), and the aphrons vanish.

Aphron drilling fluids can control fluid invasion into formations with permeabilities as high as 80 darcy. Three mechanisms are involved. First, driven by a pressure differential and high shear rate, aphrons travel much faster than the base fluid and concentrate at the fluid front. Comminution of the aphrons by shear produces bubbles of a size similar to the openings in the rock, which can serve to bridge the openings. Second, particulates in the mud form a microgel network. Bridging by aphrons and particulates, coupled with radial flow of the mud into the formation, decreases the shear rate dramatically; this enables the third element, namely the viscosity of the very-high-LSRV base fluid, to build quickly to such high levels that the fluid almost stops.

Aphron drilling fluids also protect producing formations by minimizing loss of permeability (formation damage), first through the excellent compatibility of the drilling fluids with produced fluids, and second through the lack of affinity of aphrons for each other and for mineral surfaces.

The results obtained in this work demonstrate how and to what extent aphron drilling fluids reduce whole mud loss and minimize collateral damage to high-permeability porous media. Consequently, now the industry can utilize this technology with greater confidence to drill oil and gas wells and, by doing so, recover the hydrocarbons more economically.

ACKNOWLEDGEMENTS

My sincerest gratitude goes to the Aphron Technology Team at MASI Technologies LLC that is responsible for gathering the data reported here: Arkadiy Belkin, Miranda Fosdick, Tatiana Hoff, Maribella Irving and Bob O'Connor. I also thank Gary Covatch, the DOE project manager, for his guidance throughout the course of this project, and John Rogers of the DOE for his advice and valuable and informative discussions. In addition, many thanks to the following individuals for their numerable contributions: Tony Rea and Tom Brookey of MASI Technologies LLC for their essential advice and direction; Dr. Peter Popov of Texas A&M University for the all-important bubbly flow modeling work; and George McMennamy of M-I SWACO for some critical analytical work on the composition of aphron drilling fluids.

REFERENCES

1. Montilva, J., Ivan, C.D., Friedheim, J. and Bayter, R.: "Aphron Drilling Fluid: Field Lessons From Successful Application in Drilling Depleted Reservoirs in Lake Maracaibo," OTC 14278, presented at the 2002 Offshore Technology Conference, Houston, May 6-9, 2002.
2. Growcock, F.B., Simon, G.A., Rea, A.B., Leonard, R.S., Noello, E. and Castellan, R.: "Alternative Aphron-Based Drilling Fluid," IADC/SPE 87134, presented at the 2004 IADC/SPE Drilling Conference, Dallas, Mar. 2-4, 2004.
3. Brookey, T., Rea, A. and Roe, T.: "UBD and Beyond: Aphron Drilling Fluids for Depleted Zones," presented at IADC World Drilling Conference, Vienna, Austria, Jun. 25-26, 2003.
4. Growcock, F.B., Simon, G.A., Guzman, J., and Paiuk, B.: "Applications of Novel Aphron Drilling Fluids," AADE-04-DF-HO-18, presented at the AADE 2004 Drilling Fluids Conference, Houston, TX, Apr. 6-7, 2004.
5. Sebba, F.: **Foams and Biliquid Foams – Aphrons**, John Wiley & Sons Ltd, Chichester (1987).
6. White, C.C., Chesters, A.P., Ivan, C.D., Maikranz, S. and Nouris, R.: "Aphron-Based Drilling Fluid: Novel Technology for Drilling Depleted Formations," World Oil, vol. 224, no. 10 (Oct. 2003).
7. Growcock, F. B., Simon, G. A. and Rea, A. B.: "Development of Aphron Drilling Fluids," presented at *SEFLU y CEMPO*, Margarita Island, Venezuela, May 24-28, 2004.

8. Hoff, T., O'Connor, B. and Growcock, F. B.: "Drilling Fluid Selection to Minimize Formation Invasion," AADE-05-NTCE-73, presented at 2005 AADE National Technical Conference and Exhibition, Houston, April 5-7, 2005.
9. Growcock, F. B.: **"**Enhanced Wellbore Stabilization and Reservoir Productivity with Aphron Drilling Fluid Technology," **GasTIPS**, GTI-05/0226, Vol. 11, No. 2, Spring 2005, pp. 12-16**.**
10. Popov, P. and Growcock, F. B.: "US DOE-Backed R&D Validates Effectiveness of Aphron Drilling Fluids in Depleted Zones," with P. Popov, **Drilling Contractor**, May/June 2005, pp. 55-58.
11. Irving, M., Belkin, A., O'Connor, B., Fosdick, M., Hoff, T. and Growcock, F. B.: "Avances en Fluidos de Perforacion de Afrones," presented at Primer Encuentro Tecnologico de Perforacion y Rehabilitacion de Pozos, San Tome, Venezuela, May 23-26, 2005.
12. Gregoire, M., Hilbig, N., Stansbury, M. Al-Yemeni, S. and Growcock, F. B.: "Drilling Fractured Granite in Yemen with Solids-Free Aphron Fluid," presented at IADC World Drilling 2005, Rome, June 9-10, 2005.
13. Belkin, A., Irving, M., O'Connor, B., Fosdick, M., Hoff, T. and Growcock, F. B.: "How Aphron Drilling Fluids Work," SPE 96145 presented at 2005 SPE Annual Technical Conference and Exhibition, Dallas, Oct. 9-12, 2005.
14. Growcock, F. B., Belkin, A., Irving, M., O'Connor, B., Fosdick, M. and Hoff, T.: "New Insights into Aphron Drilling Fluids," EXPL-2-FG-13, presented at V INGEPET, Lima, Peru, Nov. 8-11, 2005.
15. Chahine, G. L. and Kalumuck, K. N.: "Development of Near Real-Time Instrument for Nuclei Measurement: The ABS Acoustic Bubble Spectrometer," Proc. FEDSM'03, International Symposium on Cavitation Inception, 4th ASME_JSME Joint Fluids Engineering Conf., Honolulu, Hawaii, July 6-10, 2003.
16. API RP 13C: "Recommended Practice for Drilling Fluid Processing Systems Evaluation," American Petroleum Institute, Washington, D. C., 2nd Ed, March 1996.
17. Fann Instrument Co.: *Capillary Suction Timer Instruction Sheet*, Part No. E10280001EA, Rev. C, Houston, (1995).
18. Walker, J.: "The Amateur Scientist: Fluid Interfaces, Including Fractal Flows Can Be Studied in a Hele-Shaw Cell," Scientific American, No. 257, pp. 134-138, Nov. 1987.

19. Adamson, A.W.: *Physical Chemistry of Surfaces*, 5th Ed., John Wiley & Sons, New York, 1990.
20. API RP 42: "Recommended Practice for Emulsion Test Method," 2nd Ed., American Petroleum Institute, Washington, D. C., March 1996.
21. Perry, R. H. and Green, D. W.: *Perry's Chemical Engineering Handbook*, 7th ed., McGraw-Hill, 1997.
22. Hiemenz, P. C. and Rajagopalan, R.: *Principles of Colloid and Surface Chemistry*, 3rd Ed., Marcel Dekker, New York, 1997.
23. Darley, H. C. H. and Gray, G. R.: *Composition and Properties of Drilling and Completion Fluids*, 5th Ed., Gulf Professional Publishing, New York, 1988.
24. "M-I Drilling Fluids Engineering Manual," Revision No: A-0, Chapter 7 - Filtration Control.
25. Lee, D. J.: "A Dynamic Model of Capillary Suction Apparatus," *J. Chem. Eng. Japan*, Vol. 27, No. 2 (1994) 216.
26. Guan, J., Amal, R. and Waite, T. D.: "Effect of Floc Size and Structure on Biosolids Capillary Suction Time," *Water Sci Technology*, Vol. 47, No. 12, (2003) 255.
27. Growcock, F. B., Khan, A. M. and Simon, G. A.: "Application of Water-Based and Oil-Based Aphrons in Drilling Fluids," SPE 80208, SPE International Symposium on Oilfield Chemistry, Houston, Feb. 5-8, 2003.
28. Fraser, L. J., Reid, P. I., Williamson, L. D. and Enriquez, F. P., Jr.: "Formation-Damaging Characteristics of Mixed Metal Hydroxide Drill-In Fluids and a Comparison with Polymer-Base Fluids," SPE 57714, *SPE Drilling & Completion*, (Sept. 1999) 178.
29. Landau, L. D. and Lifshitz, E. M.: **Fluid Mechanics (Course of Theoretical Physics, Vol. 6)**, 2nd Edition, Butterworth-Heinemann, New York, 1995.
30. Popov, P.: Private Communication, Texas A&M University, September 14, 2004.
31. Barnes, H. A., Hutton, J. F. And Walters, K.: *An Introduction to Rheology*, Vol. 3 of Rheology Series, Elsevier, New York, 1989.

LIST OF ACRONYMS AND ABBREVIATIONS

A = Cross-Sectional Area of Permeable Medium

ABS = Acoustic Bubble Spectrometry

APHRON ICS^{TM} = Polymer-Based Aphron Invasion Control System

BHT = Bottom-hole temperature

BSD = Bubble Size Distribution

CSD = Capillary suction displacement (distance traveled by the fluid front)

CST = Capillary suction time

d = Distance that fluid travels in modified Capillary Suction Time test

D = Diffusion, or Transport, Coefficient of Air from Aphron to Surrounding Fluid

DO = Dissolved Oxygen

ΔP = Pressure Differential

EMI- = Experimental M-I *LLC* product

gpm = gallons per minute

h = thickness of filter cake

HTHP = High Temperature and High Pressure

HYSSTER^{TM} = Clay-Based Aphron Drilling Fluid

ID = Internal Diameter

k = Permeability

L = Length of Conduit

LSRV = Low-Shear-Rate Viscosity at 0.06 sec^{-1}

μ = Viscosity

OD = Outer Diameter

ppb = lb/bbl = Pounds per Barrel

ppm = Parts per Million

psia = Absolute Pressure

psig = Gauge Pressure, i.e. psig = psia - 14.7

Q = Volumetric Flow Rate

Q_c = Volume of the filter cake

Q_f = q = Volume of the filtrate

r = Bubble Radius

S, S_0 = Size (Diameter) of Aphron after time t and time 0

SE = SuperEnhanced

TE = Transparent Enhanced

V = Velocity of Bubble

x = Length of Permeable Medium

X = Volume of filtrate at time t

Note: Substances shown in ALL-CAPITAL letters are trademarked products from M-I SWACO.